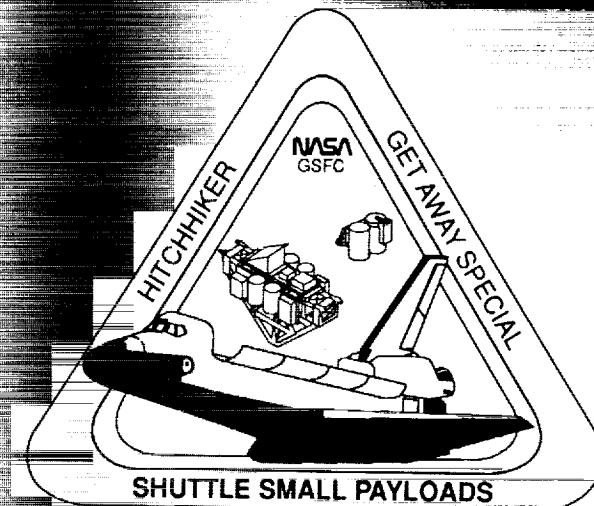


NASA Conference Publication 3171

1992 Shuttle Small Payloads Symposium



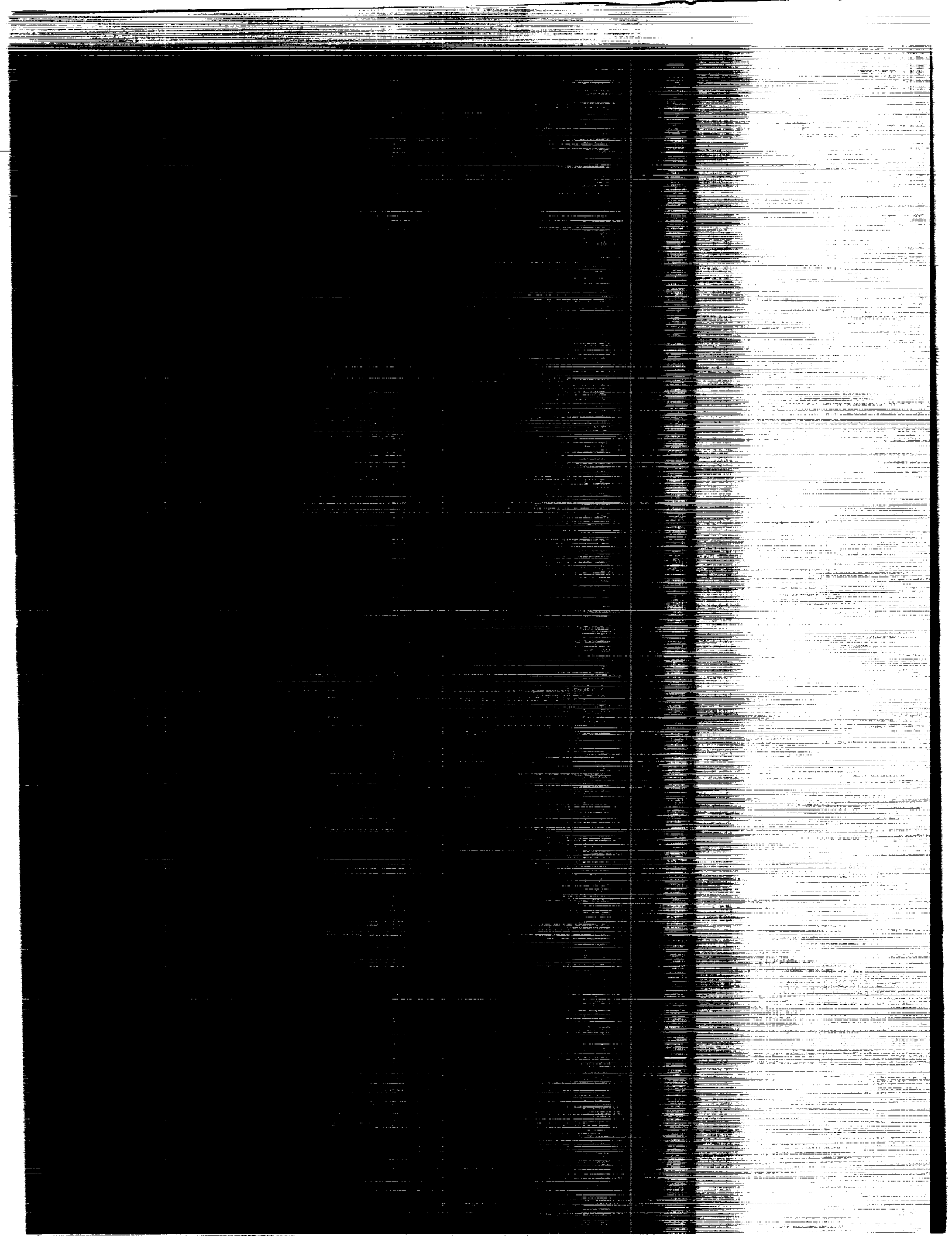
*Proceedings of a symposium held at
the Sheraton-Greenbelt
Lanham, Maryland
October 20-23, 1992*

(NASA-CP-3171) THE 1992 SHUTTLE
SMALL PAYLOADS SYMPOSIUM (NASA)
284 p

N93-13158
--THRU--
N93-13186
Unclass

H1/12 0122340

NASA



NASA Conference Publication 3171

1992 Shuttle Small Payloads Symposium

Edited by
Lawrence R. Thomas
NASA Goddard Space Flight Center
Greenbelt, Maryland

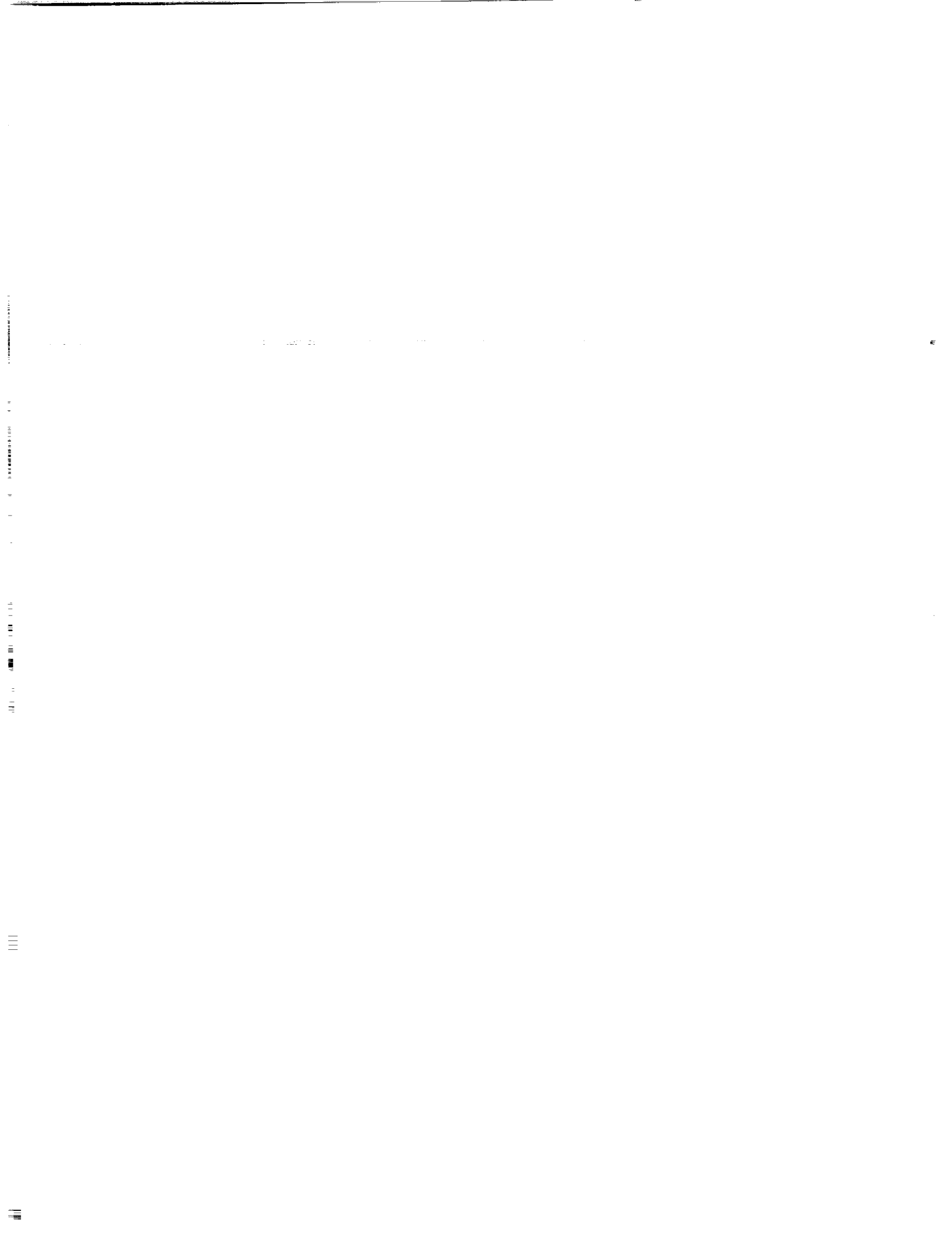
Frances L. Mosier
Interstel, Inc.
Beltsville, Maryland

Proceedings of a symposium held at
the Sheraton-Greenbelt
Lanham, Maryland
October 20–23, 1992

NASA

National Aeronautics and
Space Administration
Office of Management
Scientific and Technical
Information Program

1992



CONTENTS

	Page
1. THE ORBITER STABILITY EXPERIMENT ON STS-40 Werner M. Neupert, Gabriel L. Epstein, James Houston, Kenneth J. Meese, William S. Muney, Thomas B. Plummer, and Frank P. Russo.....	1
2. SPACEFLIGHT PAYLOAD DESIGN FLIGHT EXPERIENCE G-408 William W. Durgin, Fred J. Looft, Albert Sacco, Jr., Robert Thompson, Anthony G. Dixon, Dino Roberti, Robert Labonte, and Larry Moschini.....	9
3. POST FLIGHT OPERATION OF A HIGH PEAK POWER NEODYMIUM YAG LASER ABOARD THE G-449 PAYLOAD FLOWN ON SPACE SHUTTLE COLUMBIA MISSION 61-C M. C. Muckerheide.....	21
4. A DECADE OF DISCOVERY: EXPERIMENTS WITH THE GET AWAY SPECIAL (GAS) CANISTER Robert Brienzo.....	29
5. IlaO ULTRAVIOLET AND NUCLEAR EMULSION FILMS RESPONSES TO ORBITAL FLIGHTS ON STS-3, STS-7, STS-8, AND STS-40 E. C. Hammond, Jr., K. A. Peters, S. M. Blake, Y. Bailey, D. Johnson, S. Robancho, and A. Stober.....	39
6. EARTH OBSERVATION PHOTOGRAPHY - LOOKING BACK 20 YEARS AFTER SKYLAB James H. Nicholson, Thomas J. O'Brien, Mitchell Colgan, Ruth Ashcraft-Truluck, James R. Frysinger, and Carol A. Tempel.....	47
7. A PATH TO IN-SPACE WELDING AND TO OTHER IN-SPACE METAL PROCESSING TECHNOLOGIES USING SPACE SHUTTLE SMALL PAYLOADS David Tamir.....	57
8. A PAYLOAD TO EVALUATE PHOTODIODES FOR THE DETECTION OF SOFT AND HARD X-RAYS IN A SPACE ENVIRONMENT USING A GET AWAY SPECIAL Upendra D. Desai and AmyElizabeth C. Stewart.....	77
9. A STUDY OF THE EFFECTS OF MICRO-GRAVITY ON SEED GERMINATION Lynn Suzanne Klein, Mark McKibben, David A. Brain, Theodore C. Johnson, and Konrad K. Dannenberg.....	85

CONTENTS (CONTINUED)

		Page
10.	INVESTIGATION OF MICROGRAVITY EFFECTS ON SOLIDIFICATION PHENOMENA OF SELECTED MATERIALS Carl R. Maag and Patricia A. Hansen.....	95
11.	ENVIRONMENTAL QUALIFICATION TESTING OF PAYLOAD G-534, THE POOL BOILING EXPERIMENT J. Andrew Sexton.....	103
12.	ELECTRICAL DESIGN OF PAYLOAD G-534, THE POOL BOILING EXPERIMENT David R. Francisco.....	115
13.	G-133: A SOFT X-RAY SOLAR TELESCOPE Memorie K. Williams, Branton Campbell, Peter W.A. Roming, Mark K. Spute, and J. Ward Moody.....	125
14.	TAGGING INSULIN IN MICROGRAVITY Michael Dobeck and Ronald S. Nelson, M.D.....	133
15.	GAMCIT - A GAMMA-RAY BURST DETECTOR Derek M. Surka, John M. Grunsfeld, and Brett A. Warneke.....	143
16.	G-254 UNDERGRADUATE EXPERIMENT Doran Barton, Karilyn Bogh, Brett Evans, Steve Folkman, Marc Hammond, Casey Hatch, Neva Herr, Tina Hubble, Jeff Humpherys, Steve Johnson, Mark Lemon, Oscar A. Monje, Kristin Redd, Rich Warby, Tumkur Raghuram, and students from Kinkaid High School.....	151
17.	STRUCTURAL VERIFICATION FOR GAS EXPERIMENTS Mark Daniel Peden.....	165
18.	PROPER BATTERY SYSTEM DESIGN FOR GAS EXPERIMENTS Stephen A. Calogero.....	175
19.	A PENNSYLVANIA STATE UNIVERSITY/GENERAL ELECTRIC GET AWAY SPECIAL (GAS) EXPERIMENT George Evanisko, Theodore Grosch, Milad Youssef, Jim Yurack, and C. R. Philbrick.....	185
20.	CONCAP IV: A COMPLEX AUTONOMOUS PAYLOAD (CAP) FOR GROWING ORGANIC THIN FILMS IN MICROGRAVITY W. E. Carswell and F. C. Wessling	195

CONTENTS (CONTINUED)

	Page
21. THE ROMPS ROBOT IN HITCHHIKER George Voellmer.....	205
22. THE DSI SMALL SATELLITE LAUNCHER S. Nichols, D. Gibbons, J. Wise, and D. Nguyen.....	221
23. THE CAPILLARY PUMPED LOOP FLIGHT EXPERIMENT (CAPL) A PATHFINDER FOR EOS D. Butler and T. Hoang.....	233
24. THE VTRE PROGRAM - AN OVERVIEW William J. Bailey and John P. Gille.....	247
25. THE LDCE PARTICLE IMPACT EXPERIMENT AS FLOWN ON STS-46 Carl R. Maag, William G. Tanner, Janet Borg, Jean-Pierre Bibring, W. Merle Alexander and Andrew J. Maag.....	257
26. BATTERY SELECTION FOR SPACE EXPERIMENTS David R. Francisco.....	267
27. THE UNIQUE CHALLENGE OF MANAGING AN UNDERGRADUATE GET- AWAY-SPECIAL EXPERIMENT Peter W.A. Roming, Mark K. Spute, Memorie K. Williams, Branton J. Campbell, and J. Ward Moody.....	277
28. PREPARING SAFETY DATA PACKAGES FOR EXPERIMENTERS USING THE GET AWAY SPECIAL (GAS) CARRIER SYSTEM Jerome Kosko.....	285



THE ORBITER STABILITY EXPERIMENT ON STS-40¹

Werner M. Neupert, Gabriel L. Epstein², James Houston, Kenneth J. Meese,
William S. Muney, Thomas B. Plummer, and Frank P. Russo³

Laboratory for Astronomy and Solar Physics
NASA/Goddard Space Flight Center
Greenbelt, MD 20771

ABSTRACT

The Orbiter Stability Experiment (OSE) was developed and flown to evaluate the steadiness of the STS Orbiter as a potential platform for instrumentation that would image the Sun in its extreme ultraviolet and soft X-ray radiations. We were particularly interested in any high frequency motions of the Orbiter's orientation due to normal operations and manned activities. In this paper we present preliminary results of our observations. Other than the expected slow motion of the Orbiter within the specified angular deadband of 0.1° during our observations, we found that high frequency (above 1 Hz) angular motions ("jitter") were not detectable at the 0.25 arc sec detection limit of our most sensitive detector, for most of the period of observation. No high frequency motions were recorded during intervals that we identify with vernier thruster firings. However, one short interval with detectable spectral power to a frequency of 10 Hz has been found to date. It has not yet been correlated with a particular activity going on at the time. The results of our observations may also be of value in assessing perturbations to the Orbiter's micro-gravity environment produced by normal operations.

OBJECTIVE OF THE EXPERIMENT

The primary objective of the OSE was to obtain a characterization of the Orbiter's spectrum of high frequency angular motions (which we term "jitter"), produced by the operation of mechanical systems, thruster firings, and man motions during normal crew activity. The presence of such rapidly varying motions, although small and not detectable by visual observations, could contribute to a residual microgravity environment at locations on the Orbiter that are not at the center of rotation. The OSE measured angular displacements, and hence, angular accelerations, directly by observing changes in the orientation of the Orbiter in pitch and roll relative to the Sun, using sensors typically flown on solar sounding rockets. We recorded the position of the Sun relative to the Orbiter for upwards of 40 minutes, as the Orbiter was

¹ This research was supported by the Director's Discretionary Fund of the NASA/Goddard Space Flight Center

² Present Address: Code 410, NASA/Goddard Space Flight Center

³ Present Address: Code 728, NASA/Goddard Space Flight Center

maintained in a $-Z_0$ solar inertial attitude by vernier thruster firings.

DESCRIPTION OF THE INSTRUMENTATION

OPTICAL SUN SENSORS

The OSE detected the angular Orbiter's motion of the Orbiter's $-Z_0$ axis by measuring the direction of incoming sunlight relative to two optical sun sensors mounted externally on a GAS experiment plate. The sensors used were Lockheed Intermediate Sun Sensors (LISS) provided by the Lockheed Missiles and Space Co. SPARCS Office, White Sands Missile Range, NM, under contract to the Wallops Flight Facility of NASA's Goddard Space Flight Center. Each sensor provided independent pitch and roll measurements. These devices can detect angular changes as small as 0.1 arc sec at frequencies up to 1000 Hz. They are typically flown on fine-pointed solar sounding rockets and have been qualified at vibration levels far higher than are encountered with the Shuttle. Characteristics of the sensors and other significant operating parameters of the OSE are provided in Table 1.

The sensors were carefully aligned to the GAS bridge, which was located at the aft end of the Orbiter bay. Consequently, any change in the position of the Sun within the fields of view (FOV) of the sensors accurately represented a change in the angular offset of the direction of incoming sunlight relative to the Orbiter's inertial guidance system.

ALIGNMENT OF THE OSE SUN SENSORS TO THE ORBITER'S $-Z_0$ AXIS

Accurate alignment of the sun sensors to the Orbiter was necessary as the estimated tolerance buildup between the experiment and the orbiter navigational base, located in the nose of the Orbiter, was estimated to be as high as 1.5° , and therefore comparable to the FOV of the sensors. For this reason, also, the FOV of one of the sensors was intentionally expanded (resulting in a loss of angular sensitivity) from its nominal $\pm 2^\circ$ to $\pm 3^\circ$ to assure that some observations would be acquired, even if the worst case misalignment actually occurred. The sensors were first mounted to and aligned with a specially designed mounting plate that was in turn mounted to the top of the GAS can. This mounting plate was accurately aligned to the GAS bridge during integration, following an alignment procedure using an inclinometer and sensitive bubble level. Final alignment of the sensors to the GAS bridge was within 1 arc min in pitch and 7 arc min in roll. A unique flexible thermal blanket for the top of the GAS can was designed and built to accommodate the sun sensors while providing maximum solar isolation for the GAS can.

The Orbiter was maintained in a $-Z_0$ solar inertial mode within a $\pm 0.05^\circ$ deadband during our observations. At the time of Sun acquisition by the OSE, the alignments of the two LISS sensors to the Orbiter's navigational base were -3.2 and -2.2 arc min in pitch and -2.3 and -5.3 arc min in roll, far better than the estimated error envelope of $\pm 1.5^\circ$. One LISS was positioned with a 180° rotation about its line of sight so as to provide signals of opposite polarity for orbiter pointing deviations. This was a means of discriminating against undetected electronic noise and drifts in the shared

electronic system. Thermal stabilization of the electronics, using heaters, was incorporated to assure that observations would take place with the electronics at their nominal operation temperature range of 25-30°C. These heaters were eventually not required as the Orbiter's attitude provided a benign thermal environment, and the OSE's internal electrical dissipation quickly raised the instrument's electronic system to nominal operating temperatures. The instrument was operated both with and without a solar input to determine the level of internal electronic noise. Such noise produced a white noise spectrum against which the spectrum of vibrations recorded during Sun-pointed operation could be compared.

OBSERVATIONS

The OSE was powered up for two intervals of time totally nearly three hours (that included both dark and sunlit portions of the orbit). The periods of operation during the STS-40 mission were Mission Elapsed Time (MET) 01:23:56 (day/hr/min) to 02:02:01 and 02:07:26 to 02:08:21. Intervals of anomalous tape recorder operation (loss of synch, but not necessarily loss of data) are apparent in our data playback after the first 40 minutes of operations and make data analysis more difficult. We have therefore limited our preliminary analysis to the first 40 min of data. During that interval, the offset of the Orbiter's $-Z_0$ axis from the solar direction as the vehicle moved in its deadband about its pitch axis (Y axis) produced a signal reminiscent of a rectified sine wave (figure 1), with the Earth's residual atmosphere at orbital altitude

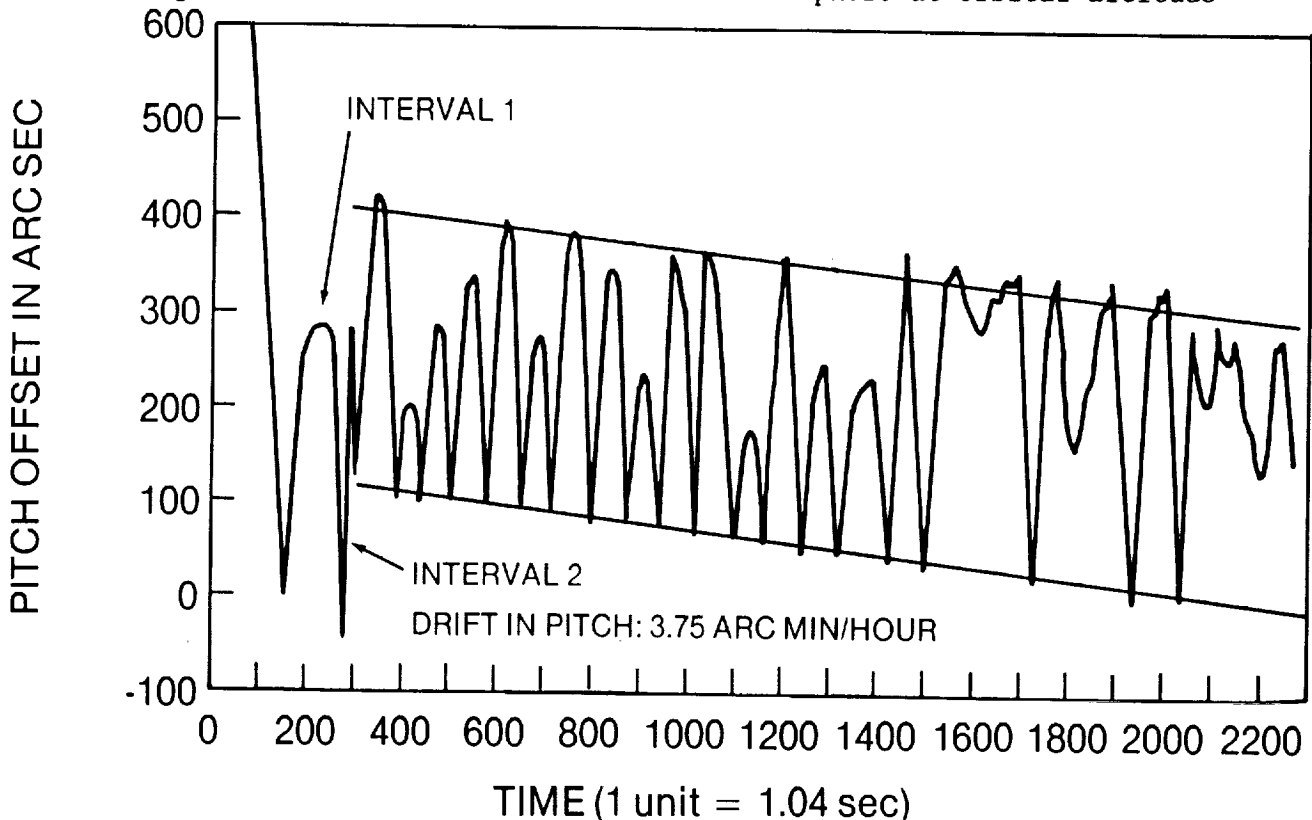


Figure 1. Deviations in Orbiter pitch as a function of time for the initial period of OSE observations on STS-40. Measurements with Sensor 1 are shown.

providing a drag force that typically rotated the Orbiter against one side of the deadband. The motions of Orbiter about its roll axis (X axis), shown in figure 2, were less regular in frequency.

The drift in the envelope of pitch deviations, shown by the sloping straight lines in figure 1, was almost exactly the same for both LISS, and therefore not due optical degradation. For this time interval, the drift was 3.75 arc min/hour, which is about 2.5 times the drift in pitch recorded by an optical sun sensor on STS-3 (data supplied informally by the SUSIM investigator on STS-3) for a much longer (10 hr) period of solar inertial pointing. In that instance, realignment of sun sensors to the center of the Sun was re-established when the Orbiter's navigational base was updated using star trackers. We propose that, in both instances, the drift in the envelope of pitch deviations was due to a drift in the Orbiter's navigational coordinate system relative to the Orbiter's structure (i.e., a drift in the navigational gyros) rather than a drift in the sun sensors relative to the Orbiter's structure. The drift in the envelope of roll deviations was approximately 3 arc min per hour, as can be seen from an inspection of figure 2.

The objective of the OSE observation was to record high frequency motions of the Orbiter bay that might be superimposed on the expected larger scale motion of the Orbiter within its deadband. Such higher frequency components, commonly called "jitter", might be attributable to the normal operation of mechanical systems or to the usual motions of the astronauts during their normal working

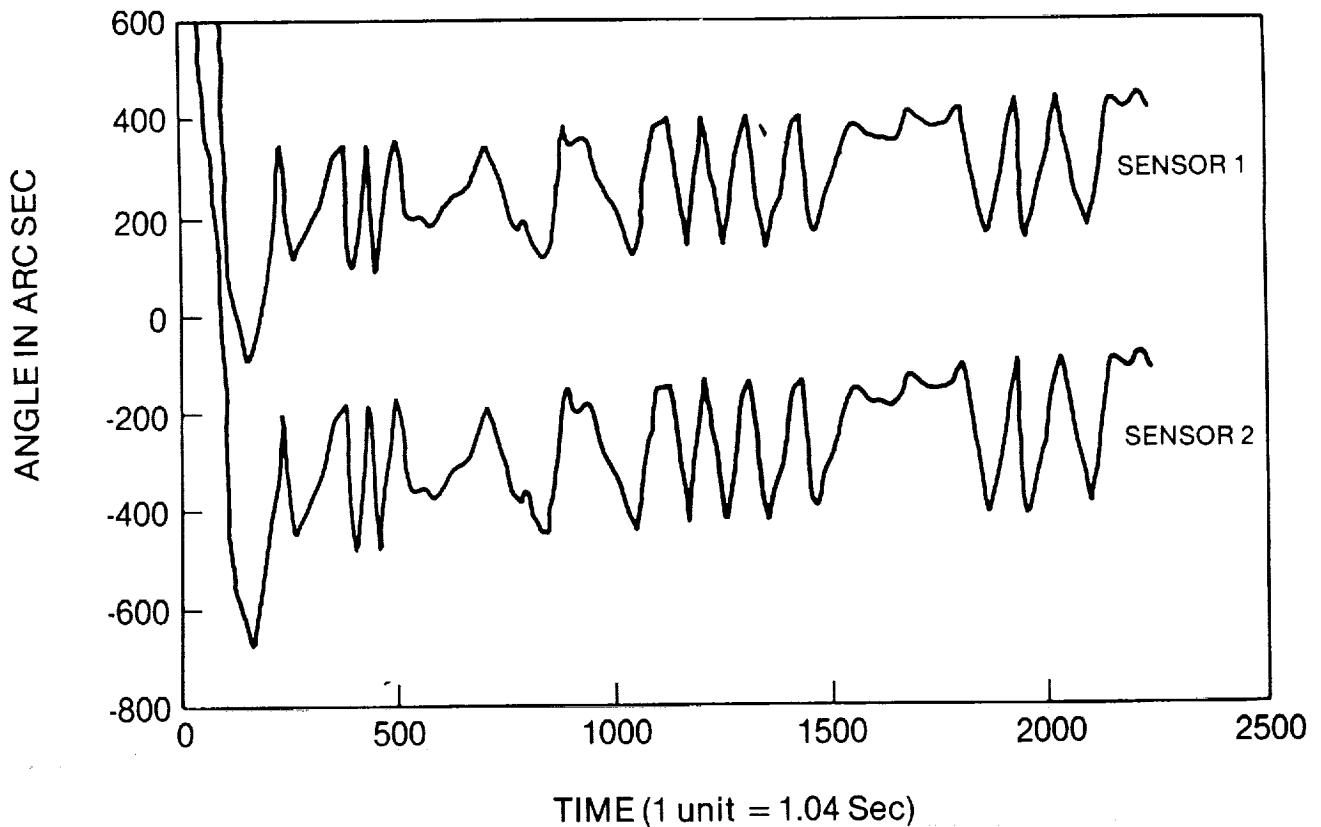


Figure 2. Deviations on Orbiter roll (about its X axis) during the initial period of OSE operation on STS-40. Outputs of both LISS sun sensors are shown.

activities. Our initial scan of the bulk of the usable observations, which occurred during the sunlight portions of one orbit, indicates that any such jitter must have been at or below the limit of detectability (0.25 arc sec) for almost the entire observing interval. An example of the signal output for the pitch channel of Sensor 1, the high sensitivity sensor, during an interval of time that included thruster firings is shown in figure 3. The Orbiter's motion appears smooth throughout, and in comparing plots of the outputs of the two pitch channels visually, we find no detectable correlation of high frequency signal variations.

Figure 3 also shows that the reversal of orbiter motion due to a thruster firing at the extremes of its deadband is smooth. No detailed correlation of our data has yet been made however, and it is not clear to what extent the smooth reversal of attitude is the result of a sequence of vernier thruster firings or whether it reflects a low frequency response by the Orbiter to a single firing. In any case, no angular vibration at frequencies above about 1 Hz attributable to a vernier thruster firing is detectable with the present instrument.

To date, we have found only one interval when pointing deviations (other than oscillations within the dead-band) were clearly present. That interval, shown in Figure 4, lasted for about 25 sec. It occurred, perhaps coincidentally, during a reversal of Orbiter motion in its deadband. The reproducibility of line of sight deviations in the two pitch channels gives confidence that the varying signals are in fact real fluctuations in Orbiter pointing at the 0.5 to 2 arc sec level.

ANALYSIS

We have begun to characterize the Orbiter's angular motions in terms of power spectral density (PSD) for intervals of time when interesting perturbations were been recorded. As a baseline, we derived the PSD for an interval of instrument operation without solar input (recorded in the laboratory during final integration activities). The PSD for such operation is flat, i.e., independent of frequency, to a limiting frequency of about 20 Hz. We have similarly calculated PSD for sample intervals of OSE on-orbit operation. For a portion of the interval shown in figure 3 that was free of thruster firings, we find no power above 1 Hz in the PSD of deviations of our high-sensitivity observations from a polynomial fit to the data. For the 25 sec-long interval of erratic pitch motions (jitter) shown in figure 4, we find no spectral power above the instrument's ambient electronic noise level for frequencies above 10 Hz. The PSD fits a power law with an exponential of -2.6 for frequencies between 0.5 and 10 Hz. Angular motions of 0.5 arc sec or greater (peak-to-peak) in pitch or roll were limited to frequencies of 1 Hz or less. The erratic pointing deviations shown in figure 4 have not yet been identified with any specific event or activity aboard the spacecraft.

SUMMARY

The Orbiter Stability Experiment performed well during the STS-40 mission

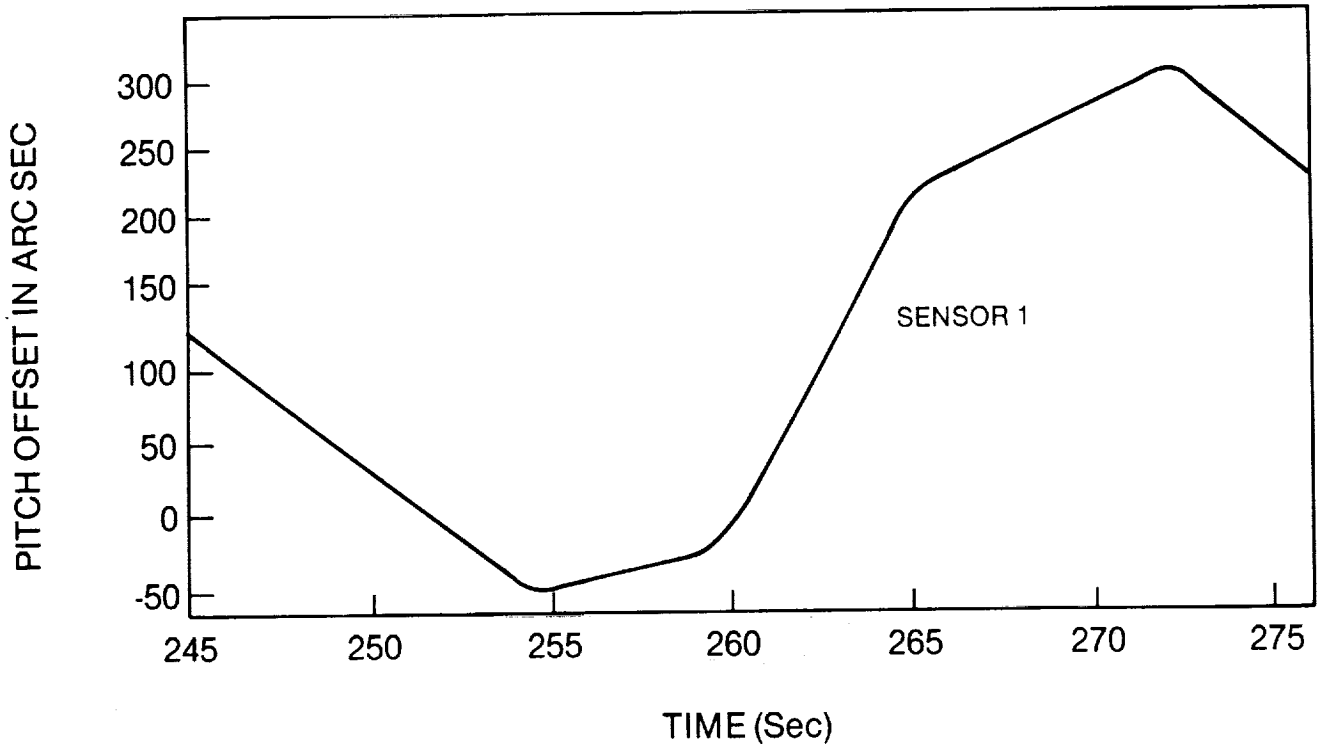


Figure 3. Output of the high sensitivity pitch channel (Sensor 1) during an interval when vernier thrusters were used to maintain the Orbiter's attitude. This interval is indicated as Interval 2 in figure 1.

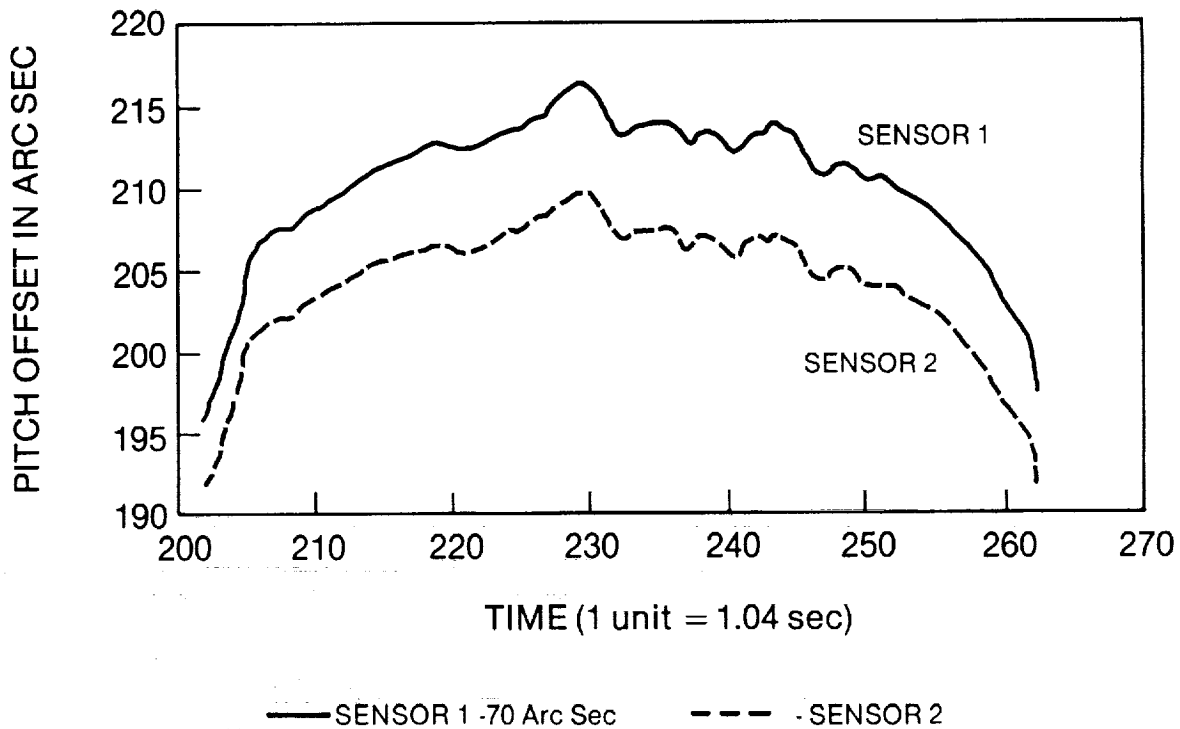


Figure 4. Comparison of pitch channel outputs from an interval near the beginning of sun-pointed operation. The small (0.5 to 2.5 arc sec) pointing deviations are exceptions to the smooth motions of the Orbiter typically encountered. This interval is indicated as Interval 1 in figure 1.

and demonstrated the relative absence of high frequency jitter about the Orbiter's pitch and roll axes. The original intent of the experiment was to characterize such motions for purposes of designing an image motion compensation system for a proposed solar optical imaging instrument (which was never built). It succeeded in making the desired measurements. We plan to perform an extended and more rigorous analysis of the observations in the future, and in particular, plan to correlate our observations with Orbiter thruster firings. The eventual data base may provide correlative data for linear acceleration measurements made on-board STS-40, and we have participated in meetings of NASA's Microgravity Measurements Working Group in an effort to disseminate OSE results to other organizations that may be able to use them in characterizing the Orbiter's motions.

TABLE I. - CHARACTERISTICS OF THE OSE INSTRUMENT

Sensors	Two Lockheed Intermediate Sun Sensors
Sun Sensor Intrinsic Noise	Typically 0.08 arc sec RMS
Angular Range	+/- 2° (+/- 3°) ¹
Angular Sensitivity	0.23 arc sec (corresponding to the least significant bit (LSB) in data digitization) for the high-sensitivity sensor
OSE Equivalent Electronics Noise	0.17 arc sec RMS (0.75 OF LSB)
Frequency Cutoff	11 Hz with a nominal 12 DB/Octave rolloff
Data Sampling Rate (Each of Four Data Channels)	58 Hz
Data Storage	Data multiplexed and recorded on a Lockheed Model 4200B tape recorder
Duration of Operation	Three hours maximum (Limited by tape recorder capacity)
Power Supply	Gates X-cells in a hermetically sealed container

¹ One sensor's field of view (that of Sensor 2) was electronically expanded to +/- 3°, with reduced angular sensitivity (0.39 arc sec) to assure that some observations would be acquired, even under worst-case misalignment to the Orbiter.

SPACEFLIGHT PAYLOAD DESIGN

FLIGHT EXPERIENCE G - 408

William W. Durgin¹, Fred J. Looft¹Albert Sacco, Jr.¹, Robert Thompson¹, Anthony G. Dixon¹Dino Roberti², Robert Labonte³, and Larry Moschini³**ABSTRACT**

Worcester Polytechnic Institute's first payload of spaceflight experiments flew aboard Columbia, STS-40, during June of 1991 and culminated eight years of work by students and faculty. The Get Away Special (GAS) payload was installed on the GAS bridge assembly at the aft end of the cargo bay behind the Spacelab Life Sciences (SLS-1) laboratory. The experiments were turned on by astronaut signal after reaching orbit and then functioned for 72 hours. Environmental and experimental measurements were recorded on three cassette tapes which, together with zeolite crystals grown on orbit, formed the basis of subsequent analyses.

The experiments were developed over a number of years by undergraduate students meeting their project requirements for graduation. The experiments included zeolite crystal growth, fluid behavior, and microgravity acceleration measurement in addition to environmental data acquisition. Preparation also included structural design, thermal design, payload integration, and experiment control.

All of the experiments functioned on orbit and the payload system performed within design estimates.

¹Worcester Polytechnic Institute, Worcester, MA

²Raytheon Company, Portsmouth, RI

³MITRE Corporation, Bedford, MA

INTRODUCTION

The small self-contained payloads of the National Aeronautics and Space Administration (NASA) - known best as the "Get-Away-Special" (GAS) program - have provided unparalleled opportunities for educational institutions to participate in our nation's space program [1]. The GAS program has also proven to be an excellent mechanism for engineering colleges and private corporations to join together in programs oriented toward the development of space flight hardware [2], thus furthering institutional and industrial relationships [3]. A companion program known as the Advanced Space Design Program, sponsored jointly by the University Space Research Association and NASA, provides opportunities for universities to focus on design issues associated with the exploration of space.

WPI undergraduates have been developing experiments for NASA's GAS program since 1982. Although these experiments were ready to fly in early 1985 [4], [5], the Challenger disaster delayed the flight of the experiments until the spring of 1991. Between 1982 and 1986, five experiments were selected, developed, and tested in sufficient detail to be flight ready. In addition to the flight experiments, there were a number of other support projects conducted by other project teams. These included the development of flight recorders for data collection, a structure for mounting the experiments internal to the GAS canister, and a technical communications project. The four payload experiments are briefly summarized below.

1) **Zeolite Crystal Growth Experiment:** This experiment [6], illustrated in Figure 1, was designed to determine if a low acceleration environment would promote the growth of large zeolite crystals. The experiment required a small, heated reactor vessel with a precision temperature controller which was optimized to use minimum power.

2) **Fluid behavior experiment:** As shown in Figure 2, several methods for measuring the properties of a liquid in zero-G environment were evaluated. A thermodynamic technique was used by recording temperature and pressure in the interior of the modules when a volume change was induced by the stepper motors. Two systems were studied, one using a wetting liquid (Freon on aluminum) and the second using a non wetting liquid (ethylene glycol and water on teflon). Valve motors on each of the modules were opened and closed to study fluid migration. Also, the experiment included the design of an ultrasonic, fluid film thickness measuring instrument accurate to 0.01 mm, and a micro-processor controller was used to sequence the different measurement schemes and to record the data [8].

3) **Microgravity Accelerometer:** This experiment is shown in Figure 3. The accelerometer system detected and recorded low level (10-6G) accelerations along three axes.

4) **Environmental Data Acquisition System:** A completely automated data acquisition system was developed to monitor the canister environment. The parameters measured were interior sound pressure level, triaxial high level accelerations, barometric pressure, temperatures, and battery voltages.

FLIGHT PREPARATION AND RECOVERY

Subsequent to development of flight hardware for individual experiments, a process of payload integration was begun which included flight readiness reviews. Inasmuch as the student project teams developed the experiments individually with only moderate knowledge of other experiments or structural constraints, the integration process quickly identified areas of concern. These included ruggedization, integration of individual experiments into the structure, and development of final check-out procedures. These items were addressed and the payload held in storage until the STS-40 flight opportunity became available.

Flight preparation included a number of rehearsals at WPI where ground procedures were developed and needed tools and supplies identified.

The G-408 payload was shipped to the Kennedy Space Center in December 1990 and the launch preparation team completed their check-out and loading of G-408 during a three day period from February 19 - 22, 1991. Three other GAS payloads, in addition to G-408, were processed through the GAS facility during this period. Although the facilities were excellent and the NASA personnel were very helpful, it is clear that a well prepared and rehearsed checkout procedure is essential. Additionally, several practical tips were developed that can be applied to the design and construction of any GAS payload to promote an efficient and successful payload check-out.

Experiment Access/Removal: Installation of all experiment mounting hardware should be convenient. Blind fasteners that are hidden by another experiment, lead to difficulties during preparation.

Maintenance/Servicing Design Allowance: Experiments should have a mounting assembly that enables an extended, self-supported positioned relative to the main support structure. For example in G-408, the servicing of the Fluid Behavior experiment could have been greatly simplified if the twin cylinder assemblies were mounted on a horizontal sliding mechanism to facilitate the filling with their respective fluids.

Assembly Orientation and Identification: Ample use of guide pins and orientation markers facilitates re-assembly. Cable connectors should be clearly marked with its mate identified. Experiments should be identified in bold markings and service points such as fill ports, test points, etc. should be clearly marked.

Fastening Hardware Selection and Fastening Design: The variety of fastening hardware should be minimized. Tiny hardware should be avoided in favor of more "human-scale" hardware. For those areas of an experiment that are frequently disassembled, the fastening design should be rugged. For example, tapped aluminum holes would not be adequate for these areas.

Protective Packaging of Experiments: Dropped tools or parts as well as spilled liquids can damage experiments because of a lack of shielding. Experiments should be adequately protected from such accidents.

Built-in Test Capability: Capability to evaluate readiness of the payload needs to be provided. For G-408, all experiments were controlled through the Environmental Data Acquisition System (EDAS) for system checking. If one experiment did not function properly, it had to be determined if the experiment, EDAS, the program, or a combination of all three were at fault. Furthermore, the EDAS had to be disassembled and its circuit boards pulled to install a test IC in place of the actual flight IC for each experiment. The control circuits for each experiment should be designed with built-in test capability. A simple fail-safe switch-over to the flight configuration should be provided, preferably from the exterior of the experimental package.

The basic components of a built-in test system for a GAS experimental package would include:

- a) Exterior panel of on/off switches to simulate the shuttle control functions for each experiment which connects to payload harness.
- b) The BIT circuitry and programming necessary within each experiment to run the test sequence.
- c) Output device to process and transfer experimental functions/response to a PC or other monitoring device.

Additionally, independent indicators for each experiment should be provided as the confirmation check that a function has occurred. On G-408, the click of an engaging relay or the whine of a turning motor was relied upon. However, the GAS Processing Facility is usually a very noisy area and these types of checks cannot be relied upon. An LED display or other such indicating devices could be built for each experiment and plugged into a built-in test tap for each experiment's circuitry.

TYPICAL RESULTS

The GAS relay for this experiment was activated at 00/10:47 MET. The times indicated on Figures 4-6 are relative to that MET. The total run time for the experiment was approximately 72 hours and acceleration data were continuously collected during that time.

Figure 4 shows a two hour record beginning at 04:00 and illustrates two basic types, A and B, of acceleration environment present during the experiment operation.

Figure 5 shows a 12 minute segment illustrating Type A data. Pairs of acceleration pulses occur approximately every two minutes and have magnitudes of 0.5 to 0.7 milli-g's. For the entire 72 hours, this type of record is present unless more substantial activity is present as represented by sequence B. This 12 minute sequence is shown in Figure 6 and includes magnitudes of the order of 2 to 3 milli-g's occurring at intervals of 10.1 seconds.

The Type A sequences resulted from an electromechanical relay used to control the oven heating system for the zeolite crystal growth experiment. The period was approximately 2.0 minutes early in the experiments and became 1.9 minutes near the end of the experiment because the payload temperature was lower resulting in faster heat loss from the oven. Similarly, the duty cycle increased from 17 to 18 seconds over the course of the experiment because lower battery voltage necessitated greater time for the heater to supply the required heat.

The Type B sequences resulted from relays in a power conservation system. Whenever precision temperature and pressure readings were required from the fluid behavior system, the analog circuits would be energized and then de-energized at approximately 10 second intervals.

Between these types of events, accelerations of the order of 100 to 200 micro-g's are found. Thus, the self-induced acceleration of the experiment package greatly exceeded the Orbiter accelerations whenever electromechanical devices were in operation.

The fluid behavior experiment was, similarly, technologically successful and at least partially successful scientifically. The non-wetting module functioned perfectly. This portion contained an ethylene glycol solution in two teflon lined cylindrical containers connected by a ball valve. Initially, the containers were filled 60 percent and 40 percent respectively. The volume of one chamber could be varied, ΔV , using a piston-cylinder assembly which caused a measurable pressure rise as shown in Figure 7. The height of the rise was a measure of the liquid volume in the chamber. Periodically, the valve was opened allowing fluid to migrate between the containers. The height of the pressure rise was a good indication of the liquid volume. The spacecraft accelerations caused the fluid migration between the chambers. The total volume transferred was not large, approximately 10 percent but was certainly measurable. Figure 8 shows the variation of $\Delta V/V$ throughout the period of experiment operation.

The second module contained Freon 11 and aluminum container walls and was, therefore, a wetting system. It was supposed to function as did the non-wetting system except that the fluid transfer would be affected by capillary action. In addition, this

system contained an ultrasonic sensing system to monitor the amount of freon in the storage container. When the experiment was retrieved, the storage container still contained the beginning amount of Freon and the variable volume chamber contained none. It appears that there was a leak from one of the chambers at some time during or after the mission.

The zeolite crystal growth experiment functioned as designed and did produce crystals of zeolite A, as expected. The autoclave temperature rose to 98°C and was held steady for 72 hours (Figure 9). Upon return to earth the autoclave was inspected for leaks, and none were noticed. The aluminum end-cap on one of the chambers was squashed and/or deformed, in both chambers. This behavior may have been caused by freezing of the solution later in the flight.

The zeolite A reaction mixture was prepared by mixing 3.8 ml of silica slurry with triethanolamine (TEA) and 5 ml of sodium aluminate solution. The reaction mixture was maintained at approximately 71°F during a 110-day launch delay after mixing, which resulted in the undesirable aging of the mixed gel solution. A parallel experiment was conducted at WPI, using the same raw materials in an identical autoclave to that of the microgravity experiment, and aged for the same period of time. A third experiment used the same solutions, but the reaction mixture was heated to 96°C in a Teflon reactor, with no aging.

Scanning electron microscopy (Jeol JSM-840 SEM) was used to determine the crystal shape, size and morphology of the products and impurity phases. X-ray powder diffraction (Cu K α radiation, Nicolet 12/V Polycrystalline Diffraction System equipped with Digital Microvax) was used to determine the degree of crystallinity of the samples. Particle size analysis of the products was performed using an Electrozone Celloscope Model 80XY. Powder samples for the size distribution measurements were suspended in deionized water and vibrated in an ultrasonic bath for a few minutes for adequate dispersion. Measurements were made in a 1 wt. % NaCl solution used as an electrolyte. Infra-red transmittance spectra of samples were recorded using Perkin-Elmer 683 Spectrometer.

Analysis of the crystals grown in microgravity showed zeolite A crystals with considerable twinning, and a very small amount of an impurity phase, polycrystalline hydroxysodalite. Some single, well developed zeolite A cubes were also found. The average size of the crystals was about 33 μm . Similar results were obtained from previous terrestrial experiments, and from the control experiment on earth using aged solutions.

The reaction mixtures that were crystallized on earth with no aging, on the other hand, showed a majority of single, well developed zeolite A cubes, occasional twinning of zeolite A crystals, and an almost imperceptible level of hydroxysodalite. The average crystal size was about 50 μm . This is the usual result

of crystallization from this reaction composition and processing conditions.

The results described were expected, and are attributed to the long delay between mixing and launch, which resulted in an aged mixed gel solution. To grow larger, more perfect zeolite crystals, it is important to suppress nucleation as much as possible, so that the smaller number of crystals nucleated can grow larger when suspended in solution in the microgravity environment. Aging of the mixed gel solution compromises this process, producing poorly formed crystals, even in the presence of TEA. It therefore seems likely that the aging process which occurred prior to launch led to the crystal growth results obtained. Thus, the microgravity environment probably played little or no role in this experiment.

All in all, the experiment may be considered a technological success, but was inconclusive scientifically. It was not possible to determine what effect microgravity might have on zeolite crystal growth from these results due to the prolonged delay after mixing.

CLOSURE

The individual experiment and control modules were all tested according to the suggested acceleration spectrum [1]. These tests were adequate inasmuch as no mechanical failures occurred. The on-orbit temperature of the payload generally decreased throughout the period of operation. Because the payload was activated relatively early in the flight, the temperatures were always above 7°C, while data were recorded. There was, however, some evidence from the Zeolite experiment that lower temperatures were encountered. The experiment package was powered by Gates J and X cells in a sealed and vented battery compartment. Nominally twice the needed power was provided to accommodate storage and loss of efficiency at low temperatures. As it turned out, the temperatures were higher than expected but the storage was much longer than expected with a net result of achievement of the predicted run-time.

REFERENCES

- [1] Get Away Special (GAS), Small Self-Contained Payloads-Experimenter Handbook. NASA Goddard Space Flight Center, Special Payloads Division, 1986.
- [2] F.J. Looft, R.C. Labonte, and F.C. Lutz, "The NASA Space Shuttle: A Vehicle for Science and Engineering Education," IEEE Front. Educ. Conf. Worcester, MA, 1983.
- [3] F.J. Looft, R.C. Labonte, and F.C. Lutz, "The Space Shuttle - A Vehicle for University-Industry Educational Interaction," IEEE Trans. Educ., pp. 100-104, 1986.
- [4] W.W. Durgin and F.C. Lutz, "Designing for Space - Undergraduate Project Education," 38th Congress of the International Astronautical Federation, IAF-87-522, Brighton, 1987.
- [5] F.J. Looft, R.C. Labonte, and W.W. Durgin, "The Evolution of the WPI Advanced Space Design Program - A Evolving Program of Technical and Social Analyses Using the NASA Space Shuttle for Engineering Education," IEEE Trans. Educ., pp. 20-26, 1991.
- [6] A. Sacco, Jr., "The NASA GAS Program: A Stepping Stone to Education," IEEE Trans. Educ., pp. 27-30, 1991.
- [7] W.W. Durgin and J.W. Matthews, "Fluid Behavior in Microgravity," GAS User's Conf., GSFC, Oct. 1985.
- [8] D. Roberti, "An Investigation Using Ultrasonic Techniques to Determine the Parameter of Voids," Master's Thesis, Worcester Polytechnic Ins., 1987.

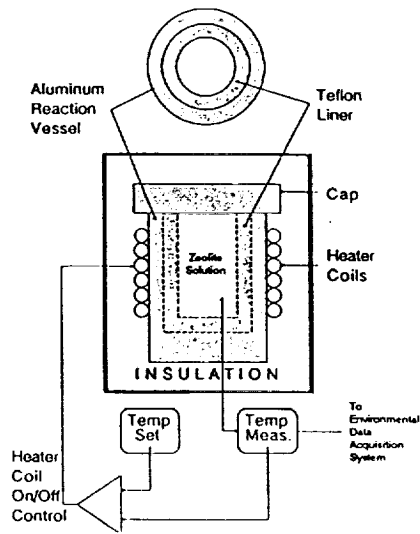


Figure 1 Zeolite Autoclave

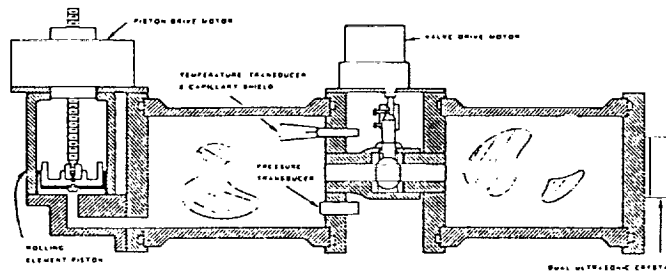


Figure 2 Fluid Behavior Module

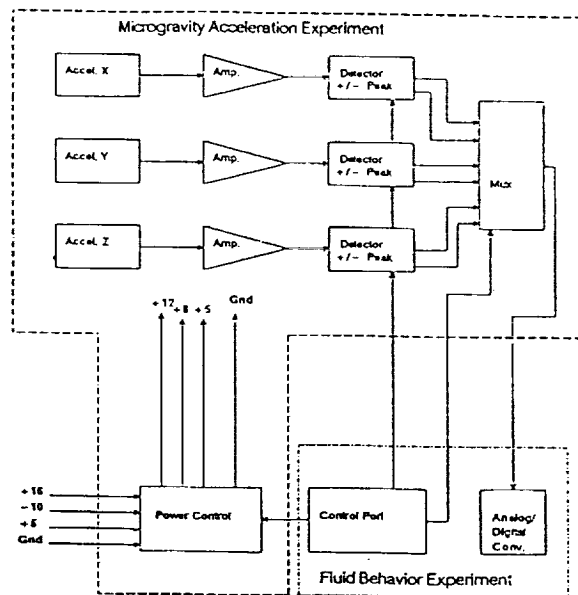


Figure 3 Accelerometer System

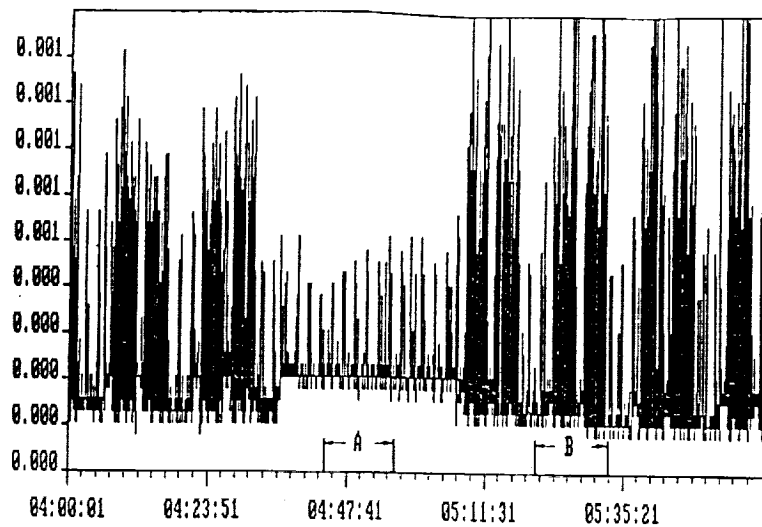


Figure 4 Two Hour Acceleration (g's) Record

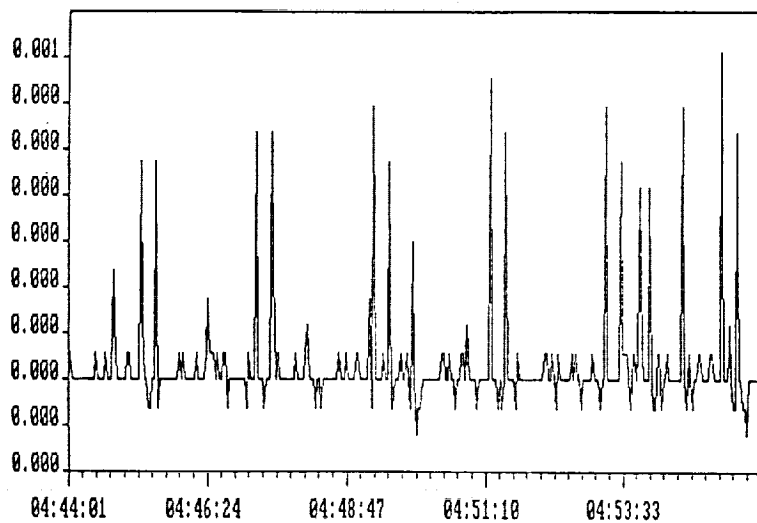


Figure 5 Type A Events

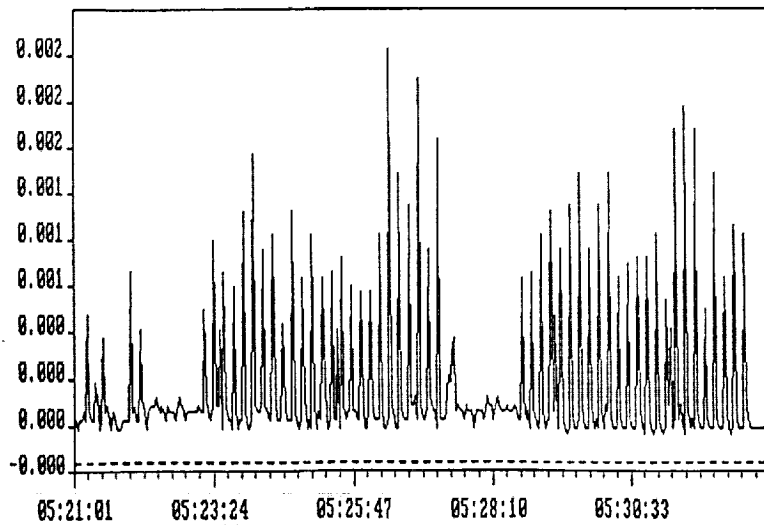


Figure 6 Type B Events

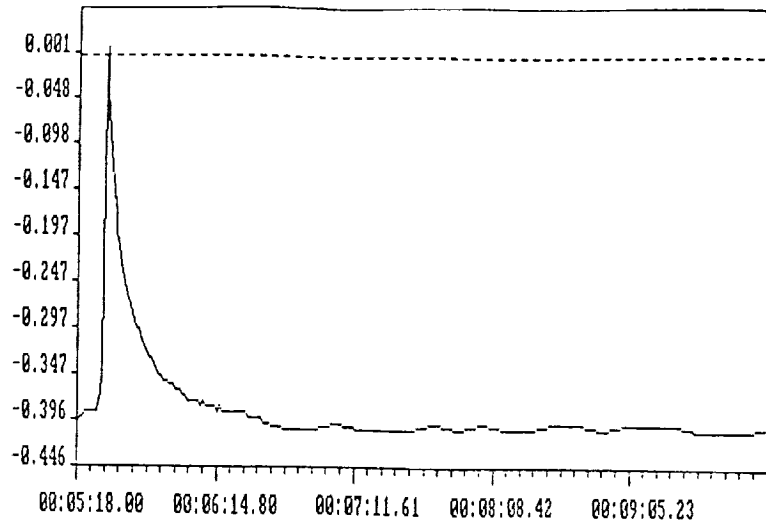


Figure 7 Pressure (psi) Curve

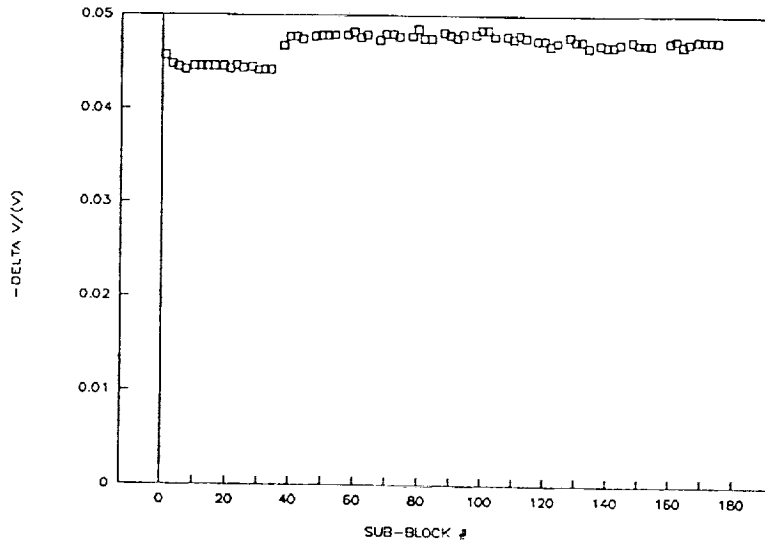


Figure 8 $\Delta V/V$ Record

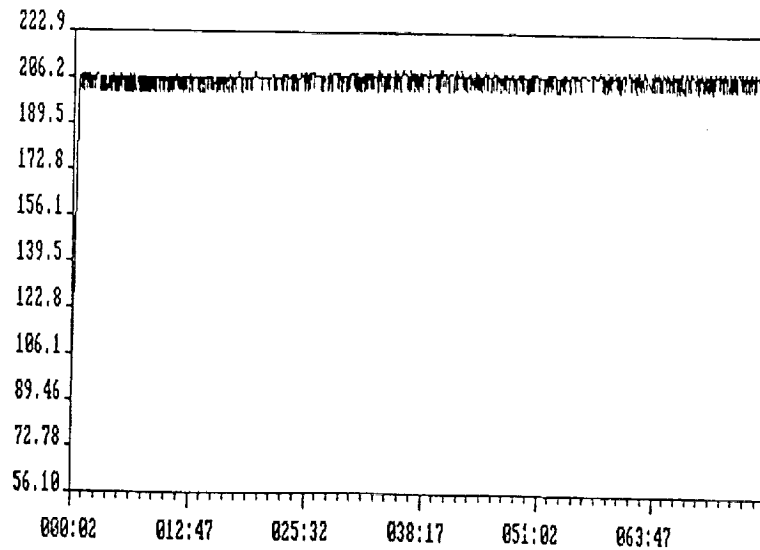
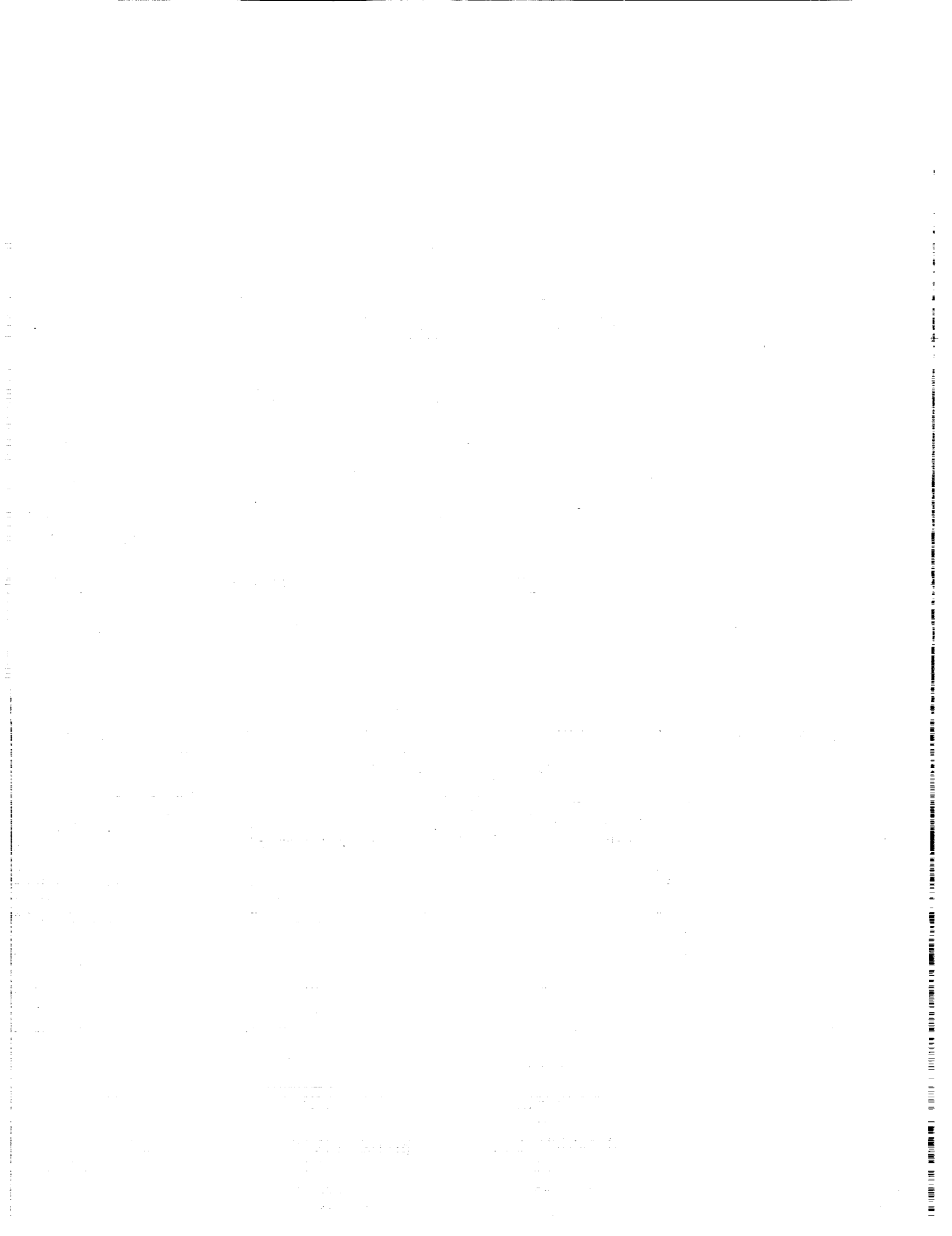


Figure 9 Autoclave Temperature (°F)



**POST FLIGHT OPERATION OF A HIGH PEAK POWER
NEODYMIUM YAG LASER ABOARD THE G-449 PAYLOAD
FLOWN ON SPACE SHUTTLE COLUMBIA MISSION 61-C**

M. C. Muckerheide
Payload Manager G-449 and Director of Laser Laboratory
St. Mary's Hospital of Milwaukee
Milwaukee, Wisconsin

ABSTRACT

The Nd Yag laser flown on board the G-449 payload completed its postflight testing successfully.

There was no indication that the laser had undergone any electronic or optical component failure. A postflight video was taken immediately following the return of the payload to the laboratory.

Early anticipation of vibration and temperature changes contributed to the successful operation of the laser.

Photographic material resulting from post flight videotape will be presented in the paper.

NASA safety reviews and recommendations supplied the insights which helped contribute to the successful operation of the Nd Yag laser. The safety review data is part of the technical presentation of this paper and gives some insight into why the system survived the severe environment of temperature and vibration during the flight of Space Shuttle 61-C.

INTRODUCTION

Following the flight of Space Shuttle Columbia on Mission 61-C between January 12, 1986 and January 18, 1986, Get Away Special (GAS) payload G-449 was returned to the Laser Laboratory. The payload was removed from the NASA shipping canister and the payload meticulously disassembled.

POST FLIGHT TEST FIRING

The large compartment cover which housed the laser was made of stainless steel. The compartment cover Figure 1 was removed and the laser which was part of the experiment package (Figure 2) was fired from its on-board power packet which consisted of two Eveready metal jacketed alkaline 6-volt batteries #520 wired in series.



FIGURE 1 - LASER COMPARTMENT COVER (ARROW)

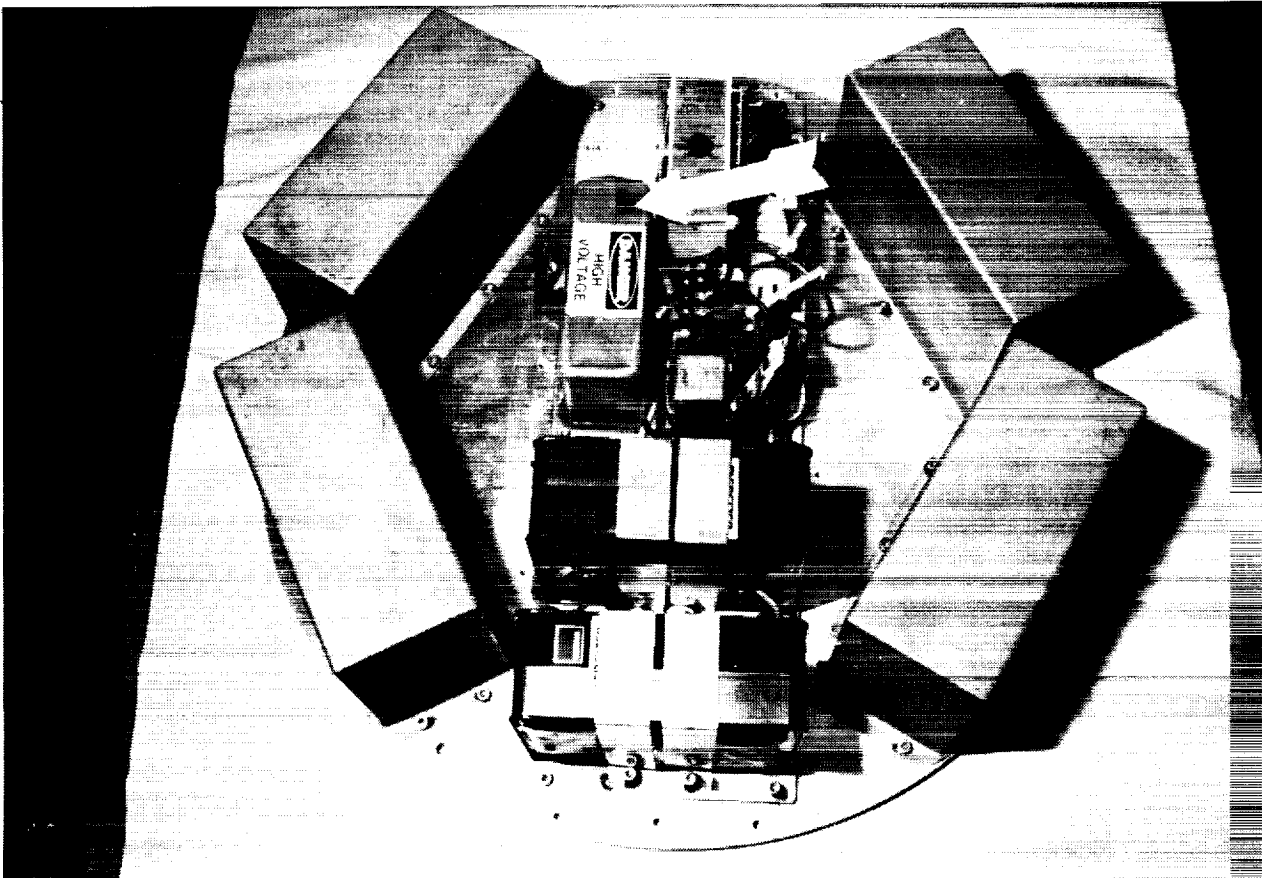


FIGURE 2 - Nd YAG LASER (ARROW)

The timer which operated the laser in space was disengaged for the post-flight test and the firing operation was initiated by manually closing the firing circuit.

The deposition of the laser energy upon a target of photographic paper demonstrated the vaporization of the exposed emulsion.

The exposed photographic paper target confirmed excellent beam characteristics as regards beam structure. The test was done upon the exposed photographic paper without using focusing optics. The three initial target tests are shown in Figure 3.

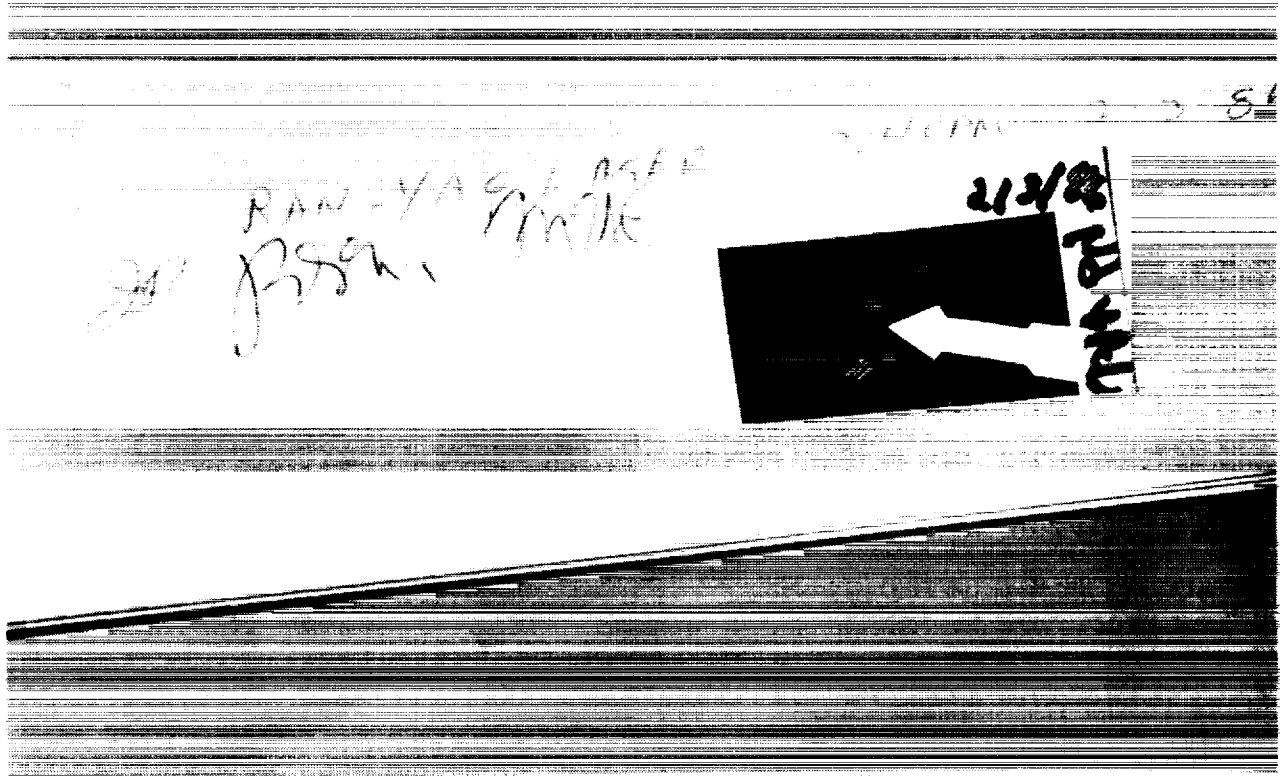


FIGURE 3 - THREE TARGET TESTS (ARROW)

Although further additional tests for diagnostics were performed, the visible ablation of the exposed photographic emulsion confirmed the lasers operational status immediately following the removal of the cover from the laser portion of the module.

VIDEO RECORD

Videotaping of the post-flight test supplied us with excellent demonstrable action pictures. Along with the videotaping, synchronized photos for the event supplied the permanently recorded proof of operation.

NASA SAFETY PACKAGE

During the Preparation of the NASA GAS safety package, evaluation of the various parameters related to the laser experiment came under scrutiny. The Laser/Optical Device Use Request/Authorization was the laser document used as part of the safety package. Attention was directed to the hazards of the laser both optically and electrically. It was decided to confine the entire laser experiment to an enclosed compartment.

The telecons with NASA provided the parameters to ensure safe flight operation of the laser.

SURVIVABILITY

Early on, the harsh environment of space drew attention to finding a laser system which had been earth proven as regards to temperature, shock, and vibration parameters. While the search focused upon operational survival, there was also a need for miniaturization. The search ended when the Laser Photonics' Yag laser was found to be available for the experiment.

Laser Module, Laser Transmitter Design, fixed mirror mounting, pump cavity, and laser transmitter/interface is data supplied by Laser Photonics and is published by their permission. The sections attest to reasons for the survivability of the MYL-100 Neodymium Yag Q-switch laser.

LASER MODULE

The laser module consists of an integrally mounted pump chamber, laser resonator, and beam expanding/collimating telescope. The single mechanical structure provides integrity and stability for the critical optical elements.

The laser resonator used on Laser Photonics' MYL-100 system is a ruggedized design developed specifically for systems encountering adverse environments of temperature, shock and vibration. The design employs the state-of-the-art in laser technology in the design of the alignment insensitive folded resonator, the high efficiency pump enclosure, and the miniature integral structure. This design concept has evolved over years of development of rugged military laser products and has proven itself in many fielded systems.

Extensive environmental and military qualification test programs have demonstrated the reliability of the laser resonator design. An extensive effort has been applied to miniaturizing the laser resonator while preserving these proven qualities.

In addition to the outstanding qualities of performance, the miniature laser resonator is designed for produceability and consistent performance.

The following data from Laser Photonics addresses laser transmitter design, fixed mirror mounting, pump cavity and laser transmitter/system interface data.

LASER TRANSMITTER DESIGN

The laser resonator design employed in the MYL-100 Laser is a version of Laser Photonics' high reliability, compact, folded resonator design. The optical resonator consists of two end mirrors (both located on the same optical substrate), the laser rod, folding corner prism, alignment wedges, polarizer, expansion/compensation lens, Q-switch, and phase retardation plate. Optical energy from the laser rod circulates between the two end mirrors with the output portion being transmitted through the partially reflecting mirror. The corner prism has the unique property of folding the optical path 180 degrees without deviation regardless of the orientation of the prism. Thus, minute movements of the corner prism will not result in misalignment of the optical resonator. The inherent stability of the corner prism folded resonator is the primary factor in the reliability and alignment stability of the Laser Photonics' design. Alignment is achieved with weak prisms (Risley prisms) located within the resonator. The prisms are rotated to the optimum position and locked into place. The beam then passes through a multilayer dielectric polarizer. The next element is the intracavity expansion/compensation lens. The lens both expands the beam on the Q-switch and adds the proper optical power to the resonator to maximize the mode volume in the laser rod. A passive dye Q-switch is the next optical component. The final element is a quarter wave retardation phase plate. The phase plate provides the proper phase shift in the beam polarization to inhibit lasing until the Q-switch is activated. The resonator elements function together to form the unique optical resonator for Laser Photonics' miniature Q-switched laser.

FIXED MIRROR MOUNTING

A fixed mirror mounting technique is employed in the folded resonator design to assure alignment stability over severe environments of temperature, shock and vibration. Laser Photonics' lasers are factory aligned modules which need no further adjustment when installed in the field. Alignment stability is assured by having both end mirrors deposited on the same glass substrate. Thus, if the mirror mount were to move slightly, both mirrors would move together in the same direction and would not become misaligned. The coatings are split to provide for the different requirements of output coupler and maximum reflector. Alignment of the resonator is achieved with a

pair of rotating prisms. The prisms each deviate the beam over a certain range. When working as a pair, these prisms can vary the amount and direction of beam deviation. Thus, the prisms can compensate for beam deviations caused by other optical elements within the resonator. Once positioned, the prisms are locked down and cannot become misaligned.

PUMP CAVITY

The pump cavity used in the laser resonator consists of a high efficiency close-coupled reflective design. The laser rod and flashlamp are linear cylinders placed near the focii of an elliptical cylinder reflective cavity. The light from the flashlamp is thus imaged onto the laser rod. The lamp is series triggered to eliminate arcing problems associated with parallel triggered systems.

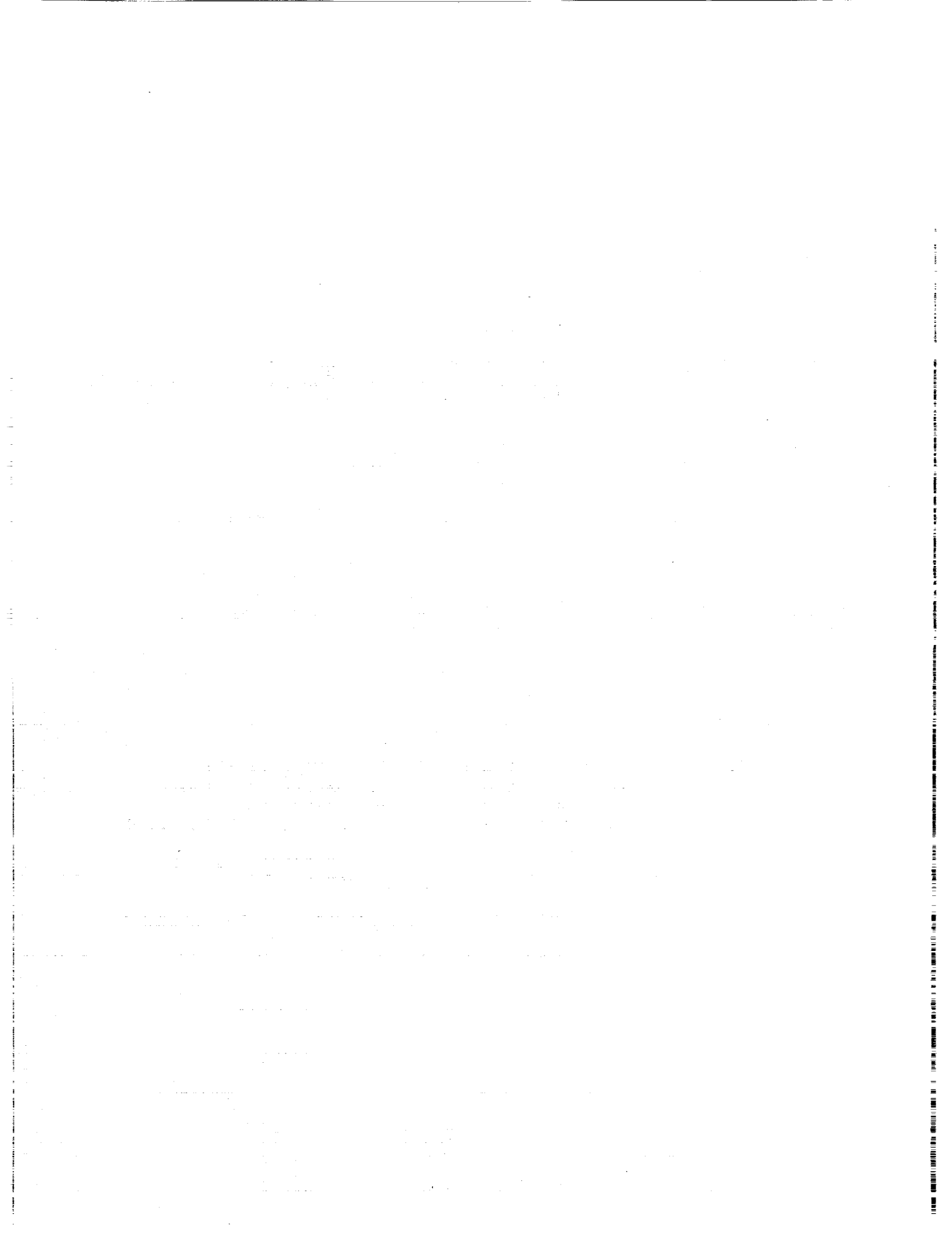
LASER TRANSMITTER/SYSTEM INTERFACE

The laser resonator is built in an optical bed case which is precisely machined. The dimensions of the case are approximately two inches (2") wide by one inch (1") high by four inches (4") long. High voltage feedthroughs are provided for all inter-connecting wiring. The output beam exits the housing through an anti-reflection coated window. Reference location holes can be machined into the outer housing for beam reference. Thus, laser modules are able to be made interchangeable without complete system realignment. Thus, the laser head is completely self-contained in a package which provides a great deal of flexibility in system design.

CONCLUSION

The successful post-flight operation of a High Peak Power Neodymium Yag laser which was flown in canister GAS-449 aboard Space Shuttle Columbia on Mission 61-C demonstrates the survivability of a high peak power laser in the harsh environment of space. The present design limit for the Shuttle is 11 G's in 3 axis simultaneously applied for worst case orientation. The outside temperature ranges are -160° C. to $+100^{\circ}$ C.

The author wishes to express his appreciation to Ms. Brenda Ballard Alfson, Technical Sales Engineer of Laser Photonics, and Laser Photonics, Inc. for supplying the technical background presented in this paper.



A DECADE OF DISCOVERY:**Experiments with the Get Away Special (GAS) Canister**

We say we live in a technical age; science is worshipped as a God - a new elemental force more powerful than Zeus, but with higher energy bills. Yet, in this new age most of the worshippers still standback, timid and afraid to approach the holy - of - holies. Sadly, one of these shy supplicants is one that could benefit the most - American Public Education. It seems ironic that the vast system of national education does not utilize one of the greatest means of expanding knowledge - the vast resources and opportunities provided by NASA in the field of space research - in particular, the relatively cheap access to extraterrestrial environment provided by the Shuttle Program. This is especially unfortunate considering the state of public education in this country; and public schools, even private ones, are in trouble are they not? Some are; some are not.

I have the privilege of teaching at Booker T. Washington's High School for Engineering Professions (HSEP) in Houston, Texas, a college preparatory school with an international reputation for educating students in mathematics and sciences. Due to the nature of the school and its location, the school and NASA have a long-standing relationship with many aerospace and educational projects. But, the school's decision to conduct student constructed and supervised microgravity experiments initiated a new level in hands-on experience. Though students with aptitudes in science at a school with its own planetarium, observatory, satellite station, wind tunnel, robotics lab, etc. are not unfamiliar with scientific experiments, the Shuttle experiments were "extraordinary". The contrast between classroom material and the experience of planning, participating in the construction and launch, and opening the canister in their own labs was incomparable. What the students gained from these experiences was one of the high points in public education and far more valuable than other educational programs of equal cost. Like HSEP's previously flown experiments, the experiments on STS-42 were contained in three layers of a GAS canister. The first layer housed the Heterogeneous Flow Experiment, to test the commercial application of space exploration; layer two housed an Artemia Salinas Growth Experiment, a test to determine the success and range of food production in microgravity for longer future missions; and layer three, reserved for the computer and monitoring equipment. What was learned from these experiments; and, more importantly, what impact they had on education on a broader scale is the subject of this paper.

LAYER ONE: The Heterogeneous Flow Experiment

The migration of an air bubble in a fluid environment (The Heterogeneous Flow Experiment) has long been a subject of expe-

rimentation; however, this phenomenon must be studied in zero gravity, that is, without the external influence of buoyancy. The findings of such experiments can be applied to the making of high technology glass, free from any imperfections; the advantages in the fields of cybernetics, high resolution optics, etc., can only be imagined. Such glass is impossible to make on earth because of air trapped in pockets in the molten glass. Theoretically, there are a number of ways in which these bubbles can be removed in a weightless environment; one of which is the application of a thermal gradient through a fluid.

A thermal gradient, is formed when the temperature of the fluid varies uniformly along its length. When an air bubble is introduced into a fluid environment containing a thermal gradient, it is acted upon by a force which moves it toward the warmer end of the fluid. This is a result of the variation in interfacial tension (surface tension at the interface between non-mixing fluids) at different temperatures. When there is a wide variation of interfacial tension, as in a thermal gradient fluids both inside the bubble (air) and around the bubble (water) are set in motion. This motion tends to carry the bubble in the direction of decreasing interfacial tension, the warmer end.

Because of a temperature gradient, the fluid on the right side of the bubble is hotter than that on the left, giving the fluid molecules on the heated right side a comparatively greater molecular motion. The rapid motion of the molecules causes inelastic collisions on the right side, forcing the bubble to move to the left. However, The fluid on the left, cooler side, is denser than the fluid on the right. As the bubble tries to move to the left, there is a tendency for the denser fluid to push back directing the bubble back to the less dense, right side, creating a counter force.

To further complicate the matter, a large bubble has a large surface area, thus increasing the number of molecular collisions and making kinetic energy the dominant force. Thus, a large bubble tends to move away from the heat source. A small bubble, however, receives less molecular hits and kinetic energy becomes a less significant force; the smaller bubble tends to move towards the heat source. The exact size needed to move one direction or another has been theorized, but there is some controversy as to the accuracy of the theories and other variables, bubble expansion, external fluid density, degree of temperature variations, etc.

Scientists have, in the past, theorized the movement of bubbles under the influence of thermal gradients. Through the years, a formula was formed through extensive experimentation. Derived from a combination of other formulas, the formula gives the migration velocity of a bubble. The formula consists of the product of two equations of velocity. The dimensionless velocity U and the natural scale velocity

V, where

$$U = 1/2 - 301/14400 N \quad (1)$$

ma

and

$$V = (T' \cdot l_0 \cdot l \cdot a) / n \quad (2)$$

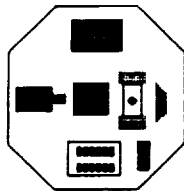
The notation in equation (2) is as follows: T' is the thermal gradient of the liquid far away from the bubble, o' is the rate of change of the interfacial tension with temperature, a is the bubble radius, and n is the absolute viscosity of the liquid. The term N is defined by

$$N = a / V$$

where N is the thermal diffusivity of the liquid.

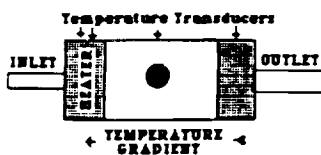
This theory was proposed and largely proven in laboratories on earth, but experimentation in weightlessness is sadly lacking. It was of considerable importance to test theories and gather empirical data in zero gravity where no other forces than the thermal gradient could affect results.

TRAY 1: HETEROGENEOUS FLOW EXPERIMENT



BATTERY (12V, 5AH)
8 MM CAMERA
HALF-SILVERED MIRROR
AIR/WATER CHAMBER

REFLECTOR LAMP
EXPERIMENT 1 CONTROLLER CARD
AIR/WATER PUMP



The Air/Water Chamber contains triple distilled water. The ends are made of aluminum. In flight, the computer injects measured amounts of air into the chamber. These air bubbles should be different sizes.

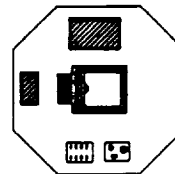
The inlet end contains a heater. Its temperature is monitored by a temperature/transducer located at the inlet end. The computer then controls the temperature gradient. Three other temperatures are recorded to allow for temperature gradient calculations.

Research indicates that the direction and speed of the bubble movement should depend on both bubble size and temperature gradient. These effects are "masked" by gravity. In microgravity, these effects will be able to be studied.



The motion of the bubble will be photographed by the 8 mm camera in a single frame mode. The half-silvered mirror will allow photographs of both experiments. The computer will energize the proper lamp to photograph the correct experiment.

TRAY 2: ARTEMIA GROWTH EXPERIMENT



BATTERY (12V, 5AH)
EXPERIMENT 2 CONTROLLER CARD
BATTERY (12V, 2.5AH)
TEMPERATURE TRANSDUCER CARD
ARTEMIA GROWTH CHAMBER & LINEAR ACTUATOR



The Artemia (Brine Shrimp) Experiment will attempt to hatch and grow brine shrimp in microgravity. The chamber contains distilled water and air.



The linear actuator will inject the eggs, salt, food and lime-released oxygen tablets in the beginning of the flight.



The eggs will hatch in 24 to 48 hours. Adequate food and oxygen will hopefully keep the shrimp alive for the flight and return.



The shrimp's hatching and growth will be recorded by the camera in tray 1 through the half-silvered mirror.

EXPERIMENTAL PROCEDURES

The Heterogeneous Flow Experiment, housed in tray one of the G.A.S. cannister, contained the following equipment: the air/water chamber filled with triple distilled water, a heater, a pump, a battery, an eight millimeter camera, a half-silvered mirror, a reflector lamp and an experiment controller card. Once orbit was achieved, the water was heated to 20°C. After the water reached the correct temperature, the computer turned on the pump which pushed an exact amount of air through the inlet. Immediately thereafter, the bubbles passed through a mesh grill and into the water chamber, a transparent cylinder with circular aluminum end blocks containing the inlet and outlet tubes. The inlet end block contained the heater and the outlet block contained a temperature transducer to remove heat. The displaced water was purged through the outlet. The water was again heated; this time to 40°C. Another set of bubbles were pushed into the water chamber. Finally, the water was heated to 60°C and the process was repeated.

The temperature in the chamber was monitored by the computer in four identical sets of EPROM's (Eraseable Read Only Memory Chips) for increased reliability. The computer also turned on the lamp and camera at five minute intervals to create a photographic record of the activity in the bubble chamber.

RESULTS

The results of this experiment were most interesting. As expected, free from the extraneous influence of gravity, the bubbles moved only along the axis of the thermal gradient, showing that this was the only force to be considered. As predicted, the bubbles entered the inlet (heated) end at the highest velocity, but the speed gradually decreased as the bubbles travelled through the cooler fluid. Gradually, some bubbles stopped in a "no man's land", the greatest fluid density at the cool end of the cylinder preventing them from actually reaching the outlet end. They remained there in an unquiet equilibrium. Some bubbles actually, after coming to a slow stop, slowly began reversing direction and moved back to the heat source. Since it was impossible to guarantee that all bubbles were of the same size, this behavior was expected.

CONCLUSIONS

This strongly indicates that theories predicting bubble movement in microgravity can be used to create optically perfect glass. It is also clear that more experimentation will be required before optically perfect glass can be manufactured in space with a high degree of reliability.

RECOMMENDATIONS

The action of the bubbles supported theoretical predictions, but some of the unanticipated behavior suggests further modification and refinement of basic theory. Interestingly enough, an observed phenomenon lent credence to a theory that a moving bubble in zero gravity is not round. Rather, it is bullet shaped with the point facing the direction of movement. Experimental data tended to support this belief. Though the experiment was largely successful, certain improvements and modifications should be considered for future experimentation.

1. More tests and refinements of macro photography, particularly when shooting through the varying viscosity/refraction index mediums, is in order.
2. Pictures should be taken more frequently than five minute intervals.
3. Experiments should be conducted with different chamber fluids.
4. In conjunction with increased photographic clarity and more frequent observations, further investigation of bubble shapes in zero gravity, particularly the bullet shape, should be conducted.

LAYER TWO: The Artemia Growth Experiment

One of the major obstacles facing further expansion in space is quite simply, food. The cost in weight and space of bulk, non-replenishable food effectively limits the length of manned space missions. This makes the space station and proposed lunar base painfully dependent on regular supply missions and interplanetary travel almost impossible. Growing food in space, however, may not be a simple proposition. Zero gravity can adversely affect, even destroy, organic systems; and an insufficient number of experiments concerning the germination and development of egg cells have been attempted in weightlessness. HSEP's experiment in tray number two was one of the experiments of this type.

EXPERIMENTAL PROCEDURES

The experiment tested the ability of Artemia Salina (brine shrimp) to hatch in zero gravity. Artemia Salina, a relative of the lobster, was picked for the experiment due to the hardy nature of the organism. It has the ability to survive in inordinately saline environments; the eggs may either hatch immediately after mating or lie dormant for extended periods. Dormant eggs develop hard, brown shells and can be dried and kept for years before being hatched in salt water. The eggs can survive temperature extremes from -190°C to $+150^{\circ}\text{C}$ and still hatch and grow normally. Not only could this organism

provide nourishment via the "plankton soup" survival diet, but also by providing a vital link in the food chain of a long-term habitation module. It would also strongly indicate that similar life forms (lobster, etc.) could be grown in micro-gravity.

The experiment contained several distinct components: a growth chamber, an actuator assembly, experiment controller and temperature transducer cards, two batteries and a silvered half mirror which allowed a camera in tray one to periodically take pictures of the activity in the growth chamber.

The 4" X 4" X 3" growth chamber was made of one fourth inch plexiglass and contained a salt water solution. The actuator assembly had an Airpax actuator and a modified syringe, which contained shrimp eggs and a food supply (rice hulls). The experiment was activated eight minutes into orbit: a heater was turned on that maintained the culture medium at a constant +23°C for the remainder of the shuttle flight. When the culture medium reached the prescribed temperature, the actuator injected eggs, food and time released oxygen tablets into the saline solution. The temperature in the growth chamber was recorded by the computer in four identical sets of EPROM's for increased reliability. The eggs hatched in twenty-four to forty-eight hours and the food and oxygen tablets provided a life-sustaining environment. The camera was used to monitor the injection of the eggs, their hatching and growth. (A light was turned on at appropriate times to allow for picture taking, with a picture taken every five minutes.) The pictures were used to compare artemia growth with a control experiment conducted simultaneously at B.T. Washington/HSEP laboratories.

RESULTS

After landing, the growth chamber solution was subjected to various examinations: a microscopic examination, comparison against the control, analysis of photographs and examination by electron microscope.

Initial microscopic examination was performed as soon as the growth chamber was delivered to Washington/HSEP laboratories. Pipettes of fluid were withdrawn from various locations in the growth chamber and examined under the microscope. In essence, a quadrant, random sampling method of counting, similar to wildlife surveys, was used. By counting the fragments of hatched shrimp and unhatched egg, while discounting food debris, it was ascertained the approximately 60 per cent of the shrimp eggs hatched. When comparing these results with the control experiment, which was terminated at the time the orbital experiment ceased, similar figures were recorded. Certain questions arose at this point; however, did an unexpected temperature rise in the growth solution kill the hatchlings? (An unanticipated, temporary temperature rise to 40°C occurred later in the mission.)

Did the long delay from the end of the experiment until the opening of the canister kill them from lack of food and oxygen; or were the shrimp, born and developed in zero gravity, literally torn apart by entry into Earth's gravitational field? Experiments are currently being designed at Washington's science labs to investigate these questions. At the time of this report, electron microscope photographs had not yet been completed by an outside laboratory, but are expected.

CONCLUSIONS

Though not all tests have been concluded, it is apparent that *Artemia Salinas* can be hatched in microgravity. This also strongly indicates that similar life forms: crustaceans, lobster, etc., could also be grown in space, thus providing a desirable food source for extended space missions. It also suggests further studies, particularly in the area of life forms born in weightlessness and their adaptability to gravitational fields.

RECOMMENDATIONS

1. A second actuator should be added to the growth chamber to inject a fixative solution at the termination of the experiment. This would preserve the organic samples in their original condition at the end of the experiment.
2. A heat sink should be added to tray one (Heterogeneous Flow Experiment) so the excess heat can be extracted from the canister interior. This was suggested because the temperature increase in the growth chamber appeared to result from heat generated in the tray one's bubble chamber. Though these two trays, were insulated from each other, there was evidence of a heat leak as tray two showed a steady 1°C/hour temperature rise correlating to the operation of the heater in tray one. At this point the cause of the heat leak can only be inferred, but thermal radiation through the mirror opening or conduction through the bolts holding the trays together are likely explanations. (See Figure 3.)
3. To prevent the liquid in the experiments from freezing in space, the canister was heavily insulated. It was speculated that, perhaps it was "too well" insulated trapping too much heat inside. Any reduction of insulation must be attempted only with considerable trial and error. Most likely, recommendation number two would be a more reasonable, cost-effective approach, with number three viewed as a last solution.
4. More experimentation and refinement of macro lense photography, is in order.

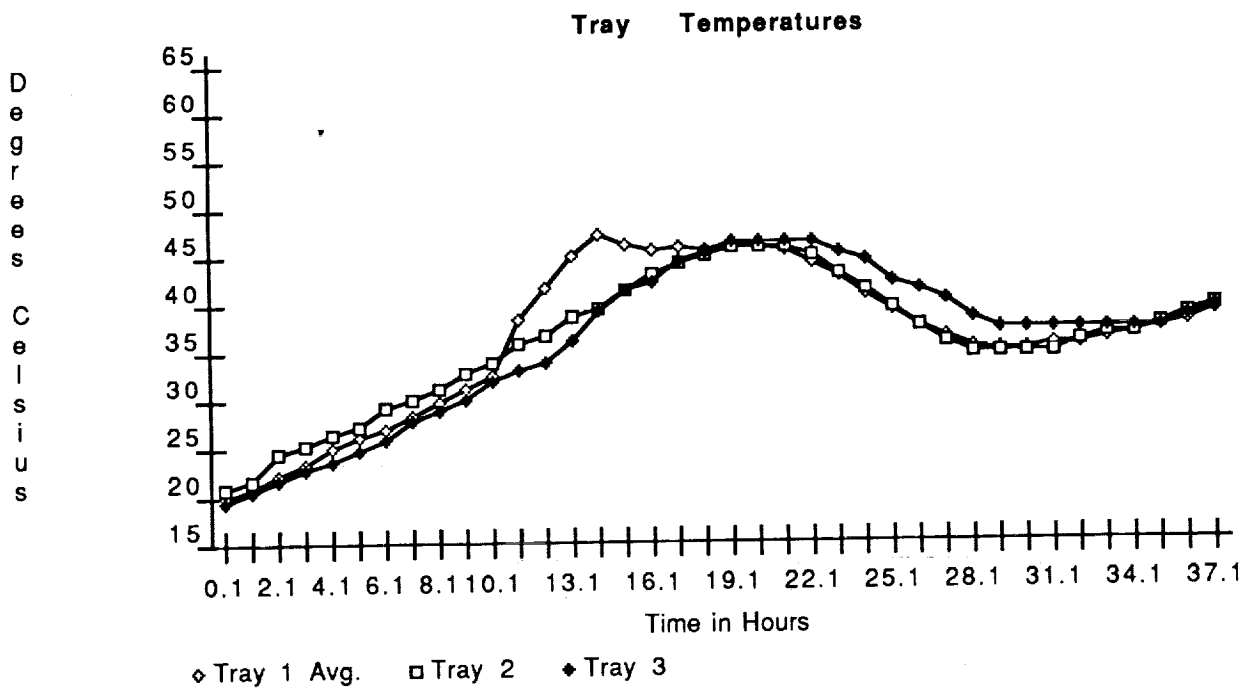


Figure 3.

These experiments, it must be admitted, are not the most important or complex ever to fly on a shuttle. To be candid, they are probably the least so. But, the main purpose of HSEP is education, and the success of the experiments can be determined by the impact on students. In this regard, the shuttle experiments were trend-setting. The actual scientific knowledge gained by the students was significant. These were not textbook experiments, not experiments suggested and set up by an instructor. Instead, these were experiments set up to serve a useful function, where real world value and potential were involved. Every student involved with the project, directly and indirectly, felt they had learned more about science and scientific method from this one project than they had in all of their traditional classes combined. They also learned how to plan larger projects. Not only were the students allowed to help plan the experiments but they also helped build the experimental hardware, plan the control experiment and plan and build the monitoring equipment. The project's student leaders and their helpers learned the importance and key steps of planning larger projects, the value of relegating duties and the significance of team effort. They also learned the value of research before, during and after the project - something very few high school students want to realize. They learned to write better technical reports, once they actually saw their value. Most importantly, as one of my students said, "There aren't really answers, just new questions."

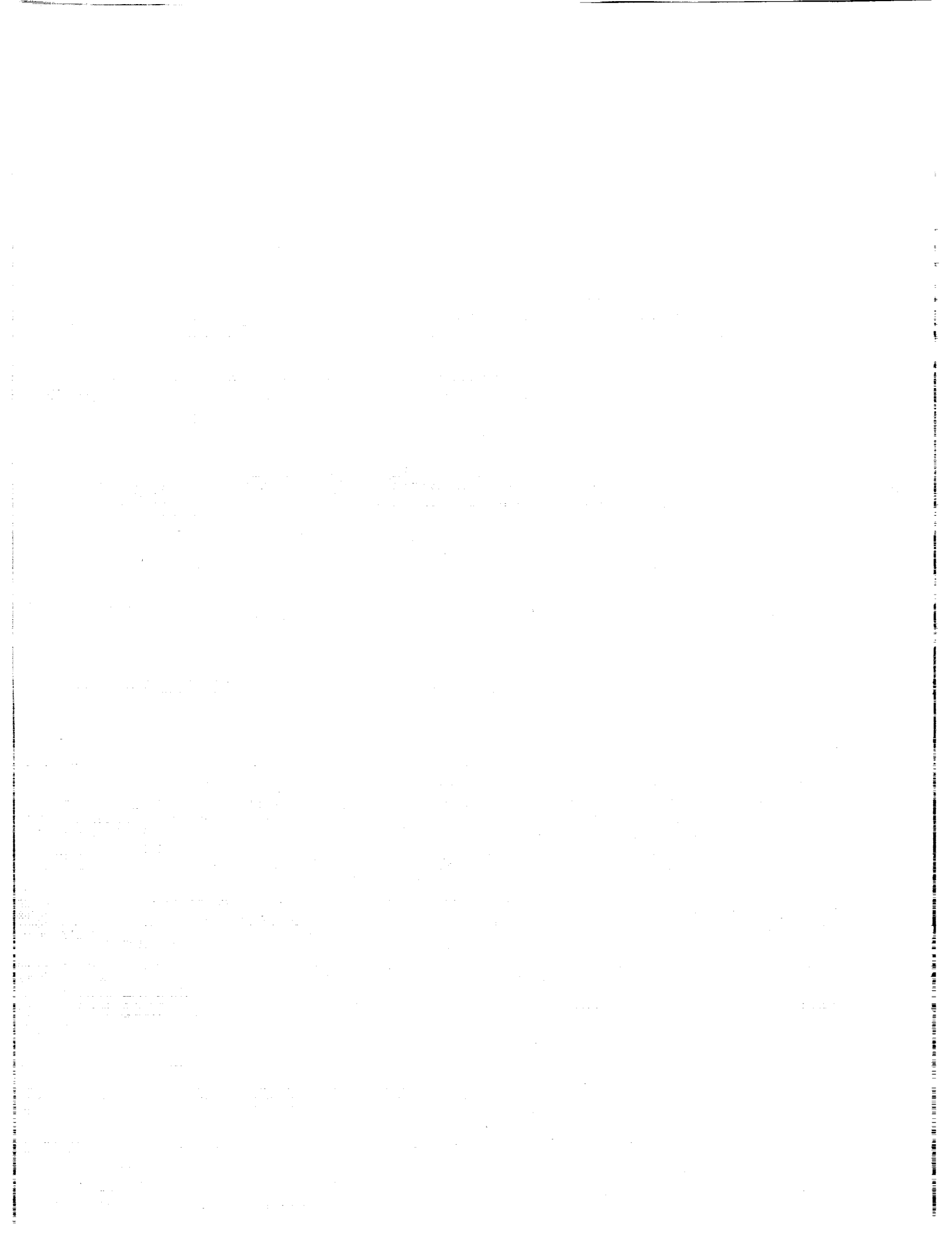
Though an increase of formal, quantitative knowledge is wonderful, the shuttle project served a more noble purpose and the

value of the shuttle experiments was the electrifying effect it had on the student body in general and their desire to learn.

Students need to feel success, to be praised for their accomplishments and to recognize value in their achievements, particular minority students, as most of ours are. The shuttle program gave our students a "shot" of self-esteem like no other educational program has. They felt good about themselves and more eager to attempt difficult and challenging tasks. They were also able to see the value of commitment to a long-term goal, and this has even carried over to classroom and textbook dedication. In fact, once they could see the material in their texts being put to practical application by other students, even the poorest student began working harder. Perhaps too, this attitude was partly the product of student realization that the administration and faculty had enough faith in them to provide this opportunity, even at the sacrifice of budgets in other areas. Pride in the school, which was never low, mushroomed. Even students in Washington's regular program who were not part of the engineering school went about the city proudly proclaiming "I go to Washington". We even saw an increase in foreign students entering our program.

Am I implying that the GAS canister experiments made an urban school a utopia? No. We had a good school before, but because faculty and students care about one another, incurring the expense of the shuttle flight and the cost of building the hardware was just another way of fulfilling our mission - education. And, the shuttle experiments were a good investment. For less than the cost of many programs of questionable worth, we gave our students something valuable for the rest of their lives. What did we get in return other than "a wonderful sense of fulfillment" and pats on the back? I can answer that in real, quantitative terms. If you would visit our school you would not see the scenes portrayed on television. Rather, you would see teachers and students smiling, telling jokes to one another, sharing a doughnut and treating each other with respect. You would see teachers giving their lunch times and sometimes Saturdays to help students, and students volunteering to come in early and stay until seven or eight o'clock to help the teachers. We have never had knives, guns or drugs in HSEP. In fact, a student has never even been sent to visit a principal in over two years. Most of our students come back one, two, ten years later to tell of their success in college and industry - and to thank us for helping them. Are some public schools bad? Yes. Are they all? No. Our teachers and students have found ways to commit their efforts to each other and create genuine learning experiences. The shuttle experiments were just some of the best.

Robert Brienzo



**IlaO ULTRAVIOLET AND NUCLEAR EMULSION FILMS RESPONSES TO ORBITAL FLIGHTS
ON STS-3, STS-7, STS-8, AND STS-40.**

E.C. Hammond, Jr., K.A. Peters, S.M. Blake, Y. Bailey, D. Johnson, S. Robancho, A. Stober
Morgan State University, Baltimore, Maryland

ABSTRACT

Two types of film were flown on STS-40 space shuttle mission in June 1991. The IlaO special purpose ultraviolet film showed continued desensitization because of various thermal and cosmic ray interactions. The films were exposed to the space orbital environment for 9 days. There were several built in launch pad delays of the shuttle mission. However, there was adequate monitoring of the temperature variations on board the shuttle that allowed for adequate knowledge of the thermal film history. This IlaO film was flown on the ASTRO I mission and is currently slated for use with the ASTRO II mission. A 50 micron thick Illford Nuclear emulsion film was also placed on a 175 micron polyester base. The exposure to space produced several cosmic ray interactions that were analyzed and measured using Digital Image Processing techniques. This same nuclear emulsion film was flown on STS-8 and produced a similar number of cosmic ray and thermal interactions. From previous experimentation of film using various laboratory electromagnetic radiation sources (e.g., alpha, beta, and neutron particles), we have been able to infer the possible orbital interactions of both IlaO and nuclear emulsion films. The characteristic responses of IlaO on STS-40 compared favorably to the results obtained from previous STS-7 and STS-8 gas can experiments. The results indicate sufficient evidence correlating increased density on the film with possible cosmic ray, thermal and shuttle out gassing interactions.

PRECEDING PAGE BLANK NOT FILMED

INTRODUCTION

Since the first major use in 1974, scientists have used over 400 rolls of photographic film in space to obtain sensitometric data. The present research team prepared 3 canisters of IlaO film along with packets of color film from the National Geographic Society, which were then placed on the Space Shuttle #3 (STS-3). The ultimate goal was to obtain accurate data concerning the background fogging effects of IlaO film as it relates to total environmental factors. This included an examination ground based packaging and loading of the film from Goddard Space Flight Center to Kennedy. In addition, the following interactions with film were examined: 1) effects of solar wind; 2) effects of humidity; 3) cosmic ray interactions; 4) Van Allen Belt radiation exposure; 5) thermal effects; 6) the effects of reentry and off-loading of film during take-off; and, 7) an examination of orbital flight of film for 8 days, 3 hours, and 15 minutes. The objective of this experiment was to examine the total densitometric changes caused by all of the above factors.

Methods

The Laboratory of Solar Physics and Astronomy, at Goddard Space Flight Center, has used large quantities of IlaO film in rockets and space shuttle flights. During the Ultra Violet Image Telescopic Experiment, the UIT launched a payload which used 70mm IlaO film. This was a requirement for the laboratory to quantitatively determine the aging effects associated with the sensitometric images on film. Spectroscopic IlaO film for this experiment (Figures 2 & 3) was obtained from the same roll of Kodak film Mfg. date 5-76 A5J. The film was loaded into specially prepared aluminum anodized packages that fit on the Space Shuttle's Getaway Special Container. One roll of film was cut from the same stock and maintained as the control. The control was maintained at a temperature of 22 degrees centigrade at Goddard Space Flight Center. After the mission, the three rolls of IlaO film were shipped back to the Small Payload Section of the Laboratory of Astronomy and Solar Physics. One film and the control film were developed as Set I, while the other IlaO sample film was developed as Set II.

Results and Discussions

Using a Macbeth Densitometer, measurements were obtained from the film every 2 centimeters, developing 3 columns of data. Significant differences were found when samples were compared with the control. Sample A and Sample B had a 5.26% increase in optical density or fogging background, while the film developed shortly after its arrival at Goddard Space Flight Center displayed a 3.8% increase in the optical density or the fogging background. An analysis of the data for each sample film aboard the Space Shuttle (Figure 5, 6 & 7) indicated variation in intensity with respect to fogging levels as a function of position on the film. There was increased random variation toward one end of the film. However, the actual orientation of the film in the Space Shuttle was not known. One hypothesis is that high energy cosmic rays penetrated the aluminum film cartridges aboard the Space Shuttle causing secondary reactions that produced variations towards one end of the film due to the wrapping procedure used in placement of the film in the canisters. Another hypothesis is that thermal effects cause density variations. Aluminum containers have been found to innately fog various UV films along with the wrapping geometry of film in the canisters.

Densitometric Response of IlaO Film Flown on STS-7

Three canisters of 35mm IlaO film were flown on STS-7 in a getaway special canister in cooperation with NASA's Plasma Physics Branch and the Naval Research's Solar Astronomy Branch. The results indicated a large degree of thermal aging during the space shuttle mission. Future requirements for films used aboard the space lab and on the UIT (Ultra Violet Imaging Telescope) will

include the following : 1) ultraviolet films may be exposed directly to a particular vacuum of space at various altitudes, thus giving rise to concern for metallic outgassing of chemicals that may cause permanent damage to the film's emulsion; and 2) the IlaO film used on the UIT may not be exposed directly to space, but may be exposed to the ionospheric fields associated with a low orbiting space shuttle. Finally, the major factor that causes fogging of film has been thermal exposure.

Experimental Set-Up

Using a sensitometer, a continuous roll of IlaO film was exposed for ten seconds using a General Electric Lamp 328 at 195 ma + 3 ma with a 10 - 18 hour calibration burn in time. The film was loaded in three 35mm canisters, sealed in air and attached to the getaway special canister containing other special ultraviolet films. The film was loaded in the canisters approximately 22 days before the launch of the Space Shuttle Columbia.

Discussion

During the loading or preflight launch and post-flight analysis (Fig. 8), that the IlaO film had been exposed to some type of thermal aging effects. The exact nature of these effects was not apparent as we examine the temperature profiles for STS-7. However, there was concern that the rapid increase in temperature from approximately -15°C - $+22^{\circ}\text{C}$ in 1.5 hours after touchdown of the shuttle on the West Coast could explain the exaggerated thermal effects. There was another real concern which was associated with the fact that the shuttle landed on the West Coast and the automatic temperature cut-off control was turned off approximately three days before the shuttle arrived at Cape Kennedy where the getaway special canister containing the film was unloaded. Analysis of terrestrial thermal and aging effects produced similar curves as observed in this experiment, but the slopes of the individual curves tended to vary dramatically. In conclusion, there were observed densitometric changes in comparing the control films and flight film, though both had been developed at the same time as the flight film received from STS-7.

Experimental Set Up for STS-8

This research team was able to use one of the canisters to place four rolls of IlaO film of STS-8, one roll of Illford G5 nuclear emulsion, and one roll of a new batch of IlaO. The Naval Research Laboratory set-up was using a very sensitive ultraviolet film to study the effects of space on the ultraviolet emulsions. The shuttle orbit was low enough to expect some minimum cosmic ray damage to the film as well as tracks on the nuclear emulsion film. The Getaway Special was aligned in the bay of the shuttle with bay portals pointed to the earth for cooling purposes as shown in Figure 9.

The temperature profiles for STS-7 and STS-8 were very similar in that, it went from a temperature of approximately 23°C degrees centigrade before launch to -22°C during the flight. This increased the optical density of the wedges. The major differences between STS-7 and STS-8 occurred because STS-7 had to land in California where the automatic temperature control devices and appropriate air conditioning units for the shuttle cargo were not present. Once the shuttle had landed, one can measure the diurnal temperature variations (Figure 8). Terrestrial experiments have shown that less dense wedges produce densitometric increases as the temperature increases over a number of days (Figure 12). The diagram shows the effects of the first 3 step wedges including the aging effect of the background at 32°C . Lowering of the temperature decreases the slope of the curve for each of the darker step wedges (Figures 11 & 14). Aging effects show the slope variation at 21°C and at 32°C over a 90-day period.

A most interesting effect occurs at the darker patterns. They tend to decrease in density, while the lighter patterns tend to increase in density. Furthermore, the IlaO film seemed to perform nonlinearly for temperature values above 67 or 68°C (Figure 13). The least dense step wedges tend to show dramatic increases in density above 68°C while the darker wedges show a reduction of temperature above 70°C. The slope of the curves of these films increased further when the ambient temperatures increased.

A brief examination of the aging effects will assist us in understanding the observed effects on the film caused by exposure to the space environment of the shuttle (Figure 14). We used a microdensitometer to contrast and compare the terrestrial film as well as the shuttle flight film (Figure 15). Using this technique we were able to calculate the signal to noise ratio for flight as well as control film. On STS-8, the signal to noise ratio increased while the control film decreased. The signal to noise ratio computed for STS-7 shows that at higher exposures, the signal to noise ratio was less than the flight films (Figure 16). But at lower exposures, the control and flight film seem to have larger signal to noise ratios (Figure 17). This difference may be caused by additional thermal activity within the canister as shown in Figure 17 and the lack of appropriate air conditioning equipment at the California landing site.

Signal to Noise Ratio of Aging Film

An analysis of the signal to noise ratios for IlaO film aged for 8,9,21, 17, and 71 days indicated that a certain amount of aging reduces the signal to noise ratio over the short term, but will increase the signal to noise ratio over long periods of time (Fig. 18). An examination of the interaction of protons at varying dosages and energies indicated that the very light wedges are very sensitive to proton interaction with the emulsion while the very dark patterns tend to be less sensitive to very high MEV protons (Figure 19). MEV vs. dosage measurements were obtained by using the Harvard University Cyclotron.

Using the Harvard University Cyclotron, we bombarded the IlaO film with alpha particles, (Fig. 18) searching for parallel interactions in the space shuttle due to cosmic rays interactions. We bombarded the IlaO film using alpha particles at 47 MEV, 79 MEV and 153 MEV for the 6.8 rad dosage. We expected to see similar results when we examined the films from the shuttle, however, we did not observe similar results (Fig. 19). There was however, difference in the toe of the curve, but the toe and the shoulders did not seem to respond. As a result we did not conclude that there was any dramatic cosmic ray activity (Fig. 20A).

Microdensitometric Analysis

When comparing similar step wedges that have been aged from 3 to 71 days, one can immediately see an increase in granularity. However, this was not consistent for all step wedges as it was for the middle wedges. The denser the wedges, the more one observes the converse of less granularity. As aging increases, granular definition between step wedges seems to decrease, while other step wedges under densitometric aging will produce a heavier granularity indicative of increased grain structure.

Microdensitometric Comparison of Control vs. Flight Film

The control film of STS-8 for step wedge 3 had a larger grain structure than flight film. Similarly on STS-8 strip 4, a new batch of IlaO film showed slight increase in granularity toward the darker wedges (Figure 24). Conversely, the least dense step wedge controls are heavier than the

traces for the flight film (Figure 25). Microdensitometric traces from STS-8 showed greater granularity for the flight film than for terrestrial controls (Figure 27).

A new approach to examination of the IlaO film emulsions is the utilization of scanning electron microscopy to investigate surface grains and structure of film. Varying the voltage of the probe electrons, we were able to examine grain structure under the surface of the emulsion at the proper accelerating voltage of the electrons. All IlaO films were coated with gold palladium using standard sputtering techniques. Using 1,000X Magnification (Fig. 27), it was evident that energy of the electrons within the scanning electron microscope striking the emulsion was crucial in viewing grain structure of film. Further experiments will examine aged film and observe exactly how the grains change (Figure 28). We found that a working voltage for SEM ISISS 40 between 2-10 kilovolts was sufficient to produce clear images without flaring. The flaring of the image from the SEM produces a 4.8% increase in the total area of the grain under investigation from direct measurements of the micrograph. As the energy of the electrons increased, there was a flare effect as each grain enlarged (Figure 29). The one grains beneath the surface of the emulsion were observed. Using scanning electron microscopy, we can examine some of the grains below the surface if the charging voltage is appropriate.

We also looked at the step wedges of film under the electron microscope. The extreme left represents the least dense, and the extreme right represents the denser wedges. (Figures 33, 34, & 36). As the density increased, the size of these grains seems to decrease. Using this technique, we measure and acquired some statistical understanding of structure (Figure 38). Qualitative analysis techniques of energy dispersion revealed a large Ag peak along with traces of Cu, Na, S, and Ar peaks as shown in Figure 38. These trace element peaks are associated with the elements used in the development process and other materials in the emulsion.

Reciprocity Failure of IlaO Spectroscopic Film

Reciprocity failure was examined for IlaO Spectroscopic Film. The failure was examined over two ranges of time from 1-31 seconds, and 1 - 180 minutes. The variation of luminance was obtained by using thirty neutral density filters. A standard sensitometric device imprinted the wedge pattern on the film as exposure time was changed. Our results indicate reciprocity failure occurred for higher density patterns within the first minute. Multiple failure occurred at 13, 30, 80, and 180 minutes.

Materials and Methods

Twenty-seven wedge patterns were placed on IlaO spectroscopic film in total darkness using a light sensitometer with a 24 hour burn in time for the bulb. Each film section was exposed to the light sources for specific periods of time. Time intervals were from 1-30 seconds, 1-11, 15, 19, 22.5, 25, 27, 30,35, 40, 45, 59, 90, 125, and 180 minutes respectively. The film was then developed using Kodak D-19 developer, rapid fixer, hypo-clearing agent and photo-flo solutions. In total darkness, and in a water bath at a temperature of $20^{\circ}\text{C} \pm 1.5^{\circ}\text{C}$, one section of film was placed in Kodak D-19 developer and gently agitated for four minutes using a specific soak and agitating pattern. The film was washed in water for 30 seconds, shaken, then placed in Kodak rapid fixer solution, using the exact same pattern of agitation and soaking, and gently agitated for four minutes. The film was then removed and rinsed in water for 30 seconds, washed in water for one minute, and then hung to dry. After developing, the optical densities of the wedge patterns were read using a Macbeth Densitometer.

Results

An examination of the reciprocity failure for the 1 - 30 second exposure periods (separate wedge pattern that was exposed to an amount of light from 1 - 30 seconds sequentially) revealed that for two separate batches of film whose histories of use were different, there was reciprocity failure occurring at the darker wedge patterns. An examination of the very light patterns further showed the trend of reciprocity failure at the 30 and 31 seconds. It should be noted that the very darkest patterns had a marked decrease in reciprocity failure around the 30 second interval, with other variations occurring at 10, 15 and 19 seconds consistently with each variation of the pattern. The results showed that the reciprocity failure minimum points occurred at 13 minutes, 30 minutes, and 90 minutes, with a less defined failure at + 80 minutes. The middle density wedges indicated the same reciprocity failure points occurring at the same time. The darkest wedges showed remarkable stability for the first 10 minute exposure, but dramatic failures occur at 11 and 20 minutes, and dramatic reductions occurred at 30 minutes.

Conclusion

For exposure times of 30 to 31 seconds, darker wedges experienced failure more than light wedge patterns. This indicated that lighter wedges are less sensitive to Reciprocity Failure at short exposure times. As the exposure times increased, there appear to be some migration of grains in the darker wedges. The last three columns gave an appearance that double exposure had occurred. There was also an increased darkening of the film with increased exposure times. Fogging of the film was prevalent at 30, 45, 58, 90, and 180 minutes with increased exposure times. An examination of the reciprocity failure from 1 to 180 minutes completely demonstrated that reciprocity failure minimum points are at 13 minutes, 20 minutes, 30 minutes, and 90 minutes, whereas, less defined failure occurred at 11 minutes, with reductions at 30 minutes.

Results on STS-40

On STS-40, flown in June, this researcher sent IlaO film in space that was flown on the ASTRO I mission and will be flown on ASTRO II missions, which is slated for 1993-1994 (Figure 39). Illford nuclear emulsion film was flown on the mission and produced five major cosmic interactions (Figures 40,41, & 42). A small container of over the counter medications was also flown on this mission in order to measure the potency of these medicines after exposure to space. Selected amounts of aspirins, and Tylenol other drug were flown with the seals left unbroken while the rest remained sealed. This research is currently being analyzed by students and faculty of the Howard University School of Pharmacy.

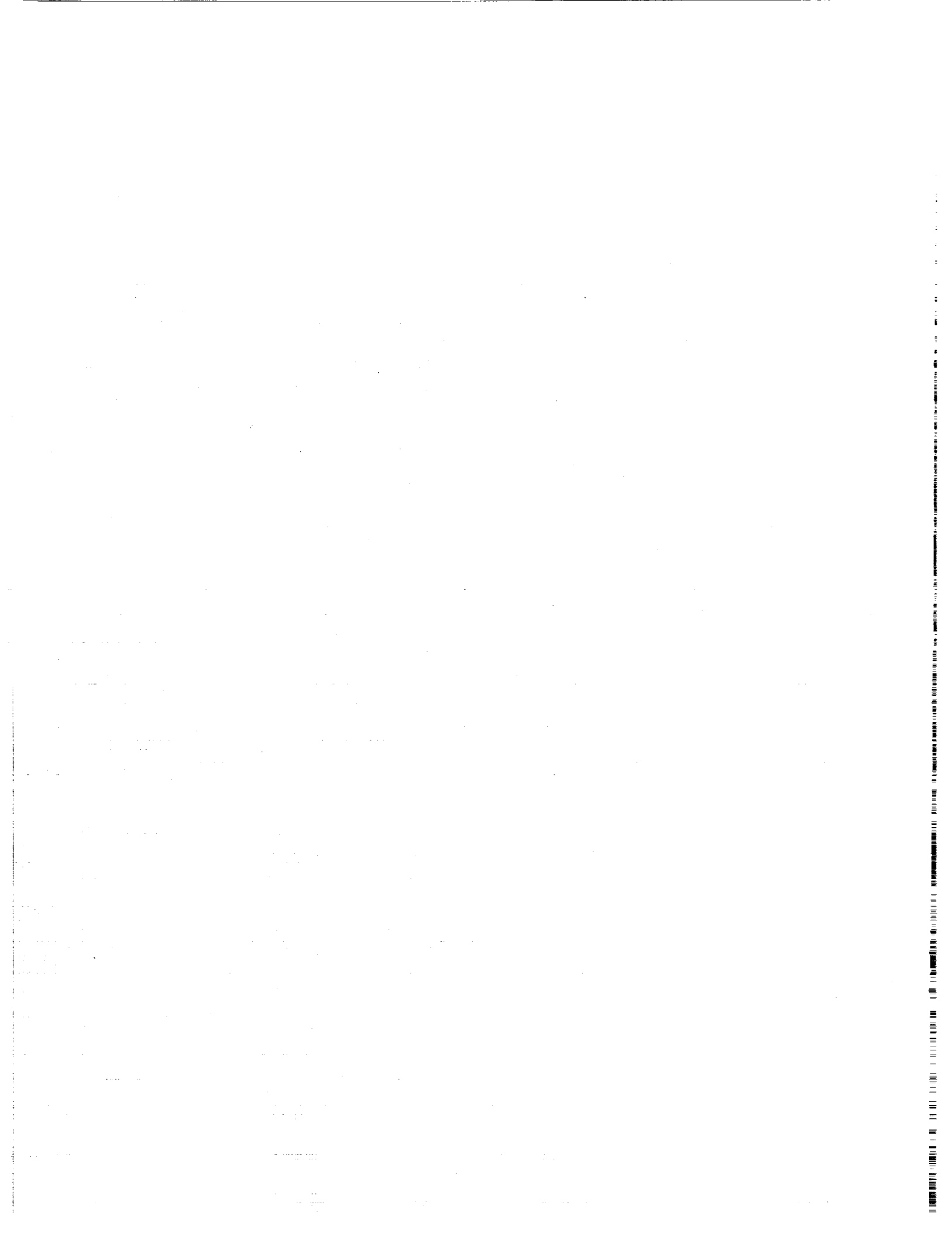
When comparing control studies with experimental studies, interesting results have appeared when the IlaO film was exposed to various wavelength of electromagnetic radiation. Alpha and Beta particles consistently interacted with the low density wedges and reacted more with the darker step wedges. The high energy gamma rays effected the middle density wedges, producing a loop. Exposure of the same film caused darker density wedges to increase substantially by neutrons, infrared and thermal radiation had an effect on the toe and shoulder of the H and D curves.

The most important result of the reexamination of the IlaO film on the STS-40 produced an effect that involved heat and beta exposure density wedge increases, while analysis of the STS-8 seem to produce exposure levels similar to the gamma ray reactions observed on Earth. The results of the density measurements indicate that the STS-40 experienced higher thermal effects than STS-7 or 8 (Figures 43 & 44). There was a hold on the launch as well, which may account for this change, but a

reexamination of the averages from all the separate density wedges seem to imply that the film was exposed to either thermal or cosmic ray influences (Figure 45).

Summary

The results of these studies have implications for the utilization of the IlaO spectroscopic film on future shuttle and space laboratory missions. These responses to standard photon energy sources will have immediate applications in a terrestrial or extraterrestrial environment with associated digital imaging equipment. The author is indebted to Gerry Baker and Al Stober of the Small Payloads Section of the Laboratory for Solar Physics and Astronomy for their hours of discussion and support. Special thanks go to Dr. Dan Klingsmith of the Interactive Astronomical Data Analysis Facility, also of the Goddard Space Flight Center, Greenbelt, Maryland for his patient assistance during the imaging processing of these films. Very special thanks go to Kevin Peters, Sean Gunther, Lisa Cunningham, and Deborah Wright for their careful assistance during the development process.



N 9 3 - 1 3 1 6 4



EARTH OBSERVATION PHOTOGRAPHY

LOOKING BACK 20 YEARS AFTER SKYLAB

GAS #324 CHARLESTON COUNTY SCHOOL DISTRICT CAN DO PROJECT

*James H. Nicholson
Thomas J. O'Brien
Mitchell Colgan
Ruth Ashcraft-Truluck
James R. Frysinger
Carol A. Tempel*

*Principal Investigator
Chief Engineer
Geology Science Advisor
Steering Committee
Orbital Physics
Coordinator*

*Medical University of South Carolina
Medical University of South Carolina
College of Charleston
Wando High School
Academic Magnet High School
Charleston County School District*

ABSTRACT

The Charleston County School District **CAN DO** project (GAS #324) was designed originally to photograph the 1986 apparition of Comet Halley. Postponed because of the Challenger disaster of that year, the project had to select new goals. Wishing to retain the already tested design, it was decided to turn the cameras towards the home planet instead. Because the various disciplines of earth science appear in curricula at many different grade levels, it was realized that high quality photographs of the Earth would have tremendous educational potential. A steering committee of trained classroom teachers, backed by a volunteer team of technical experts and academic advisors has developed a program for earth science based on photographs obtained from low earth orbit.

In selecting targeting objectives, immediate note was made of the fact nearly one generation (20 years) has passed since the United States' ambitious SKYLAB program was conducted. A critical part of those missions was the acquisition of earth photography using a six camera, multi-spectral camera system. This objective was systematically furthered through the term of three separate crew visits to the Space Station in 1973-74. Not merely an exercise in randomly photographing the Earth below, the purpose of the Earth Resource Experiment Package (EREP) was to determine what kind, and how much, photographic data could be acquired of the broad variety of Earth features witnessed on the mission's ground track. This activity was underwritten by intensive training before lift-off, real-time scientific mission planning and on-board procedural support ... qualities which have corollaries to what is here proposed.

The collection of 35,000 photos produced by EREP, in six registered wavelengths, represents still the most complete photographic coverage of the planet undertaken. Even as such, though, the body of data remains under-utilized. GAS #324 intends to operationally re-visit in part what is a considerable national asset, and to contribute an added tier of relevancy to this remarkable inventory of planetary data. Improvements in modern film technology will allow the G324 camera system to match closely the larger SKYLAB film format in both coverage and quality. The photography acquired by CAN DO should allow a direct examination and comparison of the changes that have occurred to the Globe in the last twenty years.

INTRODUCTION

THE IMPORTANCE OF EARTH OBSERVATION PHOTOGRAPHY

Later this decade, earth sensing platforms will analyze earth processes as part of a multi-national program, "Mission to Planet Earth". A rationale for the Mission comes from planetary exploration that affirms our world's special place. The Earth is the only known planet with a biosphere, abundant oxygen, liquid water, and surface renewing tectonic activity. Biogeochemical functions recycle nutrients, water, and gases that are essential to life. The Mission is concerned with changes that are occurring in such areas as atmospheric chemistry, biomass distribution, primary productivity, and population growth. By examining the past and monitoring the present, it is hoped to reach a deeper understanding of the evolution of the Earth on all time-scales. Because of the role humans now play in shaping local and global environments, a goal of this Mission is to document natural and human induced changes on the Earth over the next twenty years. Policy makers and scientists alike view the next twenty years as critical.

In twenty years the global population level will reach more than 6 billion. In less than forty years, from 1950 to 1988, world population doubled from 2.5 to 5 billion. By the year 2025, the United Nation projects population levels to reach 8.5 billion. A population growing at this rate places strong pressures on many of the earth's systems and accelerates the rate of global, as well as, local change. For example deforestation occurs at an estimated rate of 11.3 million hectares annually, industrialization pumps an additional 5,000 TgC (gigatons of carbon) of CO₂ into the atmosphere each year, and 20 to 25% of the existing tropical species are projected to undergo extinction.

Historical examinations of change often look far back into Earth's history to determine the rate and degree of natural changes. The rapid growth of human population presents fundamentally different pressures on the Earth's ecosystem. To gain new insight on human-induced changes, earth scientists focus on the changes that occurred over a shorter time span (20 years). During this time, natural and human induced changes on the surface of the earth have been photographed from space. Comparison between photos, past and present (especially, time series photography), enables documentation of the profound changes to the Earth. One of the largest data sets of earth observing photographs comes from the SKYLAB archives. These photographs covered most of the Earth's surface, and provide an important baseline to compare present and future photographs of the Earth taken from orbit. It is a major goal of the CAN DO project to provide a direct link to this resource.

THE VIEW FROM SPACE

Photographic analyses of land use practices give insight into changes. Linear functions can be used to project the rate of future change. As growing human population requires an ever increasing share of the Earth's surface on which to live, human activities change the distribution of plants and animals, alter drainage patterns, and modify natural boundaries. In doing so, mankind changes either the reflective or emissive properties of the surface. Such changes are detectable from space. Human actions that change the reflectance or color of the Earth's surface can be recorded with space photography. Activities include:

DEFORESTATION. Forests are optically dense, green areas. The cutting of the trees produces a more reflective surface and exposes a different color. Deforestation scars are seen in the rain forests throughout the world. Forests are often cleared by setting fire to the vegetation, and smoke from these fires is visible from space.

URBANIZATION. Urban areas are delineated by highly reflective paved surfaces. Because the growth of cities is at the expense of vegetated surfaces, the increase in reflectivity can be measured.

RIVER SEDIMENT LOADS. Clear cut forestry practices in many tropical countries have altered the sedimentary load of the rivers that drain the forest. Rivers loaded with sediment have a different color than "clean" rivers that drain forested areas. Sediment laden rivers, such as the Betsiboka River of Madagascar, are now red-brown when seen from space.

DESERTIFICATION. The reflective surface of deserts and eolian sediment patterns are also visible from space. The encroachment of deserts over once vegetated surfaces will register a shift in the optical and textural character.

COASTAL EROSION. Analysis of the position of the coastal features can be used to determine the rate and location of large scale coastal changes. Dramatic rates of erosion can be seen on the edge of the Nile and Ganges river deltas.

LAKE LEVELS. Changes in boundary relations can detect variation in water levels in lakes (e. g., Lake Chad) or inland seas (e. g., Aral Sea).

WETLANDS. The delineation of wetlands is sometimes difficult. Changes in vegetation color and the sea land boundary are sometimes needed to detect loss.



FIGURE 1 SKYLAB 1973

EARTH OBSERVATION AND EDUCATION

Photographic comparisons are powerful teaching tools. Their utility is particularly pronounced as regards change over time. By comparing transformation that has been documented in earth viewing photographs, changes that have occurred in our lifetimes can be observed. It is hoped that such documentation of global change will make this issue more immediate and real. There is a collateral benefit that will accrue in addition.

NASA and other federal agencies are concerned about the projected shortage of scientists and technicians able to use and understand global data sets. At the height of the "Mission to Planet Earth" program, approximately two terabytes of data per day will be generated. This staggering amount of data needs to be analyzed and assimilated to be of value. Students need training now to be able to understand and use this information in the future. An important goal of the CAN DO G324 mission is to provide a vehicle for stimulating hands-on experiences for students so that they can better interpret the global environmental changes that will determine the quality of the world that they will inherit.

THE VIEW FROM THE CLASSROOM

There has been a national movement in science education in recent years that recognizes and promotes the importance of utilizing modeling to teach process skills. These skills are used by earth scientists and may be used by intelligent informed citizens as well. Unfortunately, many students graduate from high school without an adequate foundation in this area. There is a clear need for better integration of the necessary process skills at all levels of curriculum.

The CAN DO pictures can be used as a springboard for this purpose. Students can use the photographs to make observations about land formations, weather activity, and the effect of man's presence on the planet. The destructive burning of forest land and the production of visible pollution make particularly graphic examples. Students can make inferences about these observations and model predictions of future changes that will result. Comparisons to matched SKYLAB photographs taken two decades ago will allow students to quantify the amount of change. The infrared pictures will document features not seen from the ground, such as changes in vegetation, when compared to earlier pictures. Night time shots can be dramatic for students by showing the concentration of city illumination as a measure of population density and energy usage. Such photographs can open a dialogue on world population and the problems that result, generating such questions as : what is happening to our farmlands; how much food will it take to feed the world's population; what are the problems of food distribution; and why do they occur? Students may be inspired to research the literature, communicate their findings, and even design experiments to answer their questions.

In addition, G324 is designed to contain 250 small passive student experiments. These individual experiments allow students at all grade levels to participate directly in space research. What better way to involve students in our national space program at an early age. The best learning takes place when the learner experiences hands-on involvement.

PAYLOAD DESIGN

The CAN DO payload utilizes GAS hardware and is housed in a 5.0 cubic foot canister equipped with a standard door assembly (SDA). The canister is sealed with a .92 inch fused silica window, which is optically flat and ground to a quarter wave tolerance. The fused silica window characteristics will permit photography in visible light, infrared and ultraviolet wavelengths. At the start of the mission, the motorized door will be opened, and will not close until its completion. In the event of premature battery failure, or loss of pressurization, the door closes automatically. Since the batteries are more cold sensitive than the cameras, the continued open condition of the door indicates sufficient battery power and survivable conditions in the canister.

The structure is a three strut design with a heavy structural face plate at the top, and battery compartments at the base. The cameras are hung from the face plate on struts of a length required for the lenses in use. The control electronics, heaters, and fans are mounted above the battery compartment. All structural components are fabricated of 6061-T6 aluminum and have been tested both by a detailed structural analysis and actual three axis shake and vibration testing at Langley Research Center.

All power is supplied by industrial alkaline batteries which have been thoroughly tested for cold tolerance, safety, and leakage. Because of the extremely low level of hydrogen gas generation, the alkaline batteries do not require venting. The battery stacks have been designed for redundancy and include both diode and fuse protection. Battery capacity is allotted to provide adequate power for camera operation and environmental control for a mission duration in excess of ten days. Supplemental heat and atmospheric circulation (to compensate for lack of convection) is provided by redundant mil-spec fans and strip heaters. The environmental system is designed to maintain a 0° C temperature based on experience operating the same cameras on board a stratospheric research aircraft. The electronic systems were tested for EMI at Goddard SFC and found to be interference free.

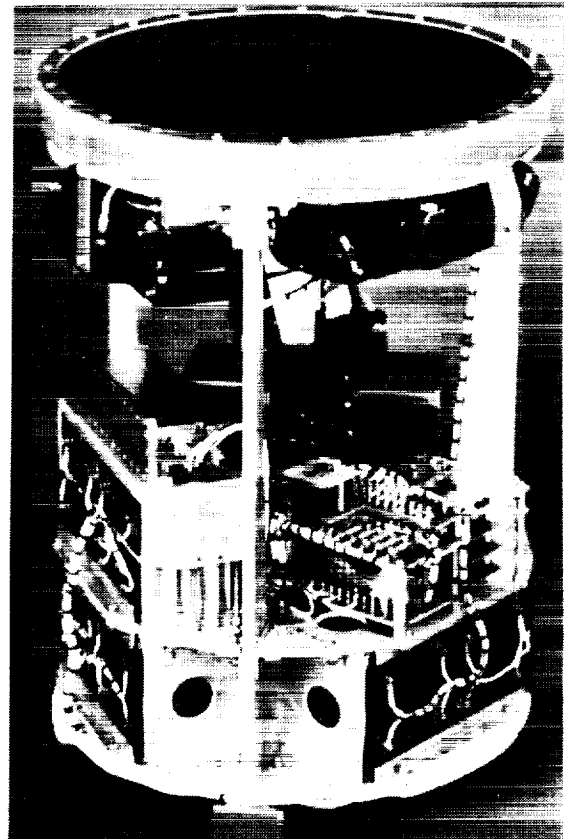


FIGURE 2 G324 PAYLOAD

PHOTOGRAPHIC DESIGN

The primary goal for the design of the optical and photographic systems is to match as closely as possible the results of the SKYLAB S190A and S190B camera systems. This includes the selection of focal lengths to match the photographic "footprint" of the cameras as well as the use of modern fine grain, high resolution films to compensate for the difference in camera format.

The SKYLAB spacecraft was launched on May 14, 1973 into a nearly circular orbit at an altitude of 435 km above the Earth. The launch azimuth inclined the orbital plane 50° with respect to the Equator and allowed observations of the Earth between latitudes 50°N and 50°S. It orbited the Earth every 93 minutes and repeated the ground track every 5 days. The photographic return from the Earth Resources Experiment Package (EREP) was as follows:

<u>MISSION</u>	<u>DATES</u>	<u>DAYS</u>	<u>PASSES</u>	<u>TOTAL PHOTOS</u>
Skylab2	5/25/73-6/22/73	28	13	5,275
Skylab3	7/28/73-9/25/73	59	48	13,429
Skylab4	11/16/73-2/8/74	84	49	17,000
TOTAL		171	110	35,704

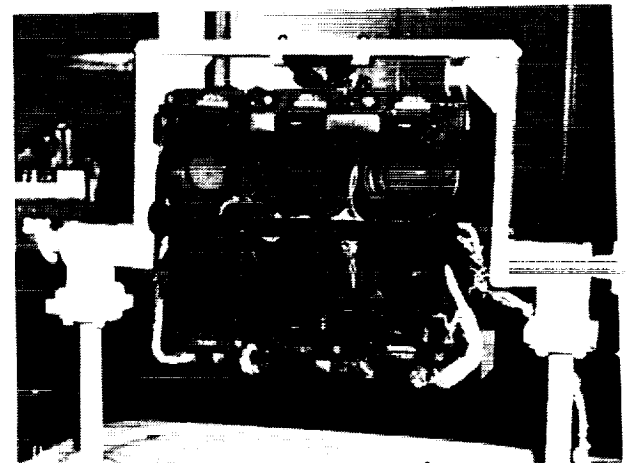
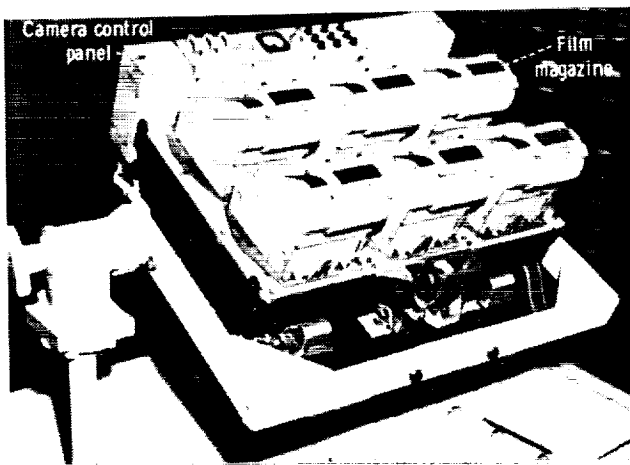


FIGURE 3 SKYLAB S190A CAMERA SYSTEM

SKYLAB CAMERA SYSTEMS

S190A Multispectral Photographic Camera System

The S190A system consisted of six bore-sighted 70mm cameras equipped with 152mm focal length lenses. Each photograph covered a square image area of 163 km on a side. Each camera was equipped with filters to cover a specific wavelength on a combination of color, black-and-white, color infrared and black-and-white infrared film. The cameras were mounted in a frame that provided programmable camera rotation to compensate for the forward motion of the spacecraft.

S190B Earth Terrain Camera

The S190B was a single 127mm camera equipped with a 457mm lens. Each photograph covered an area of 109 km square. Film could be selected from a choice of color, black-and-white or color infrared emulsions with an appropriate filter. An internal motion compensator corrected for the forward motion of the space craft.

G324 CAN DO CAMERA SYSTEM

The G324 payload is a candidate for the flight of STS-57, currently scheduled for launch in late April of 1993. STS-57 will be at a mean orbital altitude of 431.5 km with an inclination of 28.45°. During the scheduled seven day mission, approximately 46 of the planned 108 orbits are -Z axis pointing (cargo bay towards earth).

The G324 camera system consists of four 35mm single lens reflex cameras equipped with 250 exposure film backs. With an 85mm focal length lens, each photograph will encompass an area of 180.8 km by 123.9 km. The total ground area for each view will be 22,401 km² compared to 26,569 km² for the S190A multispectral system and 11,881 km² for the S190B terrain camera. The G324 film format is rectangular (24 x 36mm), while both Skylab film formats were square. The G324 camera system lacks any positive motion compensator to prevent image blur from motion over the ground, so that shutter speeds on the cameras must be selected to prevent motion degradation of the images. With an orbital speed of 7.66 km/sec (27,574 kph), an exposure of 1/250th of a second would allow 30 meters of motion. This approximates the best resolution possible at this image scale. General practice accepts motion blur as negligible when it approximates 1/2 of the image resolution; therefore, all cameras will be set to an exposure time of 1/500th of a second or shorter. By the use of 85mm lenses with a maximum aperture of f1.4, this exposure can be achieved while still permitting the use of slow speed, high resolution films. All lenses will be set at the maximum aperture of f1.4 because the subject is at infinity and depth of field is not a consideration. However, the shallow depth of focus will require careful prefocusing on an optical bench and positive securing of the focus mechanism to prevent slippage due to vibration.

SYSTEM	FILM	LENS	ANGLE	IMAGE SIZE	TOTAL AREA
S190A	70mm	152mm	21.2°	163x163 km	26,569 km ²
S190B	127mm	457mm	14.24°	109x109 km	11,881 km ²
G324	35mm	85mm	28.5°	124x181 km	22,401 km ²

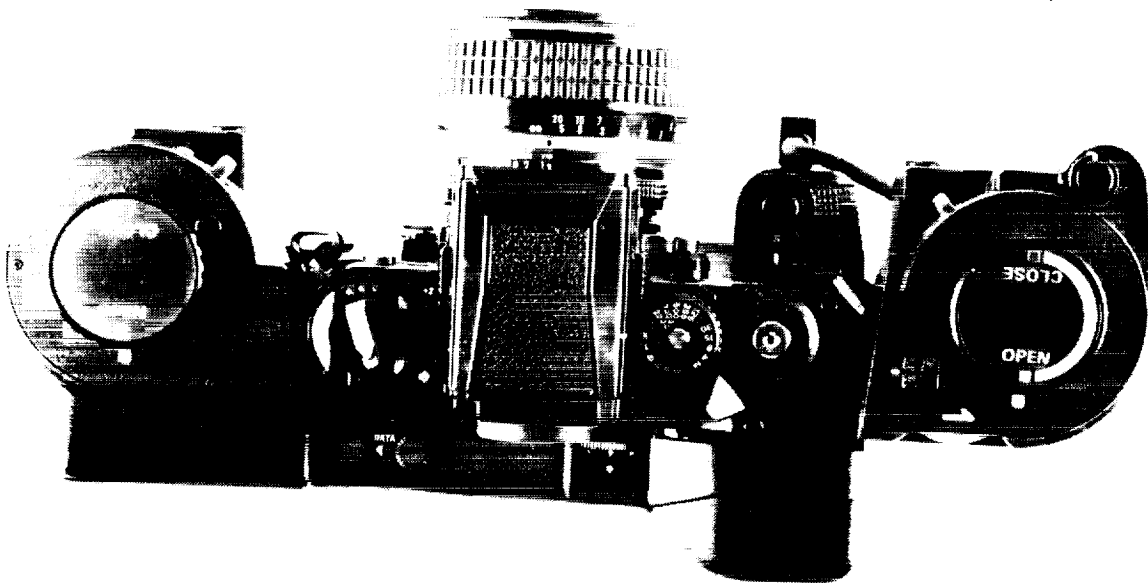


FIGURE 4 CAMERA WITH 250 EXPOSURE BACK

FILM SELECTION

The Skylab S190A camera system used four types of films; black-and-white visible (Aerial PlusX), black-and white infrared, color infrared and color visible. All films were 70mm size. The G324 cameras will be using 35mm format, which has only 1/4 the image area. Much of this difference in resolution and graininess will be made up by the use of more modern films with improved grain structure and resolution. In addition, the G324 lenses have a maximum aperture of f1.4 which transmits four times more light than the S190A lenses' maximum aperture of f2.8. This greater light transmission will allow the use of slower (lower exposure index) films with inherently finer grain and higher resolution. For example G324 will use Technical Pan film with a film resolution of 325 lines/mm as compared to the S190A Aerial PlusX with a film resolution of 125 lines/mm. This gives the G324 cameras 62.9 lines of resolution per kilometer of ground coverage as opposed to 53.7 for the Skylab system. In the case of the infrared color and infrared black-and-white films, fewer improvements have been made. No suitable lower speed films are available, so that the film format difference can not be fully compensated.

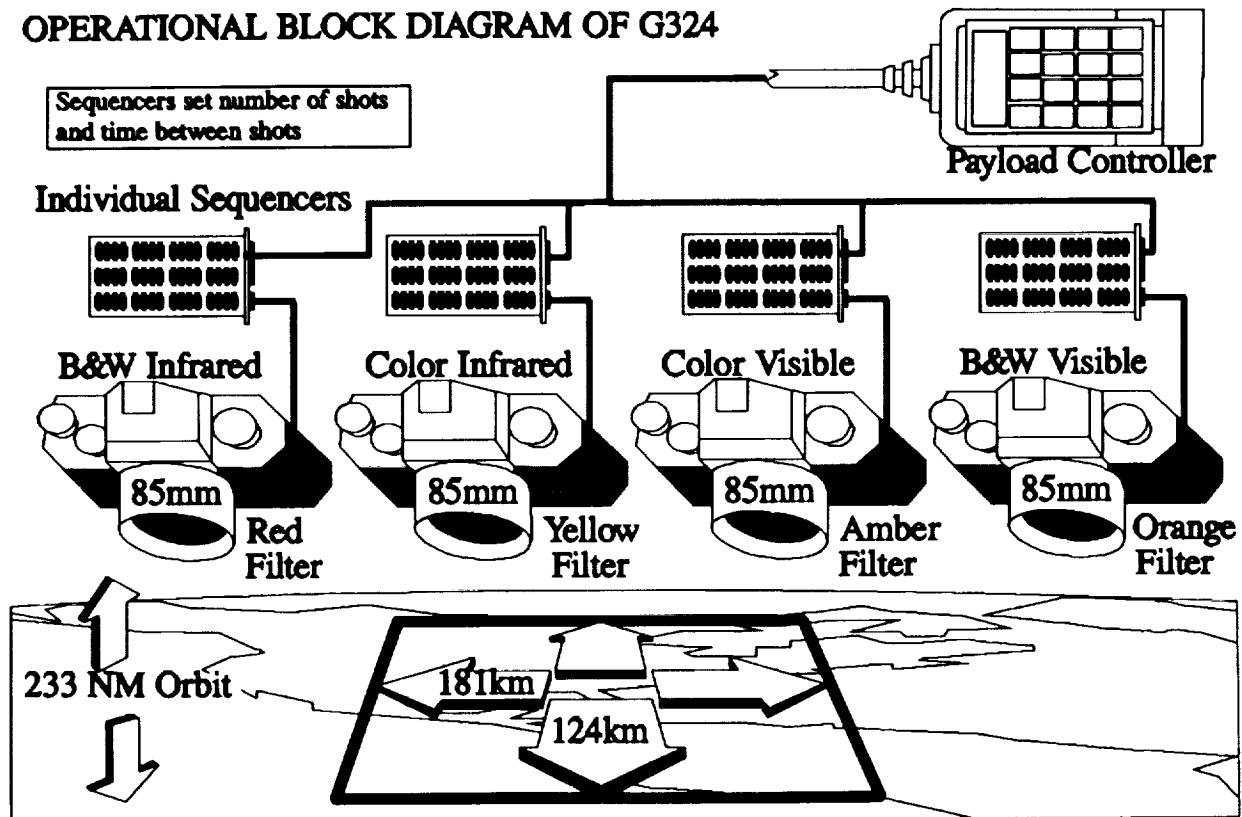
FILTER SELECTION

All of the cameras will employ filters either to limit spectral range or to correct image quality. In all cases, the filter will be used to eliminate the ultraviolet, which is the wavelength most scattered by particulates and pollutants in the atmosphere. The greatest problem in the visible color photography is the excess blue caused by atmospheric scatter of short wavelength light. This blue haze can vary from almost none over mountains and desert areas to extremely high over temperate and subtropical forests and urban areas. To achieve maximum control of this effect, the camera will be equipped with a 85B (wratten) amber color correction filter. This will remove ultraviolet and most of the blue/violet. These wavelengths are most subject to atmospheric scatter. Where scatter is not prevalent, the excess yellow can be removed by correction in color printing.

<u>FILM</u>	<u>SPEED</u>	<u>FILTER</u>	<u>COLOR</u>	<u>WAVELENGTH (μm)</u>
B&W Infrared	50	25	Red	0.7-0.9
Color Infrared	25	12	Yellow	0.5-0.88 *
Color Visible	25	85B	Amber	0.5-0.7 *
B&W Visible	25	21	Orange	0.6-0.7
"NIGHT"	6400	--	----	0.4-0.7 *

* films available in long rolls only by special order

OPERATIONAL BLOCK DIAGRAM OF G324



OPERATIONAL CONTROL

Each camera is controlled by an individual sequencer to set the interval between photographs and to control the number of shots for each crew activation. The interval is determined by the coverage of the lenses and the orbiter's speed over ground. In the case of STS-57, a 15 second interval between shots would allow a spacing of 115 km, which would provide image overlap of 9% on the short (24mm) axis of the film and 52% on the long axis (36mm). The actual overlap for any camera will depend on the orientation of the camera body to the direction of the orbiter's forward motion.

Each camera has a total of 250 exposures available. The total number of photographs taken in each "photo run" will be primarily determined by the number of crew activations available.

RUNS	#SHOTS	TIME	DISTANCE
2	125	30m15s	14,375km
10	25	6m15s	2,875km
25	10	2m30s	1,150km

FUTURE POTENTIAL

Because Earth observation has such wide reaching and enduring interest, especially in view of such long term programs as "Mission to Planet Earth", the Can Do team has been asked to consider the possibility of future use. After the flight of G324, the Charleston County School District has agreed to loan the payload and offer technical support to any suitable party that would use it for educational purposes. This use could take one of several possible forms.

FUTURE GAS FLIGHTS

Some other school groups holding GAS reservation numbers have found it difficult to construct and test a qualified payload of their own. They might consider using the Can Do structure to obtain photographs of interest to their students as well as flying their own set of small passive student experiments.

CAP PAYLOADS

The limited number of crew activations permissible under the GAS program restrict photography of specific targets of scientific interest. A CAP (Complex Autonomous Payload) secondary payload under the auspices of another NASA Earth investigation program would allow the more intensive crew involvement to perform the targeted and controlled photographic investigation necessary to support serious scientific research.

HITCHHIKER

Under suitable sponsorship, it would be possible to expand the payload to a Hitchhiker status. This would allow the use of more cameras to cover other optical and wavelength options. In addition, the availability of a radio channel would permit realtime operation of the payload from the ground, eliminating the impact on crew time completely. A suitable control room for students could be set up complete with orbital tracking and satellite weather displays. Student teams would experience the real world of decision making in choosing lighting angles and weather conditions for the completion of their photographic missions.

REFERENCES

Skylab EREP Investigations Summary. NASA SP-399, Prepared by NASA Lyndon B. Johnson Space Center, Washington, D.C., 1978.

Kodak Scientific Imaging Products. Kodak Publication L-10, Eastman Kodak Company, Rochester, N.Y., 1989.

Eyes of Nikon. Nippon Kogaku K.K., Garden City, N.Y., 1985

A PATH TO IN-SPACE WELDING

and to other In-Space
Metal Processing Technologies

Using Space Shuttle Small Payloads

presented at

1992 Shuttle Small Payloads Symposium
October 20-23

by

David Tamir
Aerospace Systems Engineer
Payload Manager G-169

Rockwell International Space Systems Division
Florida Operations
Kennedy Space Center

ABSTRACT

As we venture into space, it becomes necessary to assemble, expand, and repair space-based structures for our housing, research, and manufacturing. The zerogravity-vacuum of space challenges us to employ construction options which are commonplace on Earth. Rockwell International (RI) has begun to undertake the challenge of space-based construction via numerous options, of which one is welding. As of today, RI divisions have developed appropriate resources and technologies to bring space-based welding within our grasp. Further work, specifically in the area of developing space experiments to test RI technology, is required.

RI Space Welding Project's achievements to date, from research and development (R&D) efforts in the areas of microgravity, vacuum, Intra- / extra- vehicular activity and spinoff technologies, are reviewed. Special emphasis is given to results from G-169's (Get Away Special) microgravity flights aboard a NASA KC-135. Based on these achievements, a path to actual development of a space welding system is proposed with options to explore spinoff in-space metal processing technologies. This path is constructed by following a series of milestone experiments, of which several are to utilize NASA's Shuttle Small Payload Programs. Conceptual designs of the proposed shuttle payload experiments are discussed with application of lessons learned from G-169's design, development, integration, testing, safety approval process, and KC-135 flights.

INTRODUCTION

In recent decades, welding has become the dominant process for building metal structures on Earth. The rapid and continuing growth of welding applications is due to the inherent advantages of this metal joining method over the mechanical fastening and bonding techniques. The advantages of welding include higher joint strength and rigidity with reduced joint mass, increased design flexibility and simplicity of structural joints, more reliable hermetic sealing of pressurized structures, and broader versatility for emergency repair. These benefits dramatically reduce construction costs on Earth, and seem to be even more attractive for space-based applications. For these reasons, welding has been identified by NASA's Pathfinder Initiative as a critical enabling technology for in-space construction capabilities. There is no doubt that NASA's aggressive space exploration program for the next 30 years, which includes a permanently manned space station, a lunar base, and a manned mission to Mars, will all dramatically benefit from an in-space welding capability.

R&D ACHIEVEMENTS TO DATE

As of today, RI divisions have developed appropriate resources and technologies to bring space-based welding within our grasp. In-space welding, unlike terrestrial welding, constrains us with low or no gravitational forces in an environment which includes both pressurized-intra-vehicular operations and vacuum-extra-vehicular operations. Through internally funded programs and NASA funded contracts, RI has conducted research and developed technologies which address various constraints associated with in-space welding.

WELDING PROCESS SELECTION

Any terrestrial welding process modified for space-based applications should be amenable to both manual and automatic operations, and have the extra versatility to function inside pressurized life supported compartments as well as in the outside vacuum. Zerogravity should not pose any fundamental problems with the process. The process must conform to rigid safety standards; it should produce optimum quality welds on all aerospace metals; it must operate with available power levels and efficiently utilize energy; it should be forgiving of joint mismatch or fit-up problems; and it should use a minimum weight of consumable materials. However, to choose one single welding process, which maximizes each of these many requirements, is practically impossible. Thus, it is necessary to start with the terrestrial welding process which possesses the best overall combination of properties required for in-space welding. [1]

Gas Tungsten Arc Welding (GTAW), better known as Tungsten Inert Gas (TIG) welding, has been selected by RI as the welding process to best fulfill the requirements of a space-based welding system. When GTAW is compared with its best adversary, Electron Beam Welding (EBW), GTAW proves to have superior potential in manual operations and adaptability to joint mismatch problems. Draw backs for EBW also include the need to shield the astronaut from additional X-ray radiation inherent to the process, and the need for a vacuum which becomes impractical for welding inside pressurized life supported compartments. Furthermore, only the energy requirements of a GTAW system can be easily met by a rechargeable and relatively small battery-pack. Such versatility would be critical in repair at locations remote from a power source, or during power-down emergency scenarios (i.e. on a space station). However, it is obvious that the terrestrial GTAW process requires some modifications (specifically in the area of vacuum operation) in order to function effectively as a space-based welding system. [1]

MICROGRAVITY EFFECTS

A mass orbiting around the Earth is continually free falling about the Earth; because, the centrifugal pull on the mass is equal in magnitude but opposite in direction to the Earth's gravitational pull. Therefore, in a space station's reference frame, the environment does not have a gravitational acceleration field. Hence, any mass element sharing the space station's reference frame, such as a molten weld puddle, has no gravitational forces acting upon it; unless of course artificial gravity is introduced via some form of acceleration. But for all practical

purposes, future space-based welding applications would most likely experience low or no gravitational forces. Hence, we should question what are the effects due to the absence of gravitational forces on weld puddle formation, solidification, and joint strength. Theories to this matter are various and even conflicting, leaving much doubt as to the actual affect of microgravity on welding. If we are indeed to extend the inherent advantages of Earth-based welding out to space, it is essential to first experiment and compare the properties of a terrestrial welded joint with those of its space counterpart.

• **Development of a Get Away Special Payload (G-169)**

In 1985 RI Science Center Division began subcontracting the California Polytechnic State University in San Luis Obispo and ST International (welding systems company) to develop a Get Away Special (GAS) payload which would perform welding while on a Space Shuttle mission. NASA designated this payload as G-169 (see figure-1).

Objective -- The objective of G-169 is to allow comparison of an In-space GTAW joint to a terrestrial GTAW joint with all welding parameters held constant except for gravitational forces; welding in a vacuum is not attempted with this experiment. Upon retrieval of G-169 from its mission, the In-space (zerogravity) welded specimen would be compared to its terrestrial counterpart by RI Science Center via metallographic examinations such as macro- and micro- photography, microhardness, tensile, radiography, and scanning electron microscopy. [2]

Specimen -- One of the most attractive candidates for space-based welding application would be tubing, which may be used for structural truss elements and fluid lines. RI's Rocketdyne Division has designed Space Station Freedom's power system. The power system involves stainless steel tubing for flowing heat transfer fluids through a two-phase ammonia cooling system. Mechanical connectors which are unavoidably bulky, heavy and expensive will be used at the plumbing joints due to technology constraints. However, as learned from the Skylab Space Station, future plumbing systems should employ autogeneously welded plumbing joints, which add no mass to the joints with superbly low profile weld-beads (material at the ends of the adjacent tube sections is fused together). Such joints would be more reliable, longer lasting and dramatically cheaper. Therefore, in order to maintain a direct application for the specimen to be welded, G-169 performs a bead-on-tube (simulating a butt-joint) weld around the perimeter of an 8.9 cm (3.5 in) long X 5.1 cm (2.0 in) diameter X 1.59 mm (0.0625 in) thick wall Stainless Steel 316-L tube section; an actual butt-joint would require two adjacent sections of tube which may vibrate and separate during shuttle launch. [2]

Concept -- The basic components of G-169 include a controller, battery pack, power inverter, welding computer, welding head, and an argon gas pressure vessel. The controller manipulates and safeguards operations of the payload components. The battery pack supplies power to the entire payload via the controller. The power inverter converts the DC power-output from the battery pack to a compatible AC power-input for the welding system. The welding computer regulates power to, and operations of the welding head and argon gas purge. The welding head, housing a rotating tungsten electrode, welds along the outside circumference of the tube specimen. Lastly, the pressure vessel floods the welding zone with argon in order to imitate the gas' presence in terrestrial GTAW. Prior to launch the G-169 payload is pressurized with nitrogen gas to one atmosphere of pressure, simulating the terrestrial environment. [2]

Operation -- The sequence of operations on G-169 is regulated by a cooperation of the controller and the welding computer. Placing switch (A) of the Astronaut Payload Controller (APC) in the "HOT" position initiates start-up of G-169's (internal) controller. The controller initiates a 30 minute time delay to permit cessation of astronaut activity; scheduling activation of switch (A) within 30 minutes of crew's next sleep period should provide minimal crew induced accelerations on the Orbiter. Following this first delay, power is applied to the welding computer through the power inverter. The computer initiates an additional 7 minute time delay to permit some of its sensitive circuitry to warm up to optimal operating temperature. Following this second time delay welding is performed. The welding procedure involves 30 and 20 second periods of argon gas-flooding of the weld zone, prior and after (respectively) actual welding takes place. The actual welding (arc transfer) takes approximately 2 minutes, during which argon gas-flooding continues and the tungsten electrode rotates around the stationary tube specimen in a programmed manner. Upon completion of the welding procedure, the welding computer signals the controller to cut-off all payload power immediately. The duration for the entire experiment, including time delays, is 40 minutes. [2]

- **G-169 Flight Aboard NASA KC-135 Microgravity Simulator**

Following the Challenger Space Shuttle Accident, which prompted changes to the GAS program's safety policies and reduced space flight opportunity, RI began seeking other quicker means for microgravity simulation. Consequently, in 1990, G-169 was successfully flown on the NASA Marshall Space Flight Center (MSFC) KC-135 Aircraft Microgravity Simulation Facility.

Microgravity environment -- A microgravity environment is attainable for approximately 20 seconds by flying the aircraft through a parabolic climb and dive trajectory. G-169 produced one control specimen welded at 1g (denoted C1) prior to the KC-135 flights, three microgravity welded specimens (denoted M1, M2 & M3, chronologically), and after the KC-135 flights a second control specimen welded at 1g (denoted C2). For the microgravity welds, the operator manually started the payload's welding system just as the microgravity portion of the flight trajectory was reached, and manually stopped it as the microgravity portion was exited. This resulted in a weld of approximately 1.3 inch length along the 6.3 inch circumference of the tube. A strip chart recording of the three components of the effective gravity acceleration during each of the welds was provided by NASA MSFC. The major acceleration component for each of the three welds was as follows: M1 -- $(0.05 \pm 0.01)g$, M2 -- $(0.04 \pm 0.02)g$ and M3 -- $(0.08 \pm 0.06)g$. The acceleration trace was comparatively smooth during welds M1 and M2. During the M3 weld, however, the acceleration oscillated for four cycles about the average value, which was in itself approximately twice the acceleration level seen by M1 or M2. [3]

Analysis of G-169's specimens -- A visual comparison of the microgravity welds with the 1g control welds indicates no significant differences. Strip specimens were cut perpendicularly across each weld, taking care to select the central region of the microgravity welds. Metallographic examination reveal that the microgravity welds are microstructurally similar to the control welds, except for the sample from specimen M3 which shows an anomalous solidification pattern. Hardness indentations in the fusion zone and tensile tests were performed to compare mechanical properties and to attempt to quantify the cause of the unusual microstructure seen with specimen M3. Hardness values are the same for C1, C2, M1 and M2. But, for M3 the hardness is measurably greater. Room temperature tensile tests were performed on all samples to determine elongation, yield strength, and ultimate strength. The results (shown in figure-1) indicate essentially no difference in flow behavior or strength parameters. Fractography results were also comparable for both the control and microgravity samples. Although metallographic evidence and hardness results suggest a difference in weld M3, the important mechanical properties of M3 are still comparable to the control specimens'. One plausible explanation, for the metallographic and hardness differences, is that the relatively large fluctuation in acceleration during weld M3 caused some sort of "stirring effect" in the molten weld puddle which, in turn, influenced the microstructure during consolidation and hence the hardness. In summary, the significant conclusion to be drawn from these results is that GTAW in a microgravity environment should be able to produce satisfactory joints with mechanical properties comparable to those of terrestrial welds. If payload G-169 is ultimately flown on the shuttle, complete circumferential welds would be made in a more uniform microgravity environment and, thus, provide a more solid basis for the above conclusion. [3]

- **High Temperature Containerless Aircraft Furnace**

RI Rocketdyne Division, in cooperation with NASA MSFC, has modified and integrated a welding system into the NASA MSFC KC-135 Aircraft Microgravity Simulation Facility. The hardware comprising this microgravity welding system is known as the High Temperature Containerless Aircraft Furnace (HiTCAF). HiTCAF has been used to generate additional metallurgical data on melting and resolidifying of metal under the effects of microgravity. HiTCAF has also been used to demonstrate the feasibility of performing manned in-place tube welding and manual welding operations in microgravity. These NASA MSFC / RI Rocketdyne experiments mark the first time that American researchers have attempted manual welding tasks in microgravity and the first attempt by researchers of any nationality to perform manual arc welding tests in microgravity. The overall results of this research show that the GTAW molten weld pool, in microgravity, is "well behaved" with no tendency for metal expulsion or spatter, that the resulting joints' mechanical properties are comparable to those of 1-g joints, and that high quality manual welds can be performed in a microgravity shirtsleeve environment. [4]

VACUUM EFFECTS

The GTAW process requires a gas plasma, which serves as a medium for proper arc transfer between the electrode and work piece. This plasma is supplied on Earth by an inert gas (argon or helium) purge of the welding zone. Argon and helium also serve as shielding gases, which prevent the molten metal from reacting with the oxygen and nitrogen present in the terrestrial atmosphere. Obviously protection from oxidation and nitrogen poisoning is not required in the vacuum of space. However, the necessity for welding-arc transfer still remains. Due to the hard vacuum of space, conventional (as in terrestrial GTAW) introduction of an inert gas about the welding zone is impractical. Based on RI Rocketdyne experiments, the gas introduced conventionally into the vacuum is immediately dispersed in all directions, away from the gap between the electrode and workpiece. Consequently, ionization and arc establishment across the electrode gap is not achieved, and welding does not take place. (The arc can be forced to jump across the electrode gap with an increased voltage potential; however, the arc established in this manner is unstable and consequently unusable for quality welding.) Hence, a new method for plasma maintenance at the electrode gap is required to enable GTAW in the vacuum of space. [5]

- **Development of a Vacuum Arc Welding Patent**

Through IR&D, RI Rocketdyne has patented a method which allows maintenance of a stable and controllable GTAW arc in a vacuum. This method employs hollow tungsten electrode technology (see figure-2). The ionization gas (argon) is pumped through the hollow electrode at volume flow rates of less than 28 liters per hour (0.25 cf/h). This small flow rate is introduced at the tip of the electrode, where arc establishment is required. The arcing occurs primarily from the inside of the electrode hole, which superheats the ionization gas. This superheating combined with the pressure differential provided by the vacuum, accelerates the ionization gas to high enough velocities which overcome the vacuum's scattering force at the electrode gap. Moreover, the resulting welding arc is more constricted, yielding a more efficient and concentrated energy transfer to the work piece. Hence, deeper penetration welds, which are advantageous for thick structural joints, are achievable. Furthermore, when 28 l/h (0.25 cf/h) for the hollow tungsten process (used for arc ionization only) is compared to as much as 2,800 l/h (25 cf/h) with the terrestrial process (used also for shielding), the GTAW process consumables are reduced by 99% for vacuum welding. Hence the traditional draw back associated with GTAW, of expensive consumable transport into Earth's orbit, is eliminated. [1, 4, 5]

- **Reducing Hollow Tungsten Electrode Erosion**

A conventional nonconsumable tungsten electrode, which has been bored through its longitudinal axis with a small hole for plasma gas delivery, suffers from significant erosion when used in a vacuum. RI Rocketdyne, in cooperation with NASA MSFC, has managed to further develop the hollow tungsten electrode technology and reduce erosion to negligible levels. As a result, the hollow tungsten electrode has been modified into a hollow cylindrical ionization gas pressure chamber (shown in figure-2). The interior of the chamber provides a large surface area for the emission of electrons which form the welding arc. The flow of inert pressurized gas through this chamber inhibits vaporization of the hot electrode material. The outer end of the chamber forms an electrode disk which has a small orifice to release the inert gas and the arc. The electrode is held in a nonconductive cup, which confines the origin of the arc to the orifice; this prevents extraneous corona discharge to other spots on the outside of the welding torch. These features combine to reduce vacuum electrode erosion to acceptable levels. [6]

INTRA- / EXTRA- VEHICULAR ACTIVITY EFFECTS

In-space operations involve both intravehicular and extravehicular activities. Intravehicular activity (IVA) consists of operations which are performed inside the pressurized, thermally regulated, shirtsleeve environment of a space vehicle or station. The IVA environment only includes the effects of microgravity on the process and operator. On the other hand, extravehicular activity (EVA) consists of operations which are performed in the outside environment. This environment is much more challenging since it includes not only microgravity constraints, but also vacuum, temperature, and radiation effects on the process and operator. EVA effects on the operator become

significant due to the constraining life support systems. Therefore, robotic, teleoperated, and semi-automated systems may come into play for specific types of EVA welding operations. [7]

- **IVA Simulation**

Using the KC-135 Aircraft Microgravity Simulation Facility, RI Rocketdyne, in cooperation with NASA MSFC, has performed unprecedented manned orbital tube arc welding and manual arc welding experiments in microgravity, with results which are directly applicable to IVA operations (see above HiTCAF discussion under "microgravity effects"). The experiments' objectives were to achieve preliminary workload and dexterity studies for both semi-automated orbital tube welding and manual welding in the shirtsleeve IVA environment. The results were successful and showed no problems, due to a microgravity environment, in producing high quality GTAW joints. [4]

- **EVA Simulation**

RI Rocketdyne, in cooperation with NASA MSFC, contracted McDonnell Douglas Astronautics Company to simulate an EVA involving manual operations with a semi-automated orbital tube welding device. This evaluation was performed on McDonnell Douglas space station fluid line models, in their neutral buoyancy water tank facility, with a fully pressure-suited test subject. The results reaffirmed certain welding hardware design considerations for interfacing with the astronaut, and established time-line estimates for fluid line assembly by welding. No fundamental problems were evident with performing an EVA to support in-space semi-automated orbital tube welding operations. [4]

- **Design of an EVA Welding Experiment**

Funded by NASA's In-Space Technology Experiments Program over a twelve month period between 1988 and '89, RI Rocketdyne and the California Polytechnic State University of San Luis Obispo developed a detailed understanding, and designed a four hour Space Shuttle EVA welding experiment. The experiment design consists of both manual arc welding and semi-automated orbital tube arc welding tasks to be performed at a dedicated workstation mounted to the cargo bay sidewall of the Space Shuttle. The experiment is designed to provide the data necessary to complete development of a fully functional, highly flexible, in-space, EVA welding capability for assembly and repair of space based structures. Safety analyses, performed by NASA JSC Safety Division and Astronaut Office, found no prohibitive issues with the experiment design. However at this time, due to lack of funding, the experiment remains on RI's drawing board. [4, 8]

- **Development of Enhancement Technologies**

RI has and continues to develop a variety of technologies which should enhance in-space welding operations, especially for EVA. These technologies are primarily in the following areas: robotic, teleoperated, semi-automated and manual welding; real-time weld quality analysis and parameter control; hollow electrode filler wire feeding; and rechargeable battery powered welding.

Welding torch vision and data collection system -- RI Rocketdyne, in cooperation with NASA MSFC, has developed, employed and refined various welding torch vision systems for both open loop and closed loop operations. With advancing technology in video camera, fiber optic, lense, filtration, and electronic systems, effective real-time weld monitoring and control have been tremendously improved for remote and robotic welding operations. Viewing, through the welding torch, the magnified welding process' interaction with the workpiece, provides excellent feedback for real-time control, weld quality evaluation, and weld parameter development. A computer can also gather data from sensors while a video camera observes the weld in progress. The computer sends the data to a vision processor, which superimposes the data on the image from the camera. The operator, thus, can watch the weld bead simultaneously with the instantaneous values of such data as elapsed time, welding current, and processed sensor measurements of the weld area, such as weld back-bead width and depth of penetration, pool temperature, or top bead dimensions. The video image and superimposed data can be recorded on magnetic video tape. Consequently, the welding operation can later be reviewed in slow motion or even frame by frame. The pertinent data is always instantly available to the viewer and correlated in time with the image of the weld. In summary, implementing a welding torch vision system with a computer data collection and display system

may be critical for achieving successful in-space robotic, teleoperated, semi-automated, and even EVA manual welding operations. [9, 10, 11]

Welding with infrared thermography -- A high-resolution infrared imaging and image-data-processing system has been implemented as a thermography tool by RI Rocketdyne, in order to control welding parameters and to ensure reliable joints. The system displays a real-time image of the weld in which temperature gradients are characterized by colors. Consequently, welding defects, such as impurities, gaps, surface irregularities, porosity, and tungsten inclusions are evident from the thermographical signatures they produce. Furthermore, the system extracts data from the thermography image. This data may be processed to determine the degree of weld penetration and the effects of back-side cooling. Such a system combined with the welding torch vision and data collection system, described above, can become an effective real-time weld control and inspection tool for in-space robotic, teleoperated, semi-automated, and even manual welding operations. Employing such systems may also be valuable in developing proper in-space welding techniques and parameters, by building a data base from in-space welding experimentation. Lastly, infrared thermography of an EVA manual welding operation may become a critical monitoring and control tool for astronaut safety. [12]

Robotic welding with artificial intelligence -- For years, RI Rocketdyne has been developing robotic welding techniques for improving reliability, consistency, and efficiency of welded joints in rocket and space shuttle main engine manufacturing. Rocketdyne's efforts have been fruitful with many non-precedented achievements in robotic welding. These achievements are primarily based on artificial intelligence tools designed into robotic welding systems. The artificial intelligence tools, which have been implemented to various degrees in Rocketdyne's manufacturing lines, provide real-time automated monitoring and control capabilities of the welding process, such as weld seam tracking, weld penetration, bead height, welding current, arc voltage, wire feed rate, and travel speed. Using such technology seems imperative for the in-space environment, where manual monitoring and control are limited, and first-try acceptable quality welds are essential.

Filler wire feeding through tungsten electrode -- Filler wire feeding is necessary for welding thick joint members, gap bridging, and element reconstruction or repair. The hollow tungsten electrode technology opens new possibilities with filler wire feeding. Feeding the filler wire through the hollow electrode has been successfully applied by RI Rocketdyne in the terrestrial environment. A variety of advantages to welding in such a manner may be applicable to IVA and/or EVA in-space operations: Wire feeding is preheated and, therefore, can be fed at high speeds without spattering. High-frequency energy does not have to be supplied to the workpiece to initiate welding. The size of the arc gap is not critical; a power-supply circuit can adjust the voltage across the gap to compensate for changes. Only a low gas flow rate is needed. The welding electrode can be replaced easily as a prefabricated assembly. An external wire-feeding manipulator is not needed. Lastly, the welding process becomes more forgiving of operator error, and more tolerant of non-linear joints. [13, 14]

Rechargeable battery powered welding -- Development of G-169 as a GAS payload, required that the GAS canister contain the experiment's power source. This constraint drove RI Science Center's successful development of a welding system which is powered by a rechargeable battery pack. This technology achievement proves that in-space welding operations do not have to interfere with spacecraft power constraints, and are feasible with a rechargeable back-pack power supply at remote sites or during power-down contingencies. Battery pack performance with the GTAW process has a great potential for improvement using today's continuing technology advancements. [2, 7]

SPINOFF TECHNOLOGIES

Incorporation of the hollow tungsten electrode technology with the GTAW process, reveals spinoff applications for both in-space and terrestrial operations. Some of the in-space spinoff applications may become as important as welding and, therefore, may drive the design of an in-space welding system to also serve as an in-space surface treatment system, cutting torch system, and possibly a metal removal system.

- **Vapor Deposition of Metal**

A vacuum gas-tungsten-arc vapor-deposition process has been developed by NASA MSFC and RI Rocketdyne as a result of the hollow tungsten electrode technology breakthrough. The process yields highly reflective, smooth metallic films that reproduce almost perfectly the contours of the surfaces on which they are deposited. The rate of deposition can be controlled precisely, and the surface texture can be varied, if desired. The process is capable of deposition at rates double those of standard sputtering. This process may be applied in the making of thin metallic coatings, which can serve as electrical conductors, radio reflectors or antenna elements, and optical mirrors of partial or ultrahigh reflectivity. The potential for this surface treatment process to lend itself to in-space operations, such as refurbishing and repair of coated spacecraft elements which have been eroded by atomic oxygen bombardment, is compelling. [15]

- **Key Hole Cutting**

The vacuum GTAW system's use of a high velocity gas which transfers an arc from the hollow electrode tip to the workpiece is suited not only for welding, but for cutting as well. With a slight increase of the ionization gas's volume flow rate through the electrode, the consequent increase in the welding arc's pressure can penetrate the material thickness and produce key hole cutting. This spinoff has been experimentally demonstrated by RI Rocketdyne. This "extra feature" serves as a significant advantage for the space modified GTAW system; because it allows conversion (with a turn of a knob) of the welding mode into a cutting-torch mode. [5, 8]

- **Metal Removal**

In-space metal removal is a critical technology needed for fit-up problems and repair. Machining by grinding and chipless cutting creates debris and causes diffusion bonding. However, an improved technique has been proposed for metal removal using the hollow tungsten electrode technology. The metal to be removed would be melted with a welding arc from a hollow tungsten electrode, and then drawn off with a second hollow electrode. This approach would depend not on gravity to siphon or atmospheric pressure for force, but rather on microgravity capillary attraction which should pull the molten metal through the tube. Should such a process become workable, the benefits to be gained are enormous. [16]

FURTHER R&D REQUIRED

RI has come a long way in bringing about in-space arc welding technologies through both internal and NASA funded R&D efforts. However, the capability to perform construction and repair of metal structures in space, by welding, is still unavailable. Certain R&D must further take place in order to produce an effective in-space welding system, which may be applied by programs such as Space Station Freedom, Lunar Base, and Manned Mission to Mars. This further R&D should be based on experimentation using KC-135 microgravity simulation, Space Shuttle small autonomous payloads, and Space Shuttle IVA and EVA (see figure-4).

KC-135 SIMULATION FACILITY EXPERIMENTS

RI Rocketdyne has proposed, to NASA, the integration of a welding vacuum chamber into the KC-135 Microgravity Simulation Facility. Should such integration be accomplished, NASA MSFC's KC-135 will serve as a combined microgravity and vacuum simulation facility.

- **Hollow Tungsten Electrode Welding In Microgravity-Vacuum**

A KC-135 microgravity-vacuum simulation facility would enable first time testing of the vacuum modified GTAW process in microgravity, an essential step towards in-space arc welding capability. RI expects that further refinement of the potential in-space arc welding process would be accomplished, especially in controlling the interaction of arc force, ionization gas flow, and surface tension in the microgravity-vacuum. In addition, behavior of non-autogenous in-space arc welding, using filler wire feeding systems which lend themselves to both automated and manual operations, should be examined and refined in the simulated microgravity-vacuum environment .

- **Microgravity-Vacuum Orbital Tube Welding System**

Due to the attractive in-space applications for a semi-automated orbital tube welding system (see earlier discussion of G-169 specimen selection), it is desirable to extend the vacuum modification of the GTAW process to the orbital tube welding device. Such modifications are not as straight forward as those for a conventional GTAW torch, because the orbital tube welder consists of an electrode which is driven around the tube circumference by an orbiting gear system. The mechanical and fluid challenges, of integrating a hollow tungsten electrode and ionization gas delivery system into an orbital welding head, are considerably more complex. However, use of the KC-135 should assist in such development and testing of an in-space tube arc welding system. [8]

- **Spinoff Technologies In Microgravity-Vacuum**

Finally, RI should utilize the KC-135 simulation facility to expand on the spinoff technologies made available by the in-space arc welding process. These technologies, which include vapor deposition of metal, key hole cutting and metal removal, require further development and testing in the microgravity-vacuum environment. The KC-135 should help determine whether one versatile in-space metal processing system can be developed to perform a number of tasks including welding, surface treating, cutting, and metal removal.

SPACE SHUTTLE SMALL PAYLOAD EXPERIMENTS

KC-135 simulation of a microgravity-vacuum environment should be effective for most R&D and some testing of in-space metal processing techniques such as welding. However the KC-135 is only a simulation facility, and not the real thing. At some point along the development path of in-space welding or any other metal processing technique, we should experiment and demonstrate the process in the actual space environment. Using NASA's Shuttle Small Payload Programs, such as the Get Away Special (GAS), Complex Autonomous Payload (CAP) or Hitchhiker (HH), excellent experiment and demonstration platforms may be achieved with cost effective results.

- **G-169's Current Situation**

G-169, in its present (almost flight ready) configuration, is suffering from a variety of weaknesses, which include: overweight, outdated technology, marginal reliability, limited experiment value and lack of funding.

Overweight -- G-169 employs a single full size GAS canister with a 90.7 kgf (200 lb) weight limitation on the canister's contents. In 1990, the flight ready G-169 payload weighed in at 96.6 kgf (213 lb); 5.9 kgf (13 lb) over the limit. The payload was originally designed to weigh in at 86 kgf (190 lb) with an extremely dense and efficient package design. However, due to growing package integration complexity and NASA's post-Challenger shift to more conservative design requirements, G-169 gained weight mainly from battery box development and added structural supports. The 5.9 kgf (13 lb) cannot be trimmed from the payload without major redesign and development, and the 90.7 kgf (200 lb) limit cannot be waived due to strict GAS program guidelines.

Outdated technology -- G-169's welding system employs a modified ST International NIKA Power 100 (model 9101) computer driven, solid state, transistorized, welding power supply. This unit was developed in the early 1980's. With almost everyday advancements in electronics from the 1980's into the 90's, G-169's welding system has become an antique. The welding system is very difficult and expensive to maintain since many of its components are no longer readily available. In fact, G-169 has reached a point, where the welding manufacturer can no longer maintain the outdated system without rebuilding and upgrading it to today's technology level.

Marginal reliability -- Due to G-169's single, full size, canister volume limitation of 141.6 liters (5 cu-ft), no redundancy could be built into any of its systems. One canister provides just barely enough volume and weight capacities for a basic welding experiment. For example, should welding arc strike fail (a common phenomenon), the arc strike is automatically re-attempted a couple of times, but with the same electrode; usually arc strike fails due to a problem with the electrode itself. At least two welding heads, with one specimen each, would provide much greater odds for experiment success, and most likely additional data. Further more, G-169's extensive battery-pack has ample capacity margin for welding in room conditions with a fully charged bank (4 times). However, welding at a typical 0°C environment after 3 unattended months reduces the battery capacity by almost 50% (assuming batteries are in ideal condition), leaving only twice the required capacity. Such an experiment should realistically have a

higher capacity margin to ensure good results. In addition, the shielding inert gas supply system could use some redundancy in its design to ensure best welding results. Lastly, the welding system's numerous electronic components are marginally reliable when faced with a harsh vibration environment. Many of the components are potted, but not all. A shake table test of the payload (after its KC-135 flights) caused some breakage in the welding system's electronics.

Limited experiment value -- G-169's three successful runs aboard NASA's KC-135 Microgravity Simulation Facility and additional microgravity welding investigations using HiTCAF have yielded some good factual data, showing that microgravity effects on the welded joint's mechanical properties are negligible. Additional data, especially from a zerogravity environment, would be beneficial but not crucial. The "green light" for progressing further towards microgravity-vacuum welding experiments has already been given by the KC-135 results. Hence, flight of G-169's current configuration aboard the Space Shuttle, with its marginal reliability, no longer justifies the cost of preparing its welding system for flight.

Lack of funding -- With today's troubled economy and tight aerospace budgets, it has become unrealistic to fund G-169's final preparation for flight aboard the Space Shuttle. G-169's current configuration does not warrant any further expenditure of RI IR&D funds. The only hope remaining for G-169 is its reconfiguration, as part of a large NASA R&D contract for a series of strategic welding experiments leading to eventual development of an in-space welding system.

• **Lessons to Be Learned from G-169**

G-169's current configuration should be viewed as a prototype which has provided rich hands-on experience to university students, three microgravity welded specimens, a battery powered welding system, and numerous lessons to be applied on future similar payload systems. Each of G-169's phases of "life", including payload design, development, integration, testing, safety approval process and KC-135 flights, teaches some valuable lessons for future endeavors.

Payload design, development, and integration -- Before spending time, excitement, and effort on the payload package design, one should take the time to research and understand all the NASA requirements which the design must satisfy. The designer should understand the fault tolerances required by safety for each of the various systems. A layout of all the requirements on the drawing board is advisable. For example, if one overlooks that two pressure relief valves rather than one are required in the plumbing system, once the payload is completed NASA may catch it in a final inspection, even though they should have caught it in the early design stage. A complete design job up-front will save significant time, money, and frustration down the line; it may even make the difference between success or failure. A 3D CAD system can allow complete construction and development of the payload on "paper" without making any commitments. Such detailed development up-front should also allow accurate determination of expected payload weight. Exact weight determination, after the payload is fully built, may be too late.

When designing the payload's support structure, one should keep in mind that structural strength under compression and tension is important, but does not guarantee structural rigidity. The payload structure should be sufficiently rigid so as not to sag in a launch configuration. Moreover, the support structure should be designed to accommodate some location shifting of payload components during integration.

Employing a modular approach to the design of the payload systems may add extra weight and use more volume, but modularity provides tremendous benefits and possibilities throughout payload development, integration, testing, trouble shooting, and repair. Modular systems should be removable from the payload by simple disconnection of structural supports and single input and/or output power, control and/or fluid lines. Use of commercially available, off-the-shelf components lends itself well to a modular design approach. Components, such as a welding system that employs complex electronics, may require regular maintenance and repair. These type of components should not be reconstructed on a payload's structural shelf. Rather, their inherent off-the-shelf modularity and design should be maintained to allow easy servicing by the manufacturer. Furthermore, systems with electronics may become outdated and unserviceable within the payload's active life-span. Therefore, modularity allows relatively easy system replacement or upgrade.

Design of the payload's rechargeable battery power supply, should make provisions to allow for easy switching from payload autonomous power to bench supply power. Reliable bench supply power, simulating the battery pack, is important for payload systems development, integration, and checkout.

Payload testing -- During payload testing, which may occur throughout development, any use of rechargeable batteries should be carefully documented. Detail of battery performance (potential, current, power) before, during, and after each use, and in between charging periods should be recorded. One should construct a detailed history of the batteries' performance to determine proper care (through proper charging and discharging), and to determine reliability for the eventual flight. Furthermore, testing the battery pack's performance at 0°C, after a three month shelf period at room temperature, may be necessary to ensure payload performance during flight.

Vibration testing of the payload's structure, should be set apart from vibration testing of the remaining payload systems. The payload structure should be rugged enough to handle any of the NASA suggested vibration tests, which usually depict Space Shuttle crash landing loads. However, non-structural payload systems do not need to be subjected to vibration intended for structural testing. It is not important whether the payload can run its experiment after a crash landing of the Shuttle. But, it is critical that the payload won't structurally fail and propagate additional damage to the Shuttle in a worst case scenario. Therefore, one should use common sense and realistic launch vibration tests for the payload's electronics, mechanisms, and other sensitive non-structural components; otherwise, such components may break needlessly and set back schedules.

Should any special testing of the payload or its systems be required, such as a battery box or plumbing system proof pressure tests or an EMI test, make certain that NASA provides exact testing requirements (in writing). The standard provided literature, such as safety manuals or experimenter handbooks, may not have reliable or sufficiently detailed requirements. It can become very frustrating and costly when the safety approval process decides that some of the testing parameters or methods used are unsatisfactory.

Finally, if your testing results are marginal, it is usually easier to redesign, enhance, or fortify the system or component rather than battle the NASA safety organization for their approval.

Payload safety approval process -- For a payload with an inherently hazardous experiment, such as welding with G-169, the NASA safety approval process may become one of the toughest obstacles to cross. There appears to be some undefined requirements, inconsistent rationale, personal policies, and changing political tones which shape the progression of the safety approval process. The process itself may be clear and defined, but the safety people, who make the decisions along the process path, may be replaced by others somewhere along the way. Such situations may lead to inconsistencies. With G-169, the safety approval process began before the Challenger Accident, which drove many changes throughout Space Shuttle programs, including GAS. Consequently, G-169 experienced a roller-coaster ride; decision making people at NASA changed and so did their policies.

Early design decisions, which evolve into built products, may be reversed leading to set backs, hardships and additional incurred costs for the payload user. Be-aware, the Space Shuttle program is not a commercial airliner. The Shuttle program is still experimental and probably will always be so. The Shuttle's design lends itself to constant experimentation and uncertainties. In this day and age of un-assured access to space, the Space Shuttle is a treasure and the chance to use it is a privilege, which the payload user should not expect, even if the price to fly is paid. In order to fly a payload on the Shuttle, one must expect the unexpected in the safety approval process. Only those payload users, who are lucky or persist and have enough money to keep up with set backs, will get the chance to fly.

The payload user should try to treat the relationship with NASA, as a relationship with a contractor. The user is the paying customer. NASA is the delivering contractor. It is true that this relationship is not straight forward due to reasons mentioned above. However, by keeping tabs on all agreements reached, especially early in the design process, including record of dates, names, and exact agreement context, the payload user has a better chance of protecting the payload from set backs later down the "dark" path of the safety approval process.

When formulating hazard inhibits and safety controls, similarity analyses should be avoided. Similarity analyses are prone to personal interpretation and refutation. NASA safety may easily dismiss such analyses. Furthermore, the GAS canister should provide the payload user with some basic hazard inhibit backups, such as containment of some loosened components, pressure system failures, explosions, shrapnel, temperature

extremes, and chemical spills. However, the canister's quantitative containment capabilities are not well determined or accepted by NASA as valid inhibits.

KC-135 flights -- In G-169's case, the KC-135 flight proved to be valuable. It enforced testing of the payload system in full flight configuration (with the exception of the GAS canister shell). Consequently, several software "bugs" were detected with the welding system, which were invisible to the bench tests. The software was corrected, and three successful KC-135 flights ensued. However, it was evident that a Get Away Special experiment like G-169 is not meant to efficiently utilize the capabilities of the KC-135 Microgravity Simulator. Due to turbulence or imprecise flight control, the simulated microgravity of 20 seconds per run, at times, may be "rough" (with minor induced g-loads). Thus, the KC-135 program is designed to repetitively run an experiment as often as 40 times per day, 4 days per week, for a total of approximately 160 runs per week. Only with such repetition, can large amounts of high quality microgravity data be gathered. The G-169 payload requires some disassembly for sample removal and replacement, can only sustain power for 4 consecutive experiment runs, and requires almost two full continuous minutes of microgravity for full weld completion; hence limiting the utility of the KC-135. To summarize, the KC-135 may be useful in experiment testing and debugging, and can also yield some useful microgravity data.

Shuttle Side-Wall Autonomous Metal Processing Payload

RI should utilize its G-169 and G-170 Shuttle Small Payload reservations for development of a new dual-canister payload system, which may become known as the Shuttle Side-Wall Autonomous Metal Processing Payload (SSWAMPP); in hope that it should "swamp" the space program with a variety of in-space metal processing techniques. SSWAMPP should be developed to serve as a reliable, versatile, automated experiment and demonstration platform for in-space welding and other potential in-space metal processing techniques, such as metal vapor deposition, metal cutting, metal removal, and even pressure vessel metal casting [16]. SSWAMPP should be designed to support an extensive series of flight experiments, which may include the following phases:

<u>PHASE</u>	<u>PAYLOAD DESIGNATION</u>	<u>EXPERIMENT OBJECTIVE</u>
I	G-169 / G-170	payload system flight test with zerogravity-one atmosphere orbital tube arc welding
II	G-XXX / G-XXX+1	zerogravity-vacuum bead-on-plate arc welding
III	G-XXX+2 / G-XXX+3	zerogravity-vacuum orbital tube arc welding
IV	G-XXX+4 / G-XXX+5	zerogravity-vacuum metal vapor deposition
V	G-XXX+6 / G-XXX+7	zerogravity-vacuum key hole metal cutting
VI	G-XXX+8 / G-XXX+9	zerogravity-vacuum metal removal
VII	G-XXX+10 / G-XXX+11	zerogravity-vacuum pressure vessel metal casting

The proposed SSWAMPP design consists of two GAS canisters which are coupled via power, control, data, and fiber optic video lines. One of the canisters serves as the Power-Monitor Can, while the other is the Metal Processing Chamber Can (see figure-3).

Power-Monitor Can -- The Power-Monitor Can is designed to provide experiment power, control, and data retrieval. Elements, including a large rechargeable battery pack (with redundant capacity), a power inverter, a programmable computer controlled power supply with data storage capabilities, and an infrared thermography image processor and video recording device, are all integrated via a modular approach into one full size GAS canister. The canister is pressurized with nitrogen to terrestrial atmospheric pressure. The Power-Monitor Can is designed to

retain a constant hardware configuration, while software changes are easily made, in support of a variety of metal processing experiments.

Metal Processing Chamber Can -- The Metal Processing Chamber Can houses and safely contains the automated metal process experiments. Elements, including specimens, hollow tungsten electrode devices (i.e. welding torch), ionization gas supply system, and a Freon active cooling system, are all integrated via a modular approach into one full size GAS canister. The canister can be pressurized with nitrogen to simulate the terrestrial atmosphere or left open to ambient pressure. The Metal Processing Chamber Can is designed to support data collection sensors, such as accelerometers, barometers, video cameras, and infrared fiber optic receptors. The full size GAS canister also provides sufficient space for redundancy built into the elements described above; at least two specimens are each supported by their own dedicated systems.

- **Benefits of Dual Canister Payload Approach**

After carefully examining the experiences and lessons learned from G-169, a dual canister payload approach seems to provide the needed resources for achieving an effective in-space metal processing experiment platform such as SSWAMPP.

Improved modularity -- Two canisters force a natural split of the overall payload system into two modular parts; for example, a power, control, and data collection module coupled with an experiment chamber module. The double volume and weight capacity, offered by the dual canister approach, also allows modularizing of the individual payload systems within each canister. Rather than integrating the systems into a closely packed and inter-meshed "jungle" of wires, cables, mechanisms, fluid lines and alike, with a dual canister approach one can afford to be more organized and neat. Organization of the separate systems into compact individual modules, which can be easily removed from the payload package for maintenance, repair, upgrade or even last minute replacement with a spare, may prove to be invaluable; especially if the payload system may be re-flown to support a continuing series of experiments. Modularity prevents "ripping" the entire payload package apart to fix a problem, especially during development. Modularity also lends itself to simpler bench tests and locating of problem origins. Further more, development and successful use of generic modules, such as for power, control, or data collection, may generate a commercial market for the benefit of the Shuttle Small Payload user.

Less failure propagation -- The basic modularity established by the two canisters, and any further modularity within the canisters themselves should result in a less complex and inter-meshed system. Consequently, a failure within a particular module should remain localized and not propagate into additional system failures, due to close system packing. Protection of an individual module from an adjacent module failure becomes simpler by shielding each module from electrical surges, temperature extremes, chemical spills, foreign objects, and/or debris collision.

Higher reliability -- With the double volume and weight capacity, offered by the dual canister approach, redundant systems can be more readily employed to ensure return of at least some flight results. Systems such as power, control, data collection, experiment process, and specimens can all be duplicated to some extent and set apart as independent redundant systems.

More experiment capability -- With the added volume and weight capacity available for more extensive power supply and experiment apparatus, additional specimens can be flown and experimented with. This provides not only for redundancy, but also for added variability with experiment parameters. As an example, added variability for the welding experiment may mean some variety among specimen materials, welding schedules, and/or plasma gas mixtures.

Two separate environments -- With two separate payload canisters, at least two separate environments are easily achievable. For example, the welding experiment can employ a nitrogen pressurized canister for the electronic systems, which normally are not designed to operate in a vacuum, and a non-pressurized (ambient) canister for the in-space welding process, which is to be tested in a vacuum.

IVA AND EVA EXPERIMENTS

Space Shuttle small autonomous payloads would allow us to safely experiment and contain the in-space welding process, without the involvement of human factors. However, human factors eventually have to become an integral component of maturing in-space technologies, such as welding. Consequently, both IVA and EVA experimentation would be required to demonstrate the practical application of in-space welding and any spinoff in-space metal processing technologies.

Spacelab IVA Glove-Box Experimentation

The Space Shuttle program's use of the Spacelab laboratory module is tailored for purposes such as glove-box manual or semi-automated welding experiments, simulating IVA applications. An upgraded, space qualified derivative of the KC-135 glove-box experiment set-up may be designed for integration and flight aboard Spacelab. Demonstration of arc welding, in both the manual torch and semi-automated orbital tube modes, should be attempted in a pressurized glove-box, as well as in vacuum. In addition, demonstration of spinoff technologies, such as metal vapor deposition, key hole cutting, and metal removal, should also be attempted. Spacelab experiments would allow highly controlled in-space testing of the resulting technology, developed through the KC-135 microgravity-vacuum simulation laboratory and the SSWAMPP.

Cargo Bay EVA Experimentation

The ultimate phase in experimentation, demonstration, and application of an in-space welding capability and other potential metal processing options, is taking these new construction and repair techniques outside of the spacecraft into the EVA environment. A detailed design of a Space Shuttle cargo bay experiment has already been developed (discussed above). An EVA experiment set-up would require a specialized work station and a variety of enhancement tools and safety features to support the astronaut with such new and relatively hazardous metal processing operations. Tools, such as the RI developed welding torch vision and infra-red thermography systems, may become integral safety and data collection elements of an EVA welding experiment. Combining SSWAMPP hardware, existing Hitchhiker hardware elements (such as the SPOC adapter, SPOC mounting and cooling plates, and SPOC avionics units), and existing EVA hardware (such as foot and other body restraints), is all entirely possible. Many of the resources needed to perform EVA experimentation with potential in-space metal processing technologies, such as welding, already exist.

CONCLUSIONS

Welding is a hazardous and challenging operation to master. However, the benefits to be gained from welding capability are tremendous and continue to prove themselves time and time again in terrestrial production and repair of buildings, automobiles, ships, submarines, aircraft, and spacecraft. Just about any system employing metal structure, also employs welding as the joining method for that structure. There is no denying that welding is our most advanced and practical building methodology on Earth. We have even found ways to weld under water, in the oceans, where undersea settlements are already occurring. Consequently, it is only natural that we should find a way to extend this terrestrial methodology into space, as we begin to make our way into this next frontier which we are also bound to settle.

Today, in-space operations are restricted to tasks which on Earth are relatively simple to perform (excluding microgravity assisted tasks). Welding on Earth is not a simple task, and consequently in space it may become far more complex than its terrestrial counterpart. However, in-space welding can become a reality. It just takes development of appropriate technology. Of course, development of such technology requires time and money. The time will come, and money will be appropriated. In fact, the Soviet (now Russian) space program has already made the time and invested the money into a proven EVA electron beam versatile hand tool, which can weld, vapor deposit metal, and cut. Moreover, cosmonauts have already found practical applications for this tool during an EVA repair of the MIR space station. It is only prudent to conclude that NASA should at least have similar repair capability.

RECOMMENDATIONS

We are entering an era of imminent and permanent space exploration, habitation, and cultivation. The need for in-space welding and other metal processing technologies has already been clearly defined by NASA and demonstrated by the Soviet (Russian) space program. It is time for NASA to authorize its contractors, like Rockwell International, to develop the technologies required by NASA's upcoming, and already beginning, ventures. In-space welding technology is in Rockwell's reach. Rockwell International divisions, such as the Science Center, Rocketdyne, and Space Systems, should work together and complete the development of an in-space welding system with options for other in-space metal processing capabilities. NASA resources, including the KC-135 Microgravity Simulator, Space Shuttle Small Autonomous Payloads, and Space Shuttle IVA and EVA, should all be strategically employed to develop in-space metal processing capabilities, such as welding (see figure-4).

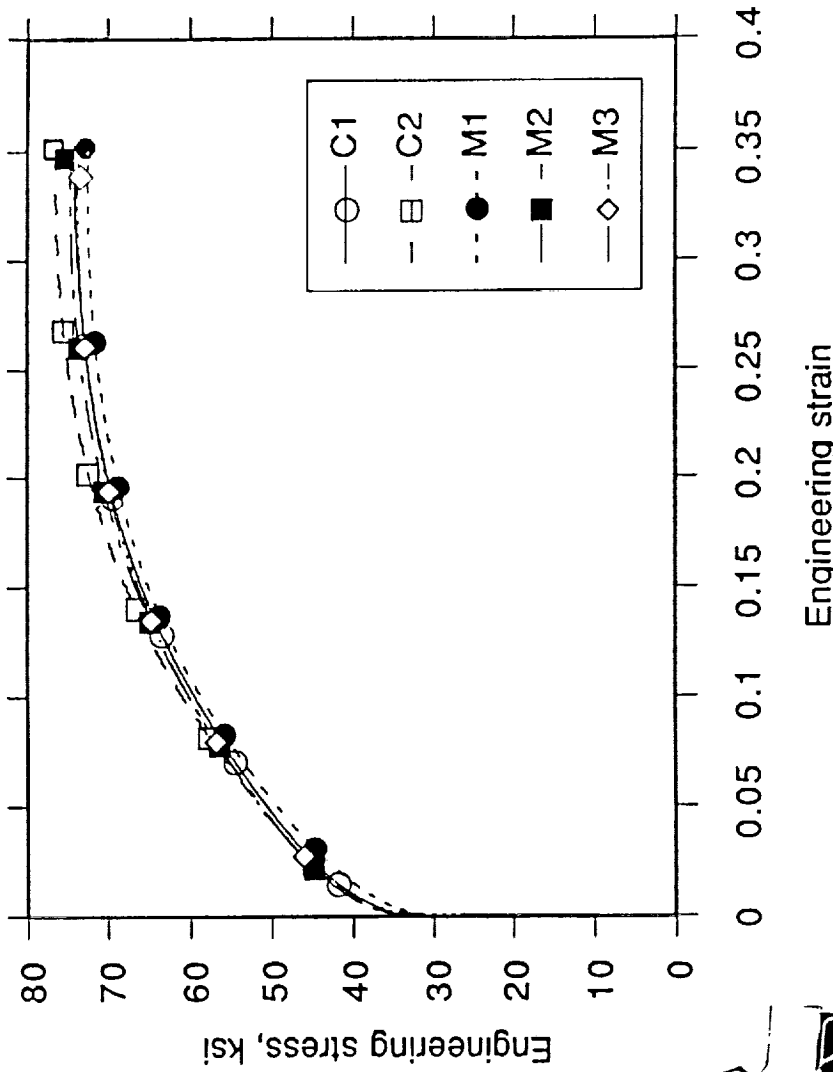
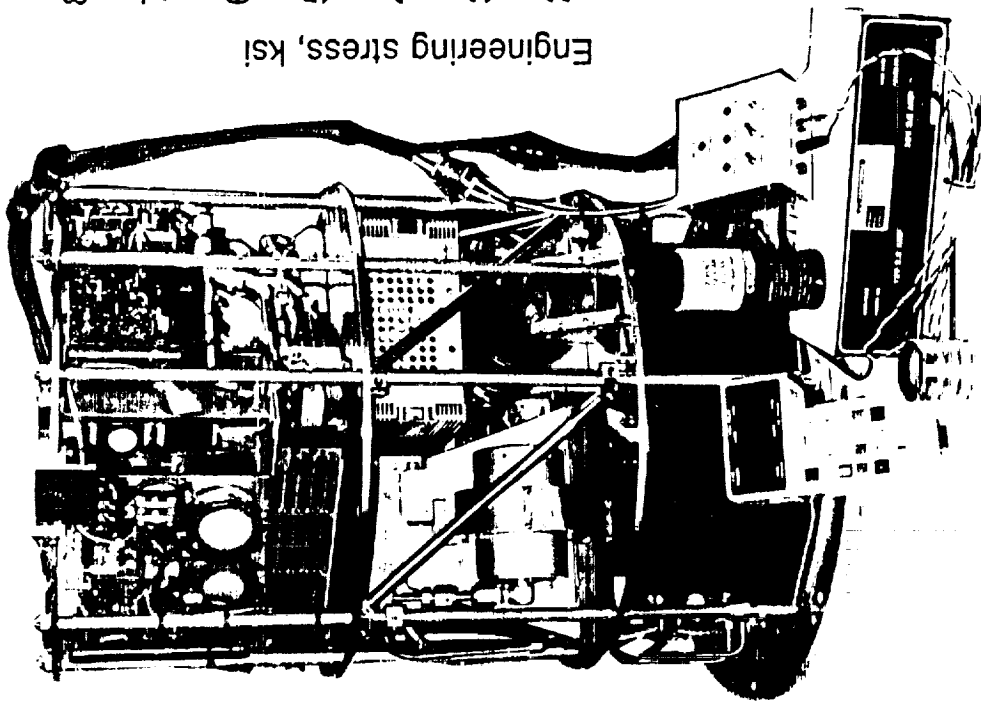
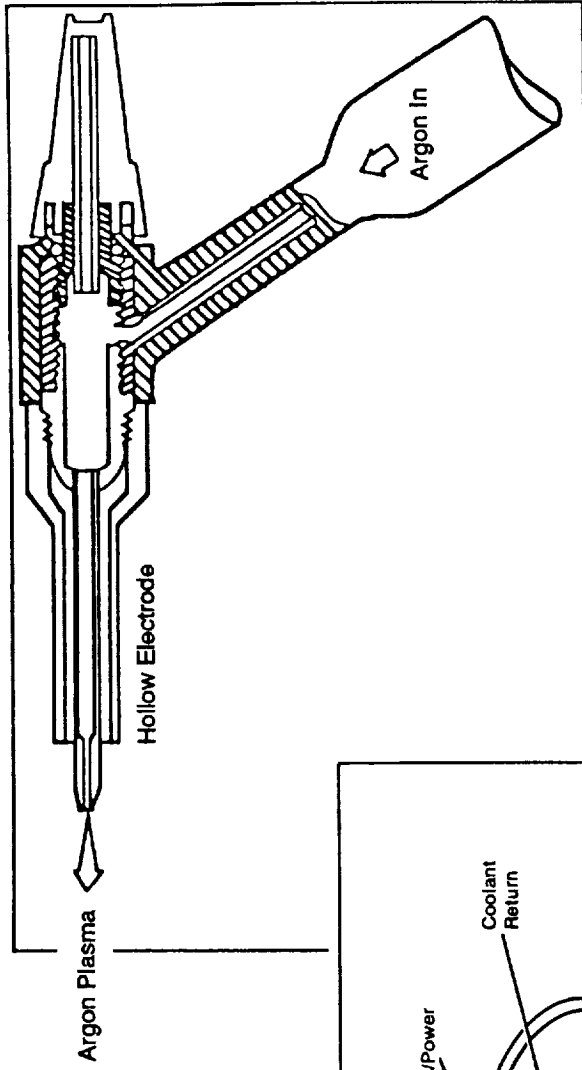


Figure-1: G-169 Get Away Special In-Space Welding Shuttle Payload with KC-135 Microgravity Flight Results.

Flow stress behavior of welded 316L stainless steel, show essentially identical properties for control samples (C1 & C2) and microgravity samples (M1, M2, & M3).
 (Courtesy of Rockwell International Science Center Division IR&D)



Rocketdyne Vacuum GTAW Torch

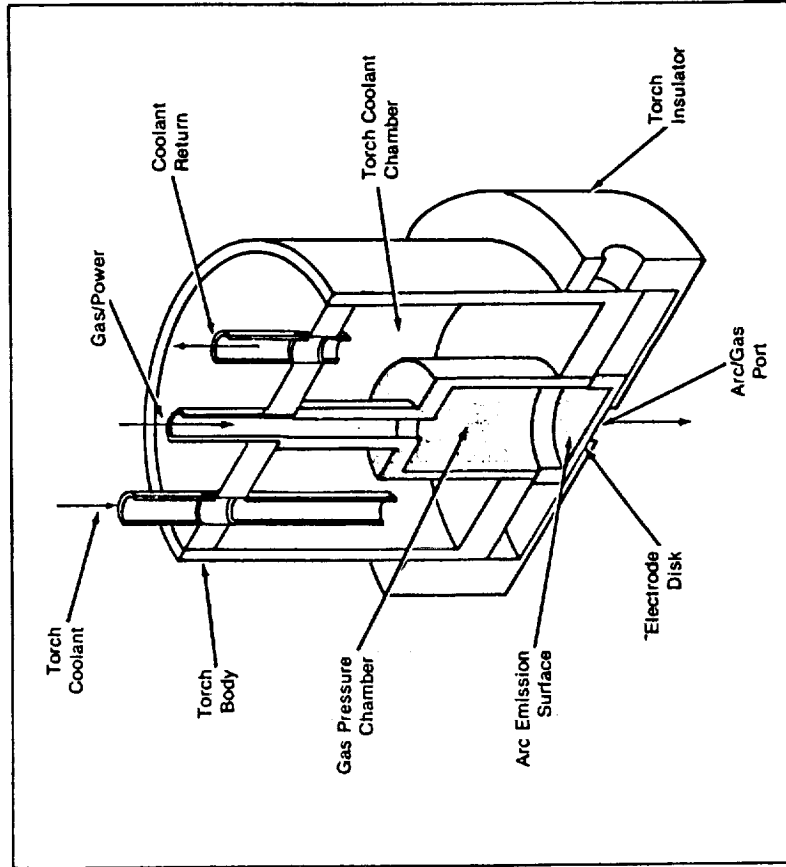


Figure-2: Hollow Tungsten Electrode Patent for Vacuum Gas Tungsten Arc Welding

(Courtesy of NASA Marshall Space Flight Center and Rockwell International Rocketdyne Division R&D)

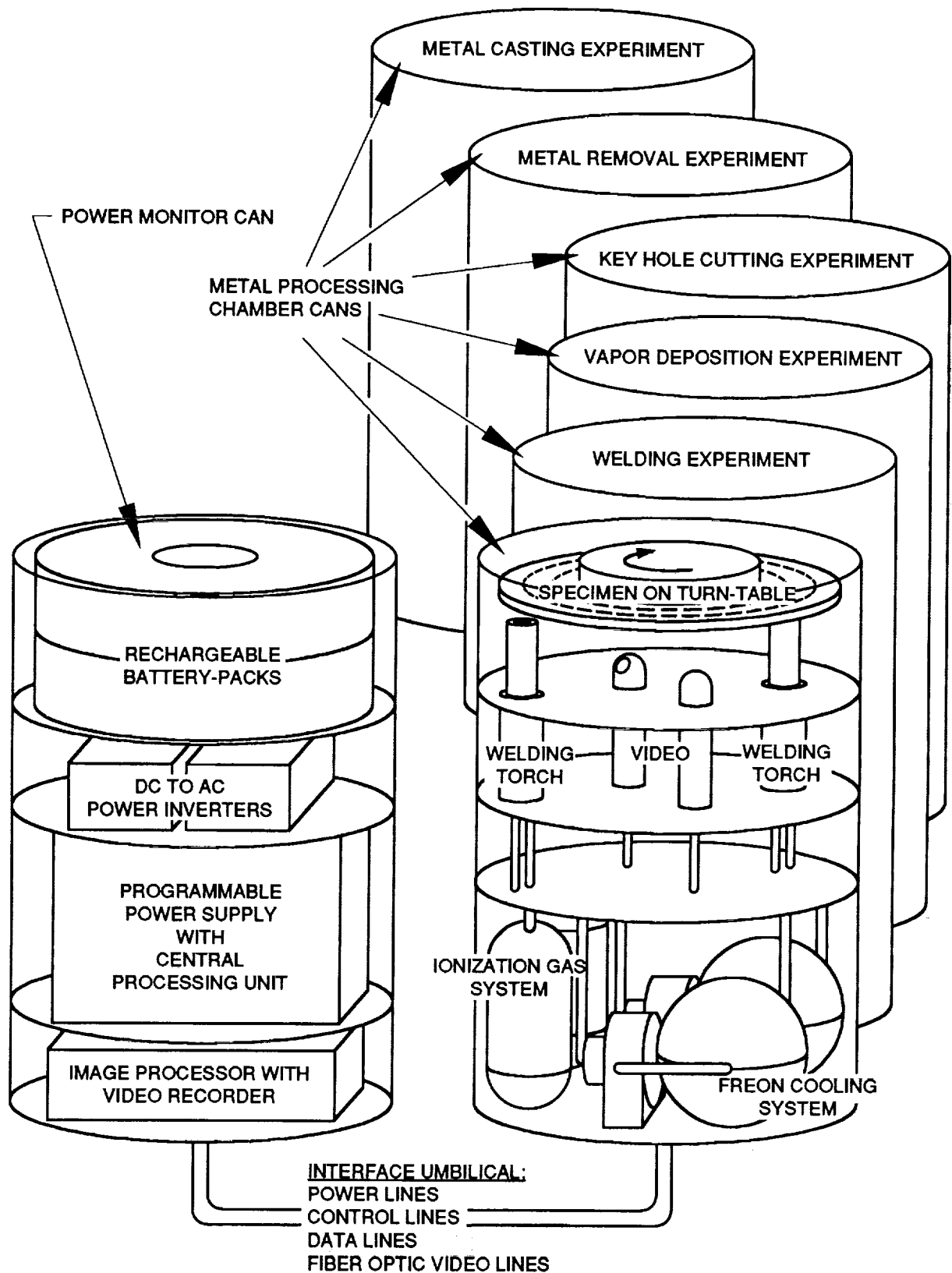


Figure-3: Shuttle Side-Wall Autonomous Metal Processing Payload (SSWAMPP) Series, Using Dual GAS Canister Approach
 (Courtesy of Rockwell International Space Systems Division)

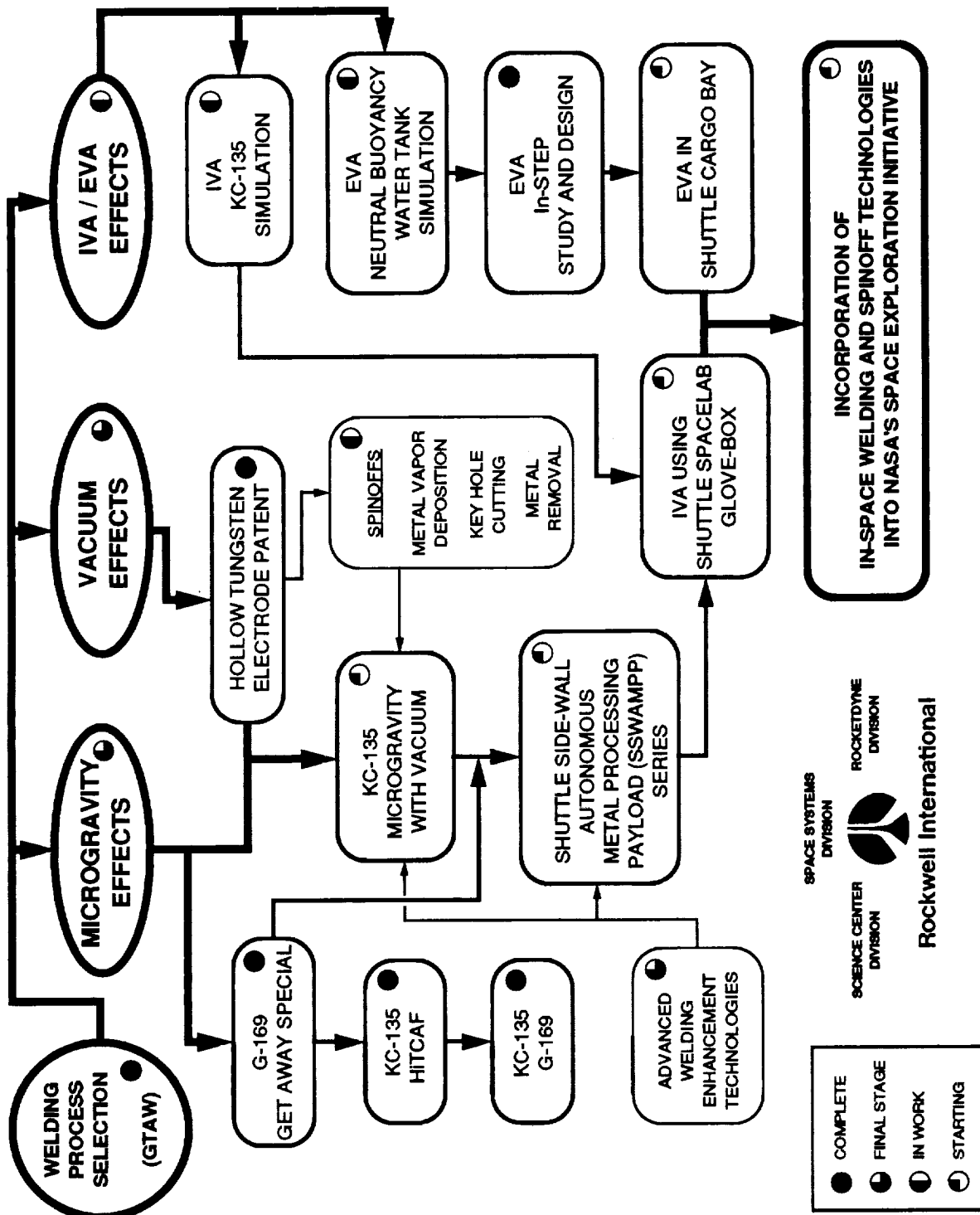


Figure-4: Proposed Rockwell International Path to In-Space Welding and In-Space Metal Processing Spinoffs

REFERENCES

- [1] Tamir, D. and Franklin, K., "Development of a Terrestrial Welding Process for Space-Based Applications," presented to California Polytechnic State University San Luis Obispo, March 1989.
 - [2] Tamir, D., "Phase-III G.A.S. Safety Data Package for Payload G-169," presented by Cal Poly Space Systems to NASA Goddard Space Flight Center, 1989.
 - [3] Muir, A. H. Jr., "FY '91 IR&D TECH PLAN: Materials Processing in Space -- Welding in Microgravity", Internal Rockwell International Science Center Report, 1991.
 - [4] Watson, K., "Extra-Vehicular Activity Welding Experiment Final Report," prepared by Rockwell International Rocketdyne Division under NASA contract NAS8-37753, Aug 21, 1989.
 - [5] Gordon, S., "Development of GTAW Welding Process for Welding in a vacuum", Internal Rockwell International Rocketdyne Division Report, 1987.
 - [6] Weeks, J. and Poorman, R., Rockwell International / NASA MSFC, "Long-Lived Electrode for Arc Welding in Vacuum," NASA Tech Briefs, Feb 1992.
 - [7] Tamir, D., "In-Space EVA Welding," presented to Florida Institute of Technology Space Systems Graduate Program, Jun 1, 1992.
 - [8] Tamir, D., "Extravehicular Activity Welding Experiment," prepared by Cal Poly Space Systems for Rockwell International Rocketdyne Division under NASA contract NAS8-37753, Aug 2, 1989.
 - [9] Gangel, K., Rockwell International, "Smaller Coaxial-View Welding Torch," NASA Tech Briefs, Dec 1991.
 - [10] Gilbert, J., Rockwell International, "Beam Splitter for Welding-Torch Vision System," NASA Tech Briefs, May 1991.
 - [11] Delcher, R., and Smith, M., Rockwell International, "Monitoring Welding Images and Data Simultaneously," NASA Tech Briefs, Aug 1991.
 - [12] Gilbert, J., Lucky, B., Spiegel, L., Hudyma, R., Rockwell International, "Infrared Thermography for Welding," NASA Tech Briefs, Feb 1992.
 - [13] Gilbert, J., Rockwell International, "Diamond-Coated Wire-Feeding Nozzle," NASA Tech Briefs, Nov 1991.
 - [14] Gilbert, J., Rockwell International, "Fast, Nonspattering Inert-Gas Welding," NASA Tech Briefs, Feb 1991.
 - [15] Weeks, J. and Poorman, R., Rockwell International / NASA MSFC, "Vapor Deposition of Metal from Gas/Tungsten Arc," NASA Tech Briefs, Jun 1992.
 - [16] Flanagan, L., Rockwell International Rocketdyne MSFC Technology Support, "Space Fabrication," presented to SAMPE, 1990.
- Tamir, D., "The Potential of a G.A.S. - Can with Payload G-169, Rockwell International Corporation / Cal Poly Space Systems, Space Welding Project," 1988 Get Away Special Experimenter's Symposium, NASA Conference Publication 3008.

A Payload to Evaluate Photodiodes for the Detection of Soft
and Hard X-rays in a Space Environment Using a Get Away
Special

by

Upendra D. Desai
NASA Goddard Space Flight Center
Greenbelt, Maryland 20771

AmyElizabeth C. Stewart
University of Maryland
College Park, Maryland 20742

Abstract

We propose to use the Get Away Special (GAS) facility to evaluate P-intrinsic-N (PIN) detectors and avalanche photodiodes (APDs) for the detection of both solar and non-solar soft and hard x-rays. We would like to fly both types of silicon detectors for the direct detection of the x-ray photons in the energy range from 1 to 30 keV with an energy resolution of about 1 keV. We would also like to use both types of photodiodes viewing CsI(Tl) scintillators to extend the energy range up to 1 MeV with ~6% resolution at 660keV. Solar flares would be detected with this instrumentation during periods of solar pointing providing high energy resolution spectra with high time resolution. Similar data would be obtained in the scanning mode on non-solar transient and steady x-ray sources with the same instrumentation. A commandable door over the detectors would be required to allow measurements to be made as low as 1 keV.

Introduction

The Get Away Special offers a unique opportunity to evaluate state-of-the-art technologies for scientific satellite instrumentation. This is particularly true for the evaluation of new detectors in a space environment. The new solid-state silicon photodiodes now becoming available offer the capability of high-resolution x-ray detection with significant reductions in weight, volume, and power requirements compared to those of conventional detector systems. New detector systems can now be incorporated for soft and hard x-ray measurements of both solar and non-solar sources. PIN photodiodes and the recently developed APDs offer significant advantages over presently used detector systems. For soft x-rays (1 to 20 keV), the conventional detectors used in space research are gas-ionization chambers, proportional counters, scintillation counters, or solid-state detectors. The ion-chamber and proportional counters have been used very successfully. They offer large area, good efficiency, good spectral resolution and imaging capability but do not offer long-term stability. Their response time also is limited. Scintillators have been used in conjunction

with photomultipliers and they have characteristics similar to those of the ion-chamber proportional counters. Among the solid-state detectors (conduction counters) lithium-drifted silicon detectors (Si(Li)) have significantly improved energy resolution and high counting rate capability, but they need to be cooled to 100K.

In 1980, Kemmer¹ reported the fabrication of silicon radiation detectors by the planar process using photoengraving. He also used oxide passivation to significantly reduce detector noise caused by surface leakage currents and achieved low reverse-bias diode leakage currents of $\sim 10\text{nA}$. Another technique used was ion-implantation which achieved a good yield in detector fabrication with uniform characteristics. Detectors fabricated with this technology were marketed in France in the early 1980's, but their high cost and high power requirements constrained their use.

The availability of large-area, low-cost PIN diodes and low-noise, low-power, charge-sensitive pre-amplifiers from various vendors have triggered new interest in PIN silicon diodes for their use in soft x-ray investigations². Avalanche-mode operation of large-area silicon photodiodes has also stimulated new interest in the use of silicon detectors for soft and hard x-rays.³ For low energy x-rays (1 to 20 keV), the silicon diodes offer simplicity, low power and high spectral resolution and they operate at room temperature. Furthermore, their fast response time ($\sim 50\text{ns}$) offers a high counting rate capability.

For hard x-rays (20 to 500 keV), scintillators viewed by photomultipliers have been used in space-borne instruments. The low-noise, high-gain capability of the photomultiplier and high detection efficiency of conventional scintillators (NaI, CsI) have proved very useful. However, even the ruggedized photomultipliers need careful packaging and handling, they are sensitive to external magnetic field variations, they need highly stable high voltage supplies, and they are bulky. Avalanche silicon photodiodes offer the possibility of replacing the photomultiplier for viewing NaI or CsI scintillators. The optical frequency response of silicon PIN diodes and APDs is wide (350 to 1100 nm) and matches very well with the CsI(Tl) scintillator emission spectrum. They have a much higher quantum efficiency ($\sim 60\text{-}70\%$) compared to photocathode quantum efficiency ($\sim 10\text{-}15\%$). Thus photodiodes have much better spectral resolution capability than photocathodes. Their usage as a replacement for photomultipliers would offer significant reductions in weight, volume, and power, with improved long-term stability for space-borne x-ray instrumentation.

Devices

Over the last two years we have procured and evaluated several PIN and APD devices for the direct detection of soft x-rays and as photomultiplier replacements in scintillation hard x-ray detectors. Table 1 lists the devices that we have tested and their manufacturers. We have used commercial charge-sensitive pre-amplifiers and monitored the spectral response of some of the devices.

Figure 1 shows the response of a typical PIN device. The resolution at the 5.94 keV ^{55}Fe line is ~ 1 keV at room temperature. For PIN devices, the energy threshold can be set at ~ 2 keV when operated at room temperature and used with a commercial charge-sensitive preamplifier.

Figure 2 shows the spectral response of an APD (1 cm x 1 cm) to the ^{55}Fe line. Figure 3 shows combined ^{55}Fe and ^{241}Am spectra taken with both APD and PIN devices. The internal gain of APD's result in a very low noise level allowing the energy threshold to be set as low as ~ 1 keV when operated at room temperature. Figure 4 shows the spectrum from an APD coupled to a CsI(Tl) scintillator exposed to a ^{137}Cs source. We get $\sim 6\%$ resolution at 662 keV with an energy threshold of ~ 30 keV at room temperature.

Payload Concept

We propose to fly silicon PIN and APD devices to evaluate them in a space environment. For soft x-rays (1 to 20 keV) we would need direct exposure to space without material absorption, i.e. we would need a lid which could be opened on command. We would also need to know the view direction (to within a few tenths of an arcsecond) of the payload with time so that we could correlate our observation. Ideally, we would like to have coarse pointing capability to a few degrees to allow us to investigate specific x-ray sources such as the Crab Nebula, Cygnus X-1, and the galactic center region in addition to x-rays from the Sun, etc. For our first GAS can instruments, this capability is not a necessity since the primary purpose would be to evaluate the performance of the solid-state devices in a space environment. We would also like to fly an optical camera for star field identification of our field of view. We will have solid-state memory to record data. Transient events will be recorded in a similar way to study their light curves. The payload would be completely self-contained.

References

- 1) Kemmer, J. "Fabrication of Low Noise Silicon Radiation Detectors By the Planar Process" Nuclear Instruments and Methods. Vol. 169, pp.499-502 (1980).
- 2) Gramsch, E. et al "Silicon PIN Photodetectors in High Resolution Nuclear Spectroscopy" Nuclear Instruments and Methods Vol. A311, pp.529-538 (1992).
- 3) James, K. M. et al "Performance Evaluation of New Large Area Avalanche Photodiodes for Scintillation Spectroscopy" Nuclear Instruments and Methods Vol. A313, pp.196-212(1992).

Table 1:

<u>device</u>	<u>dimensions</u> (mm)	<u>type</u>	<u>manufacturer</u>
S2840	0.8 (dia.)	PIN	Hamamatsu
S1223	2.4 x 2.8	PIN	Hamamatsu
S1223-01	3.6 x 3.6	PIN	Hamamatsu
S 1722-01	4.1 (dia.)	PIN	Hamamatsu
S 1723-06	10 x 10	PIN	Hamamatsu
S 3590-01	10 x 10	PIN	Hamamatsu
S 3590-03	10 x 10	PIN	Hamamatsu
S 3590-05	10 x 10	PIN	Hamamatsu
F171A	11 x 11	PIN	Siemens
SH25R	25 (dia.)	APD	RMD
SX10R	10 x 10	APD	RMD
SX8R	8 x 8	APD	RMD

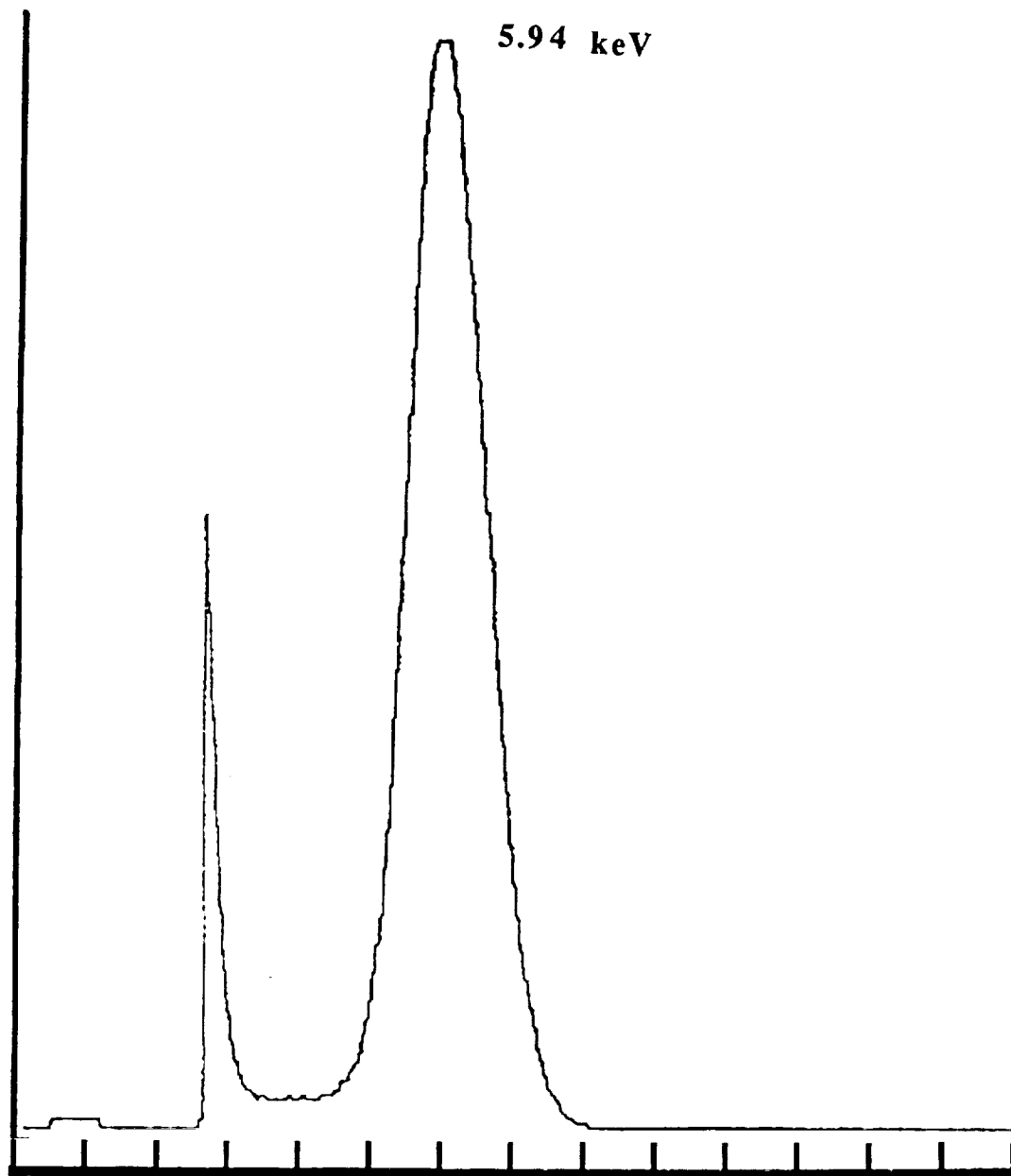


Figure 1. X-ray detection using a pin photodiode connected to the AMPTEK A250 charge-sensitive amplifier exposed to ^{55}Fe at room temperature.

^{55}Fe spectrum (5.9keV) @ 25°C
Detector: APD (RMD Model SX8S
0.64 cm²; V_s = 1350 Volts)
Preamplifier: Amptek A250
Resolution < 1keV FWHM
Peak Channel #489
Noise Threshold Channel #80

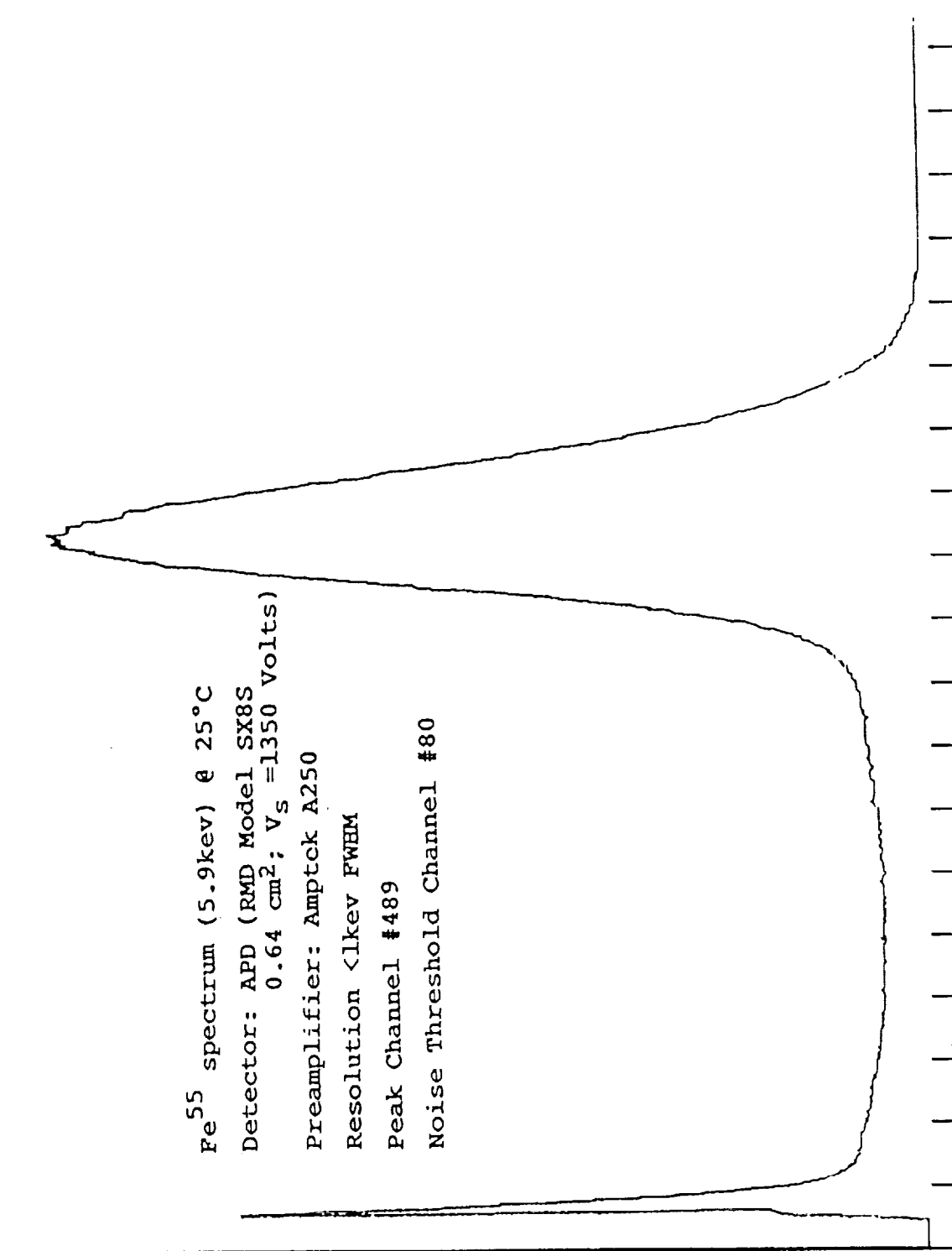


Figure 2. X-ray detection using avalanche photodiode (APD) connected to the AMPTEK A250 charge-sensitive preamplifier.

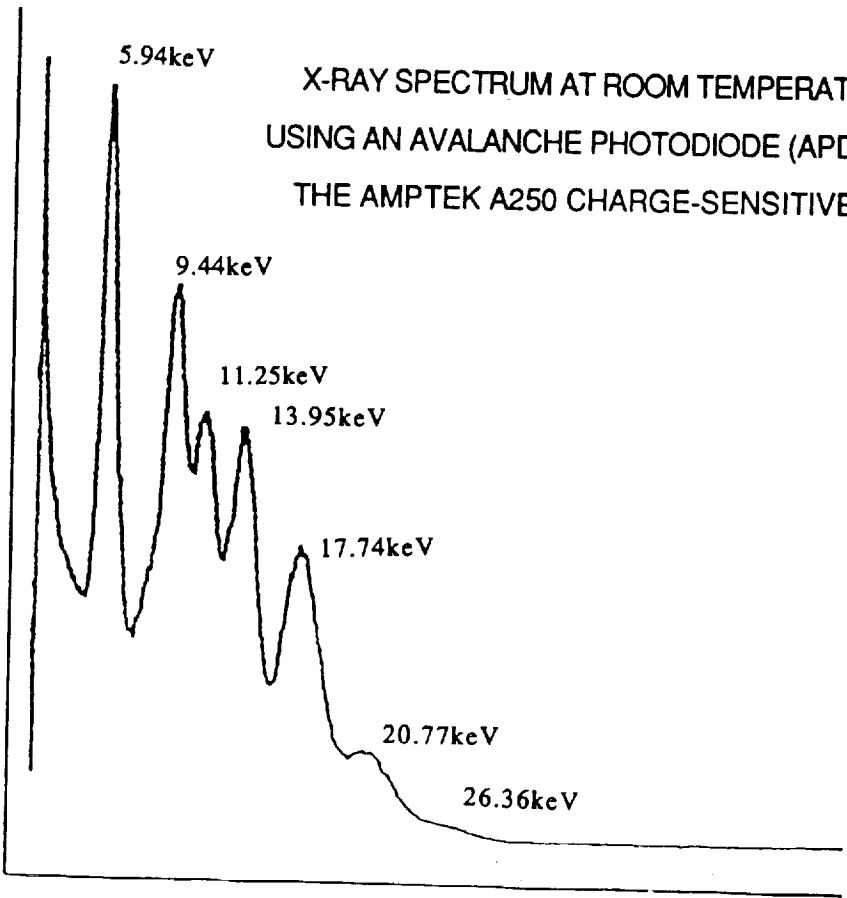
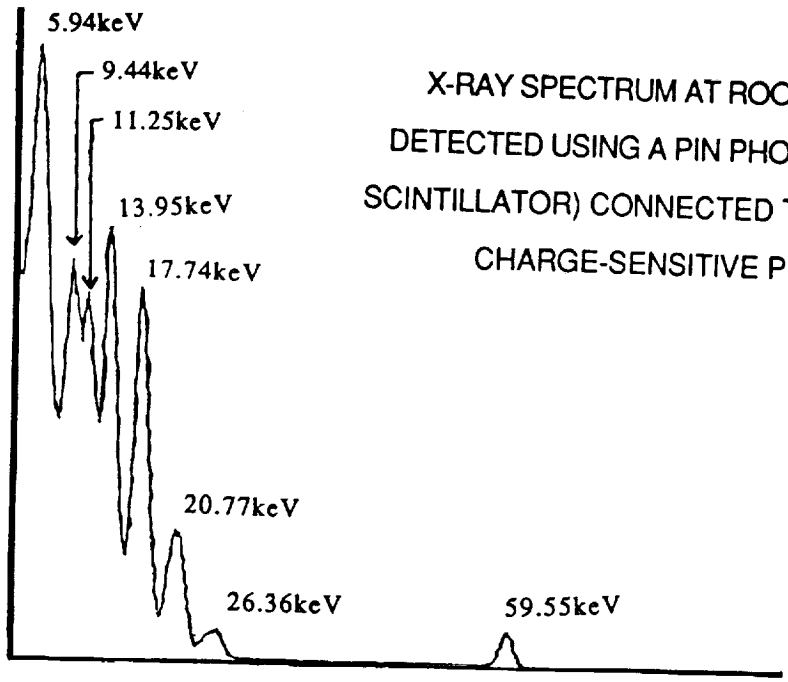


Figure 3.

Spectrum : DETA10C2.DAT
Sample Title : ref. det. A at 1220V and 10 deg. C with Cs137 source

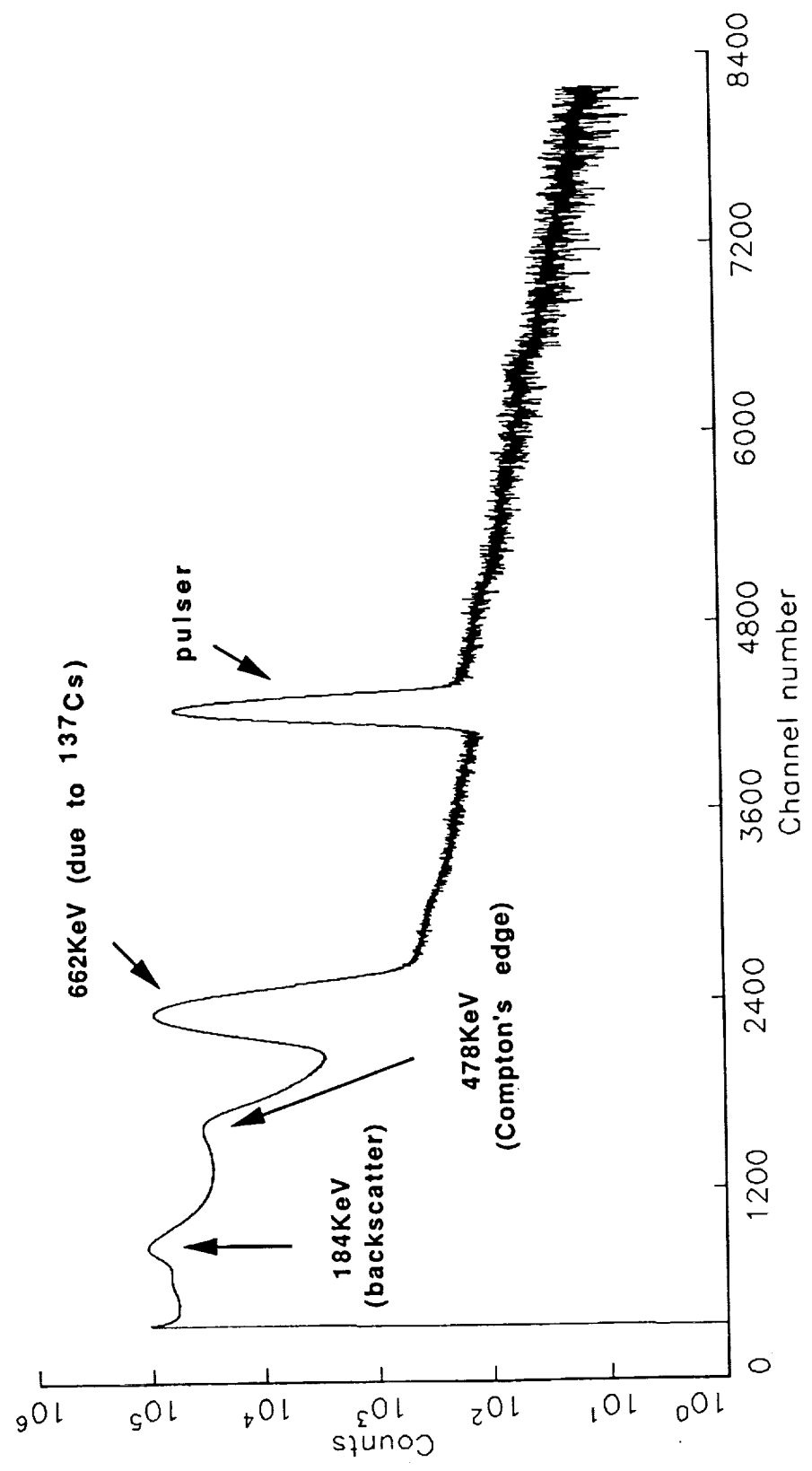


Figure 4. X-ray spectrum at 10 °C detected using an avalanche photodiode (APD) connected to a CsI (TI) scintillator.

A STUDY OF THE EFFECTS OF MICRO-GRAVITY ON SEED GERMINATION

Lynn Suzanne Klein, Washington University
Mark McKibben, Ohio University
David A. Brain, Rice University
Theodore C. Johnson, Stanford University

under the auspices
of the U.S. Space Camp, Huntsville, AL
and Dr. Konrad K. Dannenberg

ABSTRACT

This study will identify characteristics of seed germination dependent upon gravity. To accomplish this objective, four different seed types will be germinated in space and then be compared to a control group germinated on Earth. Both the experimental and control groups will be analyzed on the cellular level for the size of cells, structural anomalies, and gravitational effects. The experiment will be conducted in a Get Away Special Canister (GAS Can #608) owned by the U.S. Space and Rocket Center and designed for students. The GAS Can will remain in the cargo bay of the Space Shuttle with minimal astronaut interaction.

INTRODUCTION

The main purpose of this study is to advance the understanding of methods of agriculture in space. In the future, such methods will be required for extended space flights to Mars or for long duration space station habitation because space vehicles may not be capable of carrying all of the food necessary for these trips. By expanding the breadth of knowledge on plant growth in space, such space exploration will be more feasible.

The study focuses primarily on seed germination in space, and it will identify characteristics of germination dependent upon gravity. To accomplish this objective, four different seed types will be germinated in space and then be compared to a control group germinated on Earth. The seeds have been chosen because of their high germination rates in absolute darkness and because of their relatively small size. All four of the seeds were determined to have an optimum germination temperature range between 292 and 297 Kelvin (19 and 24 degrees Celsius). Both the experimental and control groups will be analyzed on the cellular level for size of cells, structural anomalies, and gravitropic effects.

The space germination phase of this experiment will be conducted in GAS Can #608, designated for use by students of the U.S. Space Camp. This experiment will take up roughly one fourth of the can. The GAS Can will remain in the cargo bay of the Space Shuttle with minimal astronaut interaction. The germinating seeds will be contained in a heated and insulated germination chamber in the GAS Can. This project has been

facilitated by the implementation of the previously used germination chamber (which flew in GAS Can #007) of Guy Smith at the University of Alabama in Huntsville. Due to insufficient heating and insulation, his seeds froze unexpectedly during their germination period in space. The modified version of the chamber, which will be used for this study, incorporates heating mats and foam board insulation calculated to assure the survival of the germinating seeds.

In the growth chamber, the seeds will lay between layers of filter paper employed for maintaining a moist environment and for maintaining the physical orientation of the seeds before, during, and after the Shuttle flight. For the in-flight germination, the filter papers will be wetted with de-oxygenated water containing a trace of a triple-20 fertilizer to establish a favorable osmotic gradient across the outer coats of the seeds. After the germination period has elapsed, the chamber will be filled with a formaldehyde solution to preserve the seeds for analysis after the flight. The in-flight temperature profile of the germination chamber will be monitored, maintained between 293 and 295 Kelvin (20 and 22 degrees Celsius), and recorded for later evaluation.

The seeds in the control group on Earth will be placed between layers of filter paper in the same growth chamber that will have been used for germinating the seeds in space. The control group will be germinated as soon after the mission as possible. The temperature of the control group will coincide with those temperatures recorded during the flight of the seeds germinated in space. The control group will also be preserved with formaldehyde.

Once the experimental and control groups of germinated seeds have been generated, the seeds will be compared by size, cell structure and gravitropic effects. With the results of this experiment, the understanding and feasibility of germinating food in space should be enhanced. Hopefully, this information will benefit space endeavors.

BACKGROUND ON GERMINATION

Germination is the process by which a seed, in its preliminary stages, begins to grow when the vital conditions are achieved. At first, a seed is called "spontaneously dormant," meaning it will not germinate unless some conditions; such as--an adequate supply of water, presence of air, temperature, exposure to light, and the planting depth of the seed--are met. If one of these requirements is not met, the seed will most surely not germinate.

The two types of germination processes are epigeal and hypogeal. An epigeal germination is the process by which the cotyledons come above the surface of the soil and function as leaves. It then begins photosynthesis. In a hypogeal germination, the cotyledons stay below the surface of the soil, never come out of the testa (seed coat), and do not function as leaves.

In many germination processes of various types of seeds, hormones are present that help trigger the germination process. They are gibberellin, cytokinin, and auxin. The gibberellin is actually made by the embryo; its objective is to convert the food of the endosperm to

solid substances and to take it back to the embryo. The cytokinin and auxin deal with the cell division and growth.

Going even deeper into the germination process, different parts of a plant have different functions. First, the body of the plant is called the stem. The stem's function is to support the weight of the leaves and to keep them in place against the environment. The stem has to hold up against the wind and rain. The stem is also used as a food track from the top to bottom of the plant. It contains a xylem, which is a controller of water and minerals, and a phloem, which is a controller of food from the leaves. The stem and the leaves make the food by a process known as photosynthesis. It starts at the leaves where the food is made in the chloroplasts and carried through the veins in the leaves to the stem. From there, the food moves down the phloem to the root section. This way, the whole plant is nourished. The plant uses the food it needs and then stores the rest of it in the roots.

The leaves are the next major part in the body of the plant. Their main function is to undergo photosynthesis. The leaf's structure is very delicate; it is thin and porous, allowing it to absorb light and water. The chlorophyll (the green coloring in the plant) does not stay in the leaves. It, like the food, goes to the rest of the plant. The leaves on a plant are arranged in a spiral pattern from top to bottom. Located on these leaves are leucoplasts, where the food is made for the plant.

Finally, there is the root section of the plant's structure. The root's primary objective is to anchor the plant in the ground and to draw nutrients and water from the soil for the nourishment of the plant. The roots also store food for later use.

Below (Figure 1) is a diagram of a cross-section of a bean.

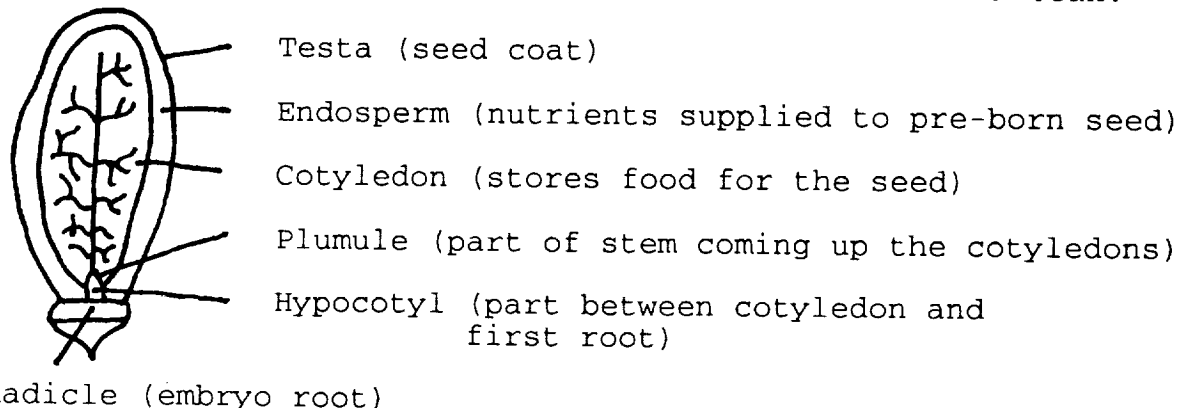


Figure 1. The location of tissues in a bean seed.

FEASIBILITY STATEMENT

In the future, we will have astronauts living in space for long periods of time to do experiments, study the earth, other planets, the sun, other solar systems, or even other galaxies. We will also have astronauts living in orbits around the earth or on the moon. Growing food in space would be practical to feed the astronauts on a space voyage, for example, on a journey to Mars, or a ninety day stay on a space station. The weight of the food products that would be required for the crew to survive would be tremendous, as experiments would take

up most of the weight on long space journeys. We could transport plants or seeds, support for the plants, oxygen, water, and the thirteen necessary elements¹ for the plants to survive instead of sending food already grown, into space for the astronauts. Even though most of the food on a long journey to Mars or beyond could be brought along, some food must be grown during the journey because of the great psychological needs of the crew. There has to be an effort to vary the monotony of rehydrated meals. Growing fresh vegetables can be used to vary this monotony according to Food Technology. We may, in the future, need more food for the people living on earth as the population rises. In space, we would not have to worry about soil. It would be easier to find defects in roots as the roots would be in chemicals, not in soil. Pests could be controlled easier in a controlled environment such as the space station.

There are many different ways to grow seeds in space including spinning drums making it possible for seeds and plants to grow in an artificial gravity. If there is a nuclear war, then the earth would be full of radiation and, we would have to depend on an alternative food supply--one in space. Or, if a world wide famine happens or some kind of early frost damages the crops, then we would have to turn to our emergency food supply in space. This project would be feasible to biological research in a micro-gravity environment because it would allow astronauts to make their own supply of food in space at the space station. This would reduce the cost of transporting food from Earth to space and would reduce the psychological effects on the astronauts.

Aside from the transportation costs, payload space would be saved; thus, more equipment could be transported into space on fewer shuttle flights. Since germination is the first step in a plant's development, if germination is impossible or impractical in a micro-gravity environment, then an alternate method of manufacturing food would have to be researched.

OBJECTIVES

The proposed GAS Can (Get Away Special Canister) has the following objectives:

- To successfully germinate one or more tomato, lettuce, radish or turnip seeds in a micro-gravity environment.
- To determine the approximate germination period of a tomato seed in the micro-gravity environment.
- To determine any peculiarities in the size and structure of the germinated seed.
- To determine any peculiarities in the length of germination.
- To determine the effectiveness of such an experiment for further research and use.

¹"Hydroponics: The Land, EPCOT Center." March 1987.

- When the project returns, to study the cellular differences at the nuclear level and possible alterations in cell divisions.

TYPES OF SEEDS

In this experiment, four different types of seeds will be germinated, including tomatoes, lettuce, radishes, and turnips. Following is information on the four seed types chosen for this experiment.

Dombello Tomato Seed

Hydro-Gardens, Inc., PO Box 9707, Colorado Springs, CO (800-634-6362). The optimum temperature is 297 Kelvin (24 degrees Celsius), but it still germinates at lower temperatures. It germinates in three to five days and can be cultivated at 70 days. 85% of the seeds germinate. It is a promising hybrid since it has a wide range of resistances and fruit of excellent shape, color, quality and size. It has a compact plant habit and a good total production. The fruit is of the greenback type with a deep red color at maturity. It is resistant to tomato mosaic virus, resistant to cladosporium races A, B, C, D and E, resistant to fusarium races 1 and 2, resistant to the most occurring pathotypes of nematodes and free from silvering.

Red Sails Lettuce (E5153-8)

Park Seed Company, Cokesbury Road, Greenwood, SC 29647-0001 (800-845-3369). The optimum temperature for germination is 294 Kelvin (21 degrees Celsius). It germinates in 7 days, with a few germinating in 3 to 5 days. Approximately 90% of the seeds germinate, and the lettuce can be cultivated at 45 days. It is an AAS award winner and a high quality red lettuce. It has an excellent flavor and a high nutritional value.

Radish Charriette Hybrid (E5747-7)

Park Seed Company. The recommended temperature for germination is 19 degrees Celsius. It can be cultivated at 24 days. It is the most attractive, vigorous rooted quality eating radish available today. The roots achieve 5 cm (2 inches) in 24 days. This variety can be grown in hot and cold weather, in Spring and Fall, and in wet and dry areas with consistent performance.

Purple Top White Globe Turnip Seed (E5469-7)

Park Seed Company. The recommended temperature for germination is 19 to 20 degrees Celsius. It germinates in 5 days and can be cultivated at 57 days. This variety has round roots 12.5 to 15 cm (5 to 6 inches) in diameter with purple tops. The flesh is white, of fine grain and is sweet.

HYPOTHESIS

While germinating seeds in an experiment in which observations are to be made between an earth controlled experiment and a micro-gravity experiment, many differences can appear when a comparison is made.

1. There are many differences that might occur between the control and the micro-gravity experiment within a time span of three to five days. Some of these possible changes are:
 - size and shape of the seed while germination occurs
 - time span of the germination process
 - root size, if there are any roots
 - temperature needed for germination
 - amount of water needed for germination to occur
 - color of the stem and leaves
 - amount of leaves, if there are any leaves
 - change in whether or not a seed is a dicotyledon or a monocotyledon

2. Micro-gravity is considered to be a state in which little strain or resistance is forced upon an object, causing it to appear to be floating. This state is created by "free-fall". For example, the orbiter falls around the Earth in an elliptical orbit. It constantly falls, creating a condition in which only one-sixth of the weight of an object is recorded, thus creating micro-gravity.

One change that may occur in the micro-gravity environment is that it will take longer for the plant to grow after the initial germination process. This would be due to the different placement of the amyloplasts. Amyloplasts detect gravity for the plant and tell it in which direction to grow. The regeneration of the root caps where the amyloplasts are found will take a much longer time due to the confusion of the amyloplasts in the strange environment. If the root caps do not regenerate at all, then the roots will contain many more vacuoles and become callous-like cells. Another possible change would be that a different amount of the chemicals needed by seeds to germinate will be required. We have not performed this experiment in micro-gravity and are unable to predict the importance of certain chemicals. This experiment will not be in space for fourteen days, so only the initial stages of germination can be observed.

EQUIPMENT

Below is a list of the equipment used in the radish seed experiment in GAS Can #007 (Figure 2).² Most of the same equipment is being used in the Seed Growth Experiment in GAS Can # 608. Modifications to this list are in the next section.

#	EXPERIMENT COMPONENT	QUANTITY	MATERIAL(S)
1	Experiment Housing	1	2024-T3 Aluminum
2	Magnetically Coupled Gear Pump	2	316 Stainless, TFE, Graphite Micropump #P11-361-70G,
3	Growth Chamber	1	Dow Corning PLEXIGLAS
4	1/8" diameter Tubing	4'	1100 series Aluminum
5	1/8" TEE Fitting	2	316 Stainless, Swagelok #SS-200-3
6	1/8" O-Seal Straight Connector	4	316 Stainless, Swagelok #SS-200-1-OR
7	Check & Adjustable Relief Valve	2	316 Stainless, Swagelok #SS-2C-3
8	1/8" 90° Elbow Fitting	4	316 Stainless, Swagelok #SS-200-2-2
9	1/4" thick Fiberglass Board	1	Owens Corning Fiberboard
10	Ceramic Fiber Insulation	2 lbs	Kaolin (High Purity Alimina-Silica Fireclay) Thermal Corp. Cat. No. 4019-10
11	Aluminized Mylar Foil	6 sq ft	0.4 mil Mylar with Alu Coat
12	Heater	1	1000 ohm, 5 watt Resistor
13	Temperature Controller	1	Bi-element Thermal Switch set to "ON" at 19°C or below.
14	Filter Paper	20 sq in	WHATMAN #4 Qualitative Filter Paper
15	Fertilizer Solution	40 ml max	20-20-20 NPK Peter's Soluble Plant "Food", 1% concentration
16	Buffered Formalin Solution	40 ml max	10% W/V (4% Formaldehyde) buffered to 7.0 to 7.1 @ 25°C with Sodium Acetate
17	Bladder	2	RTV Silicone Rubber
18	Temperature Sensor	1	Thermistor, Aluminum housing
19	Connector, ITT Cannon	1	CA3106R20-11S-A115
20	Connector, ITT Cannon	1	CA3102E20-11P-A95
21	Teflon Wire, Hook-up	10 ft	22 guage nickel plated, TFE
22	Gasket	5 sq in	1/16" thick RTV Silicone
23	Helicoils, Self-locking, 6-32	16	MS21209, AMS-7245C
24	Helicoils, Self-locking, 4-40	9	MS21209, AMS-7245C
25	Socket Head 4-40-1/2" Screws	33	304 Stainless
26	Socket Head 6-32-3/4" Screws	12	304 Stainless
27	Socket Head 8-32-1" Screws	4	304 Stainless
28	Counter Sink 6-32-3/8" Screws	20	304 Stainless
29	Flat Washers: #4, #6, #8, 1/4		304 Stainless
30	Lock Wire		Nickel Chrome 22 guage
31	Breakaway Wire		Copper with Gold Plate 24 gua
32	Hex 1/4"-20-1"	8	304 Stainless
33	Radish Seeds (<u>Raphanus sativus</u>)	30	Biological Material

Figure 2. Equipment list for use in GAS #007.

²Smith, Guy A. "Initial Project Report on ATHICAS." Huntsville, Alabama, n.d. (Report to Konrad K. Dannenberg at the U.S. Space and Rocket Center)

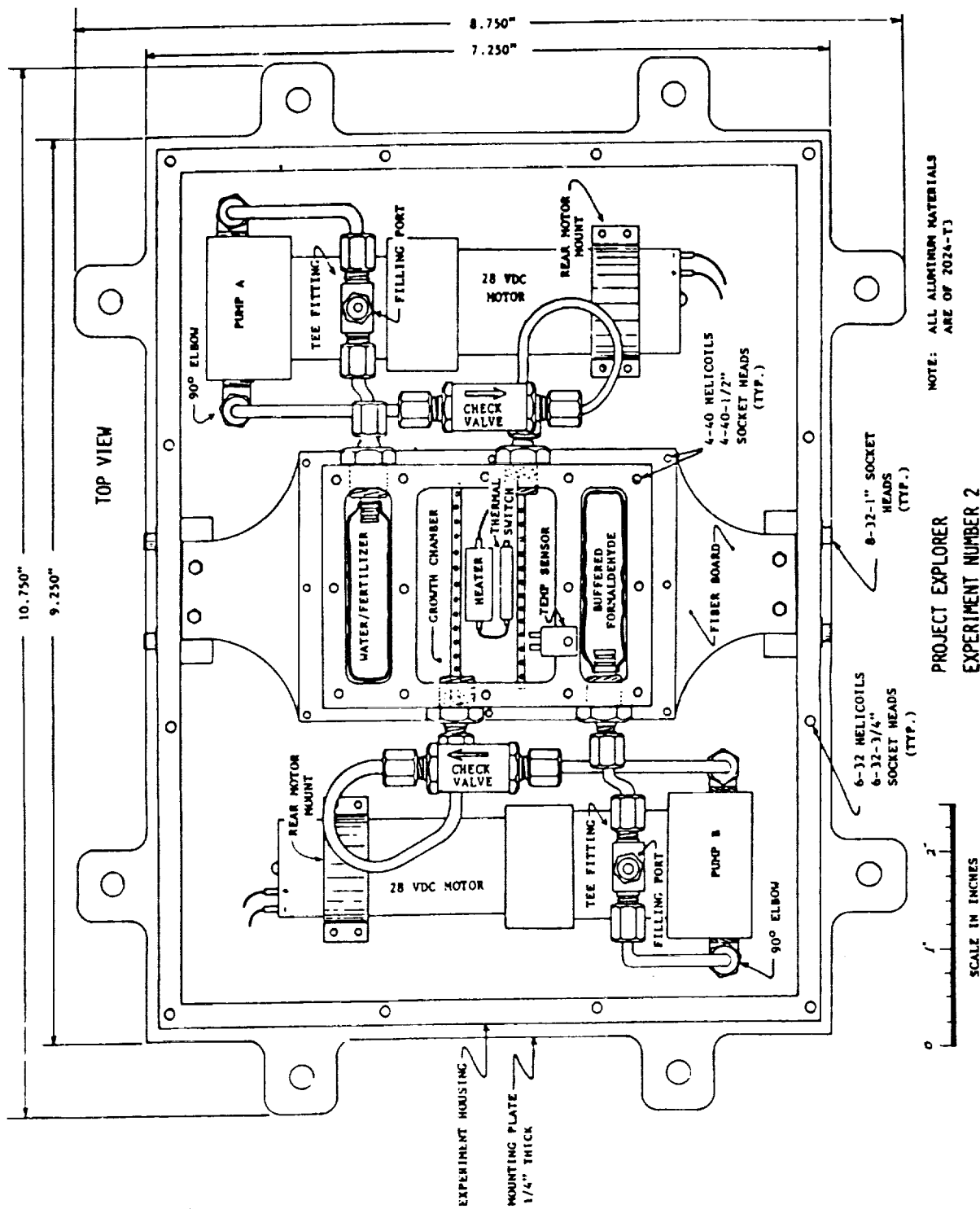


Figure 3. Growth Chamber Diagram for Guy Smith's Radish Seed Experiment from GAS Can #007.³ The same growth chamber with modifications will be used for this experiment.

³Ibid.

MODIFICATIONS

Most of the same materials will be used in GAS Can #608 as were used in GAS Can #007 with the exception of a few materials. Below is a complete list of the changes.

Under # 4 on the Radish Seed Germination Materials Listing, stainless steel tubing has been decided to be used instead of aluminum because of corrosion.

Under # 10, alternate layers of aluminized mylar (or possibly gold coated mylar) and fish net webbing (thickness of a penny) will replace the Ceramic Fiber Insulation.

Under # 12, six heating mats will be used instead of the resistor heater.

Under #17, two neoprene bladders are replacing the two rubber balloons. The neoprene bladders will be coated with activated carbon.

Under #33, ten each of the four seed types mentioned in the Seed Types section will be used instead of the 30 radish seeds used in the previous experiment.

In addition, the corrosion from the existing pumps will be removed so the existing pumps can be reused in this experiment.

PROCEDURE

Time Line for the In-Flight Procedure

- Toggle 1 - Turn computer system on in GAS Can one hour after liftoff.
- At Experimental Elapsed Time (EET) = 0, Turn the Heater On.
- Read Temperature every 1 minute and Record. Read and record continuously throughout the entire experiment.
- If Temperature > 10 degrees Celsius, then turn Pump 1 (water solution) on for 30 seconds.
- At EET=1 hour, turn pump 1 on if not on already for 30 seconds.
- If Temperature < 20 degrees Celsius, then turn heater on.
- If Temperature > 21 degrees Celsius, then turn heater off.
- Toggle 2 - One hour before last allowed time for final toggle.
- Zero seconds after Toggle 2, turn on pump 2 (formaldehyde) for 30 seconds.
- Toggle 3 - Turn off heaters 1 and 2.
- 2 minutes after Toggle 3, turn computer system off in GAS Can.

REFERENCES

- Bartok, John W., Jr. "In the Greenhouse: Soilless Mixes." Horticulture, November 1985, pp. 60-61.
- Billings, Linda. "Get Away Special." Air and Space Smithsonian, February March 1986, pp. 48-51.
- Board on Agriculture National Research Council. Genetic Engineering of Plants, National Academy Press, Washington, D.C., 1984.
- Bridwell, Raymond. Hydroponic Gardening. Woodbridge Press Publishing Co., Santa Barbara, CA, 1974.
- Christopher, Thomas. "Seeds in Space." Omni, October, 1984, p. 22.
- Get Away Special (GAS) Small Self Contained Payloads Experimenter Handbook. NASA. Goddard Space Flight Center Special Payloads Division, 1984.
- Halstead, Thora, and Dutcher, F. Ronald. "Annual Review of Plant Physiology." Plants in Space, Vol. 38, 1987, pp. 317-345.
- Halstead, Thora, and Dutcher, F. Ronald. "Experiments on Plants Grown in Space." Annals of Botany, Supplement 3, Vol. 54, Academic Press, 1984.
- Halstead, Thora W. and Scott, Tom K. Plant Gravitations and Space Research. Rockville, MD, American Society of Plant Physiologists, Waverly Press, 1984.
- Hunter, Beatrice. "Food Growth Without Soil?" (Food For Thought) Consumer's Research Magazine, January, 1986, pp. 8-9.
- Hydro-gardens Inc., Catalog 37F. PO Box 9707, Colorado Springs, CO
- Karel, Marcus. "The Future of Irradiation Applications on Earth and in Space." Food Technology, July 1989, pp. 95-97.
- Oberg, Alcestis R. Spacefarers of the 80's and 90's, Columbia University Press, New York, 1985.
- Oberg, James, E. Mission to Mars. Stockpole Books, Harrisburg, PA, 1982.
- Oberg, James E. and Alcestis R., Forward by Isaac Asimov. Pioneering Space, Living on the Next Frontier. Mcgraw-Hill Book Company, St. Louis, 1986.
- Resh, Howard M., Ph.D. Hydroponic Food Production. Woodbridge Press Publishing Company, Santa Barbara, CA, 1987.
- Thomas, Lawrence R. and Mosier, Francis L. ed., 1985 Get Away Special Experimenter's Symposium, NASA Scientific and Technical Information Branch, 1986.

Investigation of Microgravity Effects on Solidification Phenomena of Selected Materials

Carl R. Maag ¹ and Patricia A. Hansen ²

1. Science Applications International Corporation; Glendora, CA 91740
2. EER Systems; Seabrook, MD 20706,

ABSTRACT

A Get Away Special (GAS) experiment payload to investigate microgravity effects on solidification phenomena of selected experimental samples has been designed for flight. It is intended that the first flight of the assembly will a) investigate the p-n junction characteristics for advancing semi-conductor device applications, b) study the effects of gravity-driven convection on the growth of HgCd crystals, c) compare the textures of the sample which crystallizes in microgravity with those found in chondrite meteorites, and d) modify glass optical characteristics through divalent oxygen exchange.

The space flight experiment consists of many small furnaces. While the experiment payload is in the low gravity environment of orbital flight, the payload controller will sequentially activate the furnaces to heat samples to their melt state and then allow cooling to resolidification in a controlled fashion. The materials processed in the microgravity environment of space will be compared to the same materials processed on earth in a one-gravity environment. This paper discusses the design of all subassemblies (furnace, electronics, and power systems) in the experiment. A complete description of the experimental materials is also presented.

INTRODUCTION

The scientific objective of the GAS experiment payload is to investigate microgravity effects on solidification phenomena of selected experimental samples. The materials processed in the microgravity environment of space will be compared to the same materials processed on earth in a one-g environment. The basic objectives of the various materials processing experiments are:

1. The further understanding of solidification phenomena in space
2. The discovery of methods to produce new materials with improved properties over those available today.

The experiments to be included in the payload for a first flight are described in Table 1.

Payload overview

The GAS payload performing these materials processing experiments is to be contained in the "half-size" 2.5 cubic foot GAS canister, and will weigh no more than 100 pounds. The GAS canister will be sealed with a GN₂ internal atmosphere of 15 psia.

PAYLOAD DESCRIPTION

The payload assembly includes twelve (12) experiment furnaces, a power supply, an electronic control and data storage system, structural support, and mechanical/electrical interfaces to the GAS canister. The furnace interiors are plumbed to one purge port of the GAS top plate to provide a vacuum inside the furnaces.

A side view of the payload is shown in Figure 1. The subsystems are organized into two sections, the furnace module to the left and the support module (power, electronics) to the right. The GAS canister interfaces, interface plate and bumpers, are shown.

Structural subsystem

A cradle concept was developed to meet packaging requirements between the GAS container and experiment payload. The cradle provides structural support for the materials processing furnaces and associated support equipment. The payload is modular so that it can be reused for other missions with different scientific objectives.

The furnaces will operate in a vacuum environment for maximum efficiency while the remainder of the payload (support module) operates in a dry nitrogen atmosphere. Figure 2 shows a diagram of the manifold system that controls this operation. The dry nitrogen atmosphere will ensure that the batteries and electronics function properly and do not outgas. The support module is constructed in such a manner that the batteries, electronics and fuses are an integrated unit.

Furnace subsystem

The high temperature (1000°C) furnace is composed of a core and radiation reflectors that are matched to provide the best insulation, thus giving the highest temperatures with the least power input. The existing flight furnace requires 20 watts of electrical power to achieve the 1000°C design temperature. In addition, the furnace is designed to operate in a vacuum environment to eliminate convection through the gas that would otherwise fill the furnace.

The furnace core is the heating element. A nichrome heater coil coated with high temperature cement (Sauresin No. 29) provides the heat to a graphite crucible containing the sample. The furnace core and crucible are wrapped with insulation. The effectiveness of the insulation is demonstrated by the temperature measurement of 132°F at the furnace container wall during full power operation (furnace core and crucible at 1000°C).

Electronic subsystem

The electronics system for this payload is responsible for sequencing the payload furnaces during their operation, measuring and controlling the temperatures of each furnace to remain within a specified range, and recording deviations in the temperature data in non-volatile erasable programmable read only memory (EPROM) for post-flight processing of temperature profiles. In addition, the electronics will initiate these tasks upon receipt of a signal through the STS/GAS canister interface, provide electronics

ground support while the canister is in its flight configuration prior to Shuttle integration, and regulate the battery power to the electronics and furnaces.

The payload electronics design is comprised of two identical microprocessor controlled subsystems operating independently (string A and string B). Each subsystem controls, measures, and stores temperature data for up to 12 furnaces. All control is through on-board software that is programmed in Read Only Memory (ROM) before flight. Each electronics package is comprised of a central processing unit (CPU) microprocessor card, an EPROM card for data storage, a furnace select control card, an analog temperature measurement card with an analog-to-digital (A/D) converter and an STS/GAS canister interface card. Each card is linked via common data, address, and control bus to the CPU card.

Power subsystem

Alkaline batteries have been selected for the power supplies. There will be eight separate power supplies in parallel (4 supplies per string, A and B). The supplies will be based on D, C, and AA-size Duracell commercial batteries.

The furnaces are powered from 28 D-cells per string, each providing 118 Watt-hours of energy. The computers will utilize 6 C-cells per string, which will produce 10 Watt-hours of energy. The EPROM and A/D cards will operate with 25 and 10 AA-cells per string, providing each with 14 and 5 Watt-hours of energy, respectively.

EXPERIMENT DESCRIPTION

The experiment materials, along with the respective investigators for this flight, are listed in Table 1. The samples are on the order of one and one-half cubic centimeter each and are encapsulated in a hermetically-sealed quartz ampule. The ampule is contained in a closed graphite crucible. Figure 3 shows two ampules with encapsulated samples. The ring on the upper ampule is for handling purposes only. The sample subassembly is inserted into the core of a furnace. Each furnace with its contained sample is installed in the furnace module of the payload. Temperature sensors are incorporated into each furnace so that the temperature profiles may be recorded and furnace power may be controlled. Figure 4 shows the cross-section of a furnace assembly.

Experiment operation

The furnace, electronic, and power systems operate in concert with each other and without external control, except for the initial turn-on (actually a maximum of three signals) and an emergency turn-off. After the initial turn-on signal from the GAS Autonomous Payload Controller, the first furnace is actuated. The experiment controller program receives inputs from the thermal sensor in the furnace and proceeds to control power input so that an individually programmed sample thermal profile is followed. These profiles are summarized in Table 2.

After the heating and cooling cycle is completed, the second furnace is activated, and so on until the final sample is processed.

A special sequence is provided in the controller software, in the event of failure of a particular furnace to respond properly. It will be passed over and retried at the end of the furnace sequence, and shut down if operation remains abnormal. The software also enforces a shut down of each furnace run after a specified time period, nominally one hour.

All experiments will be performed twice. Each material will be placed in two separate furnaces. The six primary furnaces will contain one sample material each and will be activated first. The six secondary furnaces will allow each experiment to be repeated. Each furnace is activated sequentially until the final duplicate sample is processed.

Experiment evaluation

After flight, the sample ampules will be returned to the respective experimenters. The experimenters will examine their samples, compare them with corresponding ground-based experiments, and review the thermal profiles.

Table 1. Payload Experiments

No.	EXPERIMENT TITLE	MATERIAL	INVESTIGATORS	EXPERIMENT OBJECTIVES
1	Semiconductor Eutectic	SnSe-SnSe ₂	Alfred S. Yue, PhD Professor	Investigate the p-n junction characteristics for advancing semi-conductor device applications
2	IR Detector Crystal Growth	HgCd	Carl Maag	Study the effects of (absence of) gravity-driven convection on the growth of HgCd crystals
3	Chondrule Formation	Potassium Tetrasilicate	John Louie	Compare the textures of the sample which crystallizes in microgravity with those found in chondrite meteorites
4	Gradient Refractive Index of Glass	Zinc/Calcium Chloride Glass	Duncan Moore, PhD Professor of Optics	Modify glass optical characteristics through divalent oxygen exchange
5	Unique Aluminum Alloy	Al Alloy	Edward Eckert	Study the effects of Al Alloy casting in Zero-g.
THE ABOVE MATERIALS HAVE BEEN APPROVED FOR USE BY THE GSFC MATERIALS BRANCH				

Table 2. Experiment Time-Temperature Profiles

<p>SEMICONDUCTOR EUTECTIC Heat as rapidly as possible to 700°C, hold for 20 minutes</p> <p>(a) Cool at 5°C/min. to 630°C, power off (b) Cool at 1°C/min. to 630°C, power off</p> <p>AL ALLOY Heat as rapidly as possible to 950°C, hold for 45 minutes, power off.</p> <p>IR DETECTOR CRYSTAL GROWTH Heat to 900°C, hold for 20 minutes</p> <p>(a) Cool at 5°C/min. to 670°C, power off (b) Cool at 5°C/min. to 810°C, cool at 1°C/min. to 690°C, power off</p> <p>CHONDRULE FORMATION Heat to 750°C, hold for 20 minutes Cool at 5°C/min. to 600°C, power off</p> <p>GRADIENT REFRACTIVE INDEX OF GLASS (a) Heat to 950°C, hold for 1 min., power off (b) Heat to 950°C, hold for 10 min., power off</p>
--

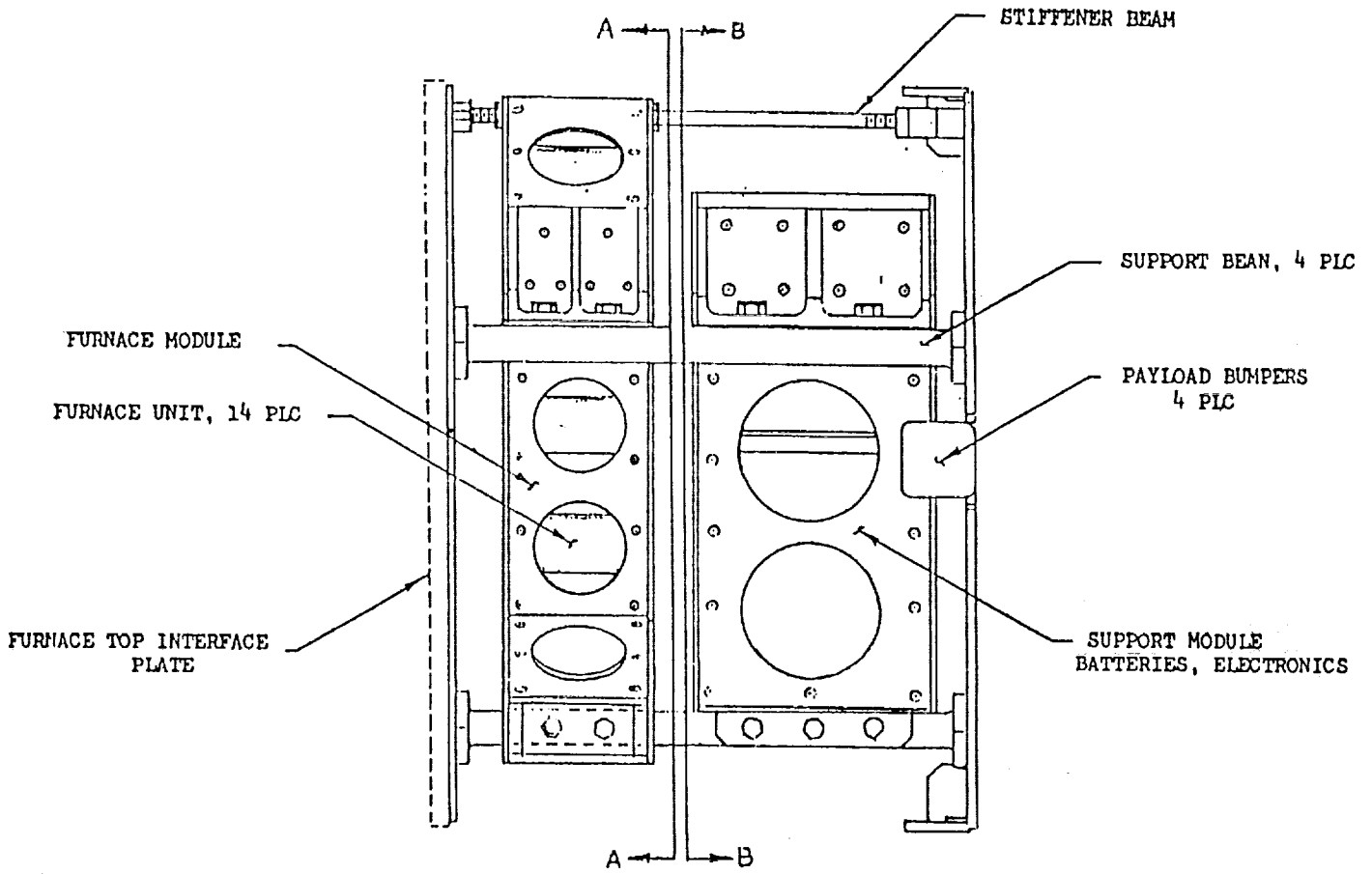


Fig.1. Cross-sectional diagram of payload

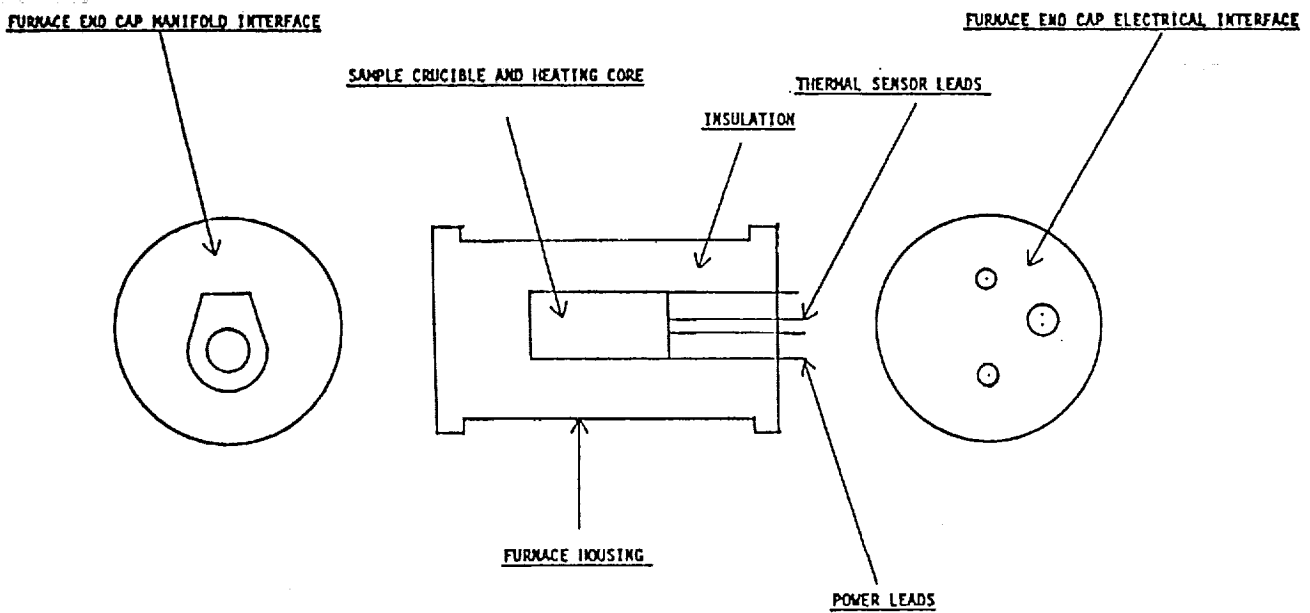


Fig. 2. Furnace manifold system

ORIGINAL PAGE
BLACK AND WHITE PHOTOGRAPH

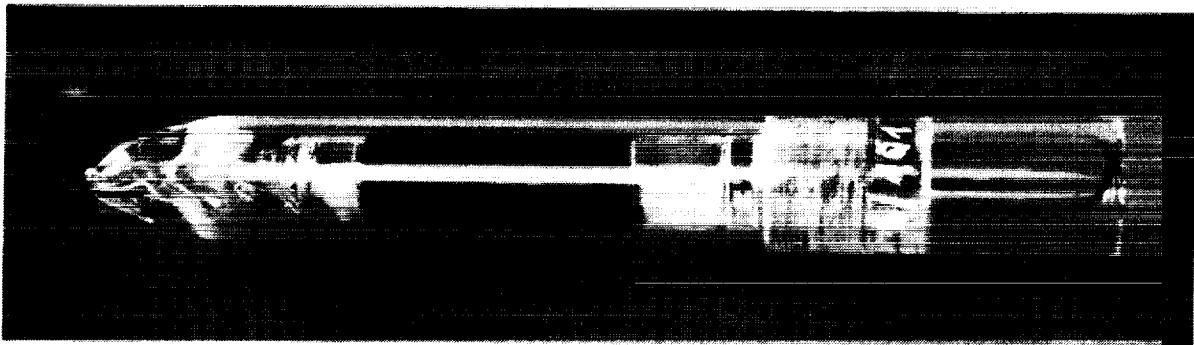
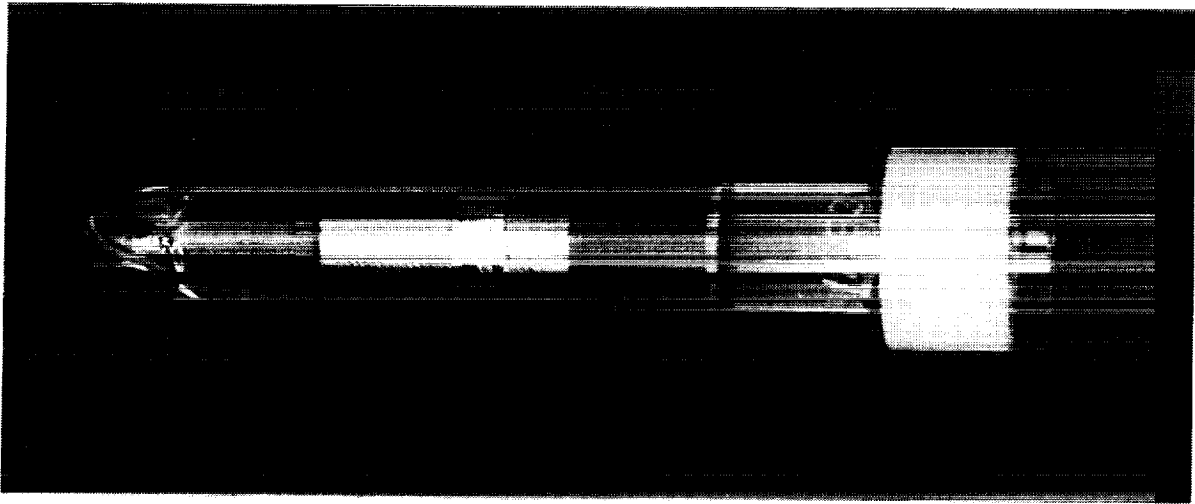


Fig. 3. Quartz ampule with encapsulated sample.

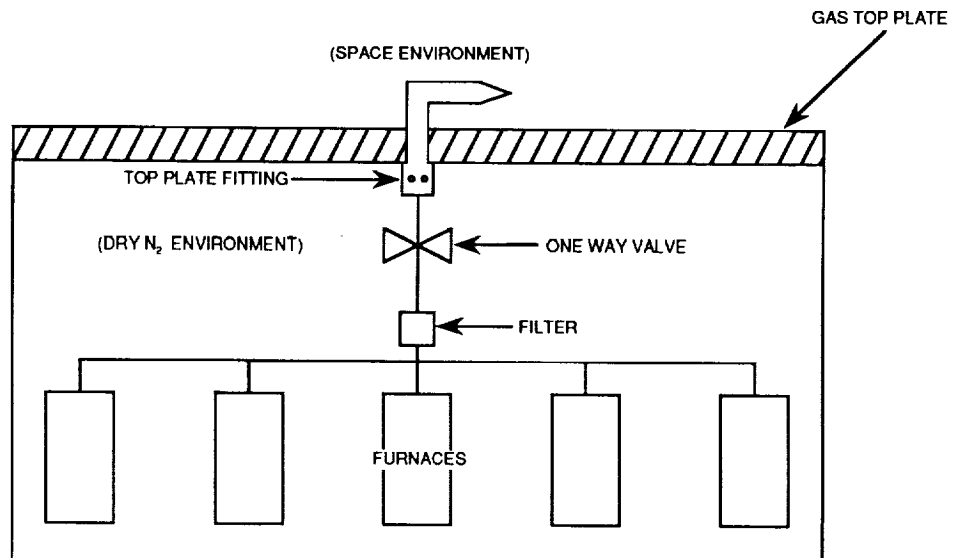
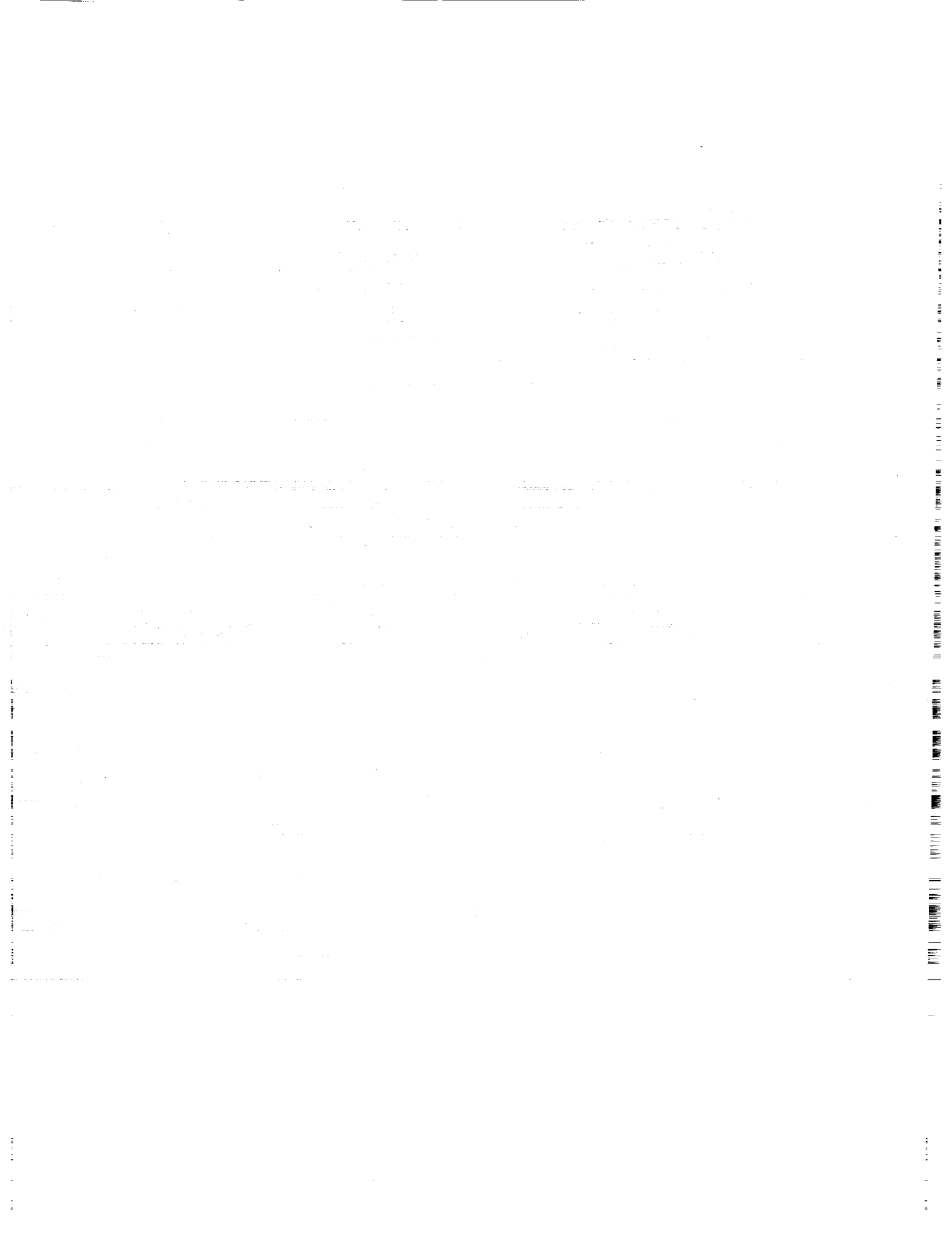


Fig. 4. Furnace assembly.



**Environmental Qualification Testing of Payload G-534,
The Pool Boiling Experiment**

**J. Andrew Sexton
Sverdrup Technology, Inc.*
Brook Park, Ohio 44107**

Abstract

Payload G-534, the prototype Pool Boiling Experiment (PBE), is scheduled to fly on the STS-47 mission in September 1992. This paper describes the purpose of the experiment and the environmental qualification testing program that was used to prove the integrity of the hardware. Component and box level vibration and thermal cycling tests were performed to give an early level of confidence in the hardware designs. At the system level, vibration, thermal extreme soaks, and thermal vacuum cycling tests were performed to qualify the complete design for the expected shuttle environment. The system level vibration testing included three axis sine sweeps and random inputs. The system level hot and cold soak tests demonstrated the hardware's capability to operate over a wide range of temperatures and gave the project team a wider latitude in determining which shuttle thermal attitudes were compatible with the experiment. The system level thermal vacuum cycling tests demonstrated the hardware's capability to operate in a convection free environment. A unique environmental chamber was designed and fabricated by the PBE team and allowed most of the environmental testing to be performed within the hardware build laboratory. The completion of the test program gave the project team high confidence in the hardware's ability to function as designed during flight.

Introduction

Payload G-534, the Pool Boiling Experiment, is a Get Away Special class payload designed to obtain data on nucleate pool boiling of R-113 (trichlorotrifluoroethane) in an extended microgravity environment. Nucleate pool boiling is a process wherein a stagnant pool of liquid is in contact with a surface which can supply heat to the liquid. If the liquid absorbs enough heat, a vapor bubble can be formed. This paper describes the environmental testing which the prototype PBE hardware was subjected to in order to qualify the design. Fig. 1 illustrates the prototype PBE system.

Normally, the prototype version of a new hardware design is subjected to qualification tests in order to qualify the design. A flight system is subsequently built and tested to lesser acceptance levels. The prototype system is not usually flown. However, an opportunity

* This work was performed for the NASA Lewis Research Center under NASA contract NAS3-25266

developed to fly the prototype PBE on STS-47 (SL-J) prior to the completion of the flight PBE system. Since the prototype system had been built with a high level of quality, and documentation was maintained to verify all of the safety critical analyses, inspections, and tests, it was determined that the prototype PBE could be flown with a relatively high chance of success. In addition, flight of the prototype system would give the project's Principal Investigator, Dr. Herman Merte of the University of Michigan, an opportunity to verify the choice of test matrix points and further enhance the science prospects for the flight system.

Qualification Testing Philosophy

The test program for the prototype PBE was derived from Goddard Space Flight Center "General Environmental Verification Specification for STS and ELV Payloads, Subsystems, and Components", GEVS-SE¹, and the GSFC "Guidelines for Standard Payload Assurance Requirements for GSFC Orbital Projects," (SPAR 3)². A project specific requirements document was prepared to summarize the test program plan.

The PBE project was conceived as a program that would incorporate the traditional prototype and flight hardware development concepts. Traditionally, the prototype system is built to the flight design specification and then subjected to qualification testing. The qualification tests seek to "demonstrate that the test item will function within performance specifications under simulated conditions more severe than those expected from ground handling, launch, and orbital operations"¹. Typically, qualification testing seeks to uncover deficiencies in design and fabrication and to provide a high degree of confidence in the end design.

The specific test levels and durations were derived from the GEVS-SE and the SPAR-3 documents. In some cases, the specifications were modified at the project teams discretion in order to tailor the tests to the project's needs.

For some of the commercial components with little or no quality pedigree, random vibration testing was performed to give early verification of the component's design integrity. These components include: a quartz halogen light, a pressure transducer, a pneumatic pressure regulator, a solenoid valve, a 16 mm film camera, and a boiling heater surface.

The project team determined that box level testing of the major electrical box assemblies would provide early verification of the designs that would otherwise be more difficult and costly to correct at a later stage of development. Box level testing was limited to three axis random vibration testing and thermal cycling at room pressure and extended temperatures (in contrast to thermal vacuum cycling).

At the system level, a wider range of testing was employed. The complete system was subjected to three axis random vibration testing, thermal extreme soak testing, thermal vacuum cycling, and an EMI signature test.

Component Vibration Testing

The three axis component vibration test specification was taken from the 1986 edition of the GAS Experimenter's Handbook³ and is summarized in Table 1. Testing was performed at the NASA Lewis Research Center Structural Dynamics Laboratory.

The component test fixtures were designed to solidly mount the components to the vibration table, and little attempt was made to accurately simulate the component's mounting on the system structure. Component level vibration testing helped provide confidence that the non-pedigreed commercial parts selected for the experiment would survive later system level vibration testing. Only one component failed during these tests: a precision pressure transducer which had a 6 cm diameter circuit board populated with discrete electrical components that were not solidly mounted to the board. One of the discrete electrical components failed during the vibration testing and caused the transducer to fail completely. A higher quality, ruggedized pressure transducer was subsequently ordered to replace the commercial item.

Box Level Vibration Testing

The box level random vibration power spectral density (PSD) curve was derived from table B-3, Appendix B of the GEVS-SE¹ and reproduced as Table 2. This PSD curve is the same as that for the entire system and was used because detailed dynamic response data at the box mounting locations on the PBE structure was not yet available. Testing was performed at the NASA Lewis Research Center Structural Dynamics Laboratory.

The test fixtures for the boxes were similar to those used for the components in that little attempt was made to accurately simulate the component's mounting on the experiment structure. As with the component level testing, a level of confidence was the desired outcome of the testing. No failures occurred during the box level testing. However, when the data acquisition and control system box was tested, one of the STD-bus boards which had relatively tall capacitors was noted to be making contact with the circuit board above it. Subsequently, the capacitors were mounted differently to allow for additional clearance between the boards in the card cage.

The completion of the box level random vibration testing gave the project team high confidence that the system level random vibration testing could be accomplished with a much reduced chance of failure.

Box Level Thermal Testing

The GSFC GAS Eleven Node Thermal Model (GEM)⁴ was used to model the overall system temperatures. The data derived from the modeling effort was used to determine the minimum and maximum expected temperatures for orbital operations. Using the guidelines set forth in the GEVS and the SPAR-3, the PBE team determined that qualification thermal test levels would be defined as 10 °C below the minimum expected on orbit temperature and 10 °C above the maximum expected on orbit temperature.

This translated into a thermal test band from 0 °C to 49 °C.

The box level thermal testing was performed in a large environmental chamber that was capable of heating and cooling, but not capable of providing a vacuum. The boxes were subjected to five thermal cycles over the thermal test band. A 4 hour soak period was observed at each temperature extreme. The electrical components inside the various boxes were powered ON for the entire duration of the thermal cycle tests.

Some of the power consuming components inside the individual boxes were instrumented with thermocouples to monitor case temperatures during the testing. Heat sensitive indicator strips were applied to the electrical components expected to dissipate the majority of the heat.

During the hot portion of the cycling, the electrical components registered temperature increases of no more than 5 °C. All of the power consuming devices were heat sunk to the aluminum structure of the experiment and this significantly reduced heat build up in the electrical components.

However, some problems did arise during the cycling. Several boards performed erratically during the testing. It appeared that humidity levels inside the chamber might have been a contributing factor. Therefore, additional thermal cycling was performed with the problematic boards using a different environmental chamber which had better humidity control. The previous anomalous results were not found to be repeatable. The circuit boards did not have conformal coating (RTV) applied at the time of the testing, but the coating was later applied.

System Level Vibration Testing

The random vibration PSD curve was obtained from table B-3, Appendix B of the GEVS-SE¹ and reproduced as Table 2. The prototype system was subjected to an overall RMS acceleration of 7.2 Grms. The GEVS-SE specification represents an overall level that is meant to take into account quasi-static, random, and acoustic induced vibration inputs. The system level random vibration testing was performed at the NASA Lewis Research Center Structural Dynamics Laboratory and at the Loral System facilities in Akron, Ohio.

The initial attempt to perform the random vibration test had to be aborted. The PBE has a number of pneumatic lines which are routed to various places on the experiment. Several of the stainless steel tubing runs were not supported as much as they needed. During the initial random vibration test, several pneumatic components went into resonance and this caused fittings to back off and parts to hit one another. In addition, the vibration test fixture was found to have its own natural frequencies which, when coupled with the experiment, were providing significant resonant couplings which ultimately caused the vibration table control system to shut down after a predetermined structure response limit was reached.

The pneumatic system problems were solved by adding additional support brackets and altering some of the pneumatic component brackets.

Solving the fixture/experiment coupling problem was more difficult. The vibration test fixture, illustrated with the experiment assembly in Fig. 2, had a cantilever resonant mode which effectively caused more energy to be coupled into the top portion of the experiment than the base. To help get around this, the vibration table control accelerometers were placed on the top plate of the experiment and on the vibration table itself. The response signals from these accelerometers were averaged for use in the vibration table control feedback loop.

System Level Thermal Soak Testing

The prototype system was subjected to system level hot and cold thermal soak tests in order to verify the system's capability to start and perform a complete mission simulation at the qualification level temperature extremes of 0 °C and +49 °C. In addition, it was felt that a level of confidence could be obtained for the system's ability to withstand temperature extremes during shipment from Cleveland, Ohio to Kennedy Space Center, Florida. In addition to verifying the system's ability to perform at the temperature extremes, the thermal soak tests also helped put operating time on all of the components so that infant mortality failures could be weeded out (no failures occurred).

A project-unique environmental test chamber was designed and fabricated by the project team and is illustrated in Fig. 3. The test chamber has internal dimensions identical to those of a GAS canister. The chamber is equipped with external cooling/heating fluid loops on the top and bottom of the chamber as well as around the cylinder side walls. These loops, used in conjunction with a constant temperature bath unit equipped with a small fluid pump, allowed the test chamber temperature to be varied from -5 °C to over +60 °C. In addition, the chamber was designed to allow vacuum operations to be performed inside of it. A variety of gas-tight electrical feed throughs were provided on the test chamber end plate to facilitate control and monitoring of the hardware inside the chamber.

The system level thermal soaks were performed with 10 psia pressure inside the environmental chamber in order to simulate the PBE's on orbit operation (the project requested a non-standard 10 psi pressure relief to be fitted to the GAS canister for flight).

The length of the thermal soak, or the time required for the hardware to achieve the desired temperature, was based upon the interior temperature of the experiment's two batteries. The system was allowed to cool or heat as needed until the battery internal temperatures reached the desired level, at which time a full mission simulation test was performed using software resident in the experiment's computer.

During the cold soak test, the battery voltages dropped significantly, from 34 to 25 Vdc. It was initially thought that the cold soak test might need to be aborted to avoid bringing the Silver Zinc battery voltages too low. However, as the batteries were discharged, they released heat which in turn warmed up the batteries and helped to bring the battery voltages back to an acceptable level of about 27 Vdc.

System Level Thermal Vacuum Cycle Testing

In addition to the thermal soak tests, thermal vacuum cycling was performed in order to simulate the convection free environment for on-orbit operations. The environmental test chamber was fitted with a vacuum pump that could provide a vacuum of about 10^{-2} Torr inside the chamber. Since the experiment's pneumatic system was not designed to function properly in a vacuum environment, Performance Acceptance Tests (PATs) were performed at the temperature extremes in order to verify the experiment's health. The PATs exercised each of the experiment's subsystems to an extent that verified functional capability.

The thermal vacuum cycles were performed over a temperature range of 0 °C to +49 °C. Sixteen hour soak periods were observed at each temperature extreme. Two full cycles were completed. The experiment remained powered ON during the entire test.

Effort Required For The Test Program

The initial component and box level test occurred over the course of approximately one year. Typically, 1 or 2 engineers and a technician would spend a week writing procedures, developing test fixtures, and performing the tests.

The system level testing was performed over a 4 month period during which the tests were conducted in a serial fashion. Preparation for most of the system level tests often occupied 3 or more engineers and a technician for one to two weeks. Preparation for the system level random vibration tests required even more team involvement.

Lessons Learned

- * Testing of candidate components early in the design process can uncover design problems which force the use of a different component (and also saves much time and money compared to fixing problems at a later stage of hardware development).
- * Box level environmental testing helps the project team develop confidence in the box level design. Also, problems found at this stage can be more readily fixed than at later stages in the project development.
- * System level testing uncovers many problems not found at the box level. The dynamic interactions of the various subsystems is difficult to completely determine ahead of time.
- * The amount of data that needed to be reduced and analyzed after the system level tests was significant. Analyzing the experiment data was just as time consuming as preparing for and performing the test itself.
- * The design of the vibration test fixture is critical to accurately simulating the GAS canister vibration environment. Having a vibration test fixture does not necessarily mean that the GAS canister vibration environment can be simulated properly.

REFERENCES

1. General Environmental Verification Specification for STS and ELV Payloads, Subsystems, and Components. GSFC designation: GEVS-SE. NASA Goddard Space Flight Center, January 1990.
2. Guidelines for Standard Payload Assurance Requirements for GSFC Orbital Projects. GSFC designation: SPAR-3. NASA Goddard Space Flight Center, March, 1990.
3. GAS Small Self Contained Payloads Experimenter Handbook. NASA Goddard Space Flight Center, 1986, p. 57.
4. Butler, Dan: GAS Eleven Node Thermal Model (GEM). GAS Experimenter's Symposium, NASA CP 2500, 1987, pp. 153-169.

Frequency, Hertz	PSD, (g ² /Hz)	Slope (dB/octave)
20	0.003	
20-80		6.0
80-1000	0.125	
1000-2000		-6.0
2000	0.25	
2 minutes per axis		
Overall RMS acceleration = 12.9 g's		

Table 1. Component random vibration specification.

Frequency, Hertz	PSD, (g ² /Hz)	Slope (dB/octave)
20	0.01	
20-50		4.77
50-600	0.0428	
600-2000		-3.64
2000	0.01	
2 minutes per axis		
Overall RMS acceleration = 7.2 g's		

Table 2. Box and system random vibration specification.

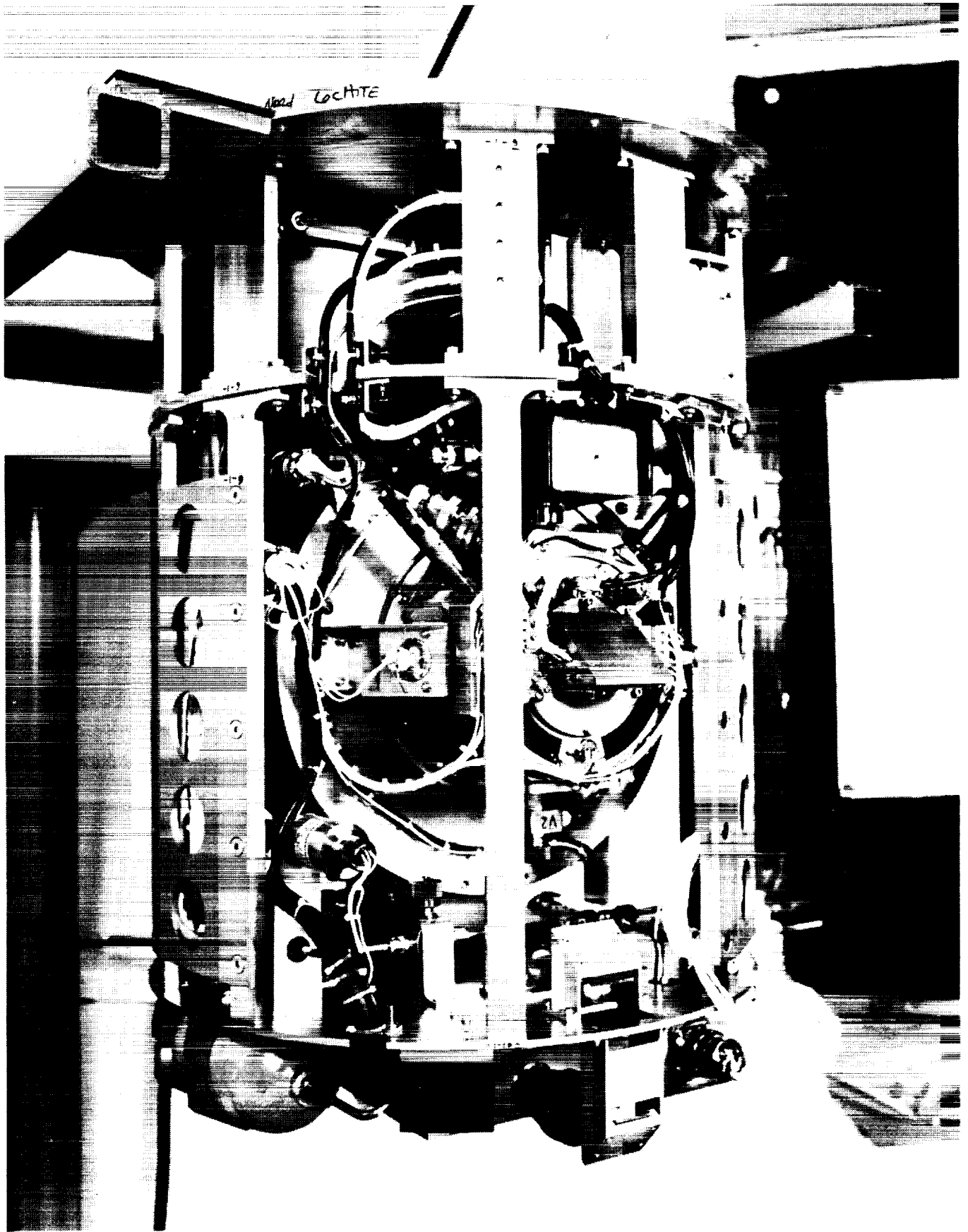


Figure 1. The PBE prototype system.

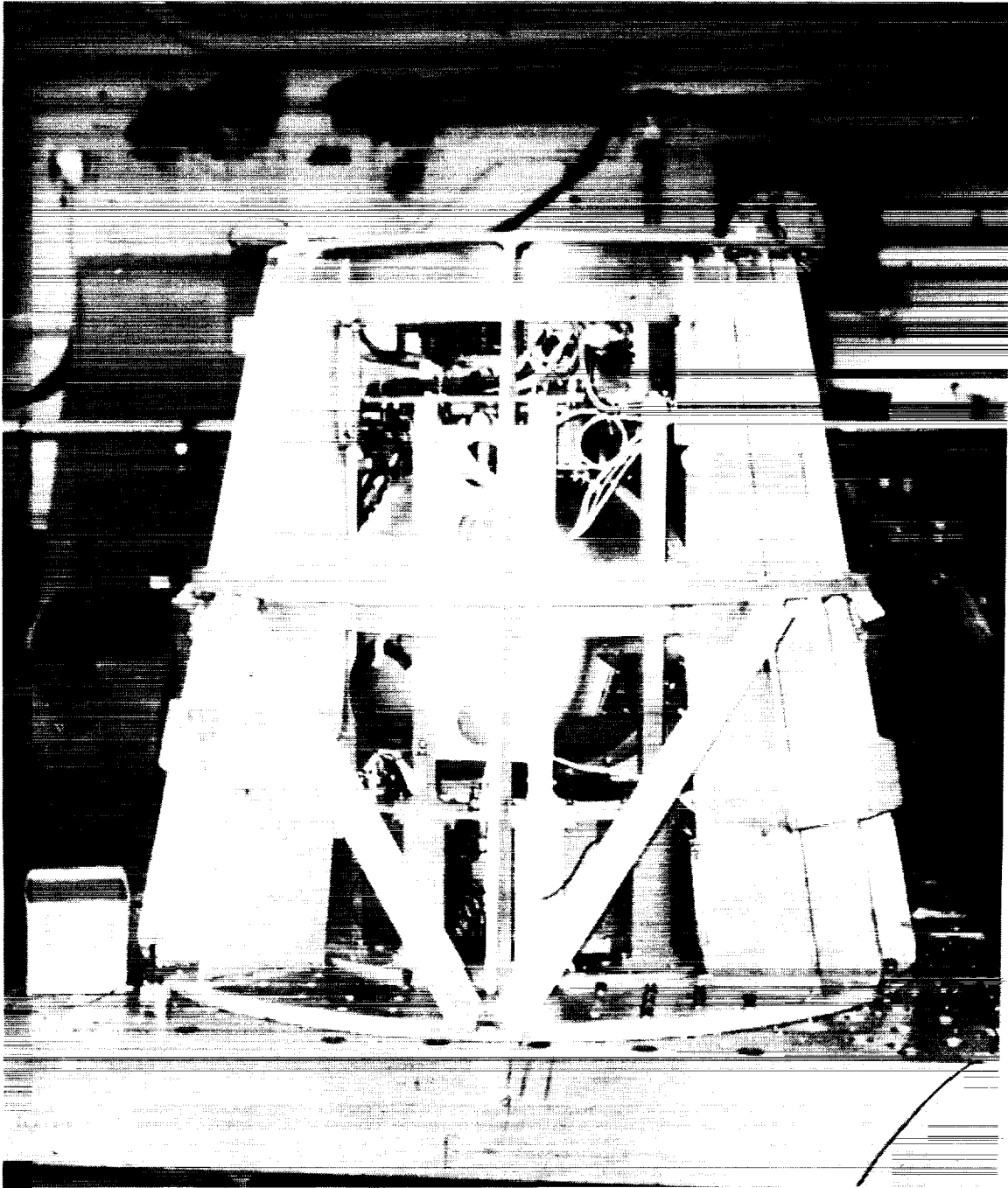


Figure 2. System vibration test fixture (with experiment).

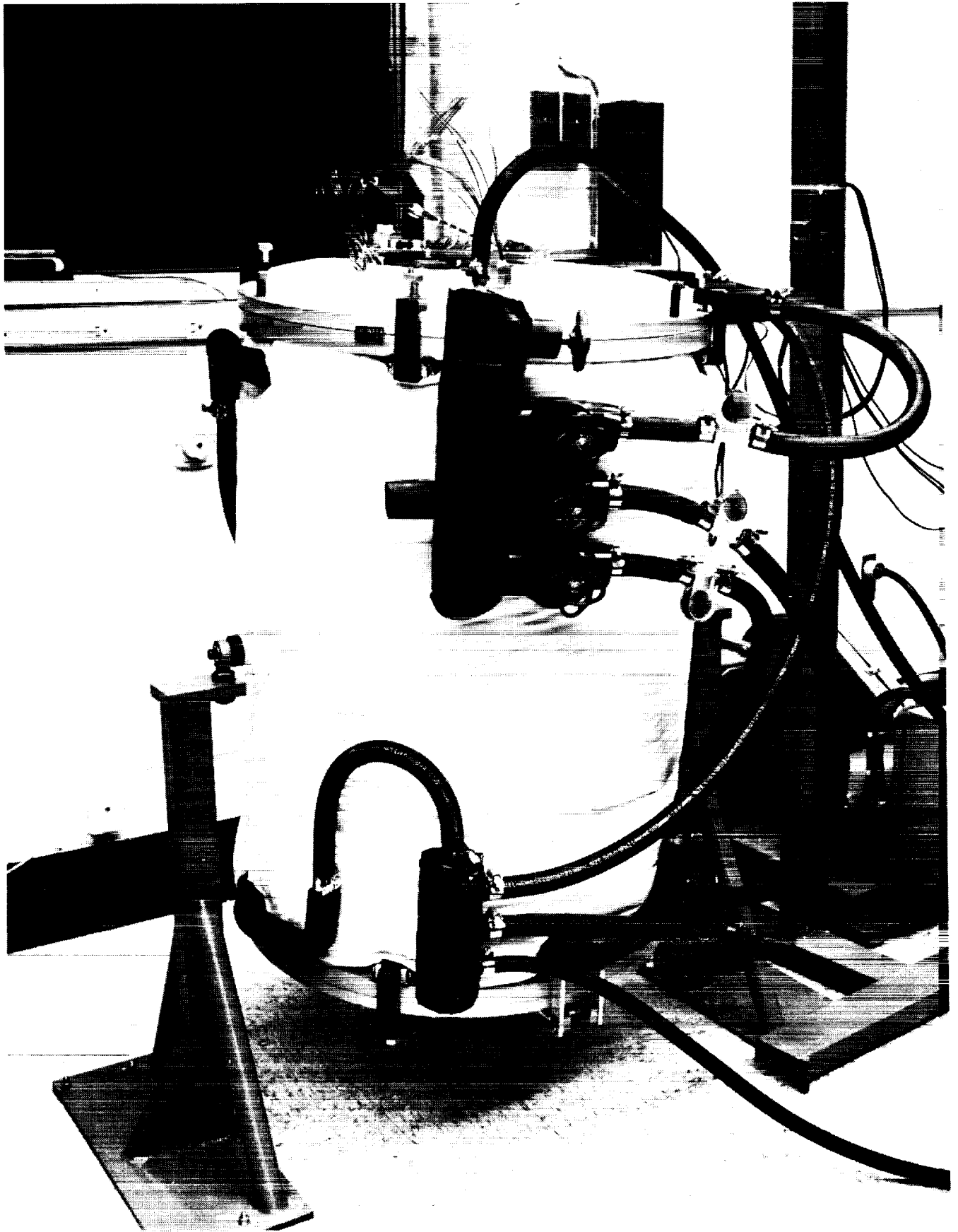
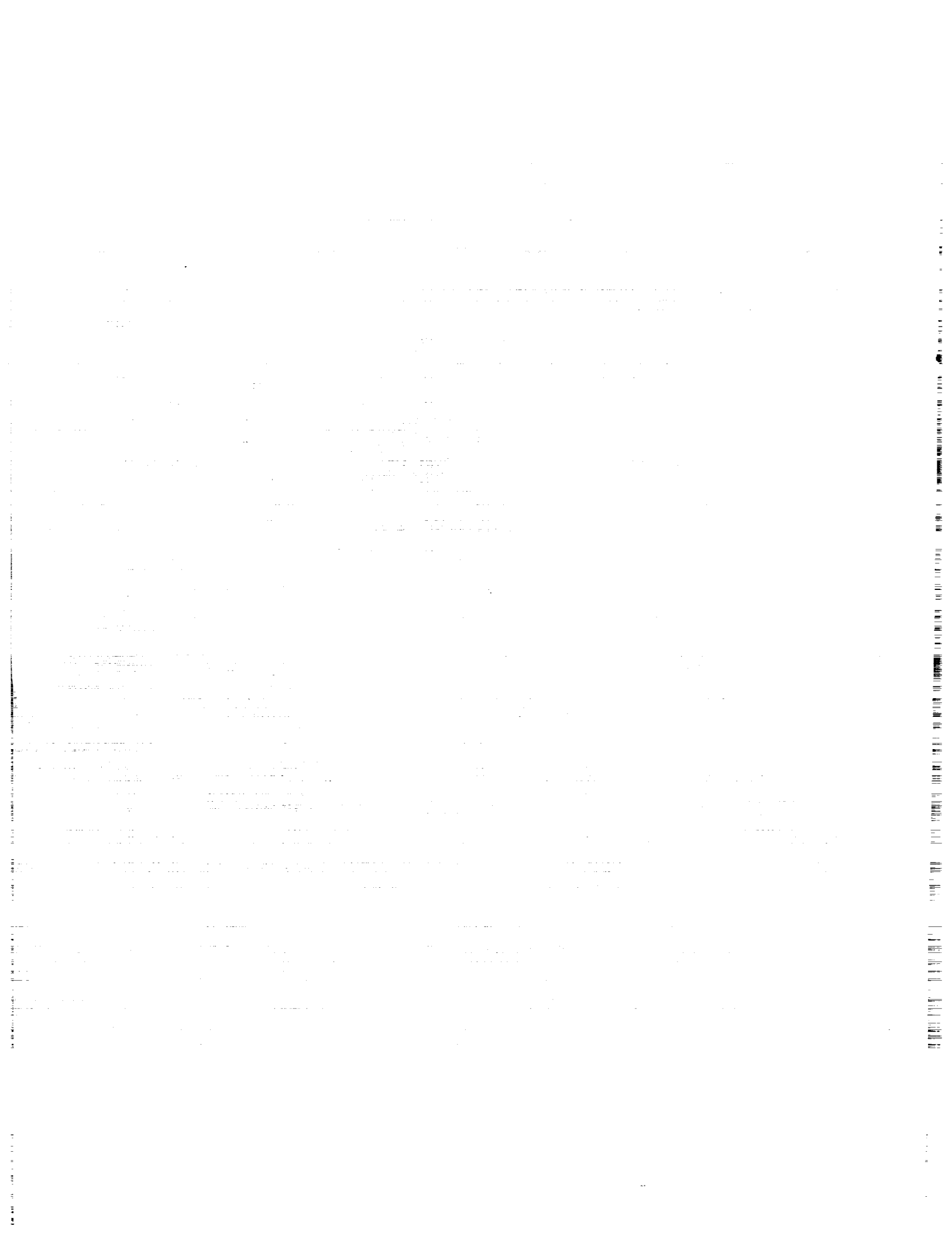


Figure 3. PBE environmental test chamber.



ELECTRICAL DESIGN OF PAYLOAD G-534
THE POOL BOILING EXPERIMENT

David R. Francisco
NASA-Lewis Research Center

ABSTRACT

Payload G-534, the Pool Boiling Experiment (PBE), is a Get Away Special that is scheduled to fly on the shuttle in 1992. This paper will give a brief overall description of the experiment with the main discussion being the electrical design with a detailed description of the power system and interface to the GAS electronics. The batteries used and their interface to the experiment Power Control Unit (PCU) and GAS electronics will be examined. The design philosophy for the PCU will be discussed in detail. The criteria for selection of fuses, relays, power semiconductors and other electrical components along with grounding and shielding policy for the entire experiment will be presented. The intent of this paper is to discuss the use of military tested parts and basic design guidelines to build a quality experiment for minimal additional cost.

EXPERIMENT OVERVIEW

The Pool Boiling Experiment (PBE) purpose is to experimentally determine the effect of heat flux and liquid subcooling on nucleate pool boiling in a long term reduced gravity environment. Nucleate boiling is a mode of heat transfer where relatively small temperature differences can provide large rates of heat transfer. This results in significantly smaller heat transfer areas to accomplish the same transfer of heat.

The experiment is performed by heating the test fluid (R-113) to 120 F with a uniformity of +/- 0.4 F. After this temperature and uniformity are achieved, the pressure on the fluid is lowered to a designated subcooling (20, 5 and 0 degrees subcooled) then power is applied to a thin (400 Å) gold film heater that has a surface area of 7.25 cm². Three different power levels are applied throughout the testing: 2, 4, and 8 W/cm². By changing the subcooling and power levels, a total of 9 different tests are performed during flight. While power is applied to the heater, temperature and pressure data are recorded. During the tests the camera is operated at 10 frames per second (FPS) and 100 FPS to capture nucleation on film. Each of the components required to perform the test is discussed in the following sections.

The PBE structure consist of two shelves that are connected together with brackets (see Figure 1.0). The experiment chamber is located between the two shelves and contains all of the science instrumentation, the thin film gold heater and the test fluid (R-113). The batteries (2) and the data acquisition and control system (DACS) are located on the top shelf. The batteries provide power to all of the components and the DACS controls all of the experiments components and acquires

the data. Other components are the triaxial accelerometer, boiling heater power supply, camera, stirrer, lights, and power control unit (PCU).

ELECTRICAL SYSTEM DESCRIPTION

The electrical system for PBE was designed using two silver zinc batteries as the power supply. The batteries power seven major components and the PCU. The components were divided into two separate groups (busses) so that the electrical "noisy" components would not interfere with the data and control system. The following is a brief description of each component and its power requirement.

Data Acquisition and Control System (DACS)

The DACS consists of a STD bus system with a CPU card and five additional cards. The CPU, memory and A/D card are bought from a commercial vendor with upgrades. These upgrades consisted of changing the parts from plastic to military screened ceramic components, see the section on Electrical Parts Selection for additional details. The CPU card is a 16 bit single board computer, 80C88, operating at 5 Mhz. The memory card is populated with eight 32K x 8 EEPROMs which gives PBE the capability of storing 256 KBytes of data. The A/D card is a 15 channel, 12 bit A/D configured in a unipolar 0 to 10 V mode. The other three cards were designed in-house and fabricated to Military Specification Mil-P-55110D. For more details on the fabrication and layout design, see the section on Printed Circuit Boards. The three in-house designed cards are the pressure control, thermistor multiplexer and the I/O-camera synchronizing.

The Pressure Control card contains a hardware logic controller which maintains the pressure in the test chamber to +/- 0.1 PSI by reading the output of the chamber pressure transducer and comparing this reading to the required setpoint (from DACS). After this comparison (this is a real time continuous process), the appropriate solenoid valve is commanded opened as required. The fill solenoid valve is connected to a nitrogen gas supply and the vent solenoid valve is open to the GAS can volume.

The Thermistor Multiplexer card provides two main functions: signal conditioning for the science thermistors (temperatures), and multiplexing 15 signals into 1 A/D channel. The signal conditioning is performed using a four resistor bridge with a highly stable voltage reference. The four resistor bridge circuit provides the greatest resolution possible over a given temperature range.

The I/O-camera synchronizing card performs two main functions. The first function is general I/O capability for the DACS. The second function is to synchronize the LEDs that are in the field of view of the camera (these LEDs display a binary time count so that each frame of film is time tagged) with the shutter of the camera. This feature prevents the LEDs from being blurred on the film.

The total power consumed by the DACS system which includes the DC/DC converter is approximately 6.25 Watts.

Thermal Strip Heaters

The experiment test chamber has strip thermofoil heaters mounted to all external surfaces. The heaters provide 5 W/in^2 of power to the chamber so that the test fluid may be heated to 120 F. The heaters have aluminum backing with Kapton insulation, 24 gauge leads and are mounted using pressure sensitive adhesive (PSA). The heaters are divided into two electrical circuits with group #1 consisting of 70 Watts and group #2 consists of 80 Watts. Each group is also over temperature protected with two thermostats.

Stirrer

A stirrer is used to mix the test fluid prior to each test sequence. This mixing provides for an even distribution of heat from the thermal strip heaters. The stirrer is a DC permanent magnet planetary gearmotor that consumes 3 Watts.

Solenoid Valves

Two solenoid valves are used to regulate the pressure in the test chamber (See DACS section). Each valve is a direct-acting, fast response, 2-way normally closed valve having bubble tight construction. Each valve requires approximately 9 Watts when operated.

Boiling Heater Power Supply

The Boiling Heater Power Supply (BHPS) is a multiple setpoint regulated voltage power supply that provides the three different power levels required for the thin film gold heater. The BHPS requires between 10 and 75 Watts of power depending on the setpoint.

Camera

A 28 Volt, 16 mm movie camera is used to film the nucleation process. The camera operates at two frame rates, 10 and 100 frames per second (FPS). Two frame speeds were required since only 18,000 frames of film were available and it is desired to capture the onset of nucleation at the faster frame rate and film the steady state boiling. The camera requires 25 Watts at 10 FPS and 45 Watts at 100 FPS.

Lights

Two lights are required to illuminate the nucleation for filming. The bulb chosen is a 24 Volt, 20 Watt halogen bulb. Each light requires 11 Watts for 10 FPS filming and 20 watts for 100 FPS filming.

Accelerometer

A triaxial accelerometer unit is included with the PBE. This device measure accelerations in the range of 0 to 50 milli-g with a resolution of 30 micro -g. The power required is approximately 1 Watt.

Power Control Unit (PCU)

The power control unit contains a triple output DC/DC converter and EMI filter. The PCU routes and controls power to all of the experiments components and signal conditions engineering instrumentation. See the section on the Power Control Unit for more details. The PCU requires approximately 5 Watts of average power during operation.

Science and Engineering Instrumentation

The science instrumentation includes the thermistors internal to the test chamber, the pressure reading of the test chamber and the voltage and current applied to the thin film gold heater. The engineering or housekeeping parameters included battery voltages, currents and temperatures. A feedback of the status of I/O lines was also stored in the data.

Power Profile and Batteries

The total energy required to operate the PBE is 420 Watt-hours. Each 28 Volt (nominal) battery is comprised of nineteen 15 amp-hour, silver-zinc cells. The total battery capacity was calculated by assuming worst case conditions. These conditions are after 3 months storage and operating at 32 F. These conditions were assumed due to the integration time for a GAS can, the shuttle attitude and the early operation of PBE during flight. The total capacity of the battery under these conditions was calculated as 765 Watt-hours. When designing an experiment with batteries it is prudent to have a 1.5 to 2 margin of energy available at worst case conditions versus energy required. This capacity must also be verified by testing.

This concludes the description of the overall electrical system. The following section describes the interconnecting of the entire electrical system.

HARNESSING, CONNECTORS, WIRE AND FUSING

Connectors

All of the non-hermetic connectors for PBE meet Military specification MIL-C-26482. The shell of these connectors are aluminum alloy with a finish of electroless nickel per MIL-C-26074. The

insulators are a rigid dielectric and the contacts are copper alloy with gold plating per MIL-G-45204. The rated operating temperature of these connectors is -55 C to 200 C. The hermetic connectors used in the test chamber and the battery boxes meet military specification MIL-C-38999. Environmental sealing is accomplished by an interfacial seal with individual raised tapered sealing barriers around each pin contact and a peripheral seal. The shell is constructed of fused tin steel with a stainless passivated finish. The insulator is compression glass. The contacts are made of nickel alloy with gold plating. The connectors are designed to operate over a temperature range of -65 C to 200 C. These connectors were chosen due to the tolerance to the environment, durability of the contacts, sure locking of the mating halves and the very low leak rate.

Wire

All of the wire use in PBE is silver plated copper conductor with Teflon insulation. This wire meets military Specification 22759/11. The wire is rated for 600 V and 200 C. See the Wire and Fuse Derating Section for criteria on selecting wire.

Fuses

The fuses used the experiment meet military specification MIL-F-23419. The fuses are subminiature high performance fast acting instrument type fuses which are classified as style FM08 by the military specification.

Wire and Fuse Derating

The policy used for wire type, size and fuse type and sizing follows the interpretation (Refer to Johnson Space Center memorandum ER-87-326) of NHB 1700.7A (NSTS 1700.7B). This memorandum covers the derating of wire and fuses for a space environment. The philosophy of this memorandum is that the circuit protectors (fuses) must be sized to protect against an educated short rather than a dead short. A smart short is defined as a current limited failure that allows current to flow in the protected wire at the ultimate trip limit of the fuse for an indefinite amount of time. Therefore the wire must be sized to withstand a load one and one half times the rating of the fuse. The design load for the fuse is equal to half of the fuse rating. The following examples use this criteria:

-20 gage, 200 C wire is not used to carry more than 3.5 amps of current and must be fused with a 7 Amp FM08 style fuse (This wire is rated for at least 10.5 Amps - 1.5 times fuse rating).

-16 gage, 200 C is not used to carry more than 4.5 amps of current and must be fused with a 10 Amp FM08 style fuse (This wire is rated for at least 15 Amps - 1.5 times fuse rating).

For comparison; If silver plated nickel conductor wire with Tefzel insulation (MIL-W-22759/18) which is rated at 150 C is used:

-20 gage, 150 C wire is not used to carry more than 2.5 amps of current and must be fused with a 5 Amp FM08 style fuse (This wire is rated for at least 7.5 Amps - 1.5 times fuse rating).

-16 gage, 150 C is not used to carry more than 3.5 amps of current and must be fused with a 7 Amp FM08 style fuse (This wire is rated for at least 10.5 Amps - 1.5 times fuse rating)

If multiple power lines are bundled together then the current capacity of each wire must be derated as follows: derate 86% if there are 2 load wires; derate 68% if there are 4 and 60% if there are 6 loaded wires in a bundle.

POWER CONTROL UNIT

The power control unit (PCU) routes power and control lines to and from the components. The PCU consist of two main sub-assemblies; a circuit card and a base with a lower compartment (See Figure 2.0). Contained within the lower compartment is a triple output (+5, +/-15V) 15 Watt DC/DC converter and an EMI filter. The EMI filter is designed to reduce the input line reflected ripple current of the DC/DC converter. The filter module also offers input voltage transient protection and reverse voltage protection. The filter reduces the conducted electrical noise, and the converter is sealed in the lower compartment to reduce the radiated electrical noise. All penetrations to the lower compartment housing the filter and converter was made via feed thru capacitors. The feed thru capacitors for the input power lines and outputs are 0.3 uF, 50V.

Mounted to the top of the lower compartment are non-latching relays. The relays are rated for 12 amps resistive load and they were derated dependent on the type of load (2 Amps for lights and 4 Amps for a motor). Non-latching relays were chosen because at power up all of the components would be at a known state (power off). Another factor for choosing non-latching relays is that only one control line is required. Since the the relays were not operated for extended duration (usually on the order of minutes), the power dissipated energizing the relay coils was not a concern. But one component, the stirrer, was operated for a longer duration (hours), so a solid state relay (SSR) was utilized. The SSR was mounted the the circuit board above the base. The SSR uses less overall energy than the non-latching electro-mechanical relay while operating. This is due to the absence of power required to energize a coil. A MOSFET driver was used to energize the relay coils. An optoisolator was also used to keep the control lines isolated from the 28 Volts required to energize the coils (which was also the same bus used for power).

The PCU also provides signal conditioning for the battery voltages and currents. The battery voltages are signal conditioned by using a simple resistor divider that divides the battery voltage by a factor of four. The current signals are conditioned by using a 0.02 Ω , 5 Watt shunt in the return line of each battery. This signal is amplified by a factor of 50 by an operational amplifier.

The fuses for the entire experiment are contained in the PCU. The subminiature fuse (style FM08) are mounted on the printed circuit board, this allowed for the minimum usage of space.

One single point ground for the batteries and the DC/DC converter output was maintained in the PCU. This allowed for a single reference for the entire experiment and the absence of ground loops (see the following section).

ELECTRICAL NOISE REDUCTION TECHNIQUES

The following guidelines were used for the PBE in reducing electrical noise.

Harnesses

- 1) Power leads twisted together.
- 2) 'Noisy' power leads twisted and shielded.
- 3) Low level signals twisted and shielded and made as short as possible.
- 4) Ground leads are placed in between signal leads and 'noisy' leads when in same connector.

Criteria For Grounding of Shields

- 1) Both ends of a shield for a noisy load are grounded to chassis.
- 2) One end of a shield for a low level signals is grounded. This ground is brought through a connector using a separate pin. This pin is directly connected to the DC/DC converter return--AT THE DACS (the point where the A/D conversion is taking place). The shield is isolated (insulated) from the connector housings and the experiment.

Other Techniques for Noise Reduction

- 1) Noisy DC/DC converters are placed in a shielded enclosure with feed thru capacitors. Ferrite beads may be placed on the leads.
- 2) Relay coils have diode suppression.
- 3) Noisy loads are on a separate power bus.
- 4) Single point ground maintained for each power bus and signal bus.
- 5) A diode is placed across inductive loads (stirrer and solenoid valves). A 0.1 micro-farad capacitor is placed across the stirrer motor. Ferrite beads are placed on the stirrer leads.

Placing noisy electrical load on a separate bus from the DACS minimizes the conduction of noise. This eliminates the need to design electrical filters for each noisy component (or for the DACS).

Circuit Cards

1) Multi-layered cards with a ground plane were used to minimize electrical noise on sensitive circuitry.

ELECTRICAL PARTS SELECTION

The electrical parts for PBE were selected with the goal of increasing reliability. The highlights of the selection policy are listed below.

Integrated Circuits (ICs)

Ceramic packages that are hermetically sealed and tested to MIL-STD-883 were selected for use on PBE.

Resistors and Capacitors

Only established reliability resistors and capacitors were used. The components used have a failure rate of 0.01%/1000 hours or better. Components with a failure rate of 0.1%/1000 hours or better were acceptable but were used only when the component with a better failure rate was not available. Use of electrolytic capacitors was avoided.

Printed Circuit Boards

The in house circuit boards are a laminate made with epoxy resin and continuous filament woven glass fabricate that is flame retardant. The material is classified under Mil-P-13949F as GFN. The circuit cards were designed to MIL-STD-275E, this specification list guidelines for all aspects of circuit board layout. The boards were fabricated to MIL-P-55110D.

GAS CAN INTERFACE

PBE uses the GSFC barometric switch to activate the GAS can Relay A which switches battery power to the experiment. Relay B is used to signal the experiment that the astronauts/shuttle is entering a quiet acceleration period. Essentially Relay B is used to switch a signal to the DACS to initiate PBE. If relay B is not activated, PBE will automatically start 14 hours after launch.

DEVELOPMENT STATUS

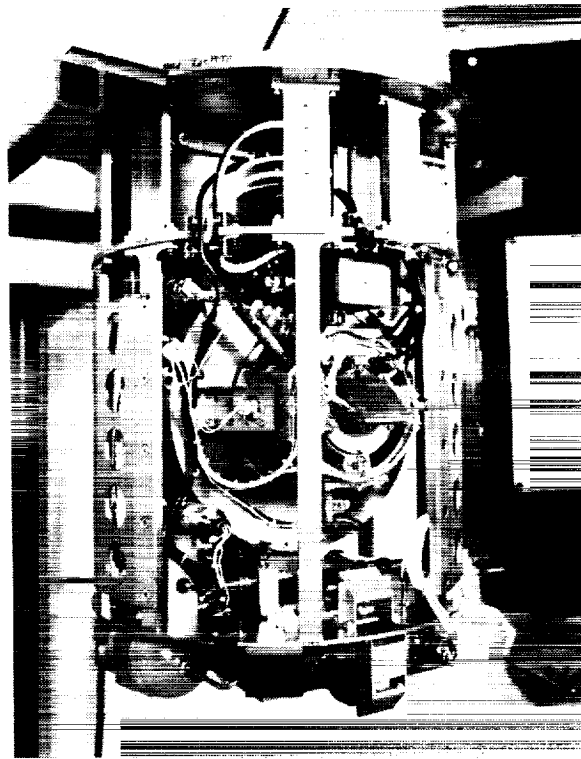
The PBE protoflight system was delivered in June of 1992 and is presently scheduled to fly on STS-47 in September of 1992. No failures due to military tested electrical parts were discovered during the test program. The test program involved thermal cycling and burn in at the box level and the system level. The flight system will be ready for launch by early 1993.

CONCLUSION

By using military tested parts with good design practices, the chances of having a failure during testing of an experiment or during flight is minimized. Even though the cost of the tested parts is higher, it's still a very small percentage of the total cost of the experiment. For the PBE the total additional cost for two flight units with spares was approximately \$25,000 which was less than 1% of total cost of the experiment. One failure of a component during testing will cost a substantial amount of money in manpower to correct. If a failure occurs during flight, the entire investment is lost. Therefore it is prudent to invest in quality parts and in good design practices.

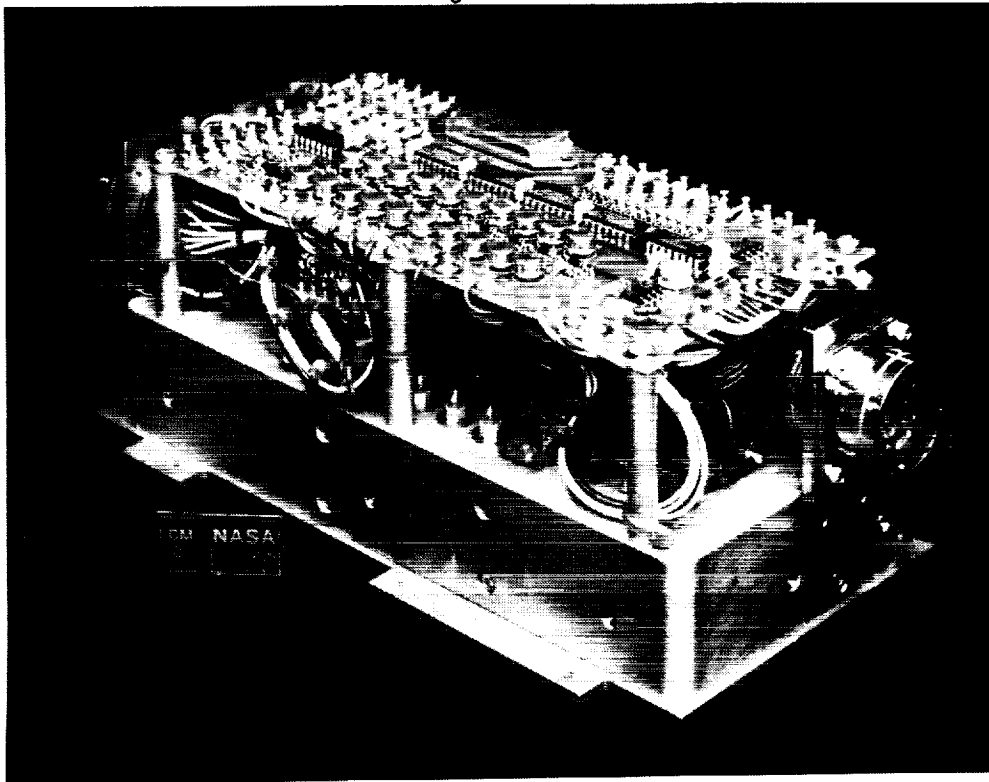
REFERENCES

1. Protection of Power Distribution Circuitry, Memorandum ER-87-326, Lyndon B. Johnson Space Center, January 1988.
2. Safety Policy and Requirements, NSTS 1700.7B, NASA, Lyndon B. Johnson Space Center, January 1989. (Formerly NHB 1700.7A).



Pool Boiling Experiment

Figure 1.0



Power Control Unit

Figure 2.0

G-133: A SOFT X-RAY SOLAR TELESCOPE

Memorie K. Williams, Branton Campbell, Peter W. A. Roming,
 Mark K. Spute, J. Ward Moody, Department of Physics & Astronomy
 Brigham Young University, Provo, Utah, 84602
 Ph#(801)378-4360, Fax:(801)378-2265

ABSTRACT

The GOLDHELOX Project, NASA payload number G-133, is a robotic soft x-ray solar telescope designed and built by an organization of undergraduate students. The telescope is designed to observe the sun at a wavelength of 171-181 Å. Since we require observations free from atmospheric interference, the telescope will be launched in a NASA Get-Away-Special (GAS) canister with a Motorized Door Assembly (MDA). In this paper we primarily discuss the most important elements of the telescope itself. We also elaborate on some of the technical difficulties associated with doing good science in space on a small budget (about \$100,000) and mention ways in which controlling the instrument environment has reduced the complexity of the system and thus saved us money.

I. INTRODUCTION

The "GOLDHELOX" Project ("GOLD" for the color of the sun and "HELOX" for HELiocentric Observations in X-rays) is a near-normal incidence soft x-ray robotic telescope being built by an undergraduate student research organization. The organization is composed of a cabinet, a science team, and three systems teams (optical, electrical, and mechanical), all staffed by undergraduate students. The project has been financed by two NASA grants, the BYU colleges of Physical & Mathematical Sciences and Engineering Technology, and by a number of private contributors. The completed telescope, after installation in a NASA GAS canister with an MDA, will fly in the bay of a space shuttle for the purpose of photographing the sun. The telescope will take a sequence of 700 photographs of the solar x-ray emissions in a wavelength band of 171-181 Å. The target date for completion of the Goldhelox payload is the fall of 1992. We are scheduled to fly our telescope on the STS-57 Atlantis mission scheduled for launch in April 1993¹. The telescope will produce full-disk images of the sun with a spatial resolution of 2-2.5 arc seconds, and a time resolution of less than 0.1 seconds. The photographs will be taken at a number of different levels of image intensification in order to investigate a wide range of intensities across the solar disk. Once obtained, the photographs will be analyzed by graduate students and professors at Brigham Young University and published.

Our bandpass was chosen to sample Fe IX, Fe X, and Fe XI emission lines. The solar plasma that emits those wavelengths corresponds to temperatures upwards of 0.8 million degrees Centigrade. These temperatures only occur in the region of the corona near the upper transition region and are characteristic of a number of solar features such as active regions, flares, micro flares, and x-ray bright spots. Our observations are designed to address the following questions:

1. What is the structure of solar plumes, and what is the source of the solar wind?
2. What mechanism causes the initial energy release in a solar flare²?
3. What is the relationship between the occurrence of coronal mass ejections, the occurrence of microflares, and the high resolution upper transition region magnetic structures³?
4. How does the transition region between the corona and chromosphere respond to the impulse phase of flares⁴?

The purpose of this paper is to introduce the project from an instrumental and operational point of view. In section 2 we present an overview of the telescope design. Section 3 addresses the principles of restricting the instrument environment to reduce cost and complexity. We discuss the methods this project has

utilized to produce a complex experimental device capable of making a contribution to solar physics on a low budget (about \$100,000).

II. THE GOLDHELOX TELESCOPE

It is convenient, for the purpose of discussion, to separate our telescope into three main elements: 1) the optical system which collects, filters, amplifies, images, and records light from the sun, 2) the mechanical structure which supports and protects the optical and electronic elements of the system as well as providing the telescope with several motional freedoms, and 3) the electrical system which monitors and controls all functions of the instrument through the use of two partially redundant computers. This section describes each of these elements.

The Optical System

The Goldhelox telescope is a two mirror optical system consisting of a concave parabolic primary mirror and a convex hyperbolic secondary mirror in a cassegrain configuration. Solar x-rays are first collected by the primary mirror, then reflected towards the secondary mirror which in turn sends them through the one inch hole in the center of the primary mirror to the detector assembly. The focal plane is 2.25" behind the primary mirror.

X-ray reflecting mirrors are more complicated than the common visible-light mirrors. When dealing with visible, infrared, or even near-ultraviolet light, it is common to find that a mirror reflects as much as 90% of the incident light intensity. In the X-ray wavelengths, however, most incident light is absorbed or transmitted by a mirror rather than reflected. To improve the x-ray reflection efficiency, we use a mirror material with an internal layer structure radiation can be reflected off the multiple surfaces in the material and then recombined. The layer thickness is spaced such that x-rays reflecting off of the individual surfaces combine constructively, resulting in a stronger reflection at certain angles. It is the thickness of the layers in the mirror material that determines these angles. These X-ray mirrors are generally one of two types: 1) grazing-incidence or 2) multilayer coated.

Grazing-incidence telescopes use the natural layer structure of crystalline materials to obtain multiple reflections. The lattice spacing in most crystals is, unfortunately, such that constructive reflection occurs only for incident light that is nearly parallel to the mirror surface. Hence the name grazing-incidence telescopes. Because effective reflection occurs only at grazing angles, these telescopes typically have to be long and bulky to effectively focus light into any sort of image.

Because of the size constraints on our telescope, we have instead elected to use multilayer mirrors, a more recent development in x-ray optics. They are made by alternately applying thin coatings of two different materials onto a smooth substrate. Our mirrors use 100 layers, each consisting of 50 Å of Silicon above 50 Å of Molybdenum. Because the layers are man made, the layer thicknesses can be chosen to produce good reflections at almost any angle desired, even normal incidence. Thus multilayer mirrors have made it possible to manipulate x-rays in almost the same way that visible light is manipulated.

Our multilayer mirrors are made to have 40% reflectivity at near normal incidence for soft x-rays in our bandpass (171Å to 181Å). They act as partial filters because light outside this range is not effectively reflected through the telescope. To properly filter out all the radiation outside our bandwidth, we have also added two additional radiation filters (1000 Å thick sheets of aluminum).

In spite of the fact that multilayer mirrors significantly improve reflectivity, intensity losses in the telescope remain a problem. The total efficiency of the optical system is only about 2%, furthermore only a very small fraction of the energy emitted from the sun falls in the wavelength range in question⁵. This makes it difficult for an optical instrument as small as ours must be (3" in diameter) to gather enough light for an adequate film exposure. Therefore, to amplify the image, we use a microchannel plate (MCP) image intensification device. The maximum factor by which the MCP can boost the incident image intensity is about 5000 times (the actual image intensification factor will vary according to a pre-programmed sequence which will be executed by the telescope's computer). When the MCP is bombarded by x-rays, the x-rays stimulate cascades of electrons that are accelerated toward a phosphor screen which emits in a visible wavelength. A visible light image is then conveyed from the phosphor to the

35 mm film via a glass cylinder composed of parallel interfused fiber optic cables, each cable having an internal diameter of 10 microns.

The Mechanical System

The telescope itself (composed of the optical elements just described and the mounts that hold them in alignment) is mounted between two vertical support walls 7 inches apart. The walls extend up from a rotating plate (see figure 1). This plate rotates upon the barrel-shaped sealed container containing the telescope control computers and other electrical components. The sealed container is airtight to maintain a normal gaseous atmosphere inside. The telescope also rotates about a pivot axis extending between its support walls. The pivot is located near both the center of the GAS canister and the center of the telescope.

The telescope has two motional freedoms: first, rotation in the azimuthal plane (the plane of the rotating table), and second, rotation in the plane of declination (the plane normal to the upper pivot axis.). The rotating table moves atop a 10 inch diameter turntable gear (see figure 2). The teeth around the outer edge of the turntable gear are matched to a smaller gear on the shaft of a stepper motor. This stepper motor which drives the azimuthal telescope motion is mounted on top of the rotating table, with its shaft reaching down through the table.

Rotation in the plane of declination is also driven by a stepper motor, but in this case a worm gear assembly is used. The motor and worm are attached to one of the support walls, and the worm gear itself is attached to the telescope body. The telescope body can assume any declination between vertical and 43° off vertical and can rotate through the entire 360° in the azimuthal plane.

Within the telescope itself, the mirrors and mirror mounts are attached to the telescope housing. The MCP flange, which is mounted inside of the camera, and acts as an image window. The camera is attached to the telescope housing, and the housing is fastened to the telescope pivot. The telescope has an alignment tolerance between 1/10,000 and 1/1,000 inches. Because this tolerance is difficult to meet with ordinary materials, we have chosen to use a composite with very low coefficients of thermal expansion for the walls of the housing and other parts of the mirror mounts. This composite is light, strong, resistant to vibration, and space environment compatible.

The Electrical System

The electrical system centers around two partially redundant computers. The first computer receives input from the tracking system and controls the positioning of the telescope. It also warms up the MCP prior to use and performs picture taking operations. The second computer is the ultimate instrument controller. It puts the instrument into a low power hibernation mode when the sun is not in view and controls the distribution of power to every other element of the electrical system. It monitors and controls the temperature of the environmentally sensitive elements of the system, and takes over control of the photographic functions of the MCP in the event that the first computer fails.

Four power supplies are required to operate the entire instrument. One power supply provides the various DC voltages between 5 and 20 Volts needed by the many electrical system circuit elements. Another high current supply drives the three stepper motors used for telescope positioning and film advancing. The last two, called switching power supplies, provide the 1000 Volt lead and the 5000 Volt lead required to operate the MCP. Picture taking is actually done by switching the MCP on and off using exposure times which will vary according to a pre-programmed sequence between .1 and .01 seconds.

Another important feature of the electrical system is the tracking circuitry. The sun-tracking system provides continuous information to the telescope control computer regarding the location or absence of the sun in the telescope's field of view. There are three tracking sensors. The first we call the "daylight" sensor, which we place near the top of the telescope allowing it to indicate to the control computers whether or not the sun is in the instrument field of view. If the sun is discovered to be in the field of view, the telescope is rotated through the azimuthal plane until the second or "coarse" sensor indicates that the sun is within 8° of the plane of declination of the telescope. When the coarse sensor tests positive, the controllers check the third or "fine" sensor. The fine sensor has a 2x2 array of photodiodes. When a light source illuminates the array, this fine sensor circuitry determines the amount of light incident on each photodiode and

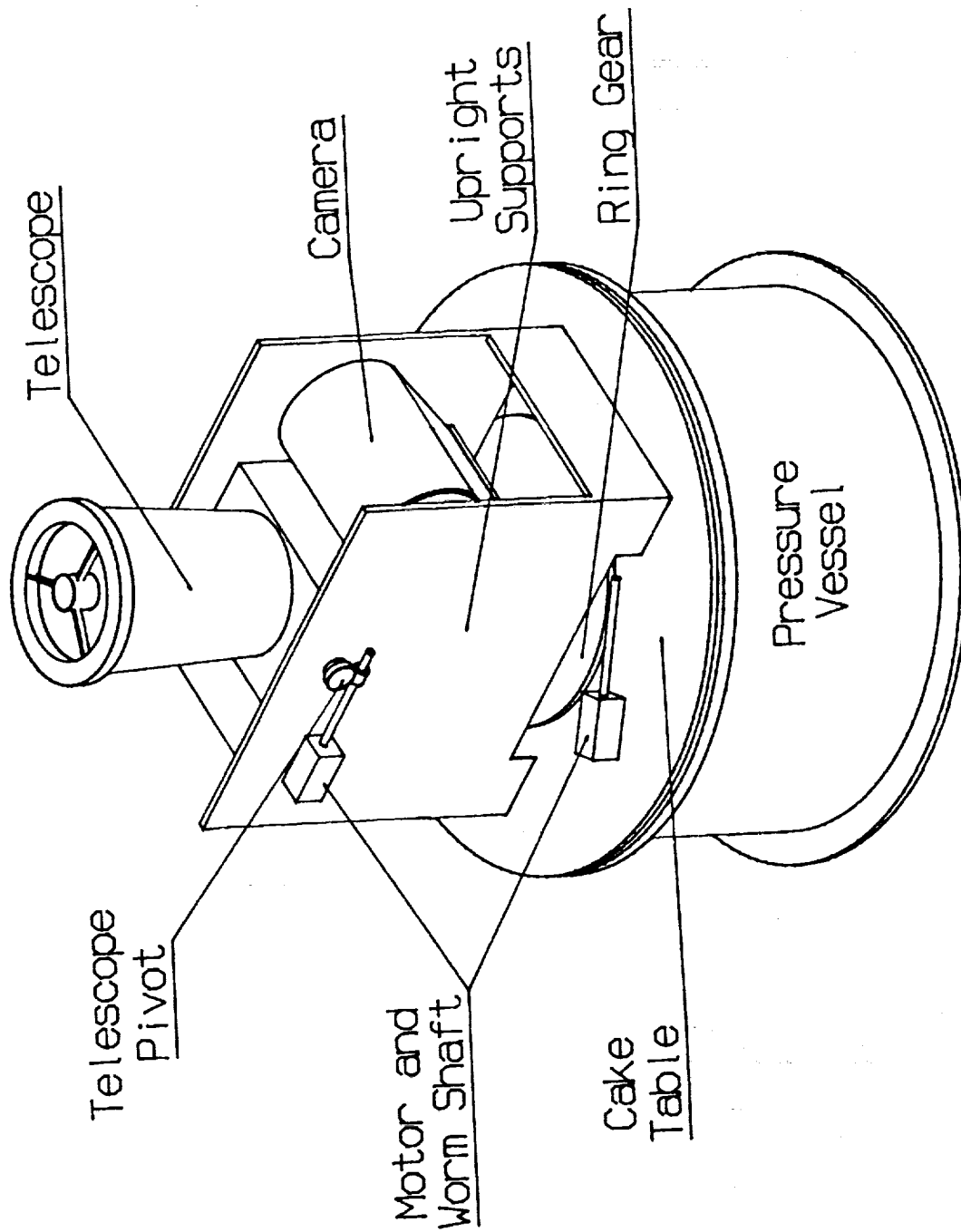


FIGURE 1: An external view of the entire GOLDHELOX soft x-ray robotic telescope, with key mechanical components indicated. Dimensions are not to scale.

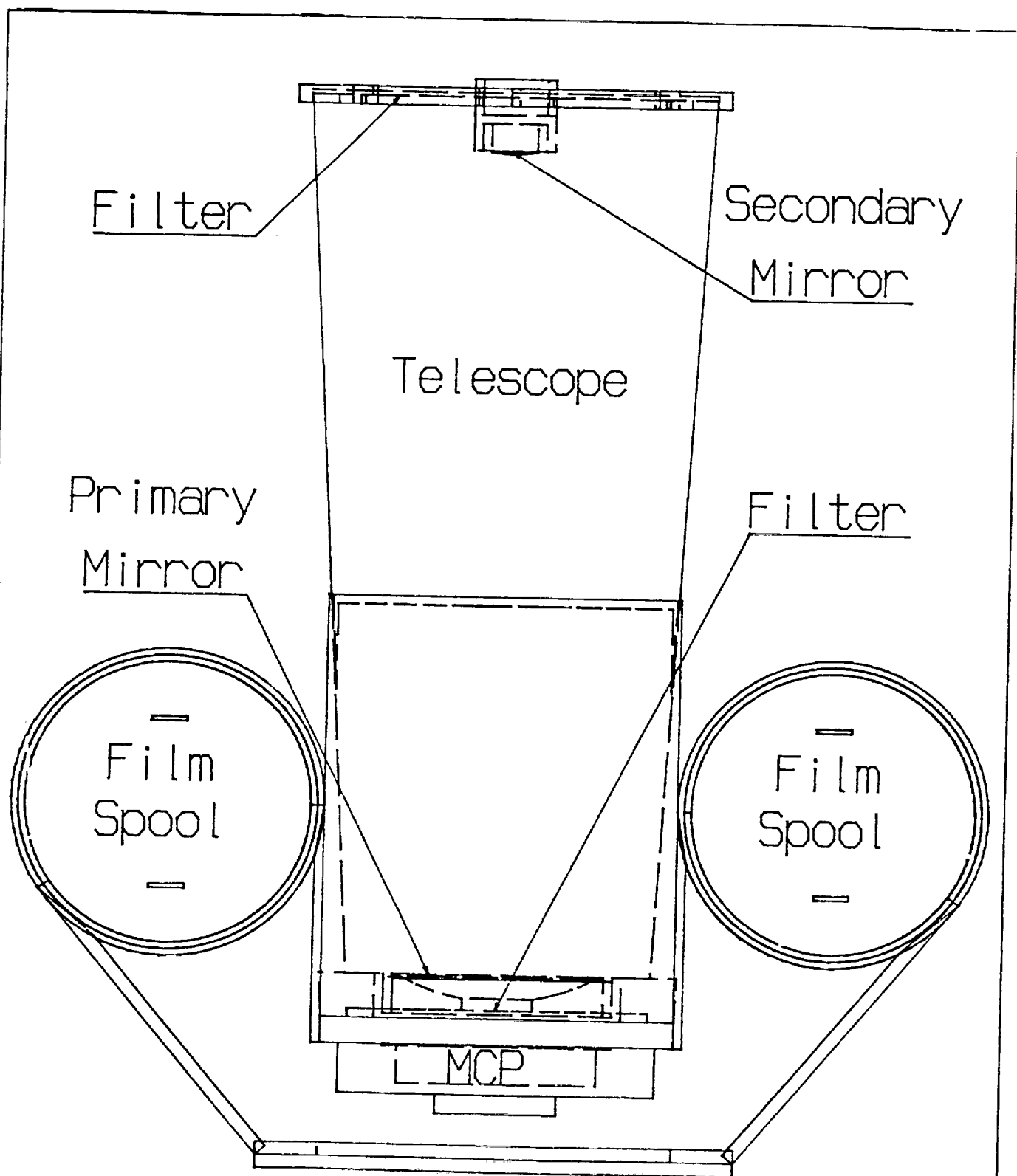


FIGURE 2: A cross-sectional side view of the GOLDHELOX telescope, with all optical components indicated. Dimensions are not to scale.

returns two voltages (an 'x' and a 'y' coordinate) indicating how far off the sun is from the optical axis of the telescope. The computer accordingly repositions the telescope and again checks the fine sensor. This procedure is repeated until the telescope is within 1/10 of a degree of being aimed directly at the sun.

III. REDUCING COST AND COMPLEXITY BY RESTRICTING INSTRUMENT ENVIRONMENT

There are many instances during the design stage of a space bound instrument in which cost and complexity can be significantly reduced by restricting the instrument's environment. In much the same way as a decision to have a barbecue in the back yard as opposed to a picnic in the park eliminates the need to pack half the kitchen into the trunk of the car, making a few restrictions on the operating environment of an instrument can eliminate the need for many of the auxiliary functions, fail-safes, and precautions that burden the instrument without increasing the value of the data that it obtains.

When we first began to plan the design of the Goldhelox telescope, we learned that much could be done on a small budget if we didn't try to do everything. For example we looked for several months for an extremely sensitive, high resolution camera film that was vacuum compatible (won't become brittle) over a wide range of temperatures, and obtained cost estimates from a few companies to custom process or even develop the film we required at a price of around \$1000/yard, with a minimum purchase requirement of \$10,000. Such an expenditure was well out of our reach. Then a team member suggested that we just use regular 35 mm film and simply not let the film be exposed to the space environment. He pointed out that this would be possible if our MCP were mounted in a standard vacuum flange and sealed onto the front of the camera with the atmosphere inside. Although the inside of the camera is now less accessible, this simple design modification saved thousands of dollars and greatly simplified our film processing requirements.

The most difficult technical problems that our project has had to deal with has been 1) temperature control and 2) tracking our target, the sun. It is difficult to find affordable optical and electronic components that won't malfunction or even fail completely at the hot and cold temperature extremes. Tracking sensors for example, can be purchased from stock, unless you want them guaranteed at temperatures ranging from -100°C to 100°C (a temperature range which is standard in a space environment). The tracking system also had three problems of it's own, in addition to the temperature problem. First, the instrument must be able to determine when the sun is in view and when it isn't, properly discriminating against all other sources including the brightly illuminated earth which frequently fills the entire telescope field of view. Second, the telescope has no advance information regarding when the sun will be in view. And third, high resolution pictures require that the telescope maintain it's orientation with respect to the sun without deviating more than two seconds of arc during picture taking. This is a challenge even for state of the art tracking systems when the many different types of orbital motion assumed by the shuttle on a typical mission are all considered.

NASA provided a way for the complexity of the electrical system to be greatly reduced through the availability of standard options, which not only solved our tracking problem but also eliminated the extreme temperatures previously anticipated, thus permitting us to purchase less expensive electrical components. By allowing for as many as six actions to be performed for a GAS payload by the shuttle crew during flight. This way the crew will be activating our instrument only during a few specific time intervals in which the shuttle bay is directly facing the sun. Hence the telescope will only have to cope with minor amounts of rotation, eliminating the need for complicated tracking subroutines. Also the MDA on our canister can now be closed during nearly all of the mission, protecting our instrument from the more extreme temperatures common to open lid flights, and saving us tens of thousands of dollars of additional expenditure on military specification electrical components. This illustrates the general principle (which many with more experience than we have already know) that for cost-effective space research, regularly consider the possibilities of trading instrument freedom for more simplicity.

SUMMARY

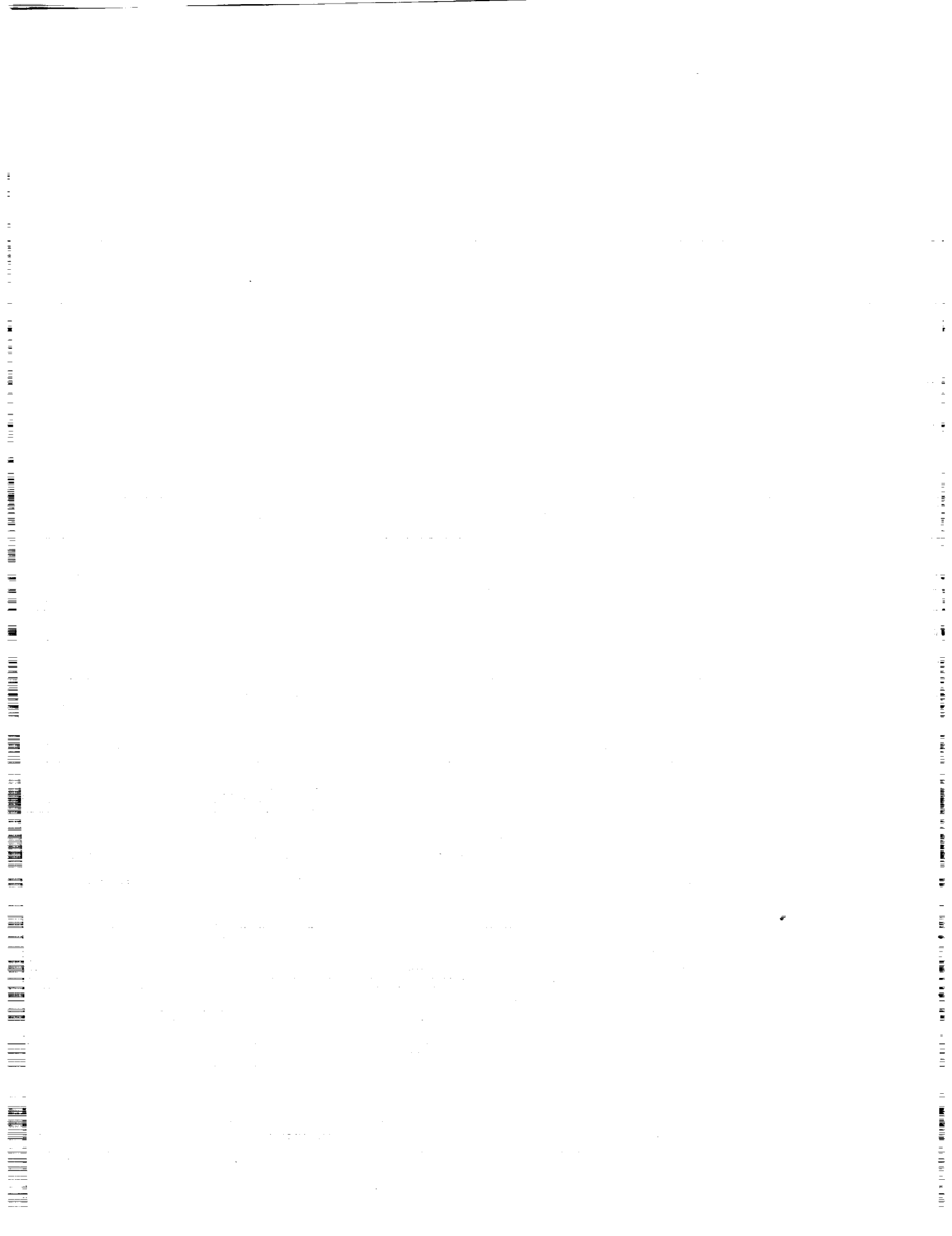
The GOLDHELOX Project is an unusual effort in that it is both managed and staffed by undergraduate students. The project, if successful, will prove that a real contribution to space research is possible in a university setting, and on a low budget. The current trend in space exploration is towards 100% reliability, requiring researchers to purchase only the highest quality components, and at great cost. If the GOLDHELOX telescope satisfies the hopes and wishes of it's makers, it will not only help us gain a greater understanding of the sun, but will set a precedence for others who are interested in space research, but believe it to be out of their financial reach.

ACKNOWLEDGMENT

This work is supported by grant #NAGW-2612 from the Education Division and the Space Physics Division of NASA Headquarters.

REFERENCES

1. "Shuttle Manifest", Final Frontier, Oct. '91, p25
2. "Solar Max 1991 Proposal", NASA publication Pg. 1-7
3. "Solar Soft X-ray Pulsations", Harrison, Astron. Astrophys. 182, p337-347 (1987)
4. "Fast Fluctuations of Soft X-rays from Active Regions", Simnett & Dennis, NASA Conf. Pub. 2449, pg123-124
5. "The Importance of Spectroscopy in the 80-800 Å Region for Plasma Diagnostics in the Solar Atmosphere", Feldman & Doschek, Space Science Reviews, 22, 1978



TAGGING INSULIN IN MICROGRAVITY

PRESENTERS:

Michael Dobeck
Computer Science Instructor
Sierra College
Sacramento, California

Ronald S. Nelson M.D.
Internal Medicine
Private Practice
Fresno, California

STATEMENT OF THE PROBLEMS TO BE ADDRESSED BY THE G-399 PROJECT

Declining Enthusiasm

A major problem seen today is the declining enthusiasm for technology among American college students. There are certainly many students which are attuned to science and technology, but their numbers are declining every year.

Declining Number of High Tech Tools

There is a declining number of high tech tools that are available to college professors which can be used to teach students the motivation to acquire knowledge in applied science. Sierra College's mission is to give students skills in applying scientific tools to industry needs. This project is to demonstrate to the students the whys and wherefores of practical and applied science, and the creation and value of teamwork in the solution of technical and scientific problems.

Diabetes Mellitus Treatment

Major advances have been made in the treatment of diabetes by the fine tuning of treatment methodologies. Up until ten years ago, all blood sugars were done in the lab monthly or less frequently with the patient only checking his urine for sugar; this resulted in poor control of glucose and a poorly controlled patient. Now, individual patients can check their own blood sugars, thus achieving better control and prolonging for a few years the complications that will surely develop.

Knowing the exact subcellular sites of action of insulin in the body has the potential to give basic science investigators a basis from which a cause and cure for this disease can be approached. The goal of this project is to create a test reagent that can be used to visualize these subcellular sites.

PRECEDING PAGE BLANK NOT FILMED

SOLUTION - THE GET AWAY SPECIAL PACKAGE FOR THE SHUTTLE

High Tech Environment

The shuttle program by itself creates a unique high tech environment which gives "infectious enthusiasm" to students, researchers, and the professors. The realistic demanding requirements that are the epitome of perfection which require the patience of Job, are inherent in the program and are part and parcel of a good business. The most rewarding personal goals of life are usually those attained by following the rules set down by someone else; working in the Shuttle environment teaches the student this lesson thus preparing them for the real business world of applied science.

Shuttle Micro Gravity Environment

The unique micro gravity environment of the Shuttle will allow the creation of a reagent that has the possibility of elucidating the subcellular sites of action of insulin.

If The Experiment Is Successful

If the procedure does indeed create the desired reagent for insulin, the same procedure modified slightly, could be used to create many other tagged entities. The list of uses for this procedure would be endless and could extend from hormones to organisms to drugs.

DIABETES AND INSULIN

Diabetes mellitus can be defined as a disease wherein the physiologic control mechanisms for the regulation of glucose levels by insulin are measurably outside of defined normal levels. This is a very complicated disease to grasp in concept since at one end of the spectrum an individual has lost his ability to make any measurable insulin, because of the destruction of the insulin producing cells from the apparent effects of an auto immune phenomenon or acute pancreatitis to the woman who only manifests the disease when she is pregnant.

The common denominator for all the diabetic states is a deficiency in tissue response to insulin. At one end of this continuum is a no-insulin state with a predictably no control over glucose to the other end of the continuum where there is an excess of perfectly good insulin that apparently is unable to influence the tissue receptors. Tissue receptors have been counted on a cellular basis and have been found to vary from tissue to tissue and between disease states. The exact location of these receptors on the cell wall or other structures is unknown.

A basic unknown is whether insulin can exert its effects from outside the cell, i.e. near it or attached to its membrane, or does it penetrate the cell and exert its actions from within the cell. Possibly, it acts at different sites with different tissues or a combination of sites.

Autoradiography

Several techniques have been utilized in an attempt to isolate the sites of action of items such as insulin. One of these is autoradiography in which the test item is obtained from animals fed radioactive materials. The test item is then radioactive and is given to another animal. After an appropriate length of time the target tissues are harvested and thin slices obtained for the microscope. A photographic emulsion is placed over the tissue allowing the radioactive material to expose the emulsion. By looking for silver granules one can infer that the target item had appeared at that point. This technique is capable of showing which cells absorb the test item, but is not even close to being accurate enough to disclose the exact subcellular site of attachment.

The Need To Visualize The Sites Of Action Of Insulin

What is clearly needed is to visualize individual insulin molecules at their sites of action. Insulin molecules themselves do not possess any attributes that would enable their visualization. A tag is needed that can be placed on the insulin molecule which will enable its localization while it is attached to the insulin receptors at its sites of action. This tag has to satisfy a number of qualifications, two of the more important are that it must not significantly alter the action of insulin, and that it must present a unique appearance on electron microscopy to allow its reliable identification.

Ferritin

Ferritin is a large molecule having a molecular weight of approximately 900,000 with iron atoms arranged in a characteristic tetrad formation which is easily identified on a molecule to molecule basis in tissues at a 160,000 magnification. Insulin with a molecular weight of approximately 6,000 has no distinguishing features in the electron microscope. The following figures show ferritin, both in its pure state and after its conjugation.

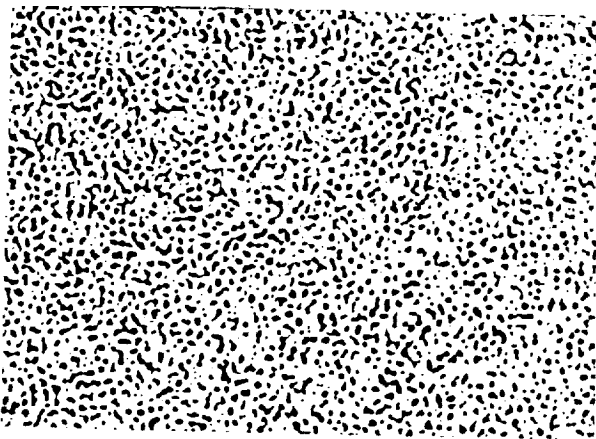


Figure 1.
Pure Ferritin 160,000 X
Note: Uniform Pattern

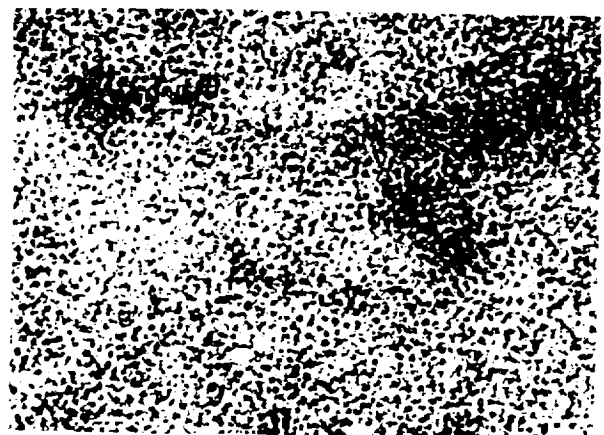


Figure 2.
Ferritin-Insulin conjugate
160,000 X, Clumped Pattern

INSULIN TAGGING

Tagged Insulin Reagent

In summary, the insulin tagging process to be used on G-399 involves the conjugation of insulin molecules with ferritin molecules to create a reagent that will be used back on Earth in an attempt to elucidate the sites of action of insulin.

During 1969 and 1970, co-author of this paper, Dr. Ronald Nelson tagged insulin with ferritin and injected it into diabetic laboratory rats. Preliminary results were obtained, but the creation of the test reagent was difficult because of the disparity in molecular weights between the insulin and its iron containing tag. The photomicrographs above clearly show that the solution of ferritin itself is very homogeneous, while the ferritin-insulin conjugate is very lumpy, even after considerable processing steps. It is hoped that in the microgravity environment of space that this disparity in molecular weights will not be a factor in the reaction that conjugates insulin molecules with ferritin.

The conjugating process that will take place on the Shuttle and its past history is as follows:

THE TAGGING PROCESS

The original process utilized in 1969 and 1970 for the creation of the test reagent occurred in a glass container stirred by a standard glass encapsulated magnet. The reaction required 24 hours at a temperature of 4 degrees Celsius. During this time the insulin molecules were conjugated (tagged) with the iron containing molecules of ferritin. After conjugation, the mixture was dialyzed against normal saline to remove any remaining traces of the very active conjugating agent difluoro-dinitro-phenyl-sulfone (DFDNDPS). Further purification steps involving filtration and fractionation through sephadex columns removed unconjugated insulin and overly conjugated insulin and ferritin complexes. A major problem with the process was the migration of the heavier iron containing ferritin to the bottom of the reaction vessel which resulted in unwanted conjugation of ferritin to ferritin, and at the top insulin to insulin.

The reactants will be mixed in the GAS container by being pumped around a continuous loop for 24 hours in the microgravity environment of the Shuttle thus avoiding the settling out of the reactants and ensuring a uniform mixture for the entire 24 hour period. The process in the Space Shuttle will end after the dialysis phase with the reactants being stored. Further purification and separation of the various conjugates will be done back on earth where the normal gravity gradient will be needed for the operation of the sephadex columns.

Post flight usage of the reagent will involve its injection into the arterial circulation of test animals that have been made diabetic.

After various lengths of time the animals will be sacrificed and electron microscopy used to search out the location of the ferritin which will be presumed to be attached to insulin. A series of controls will be utilized to make sure that the data is meaningful.

If the process proves useful for the hormone insulin, other hormones and important proteins could be tagged with ferritin and their sites of action determined.

Photomicrographs below show some of the original data which appears to indicate that at least one of the sites of action are the pinocytotic vessicles in the walls of the capillaries found in diaphragm muscle. A major site of diabetic lesions is in large blood vessels. A break through in protecting these structures would be most welcome in the medical community. Little is known about the function of insulin in glandular tissue and ferritin tagged insulin has the potential for isolating its action in these very complex and also very important tissues.

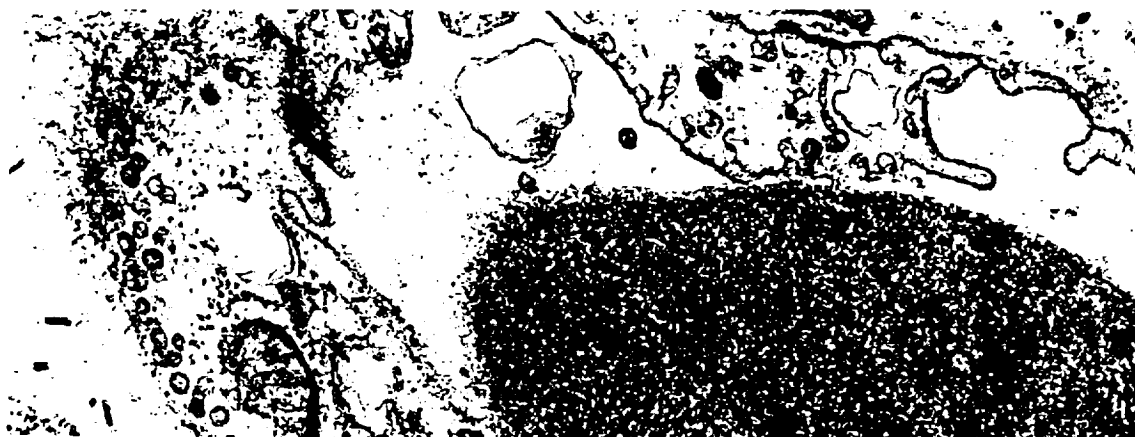


Figure 3. Orientation Picture of Tissue 50,000 X
Red blood cell lower right surrounded by endothelial cells
containing pinocytotic vessicles.
(Rat paceutatic tissue capillary)



Figure 4.
Insulin-Ferritin Conjugates within pinocytotic vessicles
(160,000 X Rat diaphragm muscle capillary endothelial cell)

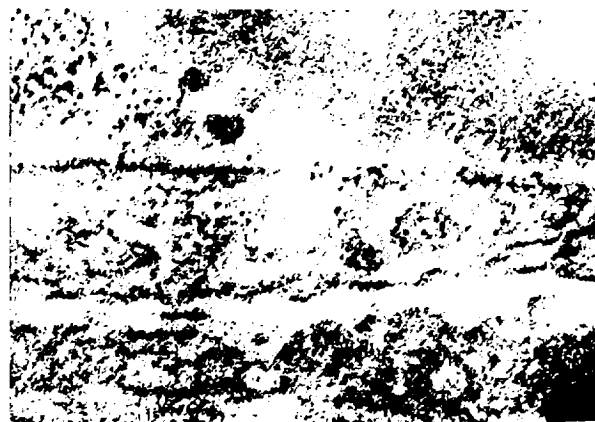


Figure 5.

INSULIN TAG EXPERIMENT HARDWARE

Experiment Apparatus

The hardware for the insulin tag experiment consists of 6 containers which hold the fluids required to complete the experiment, 7 solenoid controlled valves that keep the fluids separated prior to the start of the experiment, two fluid pumps for mixing and one air pump for fluid transfer (see figure 6).

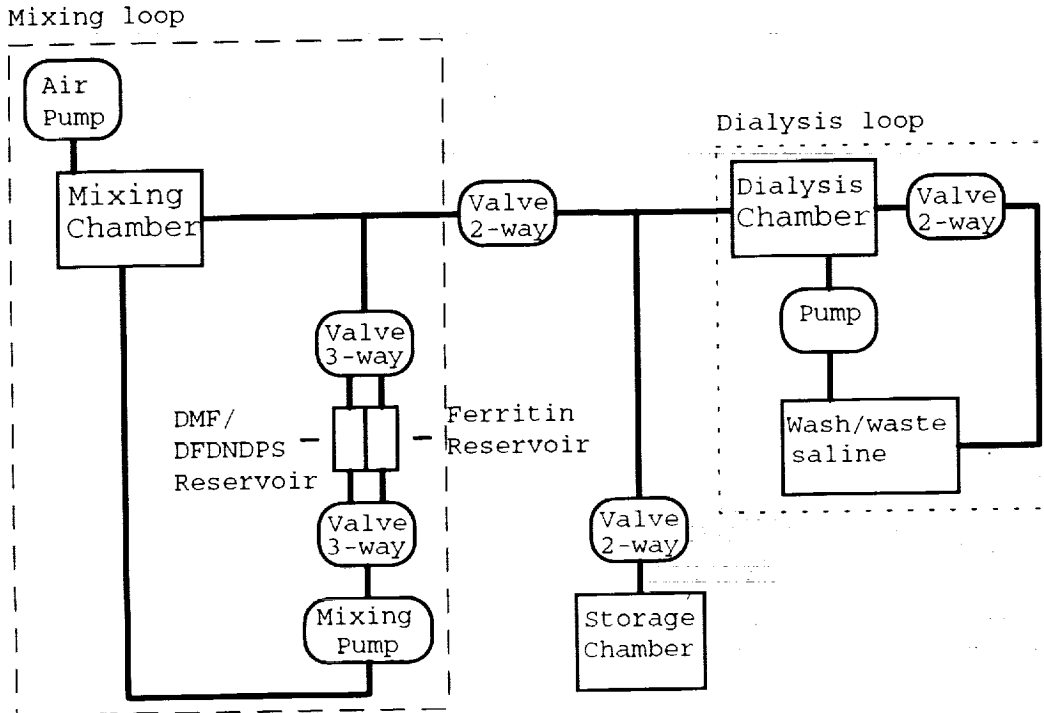


Figure 6. ITE Schematic

Mixing Phase

The insulin tag experiment (ITE) begins with a temperature check of the ferritin reservoir, mixing chamber, and DFDNDPS/DMF reservoir. If the temperature is in the 1 to 6 degree C range, the mixing phase of the ITE begins.

The goal of the mixing phase is to combine the DFDNDPS/DMF solution, which is held in the DFDNDPS/DMF reservoir, with the ferritin/ringers solution, which is contained in the ferritin reservoir, and the insulin/deionized water/sodium carbonate solution, which is held in the mixing chamber (see table 1). All three solutions are isolated by solenoid controlled valves with Teflon wetted parts. Once the proper temperature is reached, the ferritin side of the two three-way valves will open, and the mixing pump will start and run for 4 minutes. At the end of the 4 minute ferritin mix, the pump will shut down and the ferritin side of the three-way valves will close. The

DFDNDPS/DMF side of the three way valves will then open, and the pump will start and run for 4 minutes.

Table 1: ITE Solutions

<u>Component</u>	<u>Volume</u>	<u>Launch Location</u>
DMF	27 ml	
DFDNDPS	961 mg	DFDNDPS/DMF reservoir
ringers	69 ml	
ferritin	6 g	Ferritin reservoir
insulin	1.4 g	
DI water	101 ml	
sodium carbonate	3.4 g	Mixing chamber
wash saline	500 ml	Wash/waste saline
	container	

The anodized 6061-T6 mixing chamber has an internal latex bladder connected to the inside top of the chamber with a tubing clamp. The top of the mixing chamber is penetrated by two 0.125 inch NPT 316 stainless steel compression fittings which enter through the neck of the bladder. One of the fittings is connected to the multiplexed port on the 3-way valve leading into the ferritin and DFDNDPS reservoirs (see figure 6). The other fitting is connected to one side of the mixing pump. Because DMF is a fairly active organic solvent, all of the connections between the chambers, valves, and pumps are made with Teflon tubing.

Wrapped and glued to the outside of the mixing chamber is a 2.5 Watt kapton insulated electric resistance heater. The microcontroller will use the heater to maintain the temperature in the 1 to 6 degree C range.

On the end opposite the pump and valve connections, is a single 316 stainless steel compression fitting. This fitting is connected to a small air pump which will pressurize the mixing chamber during the fluid transfer phase.

The ferritin and DMF/DFDNDPS reservoirs are each of the same basic design. Each reservoir is constructed of a piece of aluminum tubing with an aluminum end cap welded on one end, and a o-ring sealed screw in cap on the other. Penetrating the end of each cap is a 316 stainless steel 0.125 inch NPT compression fitting. These fittings are connected to the 3-way valves with Teflon tubing. Fastened to the wall inside each reservoir is a flexible bladder filled with air. The air bladders leave room for fluid expansion should the chambers freeze.

Transfer Phase

After the mixing phase is complete, the fluid in the mixing chamber must be transferred to the dialysis chamber (see figure 6). To accomplish this transfer, the two-way valve between the mixing chamber and the dialysis chamber will open, and a small air pump will pressurize the mixing chamber to a maximum of 4 psig. The increase in pressure will force the bladder in the mixing chamber to collapse and

the fluid in the mixing chamber into the dialysis chamber. The two-way valve that separates the mixing and dialysis chambers will then be closed, and the air pump will be shut down.

Dialysis Phase

The dialysis chamber is constructed of 6061 T6 anodized aluminum. This chamber has a pair of 316 stainless steel compression fittings penetrating the welded end used as entry and exit ports for the dialysis fluid. The o-ring sealed screw cap end has a single 316 stainless steel compression fitting through which the tagged insulin will enter and exit. Inside the dialysis chamber, a single tube on the screw cap end opens into the flexible dialysis membrane.

The dialysis chamber is heated with a 2.5 Watt Kapton insulated electric resistance heater and has a temperature sensor for feedback to the microcontroller.

The wash and waste saline containers are 500 ml I.V. fluid bags contained in a composite structure box. The box is constructed of s-glass over foam core sides, top, and bottom. A 12 Watt heater is mounted on an aluminum plate in the bottom of the box.

The dialysis phase will last for 4 hours. During this time, saline solution will be transferred from the wash saline storage container, by a magnetically coupled gear pump, into the dialysis chamber. As fresh saline is pumped into the dialysis chamber, the waste saline is forced through an open two-way valve into the waste saline storage container.

Storage Phase

The storage phase is the final step in the ITE. The goal of the storage phase is to transfer the solution in the dialysis chamber into the storage chamber. The two-way valve that separates the dialysis chamber from the storage chamber will be opened, and the two-way valve that allows waste saline to flow into the waste saline storage area will remain closed. The wash saline pump will transfer approximately 100 ml of wash saline into the dialysis chamber. This will force the solution contained in the dialysis tubing into the storage container. Finally the storage container two-way valve will be closed.

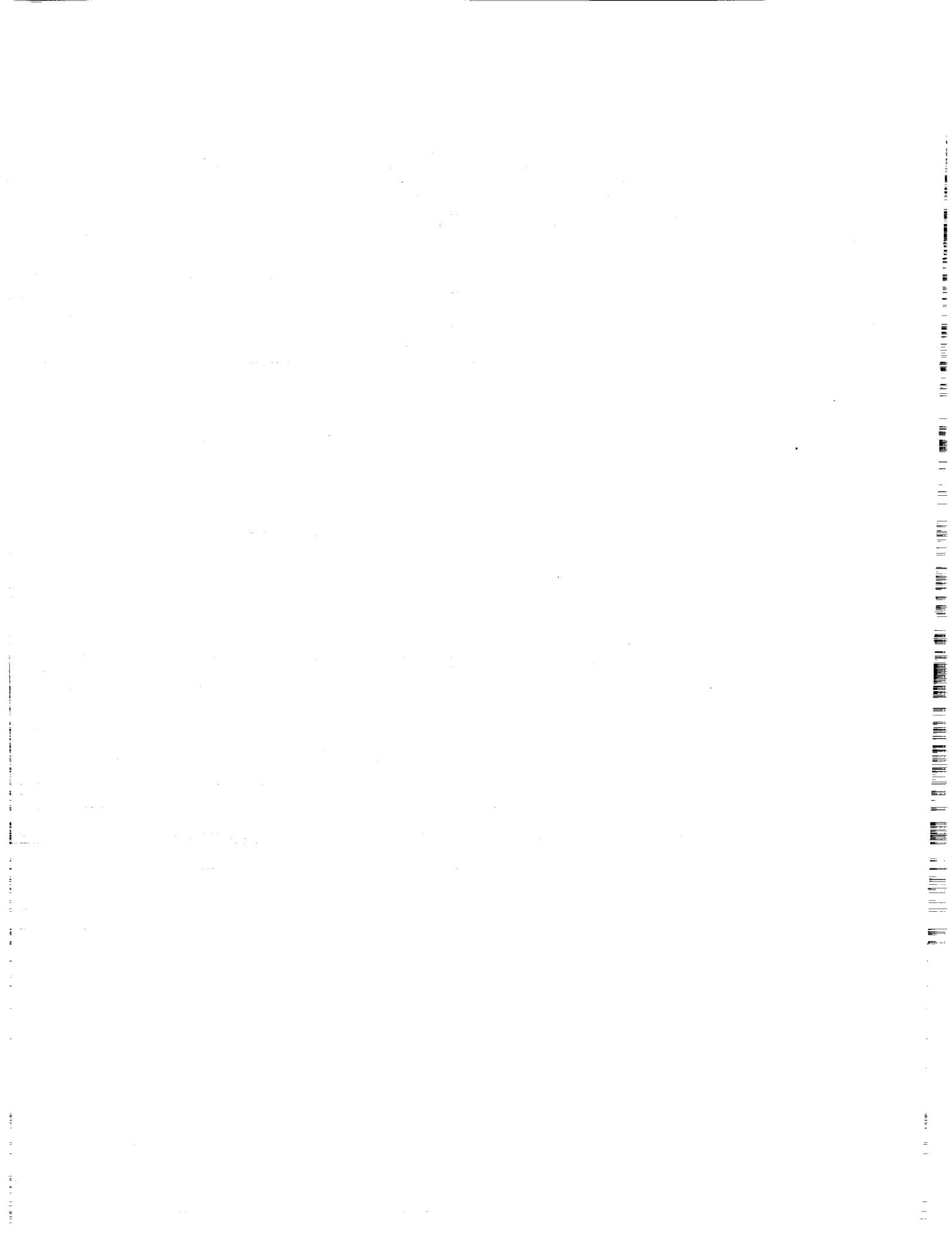
The storage container is a 250 ml polypropylene chemical storage bottle with a stainless steel tube penetrating the lid. The storage container is connected to a stainless steel "T" fitting which is connected between the dialysis chamber and the mixing chamber. An isolation valve prevents fluid from entering the storage container during the fluid transfer phase.

Safety Considerations

The fluid pumps used in the ITE are magnetically coupled, gear driven. The fluid pumps can generate a maximum of 49 psig in the unlikely event of an overpressure condition. An overpressure condition may occur if a valve failed to open and the pump was switched on. The magnetic coupling on the pump disengages within 0.5 seconds during an overpressure condition and the pressure drops to 0 psig. The ITE has been proof pressure tested to twice the maximum design pressure (100

psig). The pump housing is 316 stainless steel and the internal gears are Delrin.

Because the ITE uses a flammable organic solvent, the entire experiment must be triple contained. The ITE is fully contained in a 0.160 inch 6061-T6 aluminum containment vessel. The containment vessel will be purged with gaseous nitrogen prior to the sealing of the GAS canister.



N 93-13173

GAMCIT - A GAMMA-RAY BURST DETECTOR

Derek M. Surka, John M. Grunsfeld*, Brett A. Warneke
California Institute of Technology
Pasadena, California 91125
for the GAMCIT Team

ABSTRACT

The origin of celestial gamma-ray bursts remains one of the great mysteries of modern astrophysics. The GAMCIT Get-Away-Special payload is designed to provide new and unique data in the search for the sources of gamma-ray bursts. GAMCIT consists of three gamma-ray detectors, an optical CCD camera, and an intelligent electronics system. This paper describes the major components of the system, including the electronic and structural designs.

SCIENTIFIC OBJECTIVES

Gamma-ray bursts were first reported in 1973 from observations on earth orbiting satellites. These energetic events are characterized by a rapid increase in the observed gamma-ray flux, at photon energies from tens of keV to greater than 1 MeV, followed by a decline which may be a simple exponential, or quite complex. In Figure 1 is shown three gamma-ray bursts observed by the BATSE detector on the Compton Gamma Ray Observatory [1].

It was quickly realized that these gamma-ray bursts represent one of the most energetic and violent phenomena observed in the universe. While many experiments have been developed to study gamma-ray bursts, including the BATSE experiment, their origin is still one of the great enigmas of modern astrophysics. The BATSE observations have yielded important data on the possible origin of these events. By observing the coarse location of the gamma-ray burst events, the BATSE researchers have determined that the sources of gamma-ray bursts are distributed isotropically. Further, from studies of the intensity of the bursts, they have deduced that the sources are not distributed homogeneously but have a definite boundary [2]. In Figure 2 is shown the distribution in Galactic coordinates of a sample of the gamma-ray bursts observed by the BATSE detector showing the isotropy of their locations. These facts indicate that the bursts are either local to the solar system, distributed in a large halo around the Galaxy, or at cosmological distances. Considerable theoretical effort is currently in progress in an attempt to explain the nature of these mysterious gamma-ray burst sources.

* Department of Physics, Mathematics, and Astronomy; current address: NASA Johnson Space Center, Houston, TX 77058.

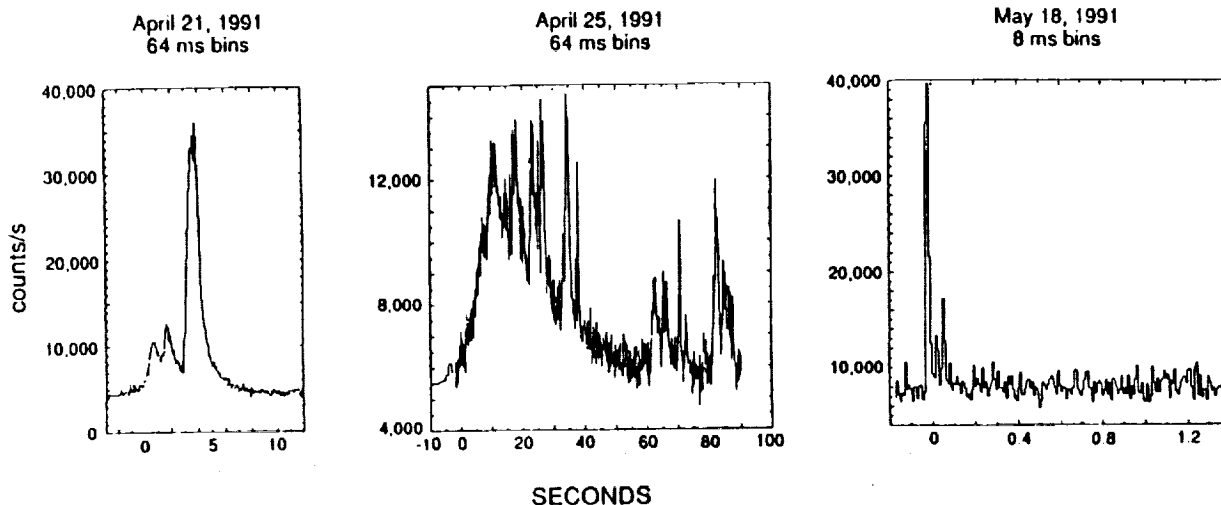


FIGURE 1. A sample of gamma-ray bursts as observed by the BATSE instrument on the Compton Gamma Ray Observatory (reproduced from [1]). These burst profiles show the wide variety of structure and varying time durations of gamma-ray bursts, from milliseconds to 100s of seconds. The energies of the gamma-rays in these plots range from 60 keV to 300 keV.

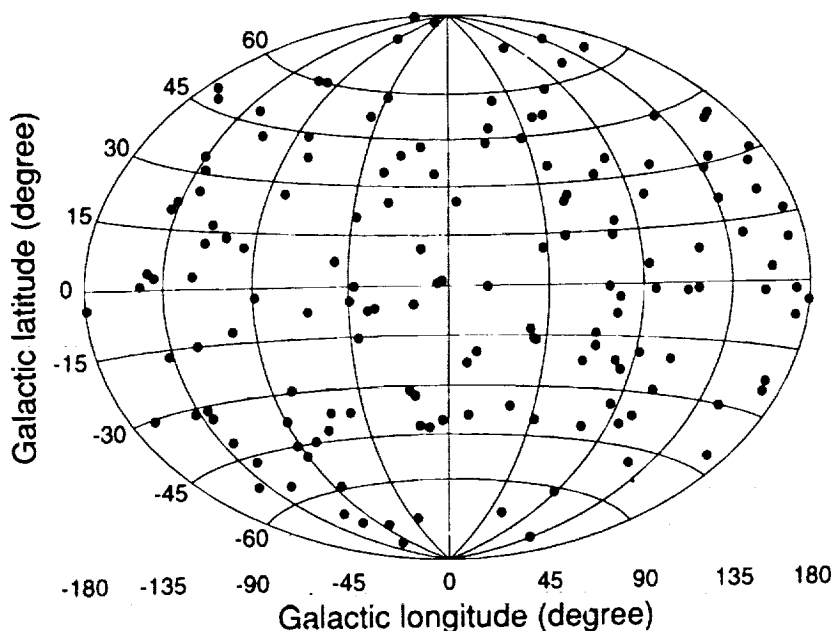


FIGURE 2. The angular location of gamma-ray bursts in Galactic coordinates as observed by the BATSE instrument on the Compton Gamma Ray Observatory (reproduced from [2]). The observed distribution shows no significant deviation from isotropy. In particular no enhancement along the Galactic plane (latitude=0) is seen, as would be expected if the sources of gamma-ray bursts had the same distribution as the stars in the Galaxy.

One theory suggests that neutron stars in binary systems are the culprit. In this scenario, a normal companion star transfers material into the extremely strong gravitational potential well near the neutron star. The energy this material gains is converted into gamma-rays near the surface of the neutron star producing a gamma-ray burst. Other models predict that comets, or other material is accreted by an isolated neutron star or black hole producing the gamma-ray burst. One interesting prediction of some of these theories is that as the gamma-rays hit the atmosphere of the companion star (or the material in orbit around the neutron star) some of the gamma-ray energy may be reprocessed into visible light. If these theories are correct, then a gamma-ray burst may be accompanied by a flash of optical light.

The scientific motivation for the California Institute of Technology Gamma-Ray Burst Detector (GAMCIT) project is to detect celestial gamma-ray bursts and to test the optical flash theory. Discovery of even a single optical flash, coincident with a gamma-ray burst, might well provide the key to crack the gamma-ray burst puzzle.

SYSTEM DESCRIPTION

Our technique is to use three conventional sodium iodide, NaI(Tl), scintillation gamma-ray detectors, combined with an image intensified CCD camera, sensitive to visible light. The GAMCIT payload provides, for the first time, truly simultaneous gamma-ray and optical observations. An intelligent electronics controller triggers the CCD camera when the gamma-ray burst is detected by the scintillation detectors. Three detectors are used to allow the requirement of a multiple coincidence between independent units, which reduces the chance of a background event mimicking a gamma-ray burst. It also provides some redundancy in the event of a hardware failure.

The time of occurrence of a burst is determined by using an on-board Global Positioning System (GPS) receiver, which provides a stable UTC clock and the position of the orbiter. This position and time are needed for correlation of the arrival time for a burst at the orbiter with the arrival time for the same burst at other satellites and spacecraft in the solar system. From these times triangulation can be performed to determine the direction from which the gamma-ray burst originated.

If we detect an optical flash, we should be able to localize the source to within a radius of less than 10 arcminutes. In addition, the CCD camera frames provide the aspect of the GAMCIT payload by determining the pointing direction of the experiment through the observations of bright star tracks.

To discriminate against solar flares, trapped electron precipitation events, and South Atlantic Anomaly crossings we also incorporate a small silicon charged particle detector. While solar flares resemble gamma-ray bursts, they are usually accompanied by a large charged particle flux, which will be registered by the silicon detector, allowing us to veto such events.

Based on input from the analog electronics and high speed logic system a microprocessor will control the CCD camera and GPS subsystem. All the data is processed by an intelligent microprocessor system and stored on high capacity hard disk drives for later analysis on the ground. A block diagram of the GAMCIT payload is shown in Figure 3.

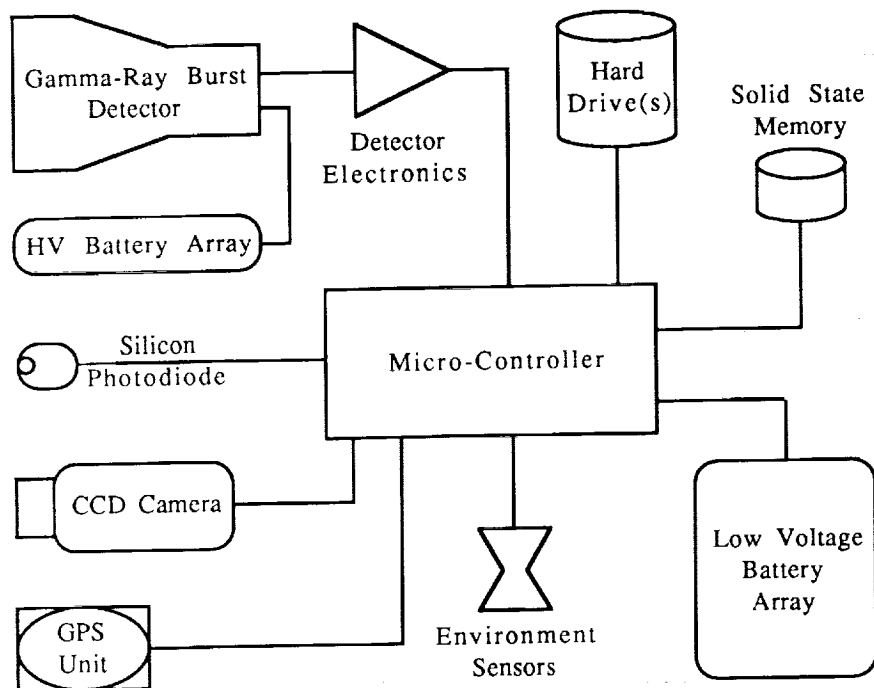


FIGURE 3. Block diagram of the Caltech GAMCIT payload.

ELECTRONICS

The challenge for the electronics design is to produce a sophisticated and intelligent data acquisition system while keeping the instrument within size, weight, and power constraints. The signal from the gamma-ray detector is conditioned by high speed analog circuitry and digitized for processing by a 16-bit CMOS, high-reliability, low-power microcontroller. This microcontroller serves the functions of instrument control, data handling, and system monitoring. The instrument utilizes hard disk drives designed for use in portable computers because of their high data density, low power consumption, and high mechanical reliability.

When the analog circuitry detects a gamma-ray burst it sends an interrupt to the microcontroller, which begins recording the burst and triggers the CCD camera to begin capturing optical information. The CCD data is compressed using image compression routines for efficient use of the mass storage resources. Additionally, the microcontroller monitors several analog sensors to aid in making operating decisions. These include the charged particle detector, a photodiode, which protects the CCD camera from the intense light of the sun, and an array

of temperature sensors. These solid state sensors are used for temperature control and to aid in post-flight thermodynamic analysis of the system. A second microcontroller is used to control the GPS subsystem, which interfaces with the primary microcontroller. The GAMCIT mission may be one of the first occasions on which this precision system will be employed aboard the Space Shuttle.

Overriding all design concerns for the electrical systems is a need to stay within the power budget. As the GAS payload is independent of the Space Shuttle power system, it needs to provide its own supply of power. To conserve energy the microcontroller powers down instruments when they are not needed, such as the CCD camera and hard disk drive. The microcontroller stores the data in solid-state memory buffer until a sizable amount of information has been collected. The hard drive is then powered up and the data stored permanently. Similarly, the CCD camera can be powered up within a fraction of a second when a burst has been detected.

To meet the power requirements of the GAMCIT system, we chose to use gel cells for their space qualified status, relatively high current density, fairly flat discharge curve, and sturdy packaging, which protects the detector and the Shuttle from possible battery leaks.

In Table I we list the power estimates of the major components of the GAMCIT system.

TABLE I.- POWER BUDGET ESTIMATES

Component	Power Estimate	Comments
CCD camera	5 Watts	low duty cycle
GPS System	1.5 Watts	
Hard Disk Drive	2 Watts	low duty cycle
Photomultiplier Tubes	1 microWatt	separate high voltage system
Logic Circuits	0.5 Watts	microcontroller
Analog Circuits	0.5 Watts	amplifiers, sensors

MECHANICAL

The challenge for the structural design of GAMCIT is to provide a one atmosphere pressure environment for the electronic components while allowing an optical window to view the sky in the search for the possible optical counterparts to gamma-ray bursts. To satisfy both requirements, a Motorized Door Assembly (MDA) and specially designed pressure vessel are being used.

A custom aluminum/Kevlar top for the pressure vessel has been designed to accommodate the gamma-ray detectors, the optical window, the GPS antenna, and the MDA. Aluminum and Kevlar were chosen both to minimize the absorption of gamma-rays and to provide a strong structure for the pressure vessel.

The circular pressure vessel lid is divided into four quadrants, three of which are of a minimum thickness for the gamma-ray detectors. The fourth quadrant contains the GPS antenna and a 2.5 cm diameter quartz window through which the CCD camera has an approximately 110-degree view of the sky. The three NaI(Tl) crystal detectors, their corresponding photomultiplier tubes, the GPS antenna, and the CCD camera are all directly connected to the lid, as well as to the main support structure.

The main support structure consists of two aluminum cross-pieces which span the full length of the payload. The electronics box for the experiment is attached to the mid-section of the cross structure while the batteries are located at the bottom of the pressure vessel, in a separate sealed and vented container. The aluminum cross structure minimizes the response of the payload to the vibrations induced during the launch and landing phases of the orbiter since it is inherently strong and resistant to vibrational modes at low frequency. The only moving parts in the payload, other than the MDA, are the hard disk drives. These units were designed for use in notebook personal computers and in all cases meet or exceed the requirements for use on the Space Shuttle by a large margin. Additionally, a finite element analysis is being performed for the vibration stress induced.

The thermal design of GAMCIT results from the goal of keeping the gamma-ray detectors, the CCD camera, and the other interior components within their operating temperature ranges. A thermal system resulting from a finite element transient thermal analysis is being designed with insulating materials and heating elements in order to maintain the interior vessel temperature at $20^{\circ}\text{C}\pm 15^{\circ}$.

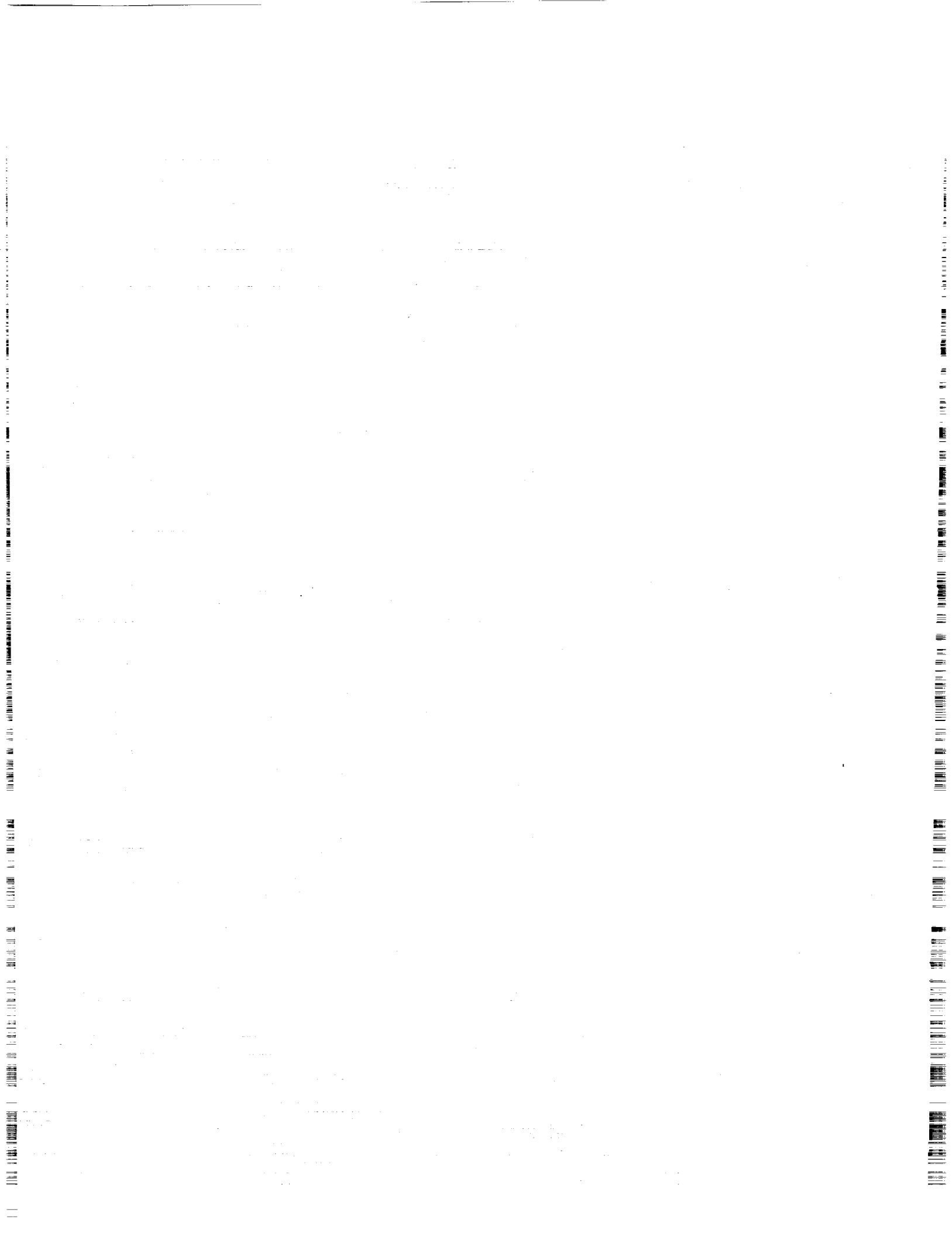
CONCLUSIONS

The GAMCIT experiment promises a guaranteed scientific return, as the gamma-ray burst observations will provide important data which can be combined with results from other detectors on ULYSSES, Pioneer Venus Orbiter and the Compton Gamma Ray Observatory. The observation of even a single optical flash would as well provide a stringent constraint on gamma-ray burst theories.

GAMCIT is the first payload being built by the Caltech Students for the Exploration and Development of Space. There are a total of fourteen undergraduate students presently working on GAMCIT, divided into four teams - electronics, structural, thermal, and safety. The real-life experience of designing and constructing space hardware isn't normally taught in a university curriculum. Thus, the Caltech GAMCIT program is providing a strong educational role in the training of future scientists and aerospace professionals.

REFERENCES

1. Fishman, G.J., Meegan, C.A., Wilson, R.B., Paciesas, W.S., Pendleton, G.N., The BATSE Experiment on the Compton Gamma Ray Observatory: Status and Some Early Results, NASA Conference Publication 3137, 1992, pp. 26-34.
2. Meegan, C.A., Fishman, G.J., Wilson, R.B., Pacieses, W.S., Pendleton, G.N., Horack, J.M., Brock, M.N., and Kouveliotou, C., Spatial Distribution of Gamma-ray Bursts Observed by BATSE, Nature, 1992, vol. 355, pp. 143-145.



G254 UNDERGRADUATE EXPERIMENT

Doran Barton, Karilyn Bogh, Brett Evans, Steve Folkman, Marc Hammond, Casey Hatch, Neva Herr, Tina Hubble, Jeff Humpherys, Steve Johnson, Mark Lemon, Oscar A. Monje, Kristin Redd, Rich Warby, Tumkur Raghuram (coordinator), and Students from Kinkaid High School.

Utah State University
Logan, UT 84322-4415

ABSTRACT

This paper describes the experiments on payload G254. Each experiment is accommodated in a spacepak and six experiments fly in a full canister. One of the experiments will be housed in a new Isospacepak structure, which will be described briefly. Five of the six experiments have dedicated controllers. The objective of each experiment is discussed. In addition, the operational scenario is provided.

INTRODUCTION

The Get Away Special (GAS) program is an academic program at Utah State University (USU) which enables students and other educational organizations to participate by designing their own engineering and microgravity science experiments. Five of the experiments on this payload utilize the "spacepak" concept similar to G-008, G-004, G-525 and G-006. The sixth uses the new "Isospacepak" concept. The external shape and dimensions of each experiment is standardized and each experiment is independently controlled so that experiments can be easily interchanged within the canister.

One of the experiments in this GAS canister has been mounted on a new Isospacepak structure that has been machined by Utah State University GAS investigator Tina Hubble and Industrial Technology and Education Department graduate student Joe Greathouse, utilizing Isogrid manufacturing techniques. The Isogrid method consists of milling a series of equilateral triangles out of solid plate stock to produce a structure which is six times as strong as a solid plate of equal weight. In addition, the nodes of the machined structure provide convenient attachment points for experiment components. Each of the nodes has been drilled and tapped, so that a regular, repeating attachment pattern is available to the experimenter. Following its demonstration in this canister, the Isospacepak will be employed in all future Utah State University GAS experiments and will be made available to other organizations desiring to adopt this concept.

The remaining "spacepaks" are a hexagonal structure made of fiberglass/polyurethane composite trays. Each tray has three aluminum mounting plates. The trays are mounted on top of each other and are held together by means of supporting struts which attach to the canister endplate. Five of the six experiments will have dedicated controllers. The sixth experiment will be controlled by a simple temperature sensitive switch.

One of the spacepaks will contain popcorn kernels and radish seeds, in addition to the regular experiment. An experiment with these will be conducted by the Edith Bowen Elementary School. After being flown in space, students will pop the popcorn and taste it. Similarly, the radishes will be grown and sampled. The scientific purpose of this experiment will be to foster interest in the space sciences amongst a younger generation.

The USU GAS program is heavily biased towards developing student skills associated with conducting individual experiments. Currently, G254 is in the integration stage. It has undergone the vibration test, and safety reviews are in progress. The experiments are targeted for delivery by December 1992.

CONTROLLERS

There are two types of controllers that are being used on this payload. One controller uses 24K bytes of user memory divided into 8K RAM and 16K ROM, 32K bytes data storage (EPROM), 16 analog inputs, 8 high current outputs, 8-bit digital input in parallel, a special energy-saving sleep circuit, and a real time clock. There are no external data storage devices and the programs are stored in the EPROM.

The other controller has 64K of internal RAM, functionally divided into 5 areas. Three of these areas are used in processing and storing measurement values. There are 6 differential channels used for analog inputs. They can also be used for single ended measurements. There are 8 digital I/O lines and a serial I/O port. It has two pulse counter inputs which are user programmable. It runs on a 12V power supply.

SPACEPAK 1

The purpose of this experiment is to examine the damping of a tetrahedral truss in a microgravity environment. An area of concern for the design of large space structures is predicting the amount of structural damping which will be present to damp out vibrations caused by orientation or docking operations. The joints used to assemble a large light weight structure like the Space Station will provide

some damping. However, an accepted methodology for predicting joint damping is yet to be established. A Get Away Special experiment was assembled to investigate methods for predicting joint damping in large space structures. A miniature tetrahedral aluminum truss will be attached to the wall of a vacuum chamber, and a tip mass attached to the free end. Oscillations will be induced in the truss structure with a solenoid and the rate of decay of the vibration modes will be recorded. The tip mass will be secured using solenoids during both launch and reentry maneuvers. The truss chamber will be evacuated through a vent to the shuttle bay.

Leak testing was conducted on the vacuum cell housing for the tetrahedral truss experiment. A vacuum pump was used to reduce the pressure down to approximately 10^{-6} Torr inside the vacuum cell and a helium leak detector was used to determine if outside air was leaking through any of the seals. A successful leak test was obtained which confirms that a high vacuum can be maintained inside the vacuum cell.

The goal of this experiment is to record the decay of the truss while it is vibrating in its fundamental vibration mode. The controller operates the experiment and measures the data. The controller pulses the solenoid at the resonant frequency of the truss for about 10 seconds. Next the resulting decay of the truss is recorded from either output of a displacement transducer or a strain gage attached to one of the truss members. The controller will excite the truss and record the decay a total of ten times. Since it is desired to measure the decay in microgravity, the experiment will be conducted during the first sleep period. A steel tip mass is attached to the truss to produce a resonant frequency of approximately 15 Hz. Additional structural support is provided to the truss tip mass during launch and reentry by the truss locking mechanism. The locking mechanism is in place during launch. Shortly after launch the stepper motor is activated to unlock the truss. After the testing is complete the truss is locked again for reentry. In the event the locker mechanism fails to relock the truss, the vacuum cell is designed to limit the deflection of the truss. The structural diagram for this experiment is shown in fig. 1.

SPACEPAK 2

The objective of this experiment is to examine the behavior of an isolated water droplet suspended in an electromagnetic field. Theory suggests that when a droplet is polarized under a very strong field (of the order of 10-20 kV) it elongates into a prolate spheroid. The forces exerted on the water droplet are the normal stress from the electric field, the surface tension from the water droplet, and the

constant internal and external pressures exerted on the droplet (1,2). Although the internal and external pressures of the droplet are constant they are not constant over the surface of the droplet (1). To balance this inconsistency there must be an induced flow arising from the viscous stress of the droplet (2). This flow is shown to be both inside and outside of the droplet. These forces are believed to be the mechanics of the deformation of these water droplets.

At some point the droplet will become unstable. This point is labeled as the critical field strength. The critical field strength for a conducting incompressible (liquid) droplet is an inverse function of the original radius of the spheroid. After the critical field strength is reached, some droplets would expand until they disintegrate while others expand until they form sharp points from which jets of liquid form. The droplet can expand to an oblate or a prolate spheroid depending on the ratios of three physical parameters of the medium of the droplet. The parameters are electrical conductivity, viscosity and permittivity. These ratios determine the shape of the droplet (1,2).

The water polarization experiment depends upon 13 lead-acid batteries for all its electrical needs. Each battery delivers 2 V and 5 amp-hrs. Four batteries are needed just to power the controller. The main component of the experiment is the water chamber. It consists of two parallel plates with a separation distance of about 4 cm. The plates are made of aluminum and are 5 cm square in area. The volume inside allows a water droplet of radius 1 cm. A needle of nylon will be used to produce the water droplet. A high voltage supply which requires 15 V and delivers about 18kV output is required. A super 8mm movie camera will be used to photograph the water droplet during the experiment.

The aim in this experiment is to confirm a relationship between the eccentricity of the ellipsoid and the applied voltage across the plates. The experiment configuration is shown in fig. 2.

SPACEPAK 3

This experiment is called Project Panchamama. Project Panchamama is a biological experiment designed to study the effects of microgravity on photosynthesis. Physiological data of this nature will be useful in elucidating the effects of microgravity on the performance of plants. Microgravity may affect photosynthesis in one of two ways: (i) by altering the diffusion of gases (i.e., CO₂) into cells or (ii) by altering cell function due to redistribution of water or altering hydrostatic forces. The experiment has been designed to study photosynthesis by using chlorophyll fluorescence measurements. Chlorophyll fluorescence is a

sensitive indicator of the efficiency of photosynthetic reactions and has been used extensively to monitor plant stress.

Biological experiments are inherently more complex than non-biological ones, because measurements must be obtained from a living organism. The GAS CAN environment is extremely harsh for living organisms because of the pre-flight dormancy period (30-90 days), exposure to high g-forces during liftoff, and followed by approximately 7 days of a potentially harmful thermal environment. Furthermore, the atmosphere of the GAS CAN is composed of nitrogen, and the experiment will be unable to provide life support during the pre-flight dormancy period. GAS payload temperatures were found to reach minimums close to -20°C . The sample temperature during the experiment must be maintained between a maximum of 30°C and a minimum of 5°C , so as to avoid thermal damage of the samples. Fluctuating temperatures also affect the thermal drift of electronic components and the heating rate experienced by the organism.

The experiment will rehydrate a lichen in orbit, and fluorescence measurements will be recorded using a simple fluorometer. A lichen, a symbiotic poikilohydric organism composed of algae and fungus, was chosen because it can remain dormant for many months without the loss of viability. The organisms will be housed within a compact life support system composed of an airtight chamber, and a water reservoir. The chamber is made of aluminum and is sealed by a static o-ring. The chamber atmosphere will be air containing 21% O_2 and 600-1200 ppm of CO_2 at 1 atm of pressure. A nylon sample holder assembly is located inside the chamber. It consists of two aluminum sample holders, six incandescent glow lights, and a sensor arm. The two sample holders are independently connected to a water reservoir. Water is pumped into each sample holder with a peristaltic pump. Sample holder temperature is controlled with a feedback circuit composed of a peltier heater. All electrical connections into the gas tight chamber are made through three 20 pin feedthrough connectors.

Water is passed into the chamber through an o-ring sealed water feedthrough connector. The reservoir consists of a 10cm long, 5cm diameter solid PVC pipe and holds 150 ml of distilled water. The reservoir will be insulated and heated by a thermofoil heater. Water flow is regulated by two individually operated, normally closed solenoid valves.

The experiment will be activated by a baroswitch, which will power up the control system. Data acquisition is accomplished through 16 single-ended input channels. Control is accomplished through a memory mapped multiplexer and switching board. The control system will heat the water

reservoir to 10°C, and then each sample holder will be rehydrated. The glow lights will then be turned on to start photosynthesis to allow for a period of normal growth and recovery from the long pre-launch dormancy period.

The data acquisition portion of the experiment will begin after a suitable time for rehydration. The data acquisition consists of a sensor arm shaped like an X, that holds a pair of photometric sensors in each leg of the X. Each leg contains a chlorophyll meter and a fluorometer. The sensor arm is moved directly over the samples during the measurement sequence by a linear actuator. Measurements will be made at five different temperatures in order to characterize the temperature response of the organism.

The power required to provide a controlled temperature regime was estimated from the expected power use of both the water reservoir and the sample holders. The water reservoir will require 2 watts of continuous power to maintain the water temperature at 10°C if the GAS CAN temperature is 5°C, and 10 watts if the GAS CAN temperature drops to -10°C. Each sample holder will require 0.88 Watts continuously to heat the sample at a heating rate of 2°C/min. The second sample holder will be rehydrated only if the payload temperature is above -5°C. This arrangement allows both redundancy and economy of power in the event of encountering an extremely harsh temperature environment.

The life support system presently being developed allows certain biological experiments to be performed in the GAS CAN. The nature of these experiments was found to be limited by the reduced capability for life support during the pre-launch phase, and thus dictated by the choice of test organism. Furthermore, the use of photometric probes for measuring physiological parameters allows simplicity of design, in-flight data acquisition, and low mass and power requirements.

SPACEPAK 4

The bubble micro-gravity experiment is designed to study the characteristics of a small three-dimensional bubble structure inside a NASA GAS canister. It is completely self-contained and requires a signal to initiate the experiment operation. The primary goals of the experiment are to: (i) observe the formation process of the bubble, (ii) look for evidence of drainage in the bubble after it has been formed, (iii) look for interference bands due to bubble wall thickness gradients, and (iv) observe surface tension induced motions on the bubble surface. The bubble experiment data will be gathered by an 8 mm movie camera. Supplemental data will be measured in analog form and stored in a memory module. The bubble itself will be formed using a fluid which

is 85% (by volume) Dow Silicon diffusion pump oil and 15% 3M FC430 surfactant.

The experiment consists of 5 major subsystems: command and control, a bubble blower, camera and lighting, power and heaters.

The command and control subsystem is run by a controller. The controller has 8 digital output lines. The controller is electrically isolated from the experiment apparatus through the use of optical isolators and a separate power source.

The bubble blower is the crux of the experiment. It consists of an aluminum block onto which other parts are attached. The block serves as a bubble material reservoir. A blower aperture is affixed to this block. The bubble is formed at the blower aperture. Two linear actuators are also attached to this block, as are the DC stirring motor, two thermofoil heaters, and two thermistors. The stirring motor is used to mix the bubble material prior to the bubble formation sequence. One of the linear actuators is used to unseat a spring-loaded check valve. This valve normally keeps the bubble material inside the reservoir. The second linear actuator is used to force the bubble material to flow to the top of the bubble aperture. The thermofoil heaters are used to keep the bubble material at a temperature above 15°C. One of the two thermistors is used in a closed-looped heater subsystem. The second thermistor is used to monitor the bubble blower temperature.

An 8 mm movie camera is used to record all of the bubble formation activity. A fluorescent lamp is used to provide lighting during the filming sequences. The light is mounted directly behind the blower block, on the other side of the camera. A small incandescent lamp is used to heat the bubble surface. The heating is not uniform, which causes a gradient in the surface tension. The induced surface tension gradient will cause movement of the material on the bubble surface. This movement will be filmed by the camera.

All energy for operation of the experiment comes from several sets of lead-acid batteries. One set of 6 cells is devoted to the controller, while a second set of 12 cells is devoted to the experiment power. This was done, in part, to completely electrically isolate the controller from the experiment.

Thermofoil heaters are attached to the base of the blower block for temperature control purposes. Once powered up, the heater subsystem does not require attention from the controller. Power is supplied to the thermofoils whenever the temperature of the blower block falls below 15°C.

SPACEPAK 5

This project was proposed by Kinkaid High School. Since USU began supporting this project, various students have assisted in its development. Since the delays that resulted from the Challenger accident, the USU GAS program has taken the initiative to complete this project. The controller has been completed and tested.

The objective of this experiment is to distill a mixture of two fluids in microgravity using a temperature differential. The fluids intended for the experiment are trichlorotrifluoroethane and carbon tetrachloride. Significant properties of these fluids that require examination include boiling point, vapor pressure, and toxicity and flammability characteristics.

This experiment is contained within a composite hexagonal spacepak. Lead-acid batteries supply four power sources of 35V, 5V, 10V, and 5V. These batteries are contained within a support structure. The fluid containment system includes one solenoid valve, two aluminum containers with a fluid capacity of 13.7 ml each, and brass fittings. A thermofoil heating element wraps around one container. It requires a 35V power supply. The controlling system consists of a mechanical relay, one USU GAS switch, two voltage regulators for each of the 5V power supplies, a printed circuit board, and Teflon coated wires. A voltage regulator stand, fluid chamber stand and two aluminum base plates secure the experiment structurally.

The experiment starts when the NASA signal is received by the USU GAS switch. The USU GAS switch activates the relay that connects all power sources to the controller. The controller receives the power and regulates all power output and operation. A thermistor is attached to the bottom of the aluminum container which has the heating element. The thermistor, in combination with another resistor, makes a variable voltage divider that provides input for a Schmitt trigger. Resistor selection controls the operating temperature and the fluctuation of temperature during feedback about the desired operating temperature. The heater turns on with the power up of the controller. When the operating temperature is reached a binary counter turns on. The valve that separates the two fluid chambers also opens up as the controller receives power. The binary counter runs for approximately three hours. During this time the Schmitt trigger of the controller powers the heater according to the resistance of the thermistor so that a temperature level may be maintained. Three J-K flip flops aid in system operation. When the counter returns to zero, the valve is closed, the controller shuts down, and the project remains dormant. Completion of this experiment involves analyses of the

chemical composition of the fluid in each container and comparison with results of distillation experiments in the earth's gravitational field. A figure of the fluid containers and the solenoid valve is shown in fig. 3.

SPACEPAK 6

Float Zone Instability Experiment (FiZIE) aims to investigate convective instabilities in float zone geometries. The primary goal of the experiment is to verify the Plateau Instability limit, which states that in zero gravity a fluid cylinder is unstable when the ratio of length L to radius R exceeds 2π . This will be accomplished by creating four independent liquid wax bridges with varying lengths and radii. In addition, by allowing the liquid wax to resolidify under "non-quiet" conditions, a sensitive test of background g -levels can be qualitatively measured by the common distortion in the resolidified float zones.

Four columns of solid parowax with radii ranging from 0.5 to 0.7cm and lengths ranging from 3 to 6 cm are suspended in an array between two copper supports. At one end of each of the wax columns is connected a heater which will be used to melt the wax. The four heaters will be operated by eight lead-acid batteries. The heaters operate at 10 watts. To melt the wax, the heaters need to reach about a temperature of 70°C. A circuit known as a Schmitt trigger will be used to reach and maintain this temperature for 30 minutes. A programmable controller will be used to control the experiment, switches and time-variables. The controller will receive its power from 4 lead-acid batteries. Upon the end of the mission, the resulting shapes of the resolidified float zones will be qualitatively analyzed.

References

1. Taylor, G.I. Studies in Electrohydrodynamics. I. The Circulation Produced in a Drop by an Electric Field. Proc. R. Soc. Lond. A 291, pp.159-166 (1986)
2. Ajayi, O.O., A note on Taylor's Electrohydrodynamic Theory, Proc. R. Soc. Lond. A 364, pp.499-507 (1978)

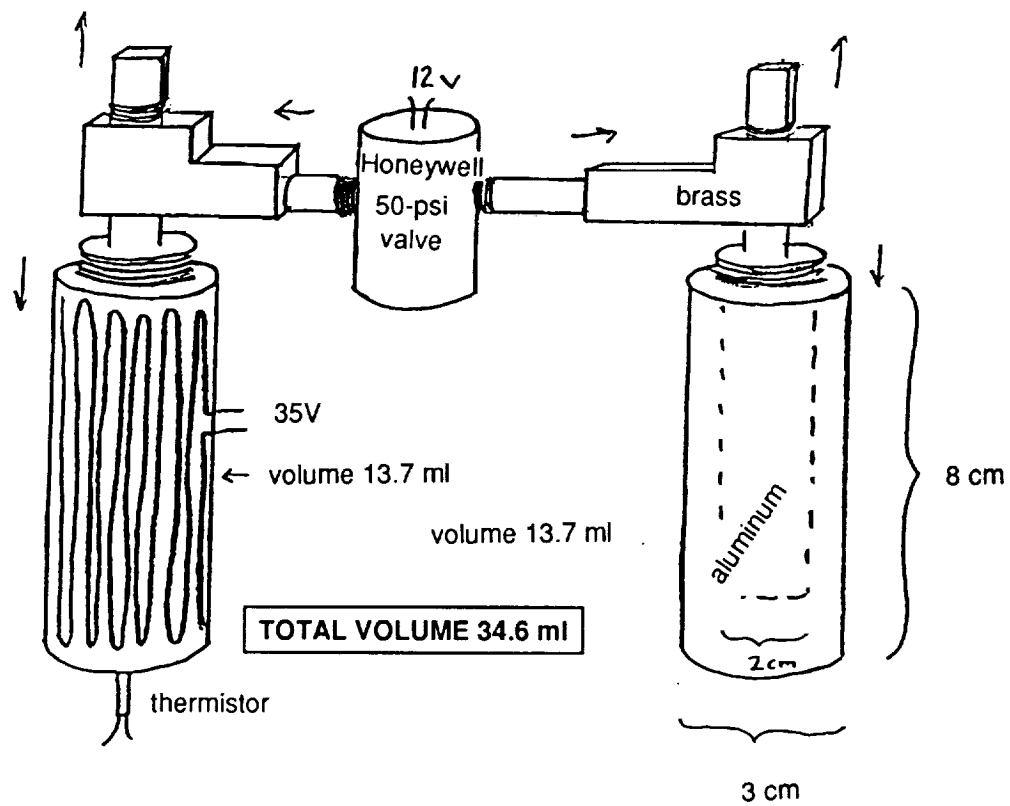


Fig. 3 Fluid containers and Solenoid valve (Spacepak 5)

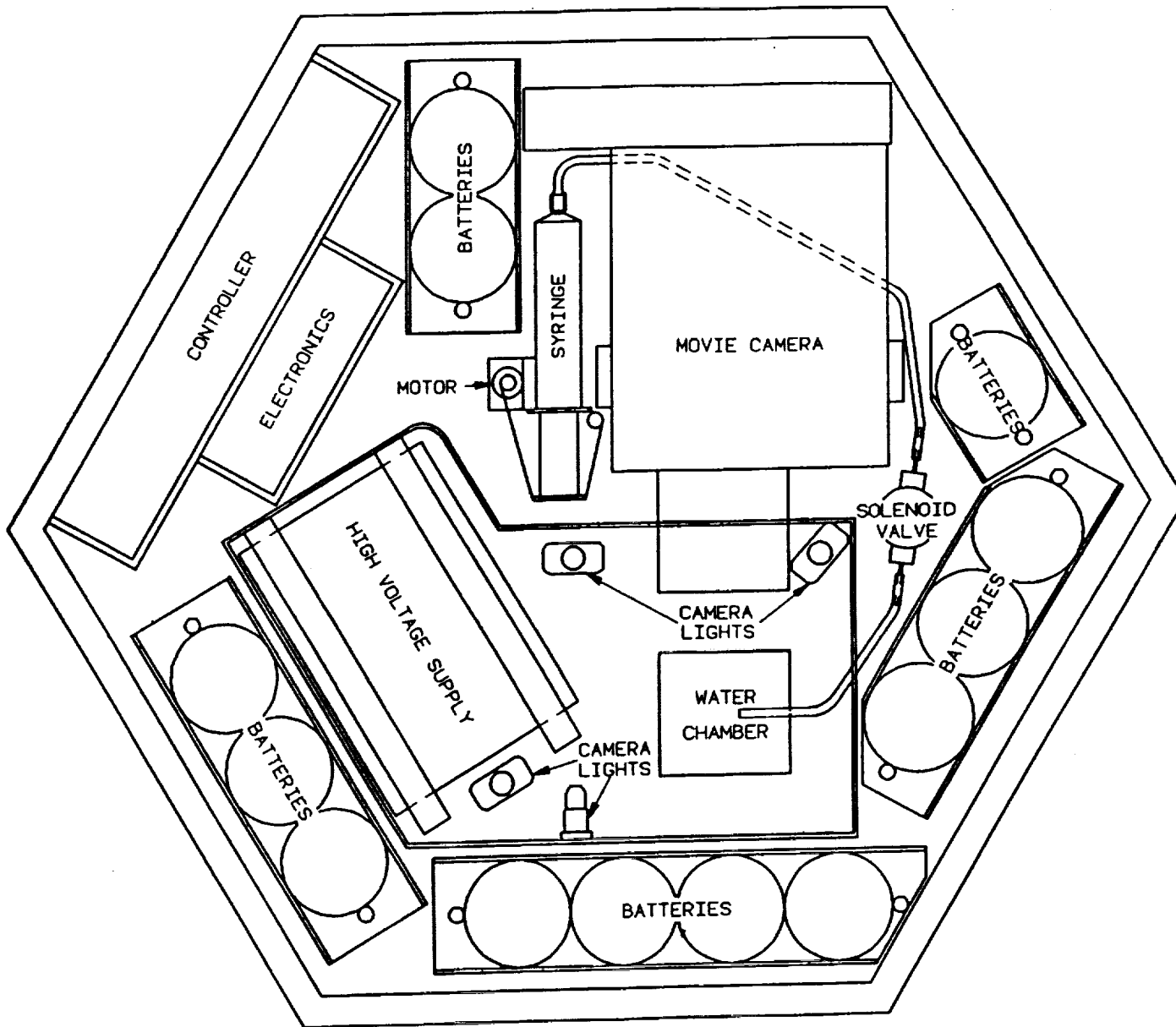


Fig. 2 Water polarization experiment configuration (Spacepak 2)

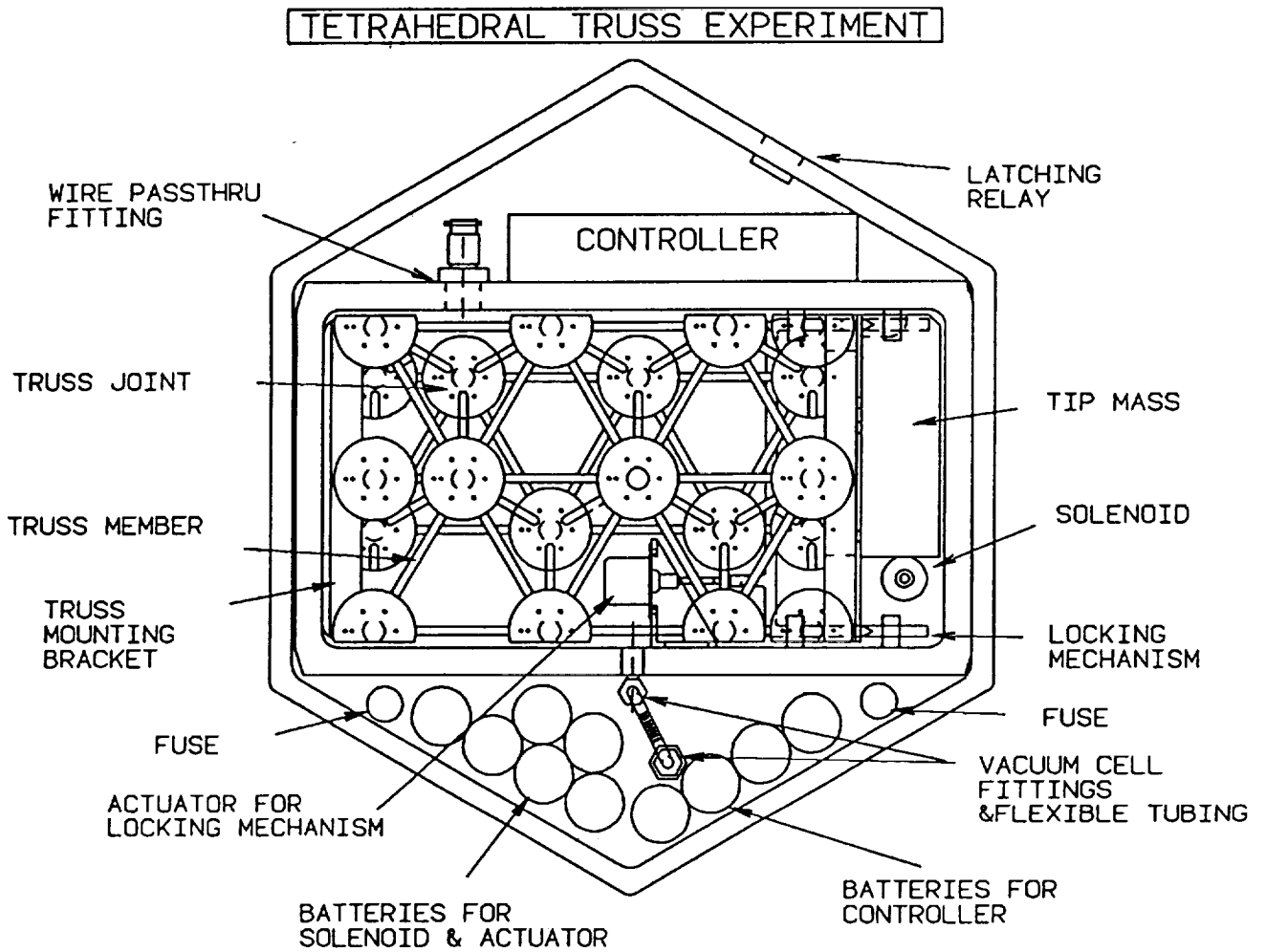
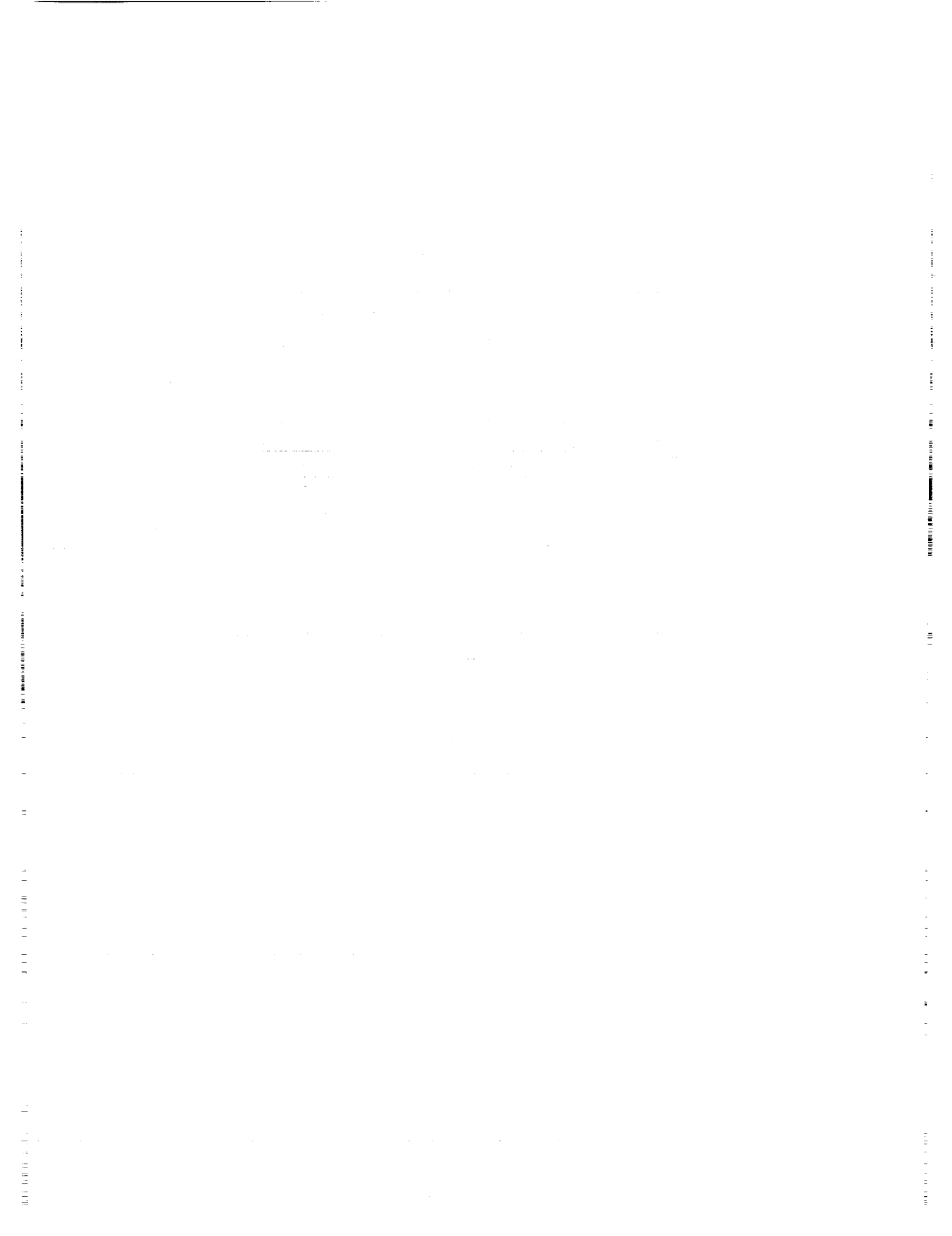


Fig. 1 Structural diagram of Spacepak 1



STRUCTURAL VERIFICATION FOR GAS EXPERIMENTS

Mark Daniel Peden
Hernandez Engineering, Inc.
Goddard Space Flight Center
Greenbelt, MD 20771

ABSTRACT

The purpose of this paper is to assist the Get Away Special (GAS) experimenter in conducting a thorough structural verification of its experiment structural configuration, thus expediting the structural review/approval process and the safety process in general. Material selection for structural subsystems will be covered with an emphasis on fasteners (GSFC fastener integrity requirements) and primary support structures [Stress Corrosion Cracking requirements and National Space Transportation System (NSTS) requirements]. Different approaches to structural verifications (tests and analyses) will be outlined especially those stemming from lessons learned on load and fundamental frequency verification. In addition, fracture control will be covered for those payloads that utilize a door assembly or modify the containment provided by the standard GAS Experiment Mounting Plate (EMP). Structural hazard assessment and the preparation of structural hazard reports will be reviewed to form a summation of structural safety issues for inclusion in the safety data package.

INTRODUCTION

All GAS experimenters must conduct a structural verification of experiment support structures in accordance with National Aeronautics and Space Administration (NASA) requirements. The structural review/approval cycle is a mandatory step in the NSTS safety process and is required for GAS experiments to receive approval for flight on the Space Shuttle.

The unique scientific objectives and mission requirements of the specific experiments being conducted will determine the experiment primary support structure. After the design of the primary support structure has been established, the structure can be further developed depending on experiment subsystems. For instance, electronics, power, or fluid subsystems may be further contained within individual boxes. The experiment structure selection process is finalized by determining the materials with which to build the support structure as well as the fasteners that will mount and hold the structure together. The experiment structure must be ultimately designed to attach to NASA standard hardware and will be cantilevered from the NASA mounting surface with lateral support in the form of bumpers at the free end of the experiment structure.

Once the experiment support structure materials and design have been selected, the payload organization is required to verify that the structure can withstand the worst case loading and vibration requirements associated with the launch and landing of the Space Shuttle. Since most Space Shuttle payloads are required to verify structures by a combination of analysis and test, the GAS experimenter is fortunate to be able to verify compliance with NSTS structural requirements by analysis only. If so desired, the GAS experimenter may verify compliance by a combination of analysis and test.

MATERIALS SELECTION

Before the support structure is verified via analysis or test, the payload organization must select structural materials that are acceptable to NASA. Particular scrutiny is given to the primary load bearing structure and the structural fasteners.

Stress Corrosion Cracking (SCC)

One of the major concerns associated with materials selection for the primary support structure, fasteners, support brackets, and mounting hardware is Stress Corrosion Cracking (SCC). SCC is defined in MSFC-SPEC-522, Design Criteria for Controlling Stress Corrosion Cracking, as "the combined action of sustained tensile stress and corrosion to cause premature failure of materials." Certain materials are more susceptible to corrosion; and when these materials are subjected to corrosion inducing environments, cracking and subsequent failure under loading will occur at lower stress levels than normal for the material. The corrosion leading to failure in many cases is not necessarily severe enough to be visible to the human eye. However, especially in the corrosive seacoast environment of the Kennedy Space Center (where GAS payloads reside for at least three months before flight on the Space Shuttle), SCC must be addressed since structures will be subjected to additive tensile stresses from assembly, transportation, storage and ultimately, the Space Shuttle mission. The Marshall Space Flight Center has conducted tests on numerous structural materials under a simulated seacoast environment that is similar in both temperature and chemical exposure to the environment that a GAS payload will experience. Table 1 of MSFC-SPEC-522 lists the alloys that exhibit a high resistance to SCC and these alloys are acceptable for all structural applications in GAS payloads. GAS payloads should select structural materials from Table 1 of MSFC-SPEC-522.

Materials listed in Table 1 of MSFC-SPEC-522 are in full compliance with NSTS 1700.7, Safety Policy and Requirements for Payloads Using the Space Transportation System, requirements concerning stress corrosion. Protective coatings such as electroplating, anodizing, alodining, iridizing, and chemical conversion coatings applied to alloys with high resistance to SCC have no affect upon the stress corrosion rating of the alloy. Surface treatments such as carburizing and nitriding may adversely affect the stress corrosion rating. Any alloy surface treatment must be identified when the experiment materials list is submitted. Use of dissimilar metals that are not protectively coated should be avoided especially in reinforcement applications (for example, brackets or braces), because the dissimilar metals may form electrical couples which could lead to galvanic corrosion.

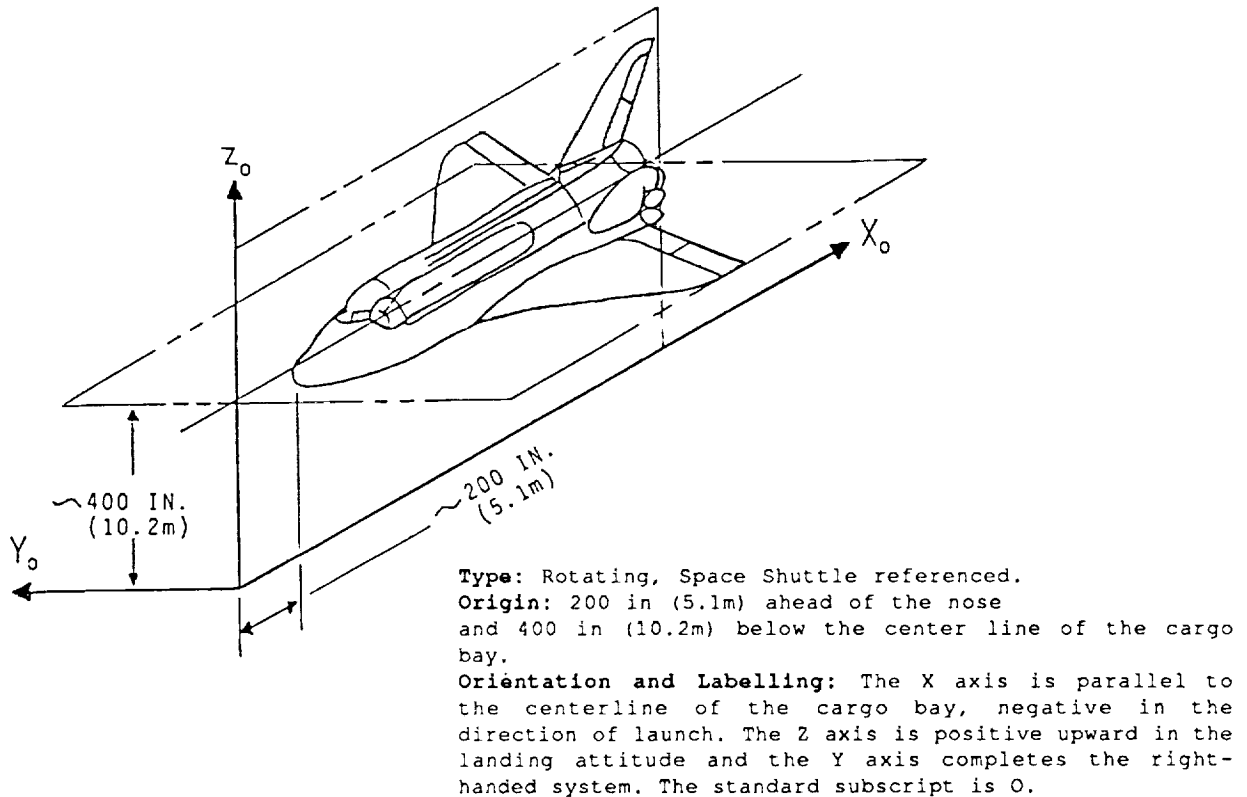
Fasteners

Fastener materials selection for GAS payloads is dependent upon the GAS canister configuration selected by the payload organization. For GAS payloads that utilize an opening door assembly or for other payloads that require fracture control due to deviance from the standard sealed GAS canister configuration, compliance with the Goddard Space Flight Center (GSFC) Fastener Integrity Requirements (GSFC Document #S-313-100) is mandatory. This means that the payload organization must either select fasteners from the GSFC approved manufacturers list (Appendix I of GSFC S-313-100) or fasteners must be in accordance with GSFC S-313-100 which may mean conducting quality assurance screening tests and inspections as well as traceability. In addition, for GAS payloads that require fracture control, the fasteners must employ positive retention such as lock wire or lock nuts. For GAS payloads that remain in the standard sealed GAS canister configuration, it is preferred but not required that the payload organization select fasteners from the GSFC approved manufacturers list.

STRUCTURAL VERIFICATION

The basic requirements for all GAS experiment support structures are as follows:

- 1) The structure must withstand flight limit loads of 10 g's in the X, Y, and Z axes with an ultimate factor of safety of 2.0 when verified by analysis only or an ultimate factor of safety of 1.5 when verified by test to a yield factor of safety of 1.25. The structure must also exhibit positive margins of safety under these loads. The loads must be combined using the X, Y, and Z loads in the worst case loading conditions (this means combining compression, tension, bending, and shear stresses). The Space Shuttle coordinate system (Figure 1) is used for defining the load direction.
- 2) The fundamental frequency of the experiment support structure about any axis must be greater than or equal to 35 Hz. This can be verified by analysis or test.



From the GAS Safety Manual

FIGURE 1 - Space Shuttle Coordinate System

Additional structural requirements are imposed on GAS payloads that utilize an opening door assembly or compromise the sealed nature of the GAS canister by modifying the containment provided by the GAS EMP (for example, payloads that attach structure to the surface of the EMP external to the GAS canister). These payloads must comply with the fracture control requirements of GSFC # 731-0005-83, General Fracture Control Plan for Payloads Using the Space Transportation System.

Verification of Basic Requirements

GAS experimenters have the option of verifying structural integrity through analysis only. Of course, the GAS experimenter may also test as long as the test results are supported by an analysis. The two basic loading and vibration requirements listed previously can thoroughly be verified using classical techniques or finite element analysis. However, conducting a series of verification tests is sometimes preferred due to the level of confidence and accuracy that it provides to the GAS experimenter. Since the structural analysis or test report is reviewed separately from the safety data package, the structural analysis/test report should not be included within the safety data package. The structural analysis/test report should be forwarded to GSFC as an independent document.

Structural Analysis

GAS experimenters are usually subjected to multiple iterations during the structural review process. The initial structural analysis is often reviewed and disapproved with a number of comments that must be answered before the structures will receive approval. Verification of the basic requirements by analysis is not always easy, and the following guidelines are provided to expedite the structural review/approval process:

- a) Description of Structure - The experimenter should introduce the structural analysis document by including a detailed description of the experiment support structure. This description should reference applicable figures that clearly illustrate mounting interface with NASA hardware, primary load bearing support structure, distribution and mounting of individual experiment components as well as lateral support bumpers. A table indicating the weight breakdown of experiment components and the location of the components on the primary support structure should be included. Components should be grouped in correlation to their location on the primary support structure (for example, all components attached to an intermediate shelf would be grouped together).
- b) Material Properties - Material properties for the experiment support structure and fasteners, such as the allowable loads and modulus of elasticity, that are used in the structural calculations should be listed in tabular form. These values should be obtained from MIL-HDBK-5.
- c) Assumptions - The experimenter should establish assumptions that are used in the structural analysis and calculations (for example, the assumption that loadings result from the specified flight limit loads multiplied by the applicable factor of safety and associated masses or the assumption that thermal effects on the loading are negligible). The experimenter must be careful when modelling the payload for structural calculations. Sometimes, the assumptions of the structural model are not accurate and the experimenter will oversimplify the model. The experimenter must clearly and appropriately model the structure so that the calculations are not only accurate but easy to follow.
- d) Abbreviations - An abbreviations list should precede the structural calculations.
- e) Primary Load Bearing Structure - The stress analysis and fundamental frequency analysis should address all main components of the experiment structure that bear loads (for example, experiment structure that mounts to the GAS EMP, experiment shelves-top, bottom and intermediate, support struts, and side walls), because experimenters often neglect to analyze key load bearing components of the experiment support structure.

f) Margins of Safety - All primary structural parts and associated attachment fasteners as well as the attachment fasteners for components that weigh 5 pounds or more must be analyzed in detail for critical stresses and must exhibit positive margins of safety. The margins of safety should be based on the interactive method that considers the combined effects of tension and shear stresses from loads applied simultaneously. This interactive relation is given as follows:

$$\text{Margin of Safety, M.S.} = [1/(R_t^2 + R_s^2)^{1/2}] - 1$$

where, R_t = Tensile load (or stress)/Allowable tensile load (or stress)
 R_s = Shear load (or stress)/Allowable shear load (or stress)

Any type of buckling analysis (taking into account pre-loads as well as inertial loads) for tubes or tube spacers and crippling strength analysis for struts should include calculations showing positive margins of safety.

g) Fasteners - When analyzing fasteners, the assumption that fastener shear force is reacted by friction is unacceptable. Shear loads must be reacted by bolts or shear pins; however, bolt threads or inserts should not be subjected to shear loads. The combined forces used in fastener analysis to determine worst case loading must take into account the effect of combining the bolt reactions. This means the loads applied to the fastener and the moments (for example, overturning moments and twisting moments due to an eccentricity of the component mounted) that result and cause additional bolt tension and shear loads must be considered in the calculations. Bearing stresses and combined local bending stresses should be examined in mounting flanges and brackets.

h) Fundamental Frequency - GAS payload structures that utilize a set of plates or shelves simply supported by struts with any number of intermediate plates can often be modelled for fundamental frequency analysis. The plates and support struts can basically be modelled as beams with equivalent loading based on the mass from the mounting of experiment components. The fundamental frequency can then be calculated by determining the properties of the modelled beams by the beam support fixtures and then using classical beam equations. The other option is to use finite element modelling with a frequency dynamics run. Once again, the experimenter must be careful not to oversimplify the structural model. Accurate assumptions and accurate beam modelling are essential to analyze the experiment support structure's fundamental frequency.

i) Finite Element Analysis - If the experimenter chooses the finite element method over classical techniques, the finite element model must be a detailed math model (analytically simulating the mass and stiffness) with a level of fidelity that accurately approximates all components of the experiment support structure. The location and values of the stresses for finite element analysis must be identified. An identification of the critical parts and components in which the stresses occur should be included as well. The mesh size used in the analysis must be appropriate to the type of run used (for example, a dynamic run or stress run). The finite element analysis should show deformed plots for both the dynamic and static load cases. This is to verify that the deformations are consistent with applied loads. The analysis should be detailed in the description of the application of accelerated loads. The acceleration loads in the three axes should encompass a worst case combination. The weight breakdown used in the analysis should be equivalent to that of all experiment components. A frequency dynamics run can be used to verify the fundamental frequency. The experimenter must clearly present the methods and assumptions used in the finite element analysis along with a clear description of the results that show structural compliance.

j) Composites - Some GAS payloads use a fiberglass/epoxy or other composite material for intermediate plates or trays to house experiments. It is desirable to avoid placing composite structural members in the primary load path. When composites are used, the experimenter must examine the connection to the primary load path and make sure that the shear strength of the composite material is sufficient to accommodate the required flight loads. The composite must not delaminate under these conditions.

k) Welds - All welds used in structural applications must be verified in accordance with MIL-STD-2219.

l) Conclusions - The experimenter should organize structural analysis results and present them in a conclusion section. Margins of safety for fasteners and the various components of the experiment support structure should be listed in tabular form. The experimenter should briefly and clearly summarize how the GAS structural requirements for loading and fundamental frequency have been met through analysis of the components of the experiment support structure.

Structural Tests

Some GAS experimenters elect to verify the experiment support structure through testing. GAS experimenters prefer tests in some cases, because tests provide more concrete results and more adequately exhibit actual experiment support structure reactions to flight loads. Before testing, structural analysis is still required to factors of safety of 1.25 for yield and 1.5 for ultimate over the flight limit loads. Structural tests are then conducted to visually verify that the structure can actually sustain the specified flight loading and still survive. The GAS experimenter should provide a description of the test set-up, test procedures followed, plots or other test results, and a summation of the test results that clearly show verification of the structural flight requirements. A number of structural tests are outlined below:

a) Static Loads Test - The static loads test is sometimes referred to as a "pull test" and consists of loading or pulling the structure to 1.25 times the flight limit loads. The experimenter can monitor the experiment support structure response using strain gages or other methods. The static test results are then correlated to determine if the stress and strain match those predicted by analysis.

b) Sine Burst Test - The sine burst test is a low frequency (< 20 Hz) sine test for 5 cycles at 100% of the test loads. The test load that should be applied is 17.7 g's in each of the three axes. This test load includes the required factor of safety (1.5) for the test. Again, the results should match the predicted values determined by analysis.

c) Sine Sweep Test - The sine sweep test is used to verify the experiment structure fundamental frequency. A harmonic vibration can be created by a vibration table or other method, and the vibration should be forced at the 1/4 g, 1/2 g, or 1 g level. A sine function vibration sweep from 20 Hz to 200 Hz is applied and the associated test result plots are used to determine the resonant frequency.

d) Random Vibration Test - The random vibration test verifies workmanship and results are not acceptable for structural verification. The GAS experimenter is not required to conduct a random vibration test but may desire to conduct such a test for confidence purposes. Appropriate levels may be found in the GAS Experimenter Handbook.

Fracture Control

Fracture control in accordance with GSFC 731-0005-83 is required for all GAS payloads that utilize a door assembly or modify the containment provided by the GAS EMP in the standard sealed GAS canister configuration. The GAS experimenter is responsible for exhibiting compliance with these requirements through test or analysis. Fracture control is required to prevent cracks, flaws, or other defects from initiating in the structure and propagating to experiment support structure failure. General requirements for such GAS payloads are covered below.

Assumptions

All structural components are assumed to have preexisting flaws in the most critical locations and orientations. Non-Destructive Evaluation (NDE) establishes the upper bound for the size of the preexisting flaw. Fracture mechanics determines flaw growth and critical flaw size. A scatter factor of 4 is used in all fracture mechanics analyses to account for material properties and uncertainties. The eventual failure and separation of any part $\geq 1/4$ lb is construed as a catastrophic hazard to the Space Shuttle or crew.

Classifications

Every part of a GAS experiment will fall into one of the following 4 categories:

- 1) Low Released Mass - part has a mass $< 1/4$ pound.
- 2) Contained - all parts or fragments of parts weighing $\geq 1/4$ pound are analyzed as being prevented by some barrier from entering the Space Shuttle cargo bay.
- 3) Fail-Safe - due to structural redundancy, the structure that remains after any single failure can withstand the redistributed loads.
- 4) Safe-Life - the largest undetected flaw that is assumed to preexist in a part will not grow to failure under the cyclic and sustained loads encountered in four complete mission lifetimes (including fabrication, testing, transportation, lift-off, ascent, on-orbit, descent, landing, and post-landing loads). Flaw growth software is often used to establish a part as safe-life.

In most cases, GAS payload parts will fall into one of the first 3 classifications and therefore are non-fracture critical. The GAS experimenter is required to assess all payload parts by these classifications and provide the analysis or test to substantiate the classification. For more specific and individually applicable requirements, the GAS experimenter should reference GSFC 731-0005-83.

SAFETY ASSESSMENT

The structural safety assessment for inclusion in the safety data package varies depending on the method of structural verification.

For verification by analysis the hazard assessment section should simply read, "To ensure sufficient structural stability, the experiment support structure was designed and built to withstand appropriate flight loads to an ultimate factor of safety of 2.0, and the fundamental frequency about any axis is ≥ 35 Hz." The hazard control verification should read, "Structural analysis has indicated compliance with the appropriate flight limit loads and an ultimate factor of safety of 2.0. All margins of safety are positive. Analysis indicates that the fundamental frequency about any axis is greater than or equal to 35 Hz."

For verification by test the hazard assessment should simply read, "To ensure sufficient structural stability, the experiment support structure was designed and built to withstand appropriate flight loads with an ultimate factor of safety of 1.5, and the fundamental frequency about any axis is ≥ 35 Hz." The hazard control verification section should read, "Structural tests have indicated compliance with the appropriate flight limit loads to yield factor of safety of 1.25 and that the fundamental frequency about any axis is greater than or equal to 35 Hz. Supporting analysis has shown an ultimate factor of safety of 1.5. All margins of safety are positive."

For GAS payloads requiring fracture control, an additional statement should be added to the hazard assessment and hazard control verification section indicating that the experiment support structure has been analyzed (or tested, if applicable) in accordance with GSFC 731-0005-83. Also, it should be indicated that structural fasteners have been selected in accordance with the GSFC Document #S-313-100 and employ positive retention.

To complete the structural safety assessment, a hazard report must be prepared for the structural failure hazard. Two generic structural hazard (Figures 2 and 3) reports are included for general reference and tailoring to specific experiment structural design and verification methods.

PAYLOAD HAZARD REPORT		No.
PAYLOAD		PHASE
SUBSYSTEM Structures	HAZARD GROUP Collision	DATE
HAZARD TITLE Failure of Experiment Support Structure		
APPLICABLE SAFETY REQUIREMENTS NSTS 1700.7B 206 Failure Propagation 208.1 Structural Design 208.2 Emergency Landing Loads 208.3 Stress Corrosion		HAZARD CATEGORY <input checked="" type="checkbox"/> Catastrophic <input type="checkbox"/> Critical
DESCRIPTION OF HAZARD During launch/landing operations, the experiment support structure fails resulting in release of the experiment inside the GAS canister.		
HAZARD CAUSES 1. Inadequate structural design for launch and landing environment. 2. Improper materials selection.		
HAZARD CONTROLS 1. (a) Fundamental frequency of experiment support structure about any axis ≥ 35 Hz. (b) Experiment support structure designed to an ultimate Factor of Safety of 2.0 (or 1.5 for verification by test) over appropriate flight limit loads with positive margins of safety. (c) GAS canister containment of the experiment in the event of experiment support structure failure. 2. Materials selected in accordance with stress corrosion requirements of MSFC-SPEC-522B.		
SAFETY VERIFICATION METHODS 1. (a) Sinusoidal vibration test or Vibration analysis. (b) Structural analysis or Test to yield factor of safety of 1.25. (c) GAS Canister Containment Analysis. Standard Sealed GAS Canister Assembly/Integration Procedure. 2. GSFC Materials Branch (Code 313) review.		
STATUS OF VERIFICATION 1. (a) Closed. Approved by GSFC (XX/XX/92). (b) Closed. Approved by GSFC (XX/XX/92). (c) Closed. GSFC Analysis GAS-CAN01-014 and Procedure GAS-CAN-08-011 to be performed at KSC and documented in the Verification Tracking Log (VTL). 2. Closed. GSFC Materials Branch approval (XX/XX/92).		
PHASE III APPROVALS	GAS P/L Manager	GAS Safety Officer
	GAS Project Manager	STS

FIGURE 2 - General Structural Hazard Report

PAYLOAD HAZARD REPORT		No.
PAYLOAD		PHASE
SUBSYSTEM Structures	HAZARD GROUP Collison	DATE
HAZARD TITLE Failure of Experiment Support Structure		
APPLICABLE SAFETY REQUIREMENTS NSTS 1700.7B:206 Failure Propagation 208.1 Structural Design 208.2 Emergency Landing Loads 208.3 Stress Corrosion		HAZARD CATEGORY
		X Catastrophic
		Critical
DESCRIPTION OF HAZARD During launch/landing operations, the experiment support structure fails resulting in release of the experiment.		
HAZARD CAUSES 1. Inadequate structural design for launch and landing environment. 2. Defective material. 3. Defects or flaws assumed to be present in the experiment structure propagate to failure.		
HAZARD CONTROLS 1. (a) Fundamental frequency of experiment about any axis ≥ 35 Hz. (b) Experiment support structure designed to an ultimate Factor of Safety of 2.0 (or 1.5 for verification by test) over appropriate limit loads with positive margins of safety. 2. Materials selected in accordance with stress corrosion requirements of MSFC-SPEC-522B. 3. The structure was designed in accordance with GSFC 731-0005-83, Rev. B, General Fracture Control Plan for Payloads Using the STS. All payload elements are either low released mass, contained, or fail-safe; therefore non-fracture critical.		
SAFETY VERIFICATION METHODS 1. (a) Vibration Analysis or Vibration Test. (b) Structural analysis or Test to yield factor of safet yof 1.25. 2. GSFC Materials Branch (Code 313) review. 3. Fracture Control Analysis or Test.		
STATUS OF VERIFICATION 1. (a) Closed. Approved by GSFC (XX/XX/92). (b) Closed. Approved by GSFC (XX/XX/92). 2. Closed. GSFC Materials Branch approval (XX/XX/92). 3. Closed. Approved by GSFC (XX/XX/92).		
PHASE III APPROVALS	GAS P/L Manager	GAS Safety Officer
	GAS Project Manager	STS

JSC Form 542B (Rev Nov 82)

FIGURE 3 - General Structural Hazard Report with Fracture Control

PROPER BATTERY SYSTEM DESIGN FOR GAS EXPERIMENTS

Stephen A. Calogero
Hernandez Engineering, Inc.
Goddard Space Flight Center
Greenbelt, MD 20771

ABSTRACT

The purpose of this paper is to help the GAS experimenter to design a battery system that meets mission success requirements while at the same time reducing the hazards associated with the battery system. Lead-acid, silver-zinc and alkaline chemistry batteries will be discussed. Lithium batteries will be briefly discussed with emphasis on back-up power supply capabilities. The hazards associated with different battery configurations will be discussed along with the controls necessary to make the battery system two-fault tolerant.

INTRODUCTION

The purpose of this paper is to discuss proper battery system design for experiments utilizing the Get Away Special (GAS) carrier system. The safety associated with the battery system will be the main point of discussion.

Before the battery system can be designed, the experiment requirements must be determined. After a full analysis of the objectives and purpose of the experiment, the designer must transform the design into concrete numbers. The first requirement will be the expected working voltage. The experimenter has a number of choices in this regard. In most cases, the experimenter will determine the voltage necessary to run most of the experiment's components and will use DC/DC convertors to operate other unique devices. The experimenter may also use two battery packs to independently operate different parts of the experiment. For example, one 5-volt battery pack could be used to operate the computer while a second 24-volt battery pack could be used to operate the rest of the experiment.

Other factors that must be determined are the maximum current draw and expected duration of the experiment. The maximum current draw and expected duration are needed in order to choose the proper fuse size and the proper battery type.

FUSE SIZE

The fuses used for the battery must be sized to protect the main power wires and the battery itself. After the maximum current draw has been determined, the experimenter should include a reliability factor to that number. Most designers will derate the system by 50%. For example, if the maximum current draw is 5 amps, a fuse size of 10 amps will be chosen. Based on the application, the designer must determine whether to use a fast-blow or slow-blow fuse. The main difference between these two types is that slow-blow fuses can withstand high instantaneous currents. Most GAS experimenters use fast-blow fuses.

The designer should also fuse all major components. The purpose for fusing major components (motors, actuators, heaters, etc.) is to protect the device from overheating. Most designers fuse major components for mission success purposes also.

WIRE SIZE

The wire size is determined from the fuse size. The wire size must be determined based on the gage of the wire and the thermal rating of the insulation. Most experiments use Teflon insulated wire with a thermal rating of 200°C. Some experimenters have also used Kapton insulated wire. It should be noted that PVC insulated wire is not acceptable because PVC is a high outgasser.

The maximum current rating for wire on the ground is different for space since there is no convective heat loss in space. In TABLE I, NASA has determined maximum current dissipation for three insulation ratings (150°C, 175°C and 200°) and for both space and ground (S/G). For example, the maximum current that a 12 gage, 200°C wire can dissipate before overheating in space is 38 amps as compared to 74 amps on ground. Consequently, the space rating must be considered when wire size is determined.

TABLE I - WIRE RATING FOR SPACE AND GROUND

WIRE GAGE	CURRENT RATING (AMPS)			WIRE GAGE	CURRENT RATING (AMPS)		
	WIRE RATING (S/G)				WIRE RATING (S/G)		
	150°C	175°C	200°C		150°C	175°C	200°C
0	235/369	285/405	340/450	14	19/56	23/62	26/65
2	155/270	190/300	215/340	16	14/39	17/42	20/45
4	115/220	140/250	160/280	18	13/37	15/39	17/42
6	85/170	100/180	120/190	20	8/25	10/27	12/29
8	60/120	71/130	80/150	22	6/19	8/20	9/22
10	37/80	42/90	51/100	24	5/14	7/15	8/16
12	29/62	34/68	38/74	26	4/13	5/14	6/15

Reproduced from NSTS 18798A, ER-87-326

The fuse selection criteria is based on the maximum continuous overload rather than the dead short condition. The rating is based on the amount of current that the fuse can handle for approximately 10 to 15 minutes before actually blowing. This is determined by extrapolating the fuse current versus time graph until it levels off (usually 10 to 15 minutes). For fast-blow fuses this tends to be approximately 1.35 times the dead short rating. For slow-blow fuses this tends to be approximately 2.4 times the dead short rating. For example, a 10 amp fast-blow fuse could possibly be overloaded to 13.50 amps before blowing. This maximum continuous overload rating must be used to determine the minimum wire size. For example, 18 gage wire rated at 200°C would be the minimum needed for the above 10 amp fuse. If the equivalent slow blow fuse was used, the minimum wire size would be 14 gage rated at 200°C.

The designer must also protect all wires when going from a higher gage wire to multiple lower gage wires. The lower gage wires must be protected such that if one of the other wires is lost, excess current will not overload the surviving wire. For example, a design may call for a 12 gage wire to be distributed to two 14 gage wires. If the main fuse size is 25 amps, both wires together could easily handle this load. However, if one of the wires open-circuited, the other wire could see approximately 33 amps. For this reason, it would be necessary to fuse each wire to 15 amps.

Finally, the designer must be cognizant of educated (smart) shorts. Educated shorts arise when three or more bus wires are used to distribute current over several smaller wires (see Figure 1). If each bus line is fused at the first bus junction, it is possible for one of the wires to overheat if a short occurs after the fuse and the short is such that it does not cause the bus fuse to blow. The designer must either place a fuse before the bus to protect the smallest wire in the bus or fuses must be placed at both ends of the bus.

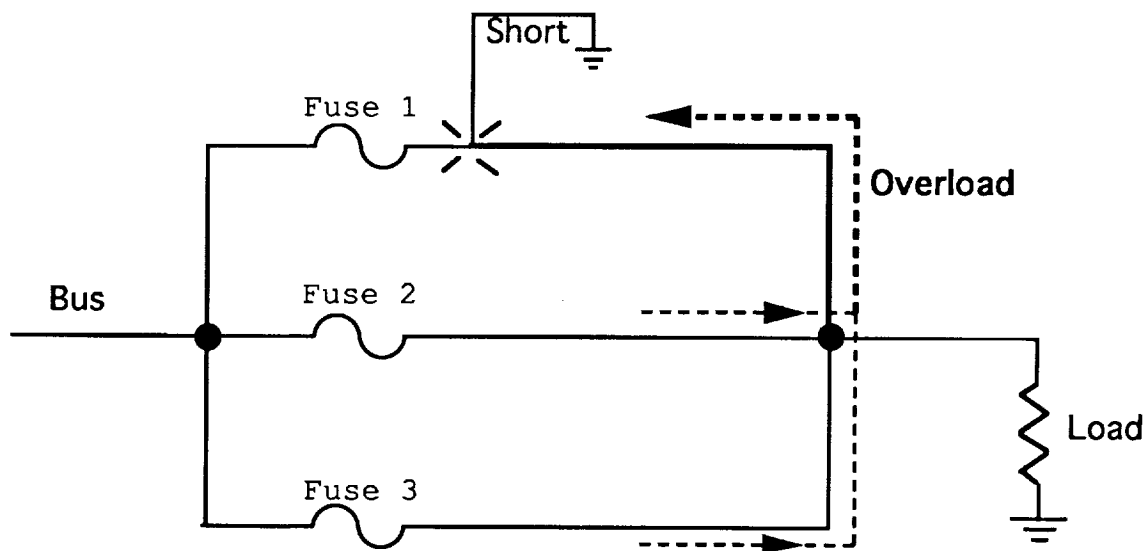


FIGURE 1 - EDUCATED SHORT

Reproduced from NSTS 18798A, ER-87-326

BATTERY TYPE

There are three types of batteries that are commonly used in GAS: Alkaline cells, Lead-acid cells, and Silver zinc cells. There are many advantages and disadvantages to each cell but cost seems to drive most decisions. Silver zinc cells tend to be quite expensive while alkaline cells are the cheapest. Regardless of which type of cell is chosen, there are some important guidelines that should be followed. The first factor to consider is the expected duration of the experiment. If the experiment is expected to run for 10 hours at a rate of 1 amp, the capacity of the cell/battery should be at least 10 amp-hours. However, the designer also needs to consider self-discharging between integration and launch (approximately three to four months). Finally, the expected operating temperature must be considered since battery performance varies significantly with temperature.

After the cell type has been chosen, the experimenter will set the voltage by placing the necessary complement of cells in series. In terms of capacity, the experimenter will probably have to decide whether to use parallel cell strings to increase capacity or to use a higher capacity cell. In most circumstances, it is cheaper, more efficient, and safer to use the higher capacity cell. When cell strings are placed in parallel, they must be protected against cell reversal. In order to control this hazard, it is necessary to diode or double diode isolate each parallel cell string. The diodes reduce the voltage output by approximately .7 volts due to the turn-on voltage of a standard diode. The designer may use Schottky diodes whose turn-on voltage is approximately .3 volts or it may be necessary to add an additional cell in series with each string to compensate for the diode voltage drop. In addition, parallel cell strings will not discharge as evenly and completely as compared to a higher capacity cell.

BATTERY BOX

The main batteries must be enclosed within a battery box. In general, all battery boxes must contain the following:

1. All interior surfaces of the battery box must be coated with a non-conductive, electrolyte resistant material.
2. All cells need to be firmly secured in order to prevent vibration damage to the cells.
3. The interior of the box should contain absorbent material.
4. If the box is constructed of a conductive material (aluminum), then the battery fuses must be placed inside the box.

The designer must also determine whether to vent the battery box to the canister or outside the canister to the cargo bay. Silver zinc batteries have always been vented to the cargo bay while lead-acid and alkaline batteries have been vented to the cargo on a case by case basis. If the battery box is vented to the cargo bay, then the box must be air-tight and the integrity of the seal verified. Most experimenters perform a leak test by pressurizing the box to 22.5 psia for 24 hours. There should be no pressure drop during this period. The experimenter will also have to provide the plumbing to the NASA pressure relief valves as stated on page 20 of the GAS Experimenter Handbook.

If the experimenter elects to vent the battery to the inside of the GAS canister, a free volume analysis must be performed. The experimenter will have to determine the amount of gas that can be evolved under worst case conditions. The data should include a standing test, cell reversal test, and a short circuit test. Using this data the experimenter can calculate whether the evolved gas will generate a combustible atmosphere in the free volume of the canister.

NASA INTERFACE

Another consideration in the battery system design is the connection to the NASA/GAS interface. As a policy, NASA must have control over the experimenter's power. In most cases this is accomplished by routing the battery supply through Relay A of the GAS Control Decoder (GCD). Relay A controls the Payload Power Contactor (PPC). The PPC contains a pair of series redundant contacts each rated at 25 amps as shown in Figure 2. This configuration gives the experimenter two options in which to route the power system. The first option is to bus the power through Circuit 1 and Circuit 2. This gives the experimenter a redundant path for the power system (see Figure 3). However, the maximum current cannot be greater than 25 amps in case one of the lines fail. If there are two independent sources, another option is to route each source through a separate circuit (see Figure 4). In this case, each circuit is limited to 25 amps.

The PPC also contains two malfunction inputs. These inputs can be used to shut the power off in case there is a malfunction (overtemperature, motor overspeed, low battery voltage, etc.). If there is a malfunction, the PPC will turn the power off and will attempt to reapply power at regular intervals until the malfunction no longer exists or until Relay A is switched to latent. It should be noted that the malfunction inputs can only be used for mission success purposes and cannot be used to control any safety hazard. Finally, external power may be applied to the experiment through the PPC during integration.

The experimenter may also use GCD Relays B and C. These relays are rated at 2 amps maximum. Most experimenters use these relays to provide signals to the experiment. A relay may be used to command a certain experiment to start during an astronaut sleep period or it could be used as a time mark for data collection purposes.

BACKUP BATTERY

The next consideration for the designer are back-up batteries. Back-up batteries are normally used to maintain memory or other data collection devices after the main power has been turned off. The experimenter may choose any battery type but special care should be taken if lithium button cells are used. Lithium cells can be a safety hazard because of the high energy capacity of these cells. If the design calls for lithium cells, the experimenter must include detailed information on the chemistry of the lithium cell, the power requirements, and the size of the cell. In addition, the lithium cell will need to be protected. The circuit should be diode isolated and fused, or the circuit should be double diode isolated (see Figure 5). These controls are meant to protect the lithium cell from being charged by the main power supply. Other cell chemistries are preferred over lithium since the safety risks are much lower.

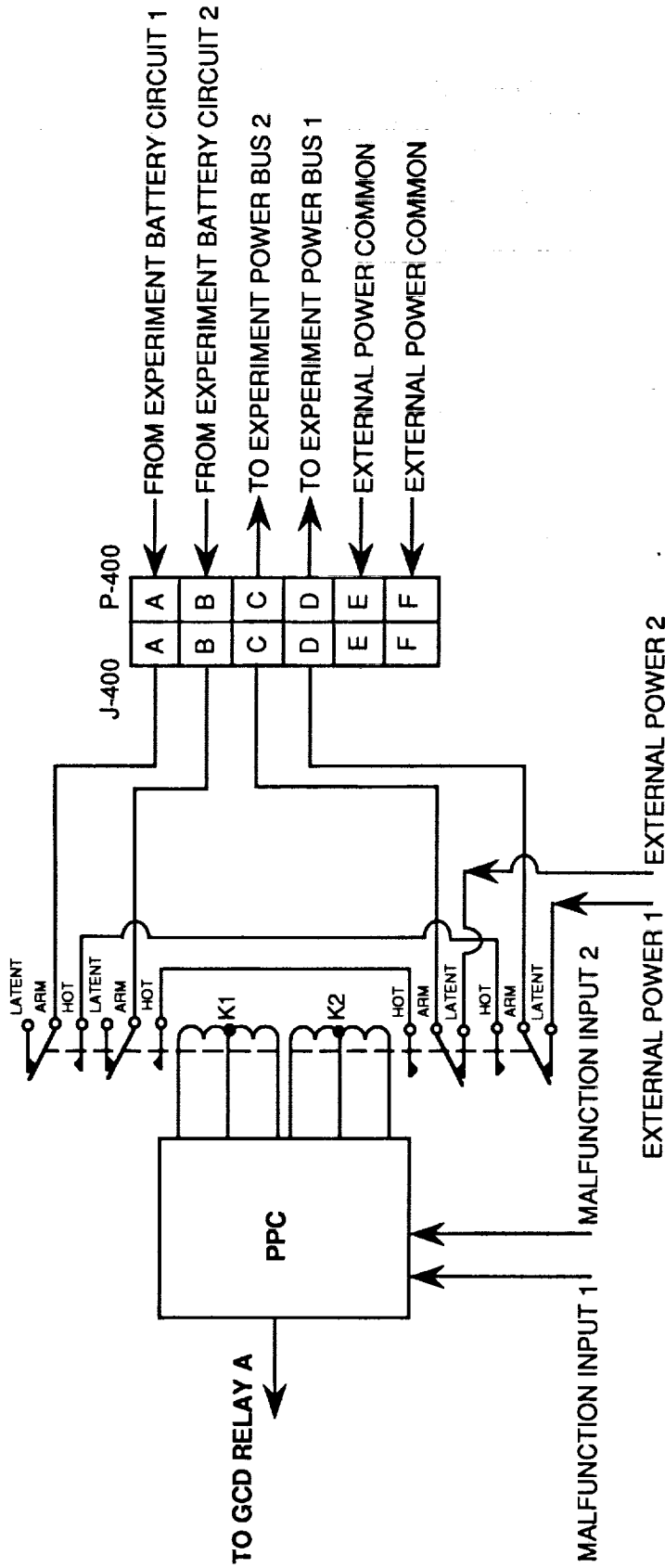


FIGURE 2 - PAYLOAD POWER CONTACTOR (PPC)

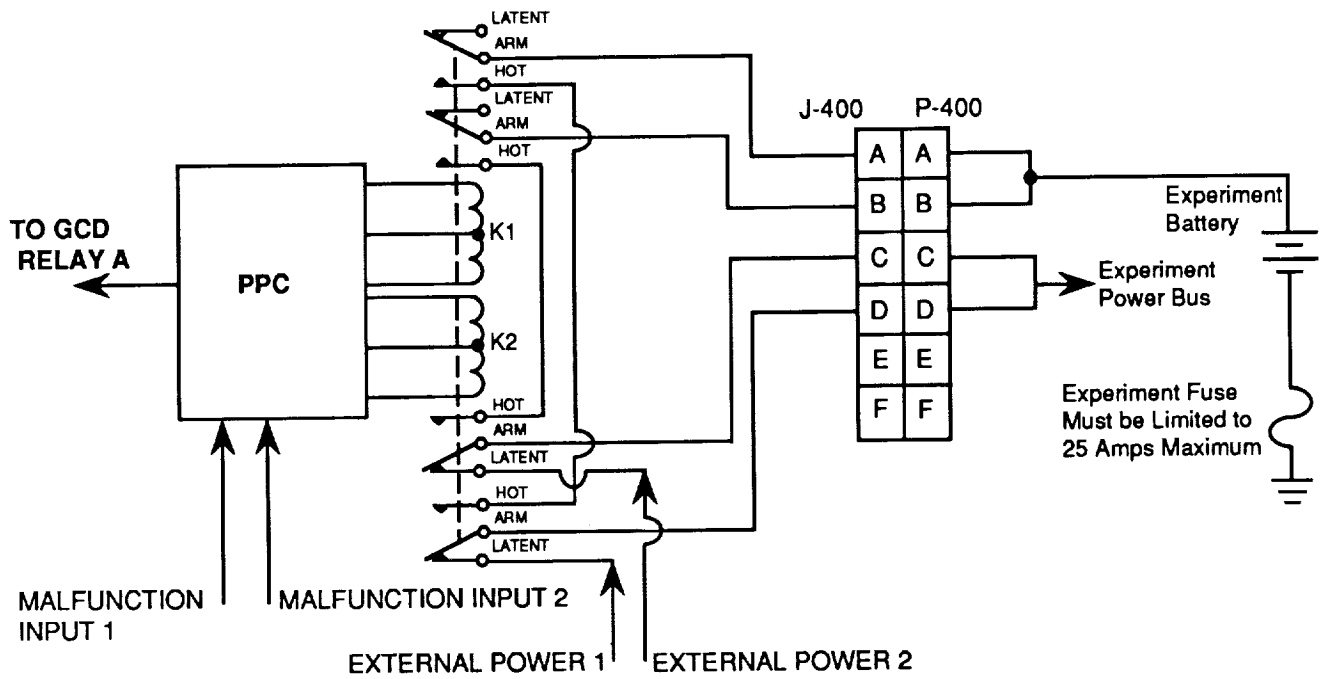


FIGURE 3 - REDUNDANT USE OF PPC

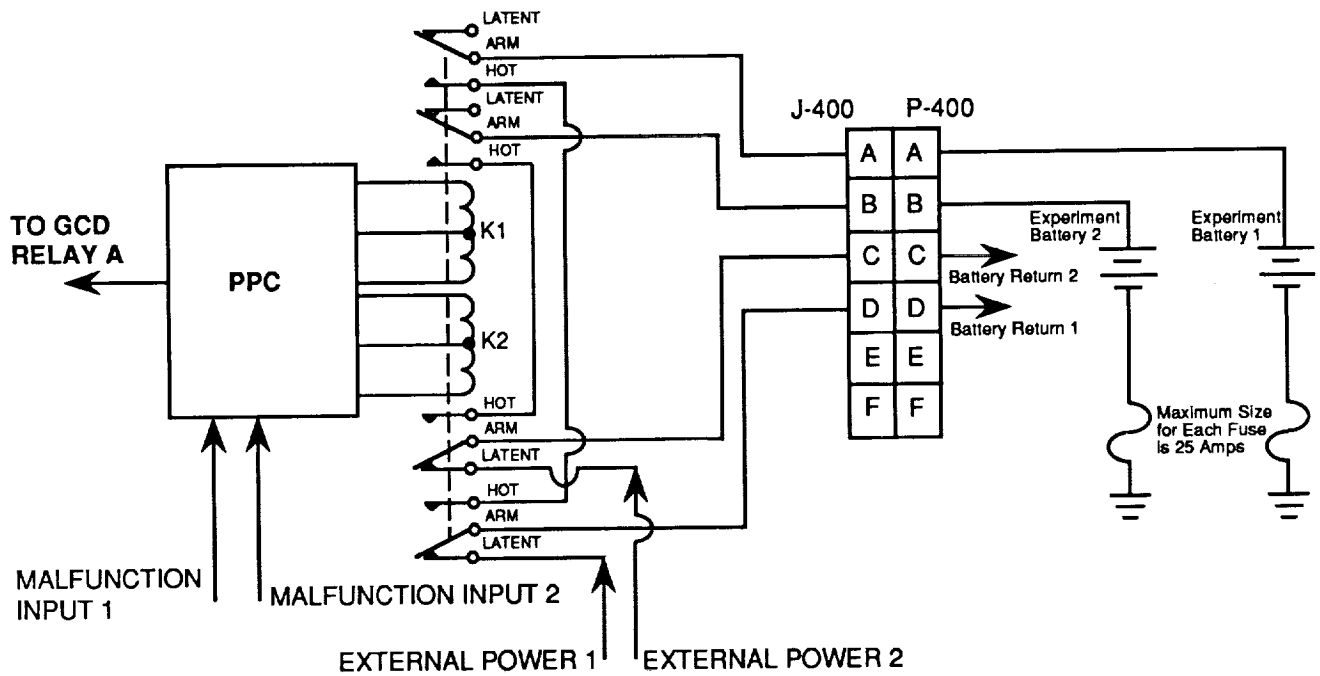
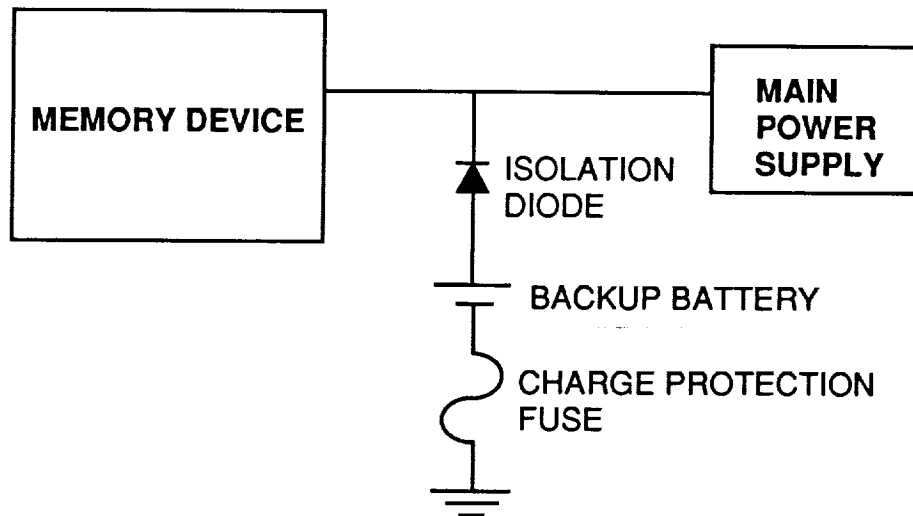
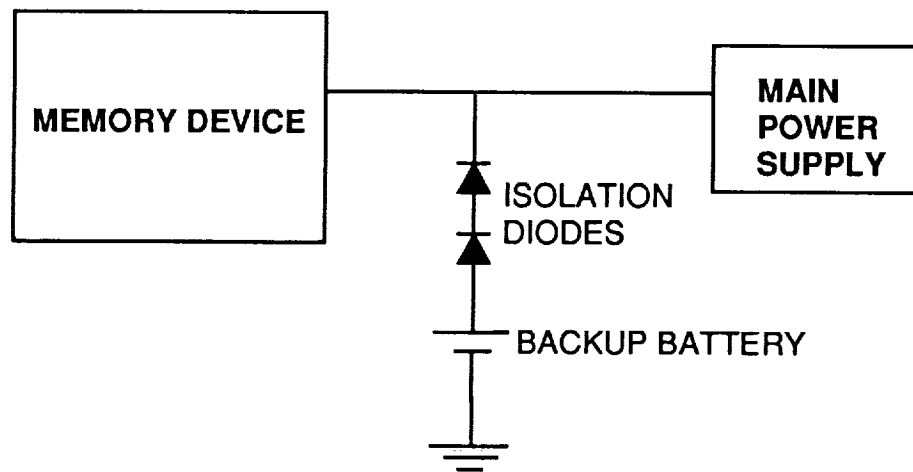


FIGURE 4 - DUAL POWER SUPPLIES



DIODE ISOLATED AND FUSED



DOUBLE DIODE ISOLATED

FIGURE 5 - PROTECTION OF LITHIUM BACKUP BATTERIES

SAFETY SUMMARY

The foregoing discussion should cover most of the safety related hazards associated with the battery system. The following is a summary of the controls needed in every battery system:

Fusing

1. The main fuses protect the battery from an overcurrent condition. An overcurrent condition is discharging the battery higher than the maximum rate. In most experiments, this should never be a problem.
2. The fuses are sized to protect the wires from overheating.
3. The fuses must be placed on the ground leg of the battery, and within any conductive battery box.

Diode Isolation

4. All parallel cell strings must be diode isolated to prevent reverse charging due to cell reversal.
5. Back-up lithium cells must be double diode isolated, or diode isolated and fused in order to prevent charging from the main power supply.

Battery Box

6. The battery box must be coated with a non-conductive, electrolyte-resistant coating.
7. The battery box should contain absorbent material in case there is a leakage of electrolyte.
8. If venting to the cargo bay, the battery box must be air-tight and the integrity of the seal must be verified. The purpose of venting is to prevent the accumulation of combustible gases.
9. If venting to the inside of the GAS canister, a free volume analysis must be performed which shows that under worst case conditions, a combustible atmosphere in the free volume of the canister is not possible. The experimenter is required to provide data in support of the free volume analysis.

Figure 6 is a sample Hazard Report detailing the hazards and controls associated with the battery system. It should be used as a guide in the preparation of the experiment's unique Hazard Report. It is also a good start for the preparation of the safety assessment. Finally, the following documents should be referenced when designing the battery system:

1. NSTS 1700.7B - Safety Policy and Requirements
2. NSTS 18798A - Interpretations of NSTS Payload Safety Requirements
3. JSC 20793 - Manned Space Vehicle Battery Safety Handbook
4. Get Away Special (GAS) Experimenter Handbook (1991)

PAYLOAD HAZARD REPORT		No.
PAYLOAD		PHASE
SUBSYSTEM Electrical	HAZARD GROUP Explosion/Corrosion	DATE
HAZARD TITLE Rupture of XXXX battery cells		
APPLICABLE SAFETY REQUIREMENTS NSTS 1700.7B: 206 Failure Propagation 219 Flammable Atmospheres 208.5 Sealed Compartments 213 Electrical Systems 209 Materials		HAZARD CATEGORY X Catastrophic Critical
DESCRIPTION OF HAZARD Rupture of XXXX battery cells and the release of battery electrolyte.		
HAZARD CAUSES 1. Battery overcurrent/short circuit. 2. Evolution of hydrogen and oxygen in the presence of an ignition source. 3. Electrolyte leakage. 4. Cell reversal.		
HAZARD CONTROLS 1. (a) Negative ground leg of each string is fused (as appropriate to wire size) within battery box in accordance with NSTS 18798A, ER-87-326 and fuse is sized to protect battery from overcurrent condition. (b) Battery box internal coating (Conathane EN-11) is non-conductive. 2. (a) Sealed battery box (proof pressure tested to 22.5 psi)/Redundantly vented overboard using 15.0 psid valves. (b) Battery box purged with nitrogen. (c) Contained in a sealed GAS canister that is purged with nitrogen. (d) Potential ignition sources conformally coated and fuses sealed. 3. (a) Battery box internal coating (Conathane EN-11) is inert to sulfuric acid electrolyte. (b) Use of absorbent material in battery box. 4. Parallel cell strings are diode isolated.		
SAFETY VERIFICATION METHODS 1. (a) Design review (see attached electrical schematic). (b) Design review; Materials review. 2. (a) Proof pressure test of battery box/Standard PRV refurbishment checkout. (b) Battery box purged with nitrogen by GAS Field Operations personnel. (c) GAS Can purged with nitrogen by GAS Field Operations personnel. Standard Sealed GAS Canister Assembly/Integration Procedure. (d) Design review. 3. (a) Design review. (b) Design review. 4. Design review (see attached electrical schematic).		
STATUS OF VERIFICATION 1. (a) Closed. GSFC Design Review (XX/XX/92). (b) Closed. GSFC Design Review (XX/XX/92) and GSFC Materials Approval (XX/XX/92). 2. (a) Closed. Test Report #xx (XX/XX/92)/To be performed at KSC (Procedure number GA37-300-11) and documented in the VTL. (b) Closed. To be performed at KSC (Procedure number GAS CAN-08-011) and documented in the VTL. (c) Closed. To be performed at KSC (Procedure number GAS CAN-08-011) and documented in the VTL. (d) Closed. GSFC Design Review (XX/XX/92). 3. (a) Closed. GSFC Design Review (XX/XX/92). (b) Closed. GSFC Design Review (XX/XX/92). 4. Closed. GSFC Design Review (XX/XX/92).		
PHASE III APPROVALS	GAS P/L. Manager	GAS Safety Officer
	GAS Project Manager	STS

JSC Form 542B (Rev Nov 82)

NASA-JSC

FIGURE 6 - SAMPLE ELECTRICAL HAZARD REPORT

A PENNSYLVANIA STATE UNIVERSITY / GENERAL ELECTRIC
GET WAY SPECIAL (GAS) EXPERIMENT

by George Evanisko, Theodore Grosch, Milad Youssef, and Jim Yurack
Faculty Advisor: Professor C. R. Philbrick
Pennsylvania State University, University Park, PA

ABSTRACT

We describe four student designed experiments by the Pennsylvania State University, which are planned for a GAS canister. The four experiments will measure; the effects of radiation on semiconductors, orbital debris impacts, the Space Shuttle's magnetic field, and the photoelectric yield of several different materials. These experiments are the result of the efforts of more than one hundred students.

INTRODUCTION

The GAS program at the Pennsylvania State University was started in January, 1991 with an organizational meeting for all graduate and undergraduate students in Engineering and Science. Students were introduced to the GAS concept and asked to suggest ideas, focused towards a microgravity and space environment, to be flown in the canister. Undergraduate students in a senior level course, Introduction to Space Sciences, were also asked to suggest ideas for experiments. A competition to select the best conceptual design was held during Spring 1992 and was open to all students in the University. Twelve proposals, with ideas ranging from a spaceborne lidar system to making optical lenses in a microgravity environment, were submitted. Professors from the College of Electrical Engineering, engineers representing General Electric (our sponsor), and two students served as judges for the competition. The experiments were judged on the basis of scientific significance, size, safety, cost, and expected performance. Four experiments were chosen; an experiment to determine the effect of cosmic radiation on semiconductors, an orbital debris detection system, a fluxgate magnetometer experiment to measure magnetic moments of the Space Shuttle, and an experiment to measure the photoelectric yield of several different materials exposed to the space environment.

The effects of radiation on semiconductors experiment concentrates on gaining an understanding of the interaction mechanisms of cosmic radiation on semiconductors and how this relates to device failure. Four memory device technologies will be tested; SIMM, CMOS, NMOS, and GaAs.

The orbital debris experiment will detect and record space debris impacting with the Shuttle. Since the LDEF satellite was recovered attention in the space community has increased concerning the effect space debris will have on space platforms or spaceborne instruments. The detection system utilizes a piezoelectric sensor's output, that is digitized and filtered with a least mean square algorithm.

The fluxgate magnetometer experiment is designed to record the three dimensional magnetic field map of the Shuttle. The data from the three axis magnetometer will be used to determine the magnetic interference in the Shuttle from other equipment and from construction used in the Shuttle and cargo bay.

The photoelectric effect experiment is intended to measure the

photoelectric yield of several different materials. The data obtained will help determine which materials can detect ambient ionospheric plasma and minimize the effects of spacecraft charging. An electrometer will measure the currents from the photoelectron yield of eight samples.

THE EXPERIMENTS

Effects of Radiation on Semiconductors

The effects of radiation on semiconductor experiment will study the susceptibility of semiconductor memory to Single Event Upsets (SEUs) and permanent damage to the memory cells. The purpose of this experiment is to simultaneously test four types of memory device technologies at an accelerated temperature. Data will be written into the Memory Under Test (MUT) and left alone for one or two hours. The MUT will be kept at 50°C to evaluate the enhanced SEU susceptibility at the higher temperature. Then, the data in the MUT is read and the test time, total radiation dose, and any errors encountered are recorded in nonvolatile memory. The experiment consists of four main components; the test memory, nonvolatile storage memory, a solid state dosimeter, and a memory test sequencer.

The current plans call for the MUT to consist of a total of 64 kbytes of SRAM. There will be 2 kbytes of GaAs, 4 kbytes of SOS, 8 kbytes of NMOS, and the remaining 50 kbytes will be filled with commercial SIMM memory. The memory will be heated to 50°C for the entire flight by several positive temperature coefficient thermistor disks. The disks have relatively low resistance until the temperature reaches 50°C. Then the resistance rapidly increases, slowing and stopping the heating process. The test memory circuits will be arrayed near the top of the GAS canister to minimize the radiation shielding effects of the canister and Shuttle.

Nonvolatile memory will be used for Long Term Data Storage (LTDS). The memory will be 128 Kbytes of low power CMOS memory with battery back-up. The memory is designed with three separate 128 kbytes of storage area connected with the data and address lines in parallel. This makes a write-only triple redundant storage area for the test data.

A solid state dosimeter (Figure 1) is used to measure the total dose accumulated during the test and the dose rate in any particular 5 minute interval. The radiation detector is a semiconductor diode connected in a short-circuit current mode. Ionizing radiation in the PN junction generates current in the diode. The current is integrated until a threshold is reached. The integrator is then reset and two counters are incremented. One counter is used as a dose rate interval counter and the other counter for the measurement of total dose encountered in the experiment interval.

The possibility of an SEU causing a controller failure was a concern. The entire test could become useless if an SEU causes the controller to go astray and scramble the data in the LTDS. The memory test sequencer was designed as a single state control circuit constructed from conventional components, such as the 54LS series circuit technology, to minimize the possibility of radiation upsets. The circuit consists of two sequencers. Each sequencer is a counter with some or all of the counter outputs connected to the address inputs of a ROM. The ROM has 16 output data bits that are used to control data direction, data flow, test address and controller resets that occur in

the experiment. The sequence controller also includes a nonvolatile alarm clock. The clock has the time-of-day and date as well as a programmable alarm and 50 bytes of auxiliary nonvolatile memory.

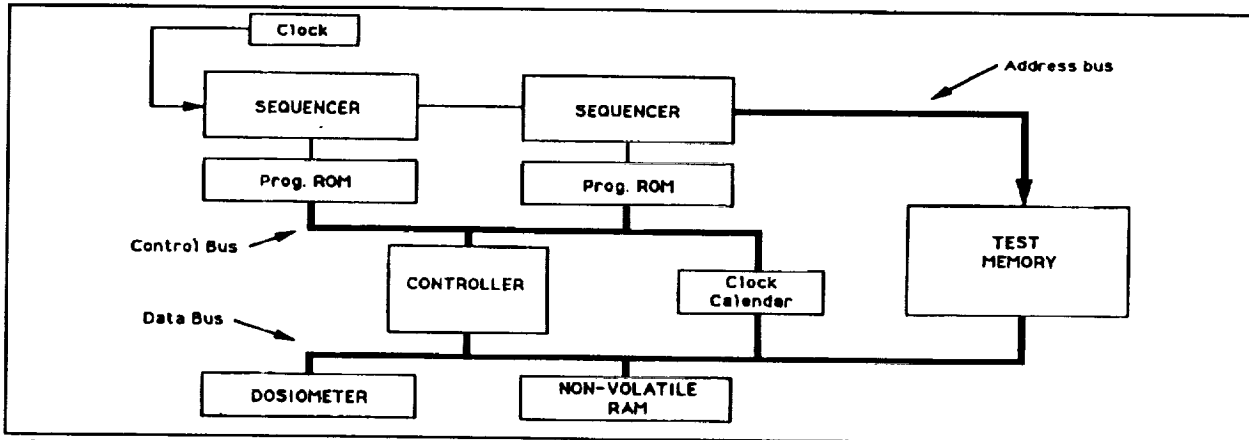


Figure 1. The Effect of Radiation on Semiconductors Experimental Block Diagram.

One sequence counter, sequencer A, initializes the test, writes the data in the MUT, reads and records the radiation dose rate and controls the time of the MUT check. The initialization procedure monitors the radiation dose for 5 hours to determine the minimum and maximum readings for these orbits. Then, the test data are written into the MUT and the alarm is set for one hour. When the alarm goes off, the radiation dose rate is measured and compared to the minimum and maximum values obtained before. If the orbit is near a maximum radiation region the memory test is not performed and the alarm is set another hour ahead. When one hour has elapsed and a low radiation dose rate is measured, or if two hours have elapsed since the last test, the control is passed to a second sequence counter, sequencer B.

Sequencer B writes a marker in the LTDS and tests each byte in the MUT four times for errors. Any error that is detected all four times is recorded in the LTDS. The error byte, the correct byte and the address of the error byte are recorded for each error detected. When all 64 kbytes are tested, the time and total dose are stored in the LTDS and the master reset is initialized.

After the mission, the data contained in the LTDS and clock will be analyzed. These data are triple redundant and should show the minimum and maximum radiation dose rates, total dose accumulated, the time of each test, and the location and type of error that has been detected.

Orbital Debris Detection System

The objective for the orbital debris experiment is to record the time and intensity of impacts on the Space Shuttle from debris encountered around the orbit. The total vibration (or noise) picked up by the sensor, an accelerometer, will come from three different types of vibrations: impacts, random noise (e.g. shuttle crew activity), and noise that has a sinusoidal dependence. The sinusoidal and random noises are considered background noise for this experiment.

One of the obstacles to this experiment is that the background

noise may, at times, mask the vibrations from the impacts. The main source of background noise normally comes from the motors, fans, and crew of the Shuttle. Because of the partly sinusoidal dependence of the unwanted noise as well as the fact that the amplitude, frequency or phase of this noise can not be known in advance, a digital adaptive filter approach is used. This digital adaptive filter is based on a least mean square (LMS) algorithm and is the heart of the software system.

The LMS algorithm estimates a signal (the impact) corrupted by noise and passes it through a filter. The filter will suppress the noise while keeping the impact signal relatively unchanged.

Now that we have a signal free of sinusoidal waves, we need a way to extract impacts from the random noise. We take the filtered signal, and run it through a "peak picker". The way this picker works is that we make a running average of 100 data points. The next point of data is compared to the running average plus a set threshold. If the data point is greater than the average plus the threshold, we conclude that it is an impact. In this case we record the amplitude of the signal and the time at which it occurred. If the data point is not a peak then it is not recorded. Each data point is then compared as it is obtained from the filter. By saving only the peaks, we have achieved a 1000/1 data compression ratio. This means that our experiment should be able to run for the entire shuttle flight.

A computer program was made to test the software on some simulated data. The results were positive. In Figure 2 we created a simulation of the output that the sensor would pick up. There are four different sources of noise with a sinusoidal dependence along with two impacts and random noise. Figure 3 shows an example of the signal of two impacts after the signal has been processed through the adaptive filtering code.

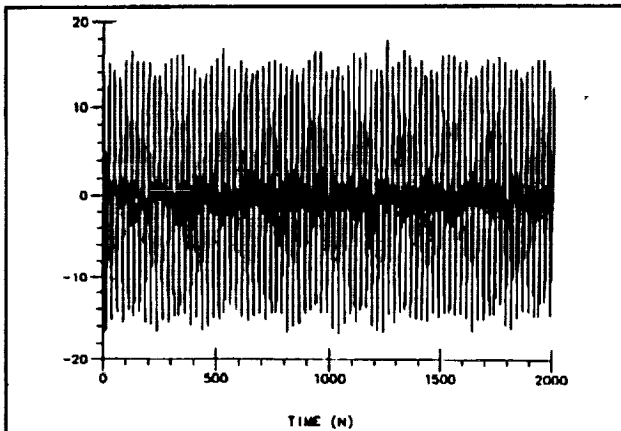


Figure 2. Simulated Output of Piezoelectric Sensor.

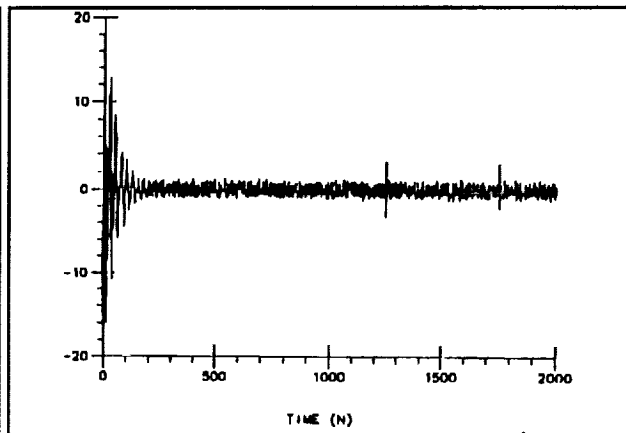


Figure 3. Processed Signal using LMS Algorithm.

The actual components needed for this experiment can all be purchased "off the shelf". Each component can be easily integrated to prepare the experiment. We have chosen certain data detecting, analyzing, and recording devices because of the power, cost, and reliability constraints. There are no moving parts in the device, with the exception of a calibration hammer, which does not affect the

design. We have chosen no disk drive recorders or the like because of their unreliability when exposed to adverse conditions.

The entire experiment will be able to function as a self-contained unit. This will be done so that, in the future, this design can be directly implemented into other orbital platforms or similar devices. However, for the GAS project, there are two exceptions. First, the piezoelectric device, which is the accelerometer used to pick up the vibrations, will be attached to the inside of the GAS canister. Secondly, our memory device will interface with the general recording device of the PSU GAS Systems Group for backup recording.

There are four basic components that need to be integrated for this experiment (Figure 4). The piezoelectric sensor, an analog to digital converter, the central processing unit, and a memory card or cards. All of the cards will be contained in a card cage. The converter will take the output of the sensor and transform it into data that can be used by the processor.

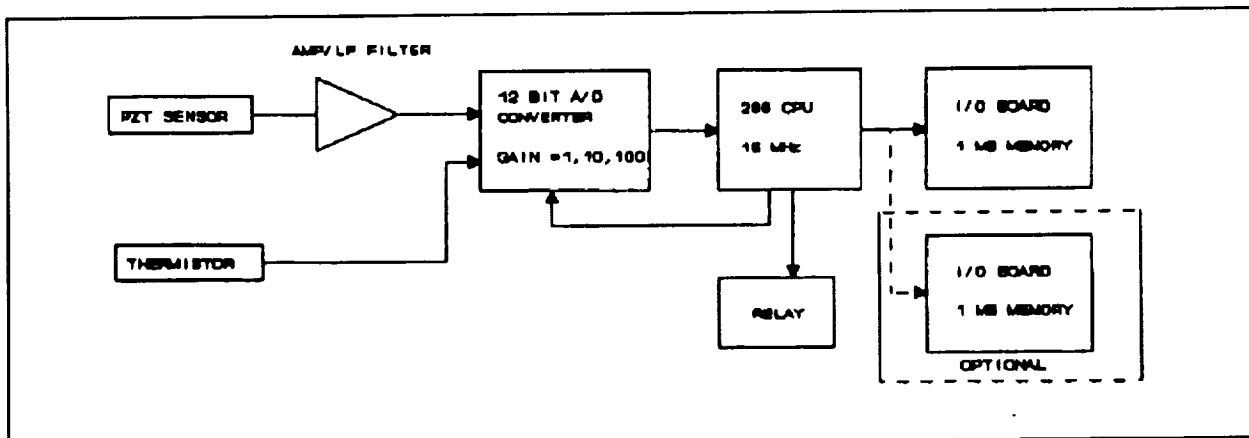


Figure 4. Orbital Debris Detection Experimental Block Diagram

The Fluxgate Magnetometer

The fluxgate magnetometer experiment is designed to record the three dimensional magnetic field map of the Shuttle. The three axis magnetometer's ability to detect changing magnetic fields is due to the nonlinear characteristics of the magnetometer's ferrite rods. The three pairs of ferrite rods (one pair for each orthogonal axis) are wrapped with three wire coils: a primary coil, a secondary coil, and a calibration coil.

The experiment begins when the accompanying drive circuitry (Figure 5) supplies a 2 kHz square wave reference signal. The signal is frequency divided to 1 kHz and sent through the primary coil, this will generate a magnetic field. Since the primary coils of each rod, in each pair of rods, are wrapped in the opposite sense, the magnetic fields in each primary coil are in opposing directions. The signal drives the ferrite core into saturation twice each cycle, changing the permeability of the core at a frequency, which is twice that of the primary current. [1] The magnetic flux in the core consists of the flux generated by the primary coil and that from the external surrounding magnetic field. The magnetic flux from the primary coil is produced at odd harmonics, since the permeability of the rods is

changing. The external surrounding magnetic field generates a magnetic flux at even harmonics because of the nonlinear properties of the core. Since the magnetic flux from the primary coils are in opposite directions, the net flux in the core from the primary coil equals zero. The flux in the secondary coil, then, is only from the external surrounding magnetic field.

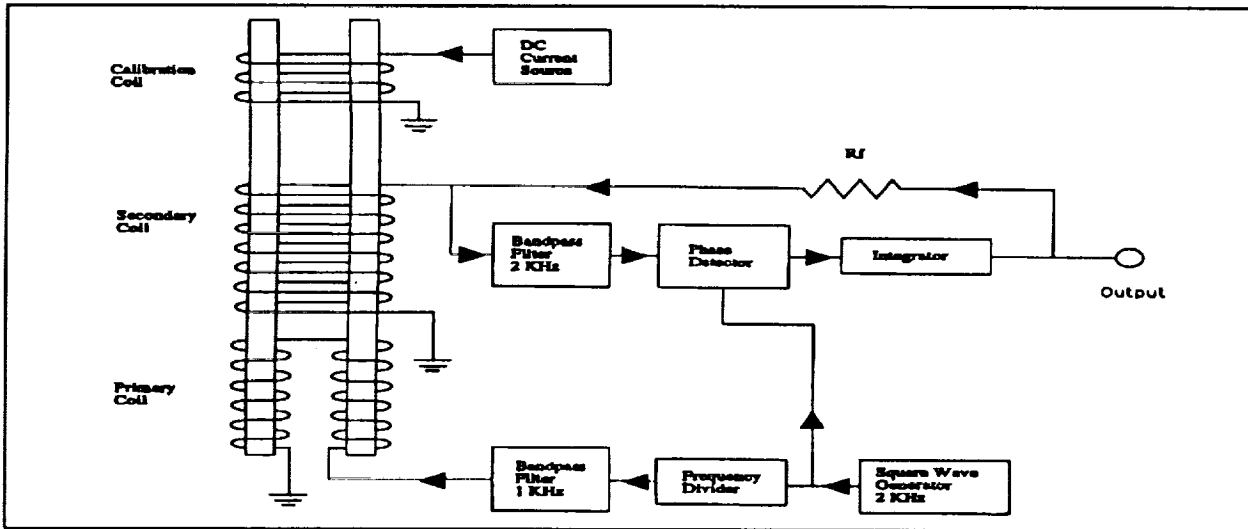


Figure 5. The Fluxgate Magnetometer

A calibration coil is used to cancel out a known portion of the signal due to the earth's magnetic field. The coil produces a magnetic field equal to and opposite the Earth's field. The equation for the magnetic field, B , produced is

$$B = \mu N I \quad \text{Equation 1}$$

where μ is the permeability of the rod, N is the number of turns of wire in the calibration coil, and I is the current passing through the calibration coil.

The magnetometer will be in equilibrium at all times. The voltage at the output of the integrator modifies the current through the feedback resistor leading to the secondary coil. This current produces an induced field in the rod that cancels the external surrounding magnetic field. The voltage across the feedback resistor is proportional to the external magnetic field, since

$$I = V / R \quad \text{Equation 2}$$

and the magnetic field, B , can then be determined by Equation 1.

The accompanying circuitry of the fluxgate magnetometer is also shown in Figure 5. The 2 kHz square wave signal generated is first frequency divided and then bandpass filtered to provide a sinusoidal signal into the primary coil. The voltage that arises in the secondary coil is then proportional to the surrounding magnetic field. The phase of the signal is compared with the reference signal to determine if the field is increasing or decreasing. The integrator modifies the voltage

across the feedback resistor to cancel out the changing external field.

The data recorded will consist of the direction and magnitude of the external magnetic field. This will be accomplished by recording the analog output from each axis's integrator. The output will be converted to digital data and stored every four seconds for five hours. In addition, the ambient temperature will be recorded every four seconds for five hours, since the temperature differences effect the core magnetization curve.

The experiment will be turned on by the GAS canister baroswitch after liftoff. Since the experiment would like to take measurements when the Space Shuttle performs a 360 degree roll maneuver, the magnetometer should be operating during the first five hours after liftoff. During the first hours of every Space Shuttle mission, rolls are executed in order to orient the Shuttle into its proper trajectory. Also, the three other experiments in our canister will be non-operational so the magnetic field produced by other experimental circuitry does not interfere with the magnetometer's measurements.

The data recorded from the magnetometer will be used to determine the magnetic interference in the Shuttle from other equipment and from construction used in the shuttle and cargo bay. The data will also be used to determine the magnetic properties of the shuttle.

The Photoelectric Effect Experiment

The purpose of measuring the photoelectric effect of materials in space is to obtain data on the photoelectric yield of several materials. The results from this experiment will be useful in design of ionospheric plasma probe experiments and in describing the local plasma interaction of satellites in orbit. The samples that will be used in this experiment are gold, aquadag, stainless steel, and aluminum. The reason why these materials were chosen is that all of them are common in spacecraft structures. For each of these materials, there will be a clean sample and a dirty (oxidized) sample, thus making a total of eight samples to be tested. The clean samples will have all surface oxides and organics removed through a chemical cleaning process. The eight samples as well as a solar cell will be placed on top of our structure to allow as much sun to impinge on the samples.

The photoelectric effect experiment will only operate when the shuttle bay is facing towards the sun. A special housing for the solar cell and the samples will be built in the shape of a cylinder. This housing will make sure the solar cell does not cause the system to run prematurely.

When the solar cell detects full illumination, the experiment will run as follows. The specimens, when illuminated, will emit photoelectrons which will be picked up by their respective electrometers. Each electrometer will amplify the current and give a voltage signal as an output. The voltages will be negative, so an inverting op amp is used to invert the signal and to set the gain. This signal will then be processed by the A/D converter for storage by the data system of the PSU GAS. A diagram of the circuit layout can be seen in Figure 6.

The electrometer needed for this experiment is one that can accept a wide range of currents (up to five orders of magnitude). For this

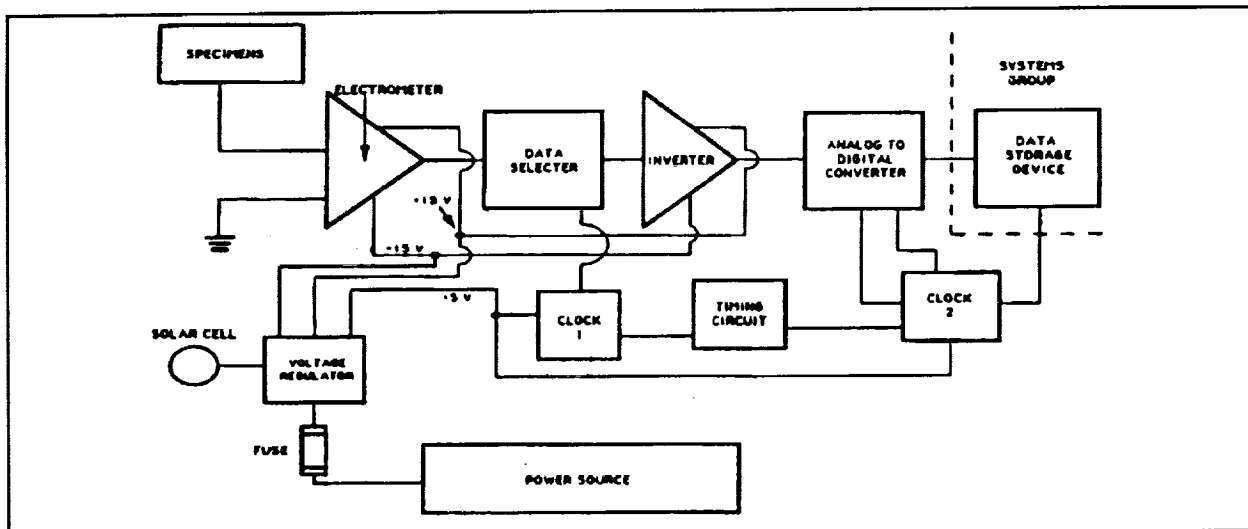


Figure 6. The Photoelectric Effect Experimental Block Diagram.

reason a logarithmic electrometer was chosen. A logarithmic electrometer has a range of up to 6 decades, which will allow the currents to be in the field of 100 pA to 10 μ A. Most of the design for the logarithmic electrometer was taken from Weihsing Liu's M.S. thesis. [2]

The data selector is an 8:1 analog multiplexer that is used to select a voltage output of one of the samples. Each sample has its own electrometer, so the selection insures that only one voltage is sent to the op amp and the converter to allow recording of these signals to the data storage device. An analog mux was chosen over its digital counterpart due to the analog's low power consumption.

The timing circuits box in Figure 6 contains two timers, one operating at 1 Hz and the other at 500 Hz. These timers control counters 1 and 2 respectively. The counters then select which specimen's data will be changed from analog to digital and eventually stored.

The experiment is designed to write data to memory once every second for the eight samples. The system will take two seconds before repeating the writing sequence, thus taking ten seconds to write the data to memory. The data system will be time stamped and will show which sample was recorded along with its photon count. If the solar cell indicates full solar intensity, the process will be repeated. The photoelectric effect experiment will select and convert data until there is no more space in memory or until the solar cell is no longer registering power.

While designing the circuit layout of the photoelectric effect, several parts received special consideration. Due to the wide variations of temperature in space, military specified components were chosen over commercial integrated circuitry. Also, low power Schottky chips were used in the design. As an example, the analog multiplexer chosen has a delay time of 1 μ s, and the A/D converter has a conversion time of 100 μ s. The PSU GAS data recorder requires 1 ms to write data, therefore the second timer is set at 500 Hz to allow data to be

transferred from the multiplexer to the data recorder without causing a data sample to be missed.

After the Shuttle mission, the data will be processed to provide a deeper understanding of which materials can be used to minimize spacecraft charging.

CONCLUSION

The four experiments will be integrated into a five cubic feet GAS canister. The entire operation will be activated by the baroswitch during liftoff. The magnetometer experiment will start taking data for the first five hours of flight. Then a timer will activate the other three experiments.

The four experiments are focused towards gaining a better understanding of the space environment. The semiconductor experiment will provide data on the susceptibility of different device technologies to the space radiation environment. The orbital debris experiment tests a system for the detection and recording of impacts to spaceborne systems. The fluxgate magnetometer provides information about the magnetic fields in the Shuttle bay. The photoelectric experiment will aid in determining what materials could be useful to minimize spacecraft charging.

It is expected that the engineering designs developed during Spring 1992 will be used to develop the experimental hardware for flight in Fall of 1993.

The experience and knowledge gained from this program will give valuable data on materials and operations in space and introduces students (Table I) to the challenge of design and construction of spacecraft systems.

Table I. Student Experimental Design Teams

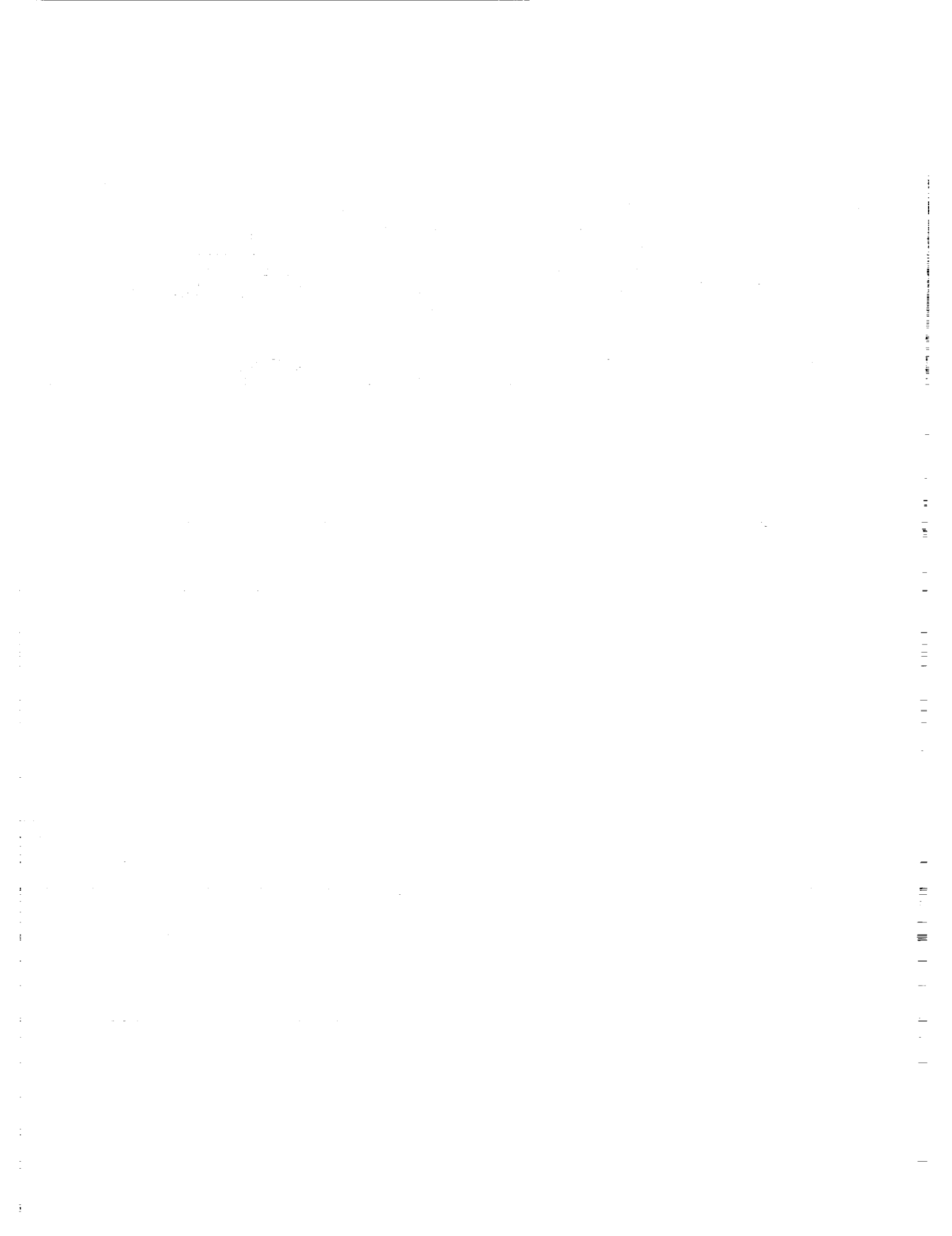
Semiconductor Experiment	Orbital Debris	Fluxgate Magnetometer	Photoelectric Effect	Systems Group
D. Bower	M. Youssef	J. Costa	T. Dembiczak	T. Boris
T. Decarbo	J. Schwartz	C. Flotta	P. Olah	M. Makdad
T. Grosch	P. Stack	D. Smuck	B. Richie	R. Williams
B. Klus	J. Martone	G. Traub	M. Schaefer	J. Yurack
D. Nguyen	J. Szabados	W. Walker	B. Werner	K. Cha

Management Team: G. Evanisko, K. Dewitt, M. Weinel, and C. Stubner

REFERENCES

[1]. Adolph S. Jursa, *Handbook of Geophysics and the Space Environment* (National Technical Information Service, Springfield, Virginia, 1985).

[2]. Weihsing Liu, "A Logarithmic Electrometer for Rocket Probes" M.S. Thesis, The Pennsylvania State University.



**CONCAP IV:
A COMPLEX AUTONOMOUS PAYLOAD (CAP)
FOR GROWING ORGANIC THIN FILMS
IN MICROGRAVITY**

W.E. Carswell, F.C. Wessling

Consortium for Materials Development in Space
The University of Alabama in Huntsville, 35899

INTRODUCTION TO THE SCIENTIFIC MISSION

The Consortium for Materials Development in Space and the Center for Microgravity and Materials Research at the University of Alabama in Huntsville are collaborating to grow Nonlinear Optical (NLO) organic crystals and thin films. NLO materials play a key role in the fields of optics and optoelectronics. Loosely, they can be said to play the same role in optics that semiconductors play in electronics. There are many advantages to using organic materials over inorganic materials for NLO applications. The two advantages we are concerned with are that organic NLO materials frequently have a much higher nonlinearity than inorganic materials do and in some cases can transmit higher power densities.

One of the major drawbacks to organic NLO materials lies in the preparation of samples to be used in devices. Organic crystal growth is made difficult by weak crystal binding forces, low thermal conductivity, and, frequently, thermal instability at growth temperatures. A ground-based crystal and thin film growth facility has been developed which addresses these limitations. After carefully fine-tuning the ground-based facility it was adapted for use in the Get Away Special Canister. By growing crystals in space we hope to obtain more uniform compositions and avoid defects caused by plastic deformation of the crystals under their own weight at the elevated growth temperature. By growing thin films in space it may be possible to obtain more uniformly ordered films in terms of both crystallinity and composition.

GAS-105: THE FIRST NLO MISSION

The first microgravity NLO crystal/thin film experiment was GAS-105, flown in June 1991 on the STS-40 GAS bridge. The results were both encouraging and disappointing. Four crystal growth cells and two thin film growth cells were flown with a four-day growth time. Neither thin film cell produced a thin film, two of the crystal seeds shrank instead of growing, another decomposed, and the remaining crystal grew well. In most cases the quality of the starting material proved to be of prime importance. The temperature controller and software provided extremely high stability ($\pm 0.01^\circ\text{C}$) in some cases. The insulative technique we employed was very efficient, using approximately 3W of power to operate two growth cells at 125°C in a single oven chamber. This hardware will be described in more detail in a later section of this paper.

The thin films are being grown from a diacetyline monomer starting material, with polymerization being induced after the thin film is grown. Each of the thin film cells on GAS-105 experienced different problems, both due to the presence of impurities. In one case the monomer polymerized prior to thin film transport. Vapor transport is impossible once polymerization has taken place due to the subsequent low vapor pressure. Although the elevated temperature contributes to polymerization once the process has begun, it was the presence of impurities which initiated polymerization at the growth temperature. The other thin film cell did undergo vapor transport, but when the cell was opened after the mission it was observed that the transported material was a brown, viscous liquid instead of a white (monomer) or purple (polymerized) fibrous film. It was determined that the material decomposed to a diol after transport due to the presence of impurities.

Four crystal growth cells were flown. Two contained a substituted nitroaniline compound (DAN), the other a proprietary material from our industrial sponsor, Teledyne Brown Engineering (TBE-1). Each crystal growth cell was equipped with small starting seeds on the growth sting to avoid nucleation problems. In both of the DAN cells the seeds actually shrank during the mission, rather than growing. This was due to improper selection of growth temperatures. In the case of the first TBE-1 sample, the source material and the seed crystal decomposed. This decomposition was stimulated by the presence of impurities in the sample material. The second TBE-1 sample exhibited excellent growth in terms of both transparency and faceted morphology. The seed crystal, however, was polycrystalline to begin with, so the grown crystal was a polycrystal also. However, even if the crystal had been a single crystal, it still would have been too small to characterize optically. TBE-1 grows so slowly that it takes nearly three weeks to obtain a crystal large enough on which to perform NLO characterization.

FUTURE NLO MISSIONS

The nature of crystal and thin film growth has led to the separation of follow-up missions into two categories, short-term and long-term. Short-term missions will be dedicated to growing thin films, which takes only a few hours. Long-term missions will be dedicated to growing crystals, which takes from two to four weeks. The short-term experiment platform will be Complex Autonomous Payload (CAP) missions on the Space Shuttle. Vapor transport is not disturbed by gravity levels less than $10^{-2}g$'s. It is not too difficult to find Shuttle missions which provide five hours of stability at $10^{-3}g$'s or less.

The long-term platform will be the Commercial Experiment Transporter COMET. This is a free-flying satellite which is expected to provide 30 days of microgravity at $10^{-5}g$'s. The COMET NLO crystal growth experiment is currently scheduled for launch in the first half of 1993. No further discussion will be made of this aspect of the program since the focus of this paper is the CAP payload.

CONCAP IV: SPACE SHUTTLE NLO THIN FILM GROWTH

The Consortium for Materials Development in Space is developing a series of CAP missions, called CONCAP. The NLO project is the CONCAP IV series. The first NLO mission, CONCAP IV-01, is currently slated for launch on STS-57 in the spring of 1993.

CONCAP IV-01 Requirements

Power Requirements

Each oven, containing two growth cells, consumes approximately two watts of power when operating at 95°C. CONCAP IV-01 will accommodate six pairs of cells, yielding a total steady state power consumption of 12W by the heaters during thin film growth. Initial heat-up demands will, of course, be higher, roughly a total of 40W for one hour. In addition to this, the controller and other electronics draw about 3W. Thus the total average power draw during thin film growth is about 15W with a total growth time of 3 hours. The total battery requirements then are 40W-hrs plus 45W-hrs, or roughly 85 W-hrs.

Vacuum Requirements

The CONCAP IV experiments require access to the vacuum of space for three purposes: 1) vacuum is one of the insulative techniques used to obtain the highly efficient thermal conditions, 2) vacuum enhances vapor transport process, and 3) exposure of the source materials to non-inert gases (i.e. oxygen) increases the likelihood of decomposition at elevated temperatures.

Experiment Time

There are three distinct phases in the thin film growth experiment: 1) heat-up, 2) thin film growth, and 3) cooldown. The exact nature of each phase will be discussed in a later section, but the times required are one hour for heat-up, three hours for thin film growth, and one hour for cooldown.

Microgravity

It has been shown that, while melts and fluids are subject to gravitationally-driven convection at $10^{-5}g$'s to $10^{-6}g$'s, vapors tolerate g-levels as high as $10^{-2}g$'s. Therefore the CONCAP IV missions require gravity levels of $10^{-2}g$'s or greater.

Gas Backfill

After thin film growth is complete it is necessary to backfill the growth cells with enough inert gas to quench vapor transport, roughly two orders of magnitude more pressure than the vapor pressure of the grown thin films. This turns out to be roughly 2 psi.

Experiment Hardware

The overall payload layout is shown in Figure 1. The experiment subsystems are: 1) the primary experiment support structure, 2) the vacuum vent valve assembly, 3) the inert gas backfill assembly, 4) the primary battery, 5) the controller, and 6) the physical vapor transport (PVT) hardware.

Primary Experiment Support Structure

Figure 1 shows the primary experiment support structure. It consists of three parts: 1) a round baseplate, to which is attached 2) a rectangular mounting plate, and 3) bumpers to secure the free end of the rectangular plate. The assembly is aluminum and weighs about 50lb.

Vacuum Vent Assembly

The vacuum vent assembly is shown in Figure 2. The valve consists of a bellows vacuum valve coupled to a polarized gear motor. The motor is controlled by the experiment controller and can be operated in either direction via polarity switching. Venting is done through the modified battery vent turret supplied by GSFC. The modification consists of a 9/16-18 thread into the side of the top of the turret. Into this thread is attached the vacuum vent tube, consisting of a corrugated metal hose with a 9/16-18 straight thread/o-ring terminus.

Gas Backfill Assembly

Figure 3 shows the gas backfill assembly. It consists of a 500ml DOT-rated pressure vessel, a motor/valve assembly, and a connecting stainless steel tube. Use of the DOT cylinder greatly eased the safety process. The cylinder is held in place by an aluminum bracket on either end. The connecting tube is welded into the valve port and swaged into the cylinder connector.

Primary Battery

The primary battery is undergoing a design change as of the deadline for this paper. The original experiment configuration called for a 13-day crystal and thin film growth mission. With this mission requirement in mind we selected a 200A-hr 15-cell silver zinc battery (4500W-hr). Subsequently, however, we obtained the COMET free-flyer long duration mission opportunity and changed the focus of CONCAP IV-01 to thin films only. This greatly reduced our power needs to less than 200W-hr. Currently we are investigating the use of lead-acid cells for this application.

Controller

The controller consists primarily of three printed circuit cards: 1) the smart card, 2) the power switching card, and 3) the thermistor signal conditioning card. The smart card is built around a Z80-based microprocessor chip. The signal conditioning card has 64 8-bit A/D channels for temperature acquisition. The current configuration uses a gain of twenty to achieve better than 0.01°C resolution in a 4°C window around the set-point. We also have un-gained resolution of about 0.2°C over the range from 0°C to 130°C. The power switching card uses P-FETS to provide 24 channels of 28V on-off supply. A control algorithm using proportional PID on/off control is capable of maintaining the temperature to within $\pm 0.012^\circ\text{C}$.

Figure 4 shows the controller assembly. The mounting structure consists of two aluminum angles with slots running down their lengths into which the cards are placed. Expanding wedges are used to hold them in place. A bottom plate is used to hold the assembly together during mounting and bench-top activities. The top and end are for mechanical and dust protection and can be eliminated from the flight configuration if weight is a problem.

PVT Hardware

The PVT hardware is shown in Figure 6. It consists of the insulative assembly, referred to as the NLO ovens, and the thin film growth cells. The NLO oven is made of two polished aluminum concentric cylinders. The inner cylinder is held into place with small kevlar strings. The strings are the only mechanical contact between the two cylinders, thus minimizing conductive heat loss. The concentric cylinder arrangement minimizes radiative heat loss and the vacuum between the two eliminates air as a heat path. In this way the primary heat loss path is the heater and thermistor wires leading from the growth cells. In this way the highly efficient thermal behavior (125°C at 3W) is obtained. Each NLO oven is approximately 12 inches long and houses two PVT (thin film or crystal) growth cells.

The PVT cells consist of three parts: 1) the source chamber, 2) the growth sting, and 3) the flange. The source chamber is a glass tube 2.5cm diameter by 5cm long closed off at one end. The source material for thin film growth is placed into this chamber and is held in place by a stainless steel screen epoxied in place across the middle of the tube. The heater is a 165Ω kapton thin film heater wrapped around the glass cell with shrink band. The thermistor is epoxied directly onto the shrink band.

The growth sting is made out of a copper rod 2.5cm long by 1cm diameter. The heater, which is a 1.6KΩ .5W resistor, and a thermistor are epoxied into a hole drilled through the center of the copper rod.

The flange is made of teflon and serves three purposes: 1) mechanical support, 2) thermal isolation, and 3) leak to vacuum. Mechanically, the teflon flange serves to hold the copper sting in place relative to the glass cell. Thermally, the flange separates the sting and the cell so that significant (16°C) temperature differences can be maintained over a relatively short distance.

The third role of the teflon flange is providing a leak to vacuum through 4 small holes drilled through it. The leak to vacuum is necessary to provide more efficient vapor transport and to remove decomposition impurities which would otherwise accumulate in front of the growing thin film.

SUMMARY

A GAS facility has been developed for carrying out low temperature experiments. The arrangement being used on CONCAP IV-01 is designed for thin film growth in microgravity and can process up to twelve samples per mission. The NLO oven hardware can also be made suitable for other low temperature applications, such as gradient freeze and solution growth of crystals.

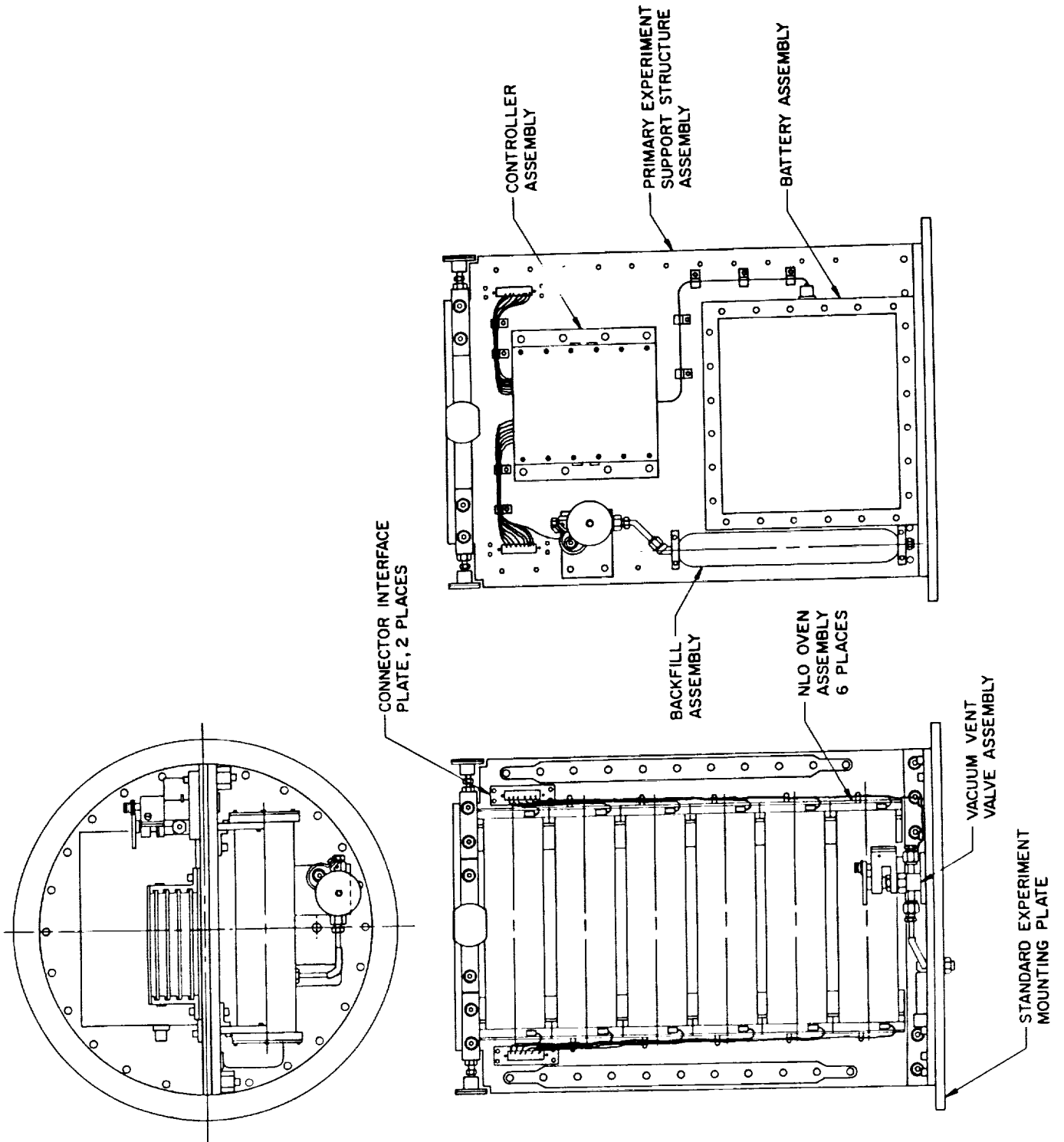


Figure 1: CONCAP IV Payload Layout

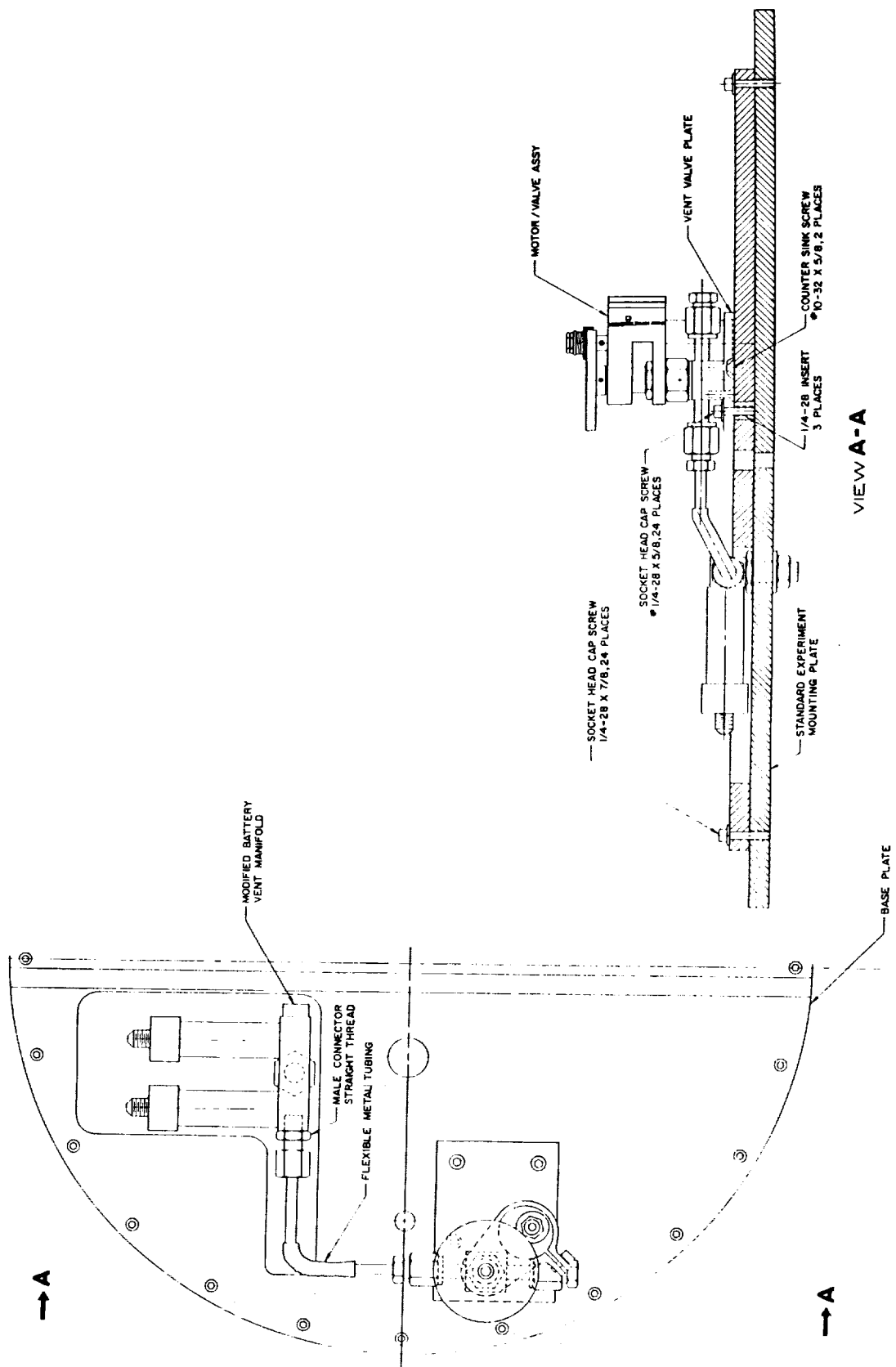


Figure 2: CONCAP IV Vent Valve Assembly

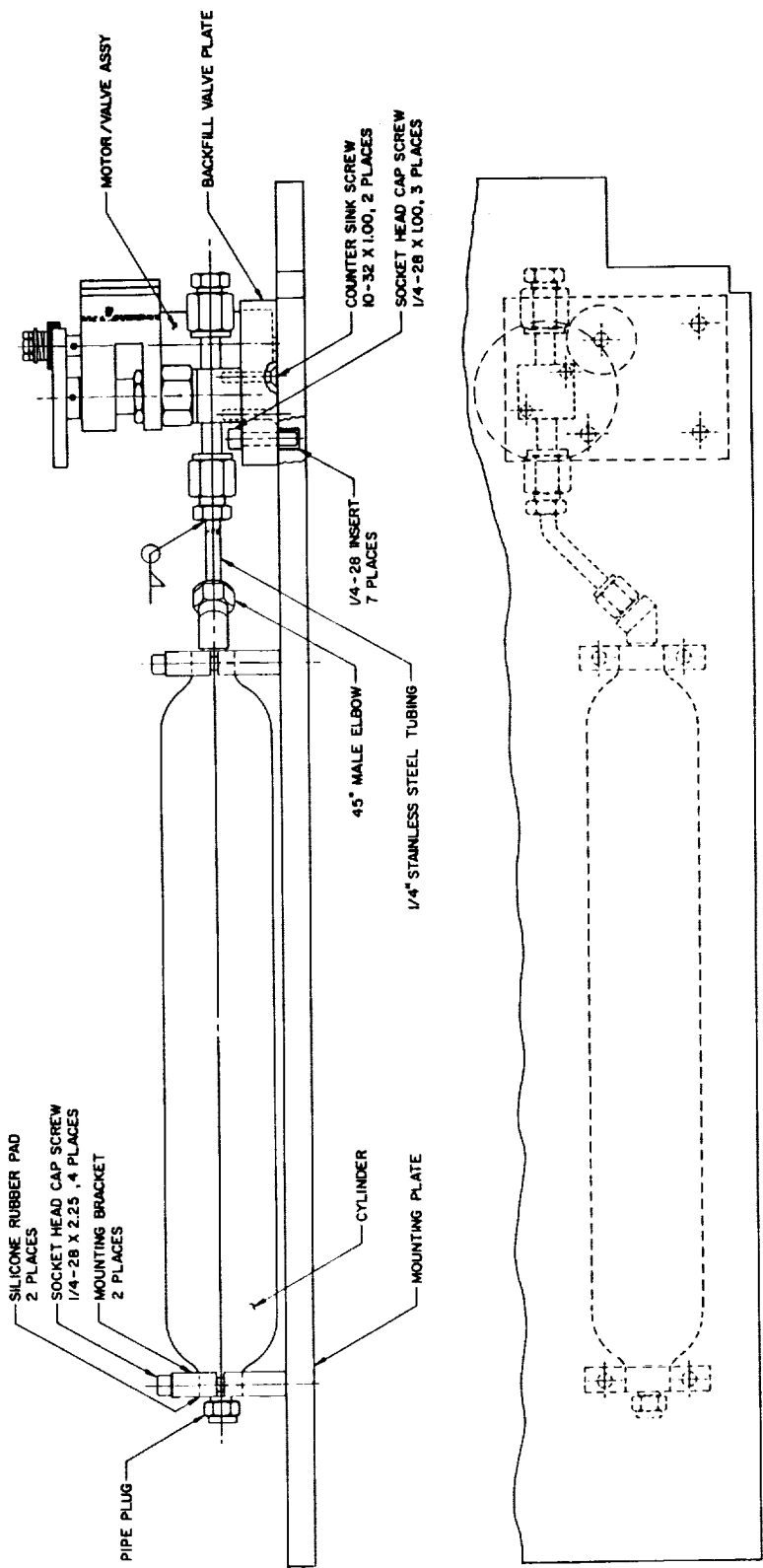


Figure 3: CONCAP IV Backfill Valve Assembly

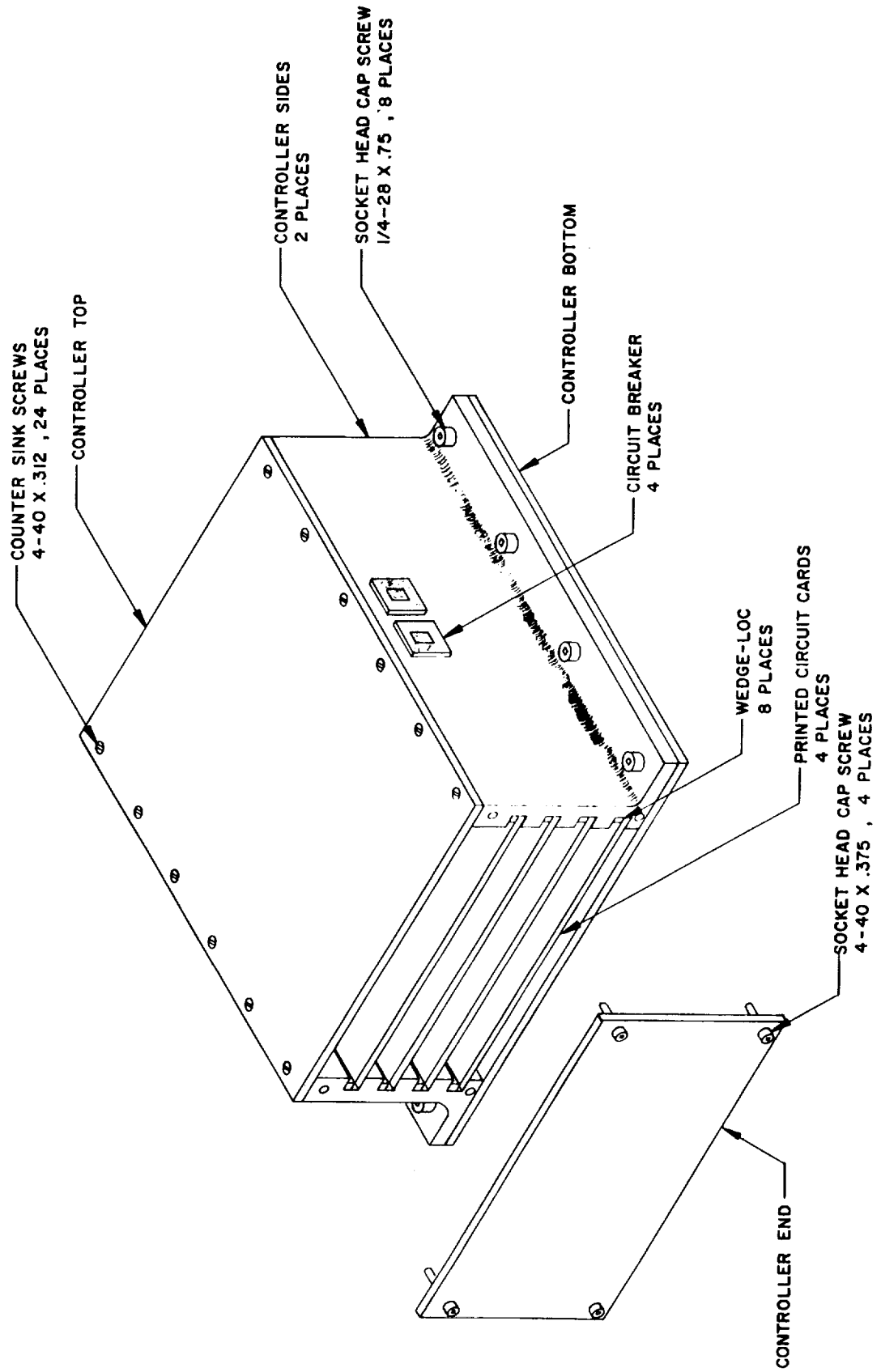


Figure 4: CONCAP IV Controller Assembly

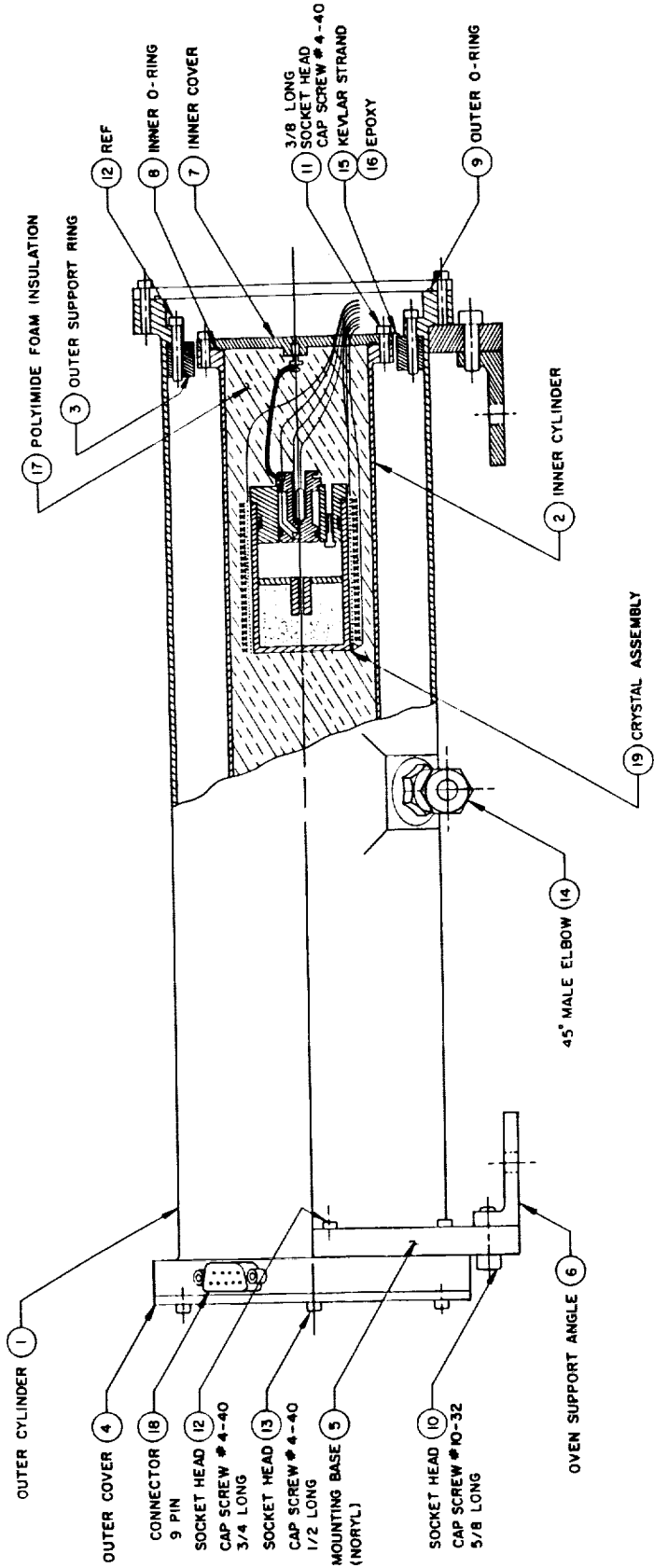


Figure 5: NLO Oven assembly with PVT cell

N 9 3 - 1 3 1 7 9

The ROMPS Robot in HitchHiker

George Voellmer

714/Robotics Branch

NASA/GSFC

Introduction

The Robotics Branch of the Goddard Space Flight Center has under development a robot that fits inside a Get Away Special can. In the **RObotic Materials Processing System (ROMPS)** HitchHiker experiment, this robot is used to transport pallets containing wafers of different materials from their storage rack to a halogen lamp furnace for rapid thermal processing in a microgravity environment. It then returns them to their storage rack.

A large part of the mechanical design of the robot dealt with the potential misalignment between the various components that are repeatedly mated and demated. A system of tapered guides and compliant springs was designed to work within the robot's force and accuracy capabilities.

This paper discusses the above and other robot design issues in detail, and presents examples of ROMPS robot analyses that are applicable to other HitchHiker materials handling missions.

Overview

The robot

The ROMPS robot (figures 1 and 2) is a three axis, cylindrical workspace robot, with a gripper. The Z axis joint consists of a motor and a ball screw shaft, which together move the carriage arm, and with it the rest of the robot, on linear bearings, up and down along the axis of the can.

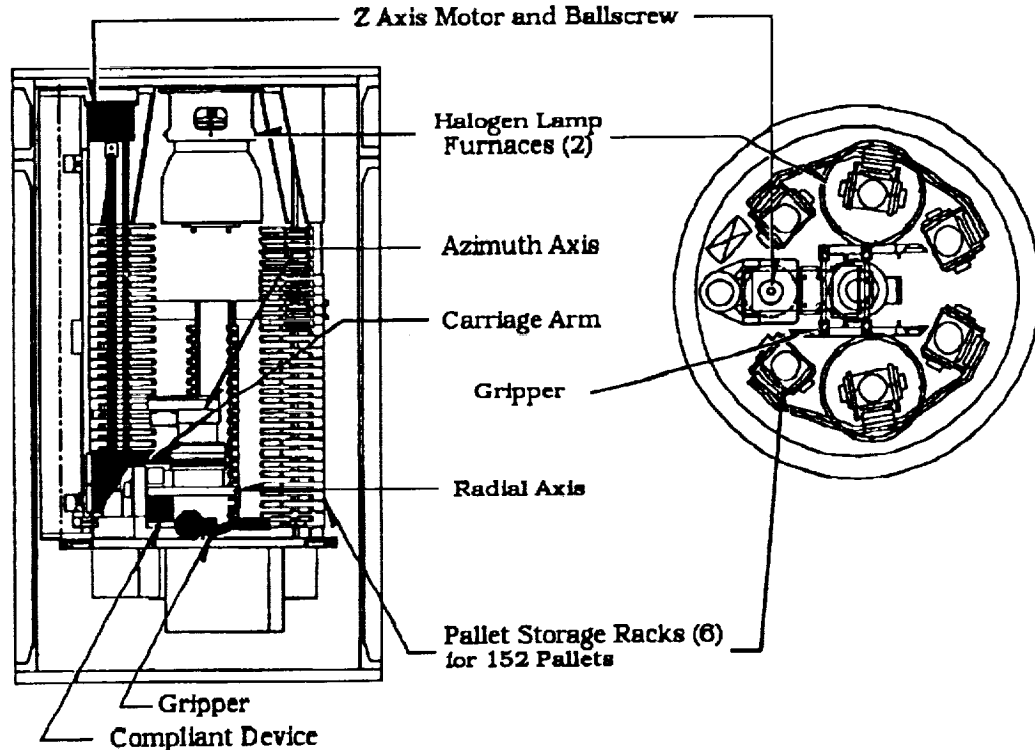


Figure 1): ROMPS experiment side and top view showing robot, furnace, sample racks with samples, and the location of the gripper and the compliant device.

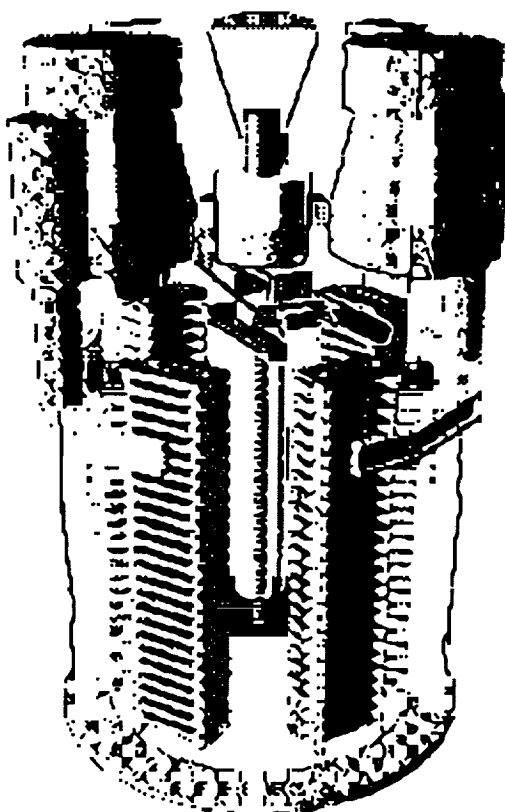


Figure 2): A computer-generated perspective view of the ROMPS experiment.

The azimuth axis is mounted to the carriage arm. It consists of a motor and a harmonic drive speed reducer, which then forms the base for the radial axis. The azimuth axis is located at the geometric center of the can, so that the robot's radial axis joint is always perpendicular to the GAS can's inner surface.

The radial axis consists of a motor and spur gear set, which drives a ball screw. The ball screw pushes a linear bearing back and forth, radially out towards the can wall.

The gripper (Figure 3) is mounted to this linear bearing via the compliant device. The gripper fingers are driven by a hollow motor and small harmonic drive. An acme screw with left hand threads on one end and right hand threads on the other goes through the hollow motor / harmonic drive assembly, and engages nuts mounted in the fingers. These nuts press against springs in the fingers, moving the fingers. The springs provide compliance for the gripper finger throw axis, as well as the azimuth rotation axis.

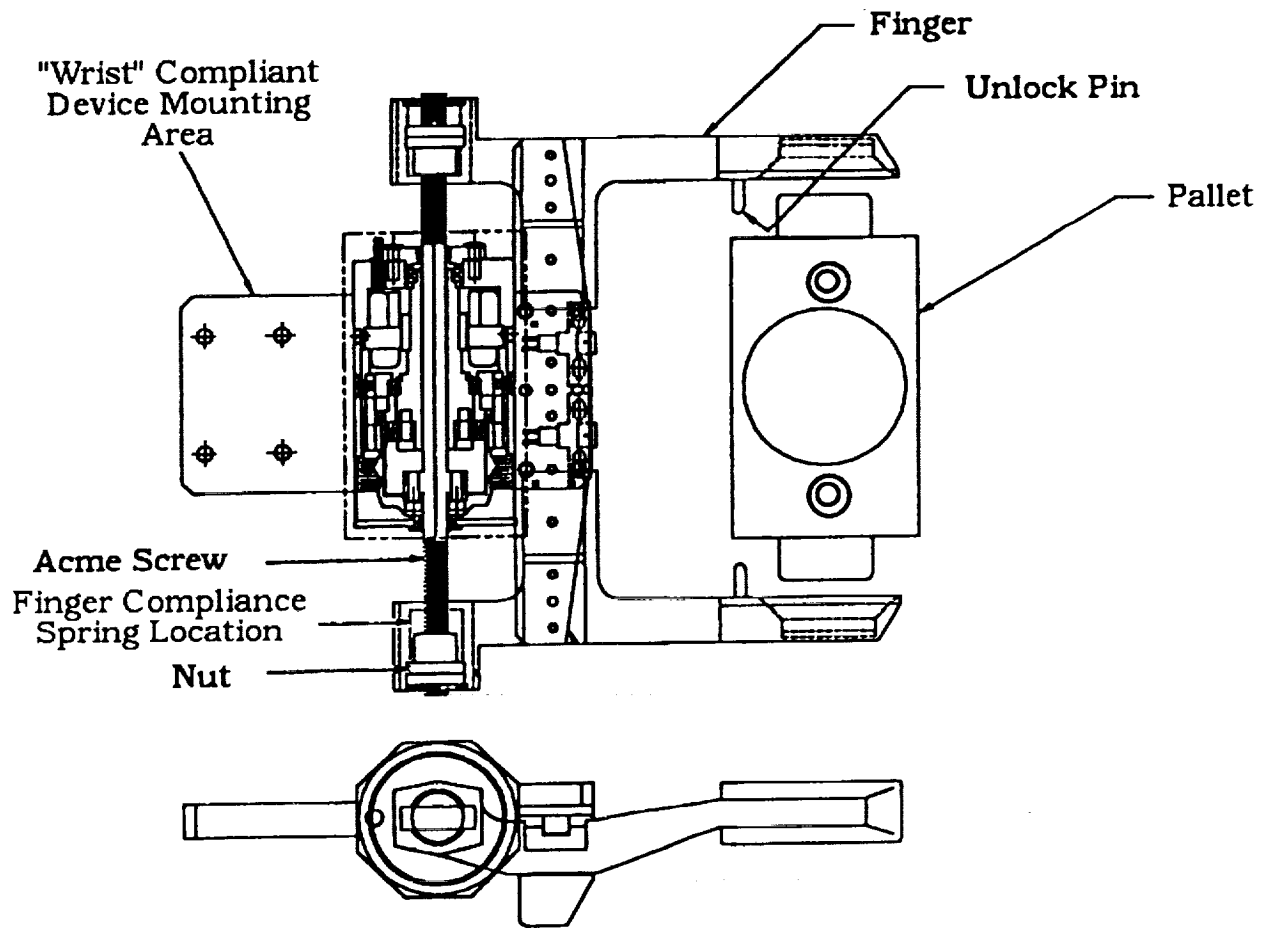


Figure 3): The ROMPS robot gripper.

In operation, the robot moves into position in front of the pallet in its storage rack by rotating the azimuth joint and moving to the appropriate elevation with the Z axis drive. During these moves, the radial axis is retracted. Once in position, the radial axis extends, with the gripper fingers open. When the radial axis is in the correct location, the gripper fingers close on the pallet. After a secure grip has been established, the radial axis retracts, pulling the pallet out of its storage rack.

Once free of the rack, the robot moves the pallet into position in front of, and slightly below, one of the ovens. The radial axis then extends until the pallet is directly below the aperture in the halogen bulb furnace. Two pins extend down from the furnace, which engage two holes in the pallet as the pallet moves up into contact with the base of the furnace, aligning the material sample in the pallet with the focus of the light in the halogen furnace.

Removal of the sample from the furnace and its return to the storage rack are the reverse of the above sequence.

Before and after all robot operations, the robot gripper is locked to the z axis support column by the fingers closing on a launch lock fixture. The fingers simply close to grasp the fixture, and open to release it. This serves to isolate the gripper's compliant device from the launch and landing loads.

The ROMPS robot will only use position control; the force will not be controlled, only monitored. When the robot needs to apply a certain force, such as when it is pressing the pallet against the furnace, the robot behaves as though it were moving the pallet past the furnace a certain amount, usually .13". When the pallet contacts the base of the furnace, the compliant device is compressed .13" (plus or minus the accuracy of the robot), and the force is then a function of the compliant device's stiffness in that axis.

Object Hand-off

When an object is being moved from one location to another by an autonomous mechanism, there will always be some uncertainty about exactly where the object is located by the mechanism. This can be due to thermal distortions of the structure, backlash in the drive train, manufacturing inaccuracies, limitations on the resolution of the position feedback sensors, accuracy of the control system, or a host of other reasons.

This is of particular concern when a hand-off of the object is to take place. In these situations, the inaccuracies of both parts of the mechanism contribute to bring about a large misalignment between the mating parts.

In order to perform the hand-off despite this inaccuracy, three things are necessary: 1) a capture range, 2) compliance, and 3) sufficient force.

1) The interfaces need features which will draw the mating objects into alignment, such as tapers or chamfers. The capture range provided by these features must be greater than the expected misalignment.

2) There must be sufficient compliance, or give, built into the system to allow the alignment devices to move the object into alignment.

3) The mating parts must be brought together with enough force to allow the alignment features to deflect the compliant device by the amount of the misalignment.

In the design of the ROMPS robot, the inaccuracy was estimated first, which fixed the required capture range. The force level was then set. Finally, the required stiffness of the compliant device in the various directions where compliance was needed was calculated. This design sequence is illustrated in flowchart form in figure 4.

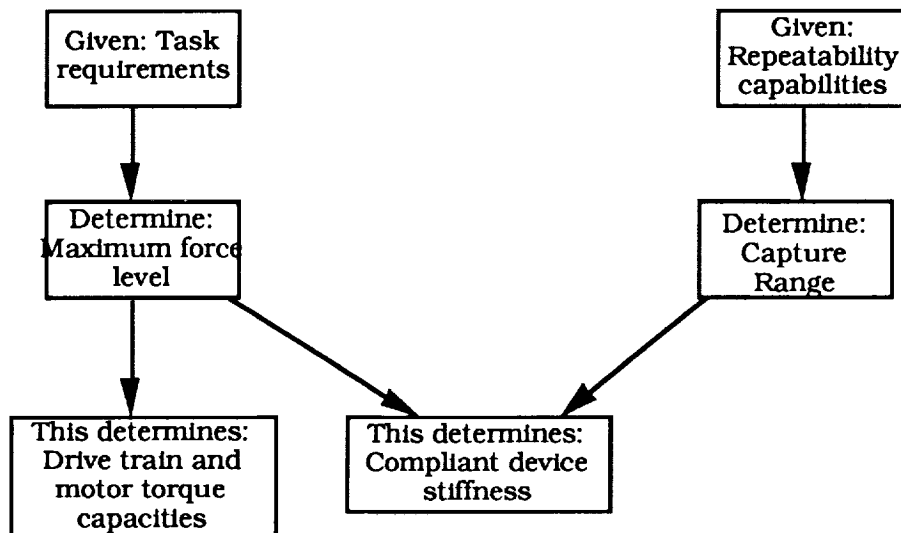


Figure 4): The ROMPS interface design flowchart.

Capture Range

The easiest way to keep the cost of the robot down was to use a position controlled robot, relax the accuracy requirements, and provide a large capture range. This allowed the use of cheaper and simpler control electronics, bearings, other drive train components, and position transducers. It allowed us to use lighter structural elements, and reduced our concern for thermally- and load- induced distortions. Additionally, ground testing of the experiment will be much easier: since the misalignment effects of gravity deflecting all the structures and biasing all the backlash will be a small percentage of the capture range, it can therefore be neglected, and no gravity off-loading schemes need to be devised.

The ROMPS robot will be taught the positions of all the interfaces it must reach: hence, the absolute accuracy of the robot is less important than its repeatability. The repeatability of the robot is governed by the controller repeatability, backlash in the drive train, the distortions in the structures due to thermal gradients, thermal expansion coefficient mismatch, and deflections due to loading of the structure. Because of the complexity of the mechanism, many simplifying assumptions were made, and a large margin for error was used.

The controller accuracy was designed to give a repeatability of at least .030" in all three linear axes, measured at the tool tip.

Drive train components with a total, combined backlash of less than .030" per axis are readily available.

Thermally matched materials will be used in all the pallet storage rack structural members and the robot structural members, and deflections of any part of the experiment with respect to another part due to thermal gradients will be less than .007", according to the thermal model.

Finally, deflections of the system due to gravity loading were analytically determined to be less than .050".

The sum of these errors is .117". This is a very conservative number, as the errors are not likely to occur at the same time in the same axis. A target capture range of ± 0.250 inches was chosen. This allowed for a relatively large position error for the robot, given the size of the GAS can (approximately 28" long x 20" diameter). At the same time, capture features and a compliant device for a 0.250" capture range did not appear to be too difficult to design for the available space. The only error which will cause a misalignment in an axis in which the robot does not move, such as rotation about the gripper, is the thermal gradient distortion. This misalignment is expected to be small, and easily within the capture range of the interfaces.

Having selected the capture range, it was then necessary to design the interfaces with the appropriate capture features.

The interfaces, shown schematically in figure 5, consist of

- 1) the pallet fitting into its storage rack,
- 2) the fingers grabbing a pallet,
- 3) the pallet fitting against the furnace, and
- 4) the gripper fingers grabbing the launch locks.

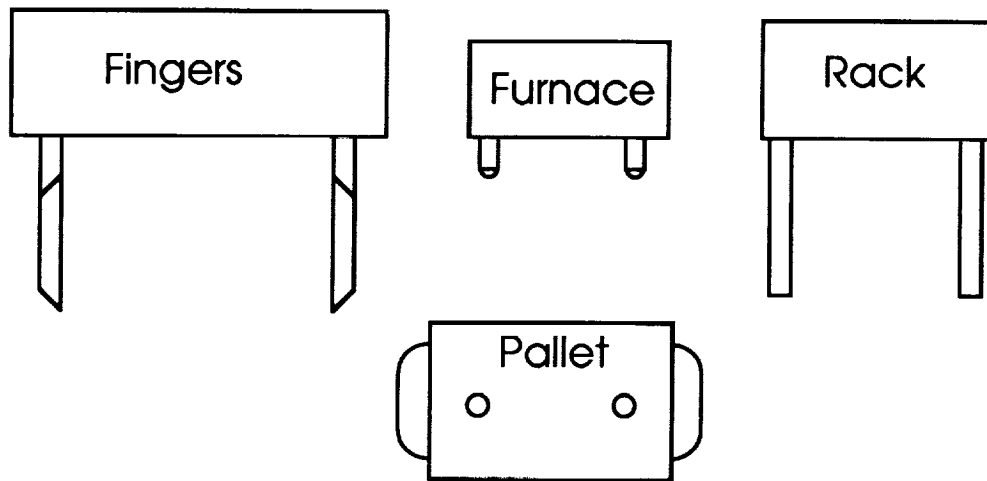


Figure 5): ROMPS mechanical interface schematic.

The Pallet / Storage Rack Interface

The transfer of a pallet from the pallet storage racks to the gripper fingers constitutes a hand-off, hence the alignment fixtures need to take into account the potential misalignment of the storage racks, as well as that of the pallet in the gripper, and that of the robot. In the other interfaces, the 0.250 inch capture range was used as a guideline; here, it was strictly adhered to.

Figures 6 and 7 show the pallet near the rack. The pallet is essentially a flat tray, and the rack is made up of two rows of tines. The rack resembles two combs, aligned parallel to one another, with the tines facing the same direction. The pallets fit into the tines of the combs, and are thereby neatly stacked.

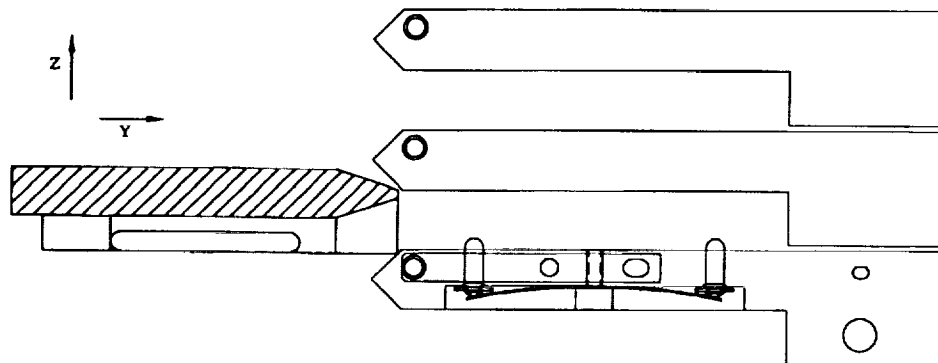


Figure 6): Side View, the pallet entering the rack, misaligned in +Z.

On insertion into its particular set of rack tines, the pallet's largest potential misalignments are in the Z direction (up and down), and in the Y axis (left and right). These are the robot's motion directions. Other potential misalignments, such as rotations about X, are not in the robot's motion directions, and would therefore not be caused by the robot's position error. Rather, misalignment in these directions would be caused by manufacturing and assembly inaccuracies. These can be controlled much tighter than the robot's position inaccuracy, and the potential misalignment here is much smaller. Simply having a loose fit at the interface will take care of these misalignments.

To align the pallet to the rack in the Z direction, the pallet leading edge is chamfered, as well as the top and bottom of the rack tines. The pallet leading edge is only chamfered where the tines can contact it, assuming the worst case misalignment in the y axis. The chamfer on the pallet extends 0.1 inches inward on both sides, and the chamfer on the rack tines extends 0.17 inches in. These chamfers combine to provide a total capture range, for this axis, of .27 inches. The chamfer on the pallet has an angle of 18 degrees, and the chamfer on the rack tine has a chamfer of 45 degrees. Therefore, if the misalignment is less than the .1" capture range of the pallet chamfer, the pallet will enter the rack until the corner where the chamfer on the rack starts contacts the 18° slope of the pallet chamfer, and the position correction is done by the 18° slope. If the misalignment is greater than .1", then the leading edge of the pallet will contact the 45° slope of the chamfer on the rack tine, and the correction will be done by the 45° slope, until the misalignment becomes less than .1". The system then corrects as described earlier.

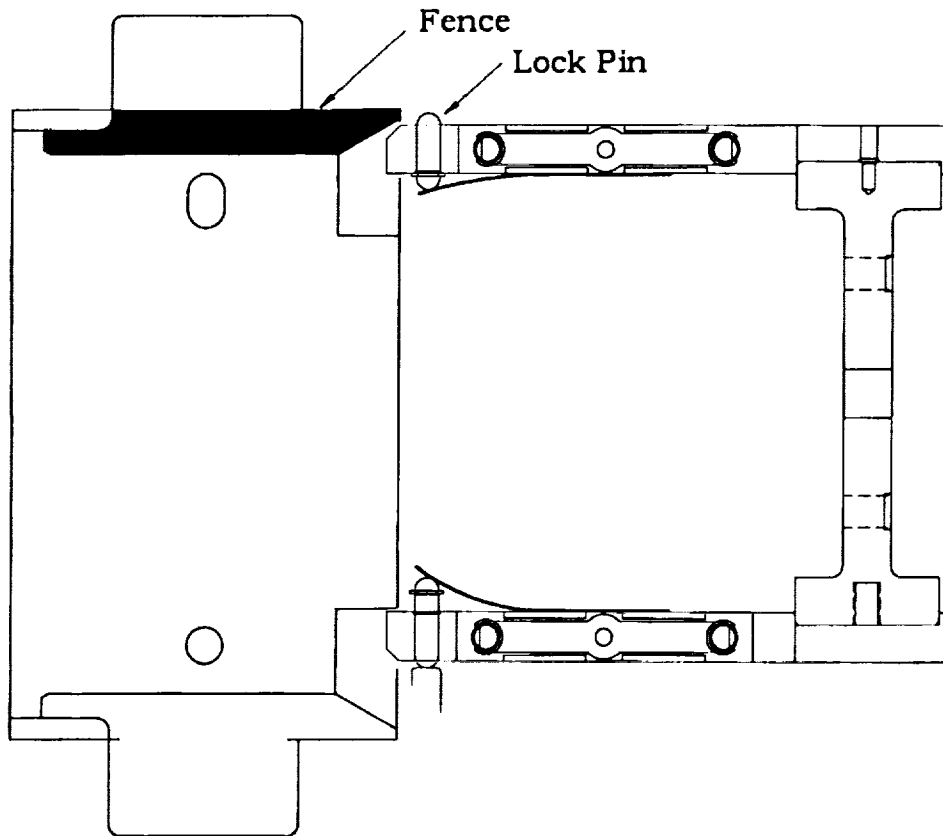


Figure 7): Top View, the pallet entering the rack, misaligned in X.

To align the pallet in the Y direction, the pallet has two "fences" extending down from its bottom surface. When the pallet is in its rack, these fences fall to the outside of the respective rack tine. This prevents the pallet from being moved out sideways, and locates the pallet. There is nominally 0.030 of play between the pallet and the racks, to prevent binding as the pallet slides in and out of the rack, and to allow for small misalignments in off directions, as discussed earlier. It should be noted that while this play is necessary for the smooth operation of the interface, it contributes directly to the uncertainty in the position of the pallet, and hence to the total capture range required.

Detent spring-loaded pins in the lower rack tines press the pallet up against the upper rack tine with about one pound of force, preventing rattling of the pallets in their rack during launch and landing. A lock pin in each of the tines extends out behind the fence

under each pallet, preventing the pallet from coming out of its storage position. An unlock pin in the finger pad presses against the lock pin as the fingers acquire a given pallet, depressing the two lock pins for that pallet, and allowing the pallet to be removed.

As can be seen in figure 6, the fences on the pallet are chamfered, and the rack tines are chamfered in this direction as well, although only on the outsides. The chamfer on the fence extends into the fence 0.17", and the chamfer on the outside of the rack is .15" deep, for a total of .32" of capture range.

The Pallet / Finger Interface

The pallet / finger interface, shown in figures 8 and 9, is the second part of the hand-off of the pallet from the rack to the fingers. The pallets have .105" thick, rectangular "ears", or tabs, which extend out from the edges of the pallet. When the pallets are in the rack, the ears extend out the sides.

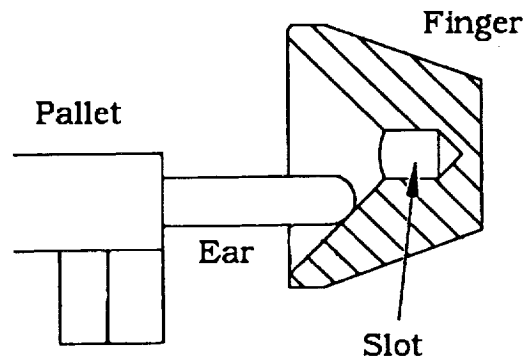


Figure 8): End view (cross section) of the finger / pallet interface, pallet misaligned in Z.

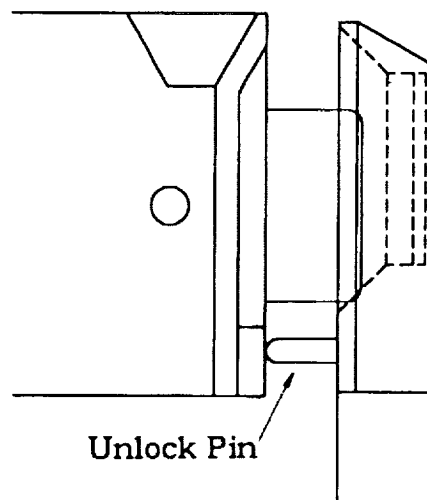


Figure 9): Top view of the finger / pallet interface.

The finger pads each have a slot in their inner faces into which the pallet ears fit, which is .020" wider than the pallet ears. The outside edges of the ears are given a full radius, and the bottom of the slot in the finger is V-shaped. Thus when the finger is closed upon the pallet with a force, the ears enter the slots and rattle about until they encounter the

bottom of the slot. There, the 45° V-shaped bottom centers the ear in the slot. This locates the pallet more repeatably with respect to the finger. If the pallet should encounter a force trying to pry it out of the fingers, however, the ear would tend to spread the fingers until it contacted the side of the slot. At this point, any additional force would not tend to spread the fingers any further, but would be taken up by the finger structure. This feature provides the fail-safe, non-backdriveable grasp of the object necessary for safety in space applications.

As an alignment feature, the slot has a 45° chamfer of .250 inches width around it. This fixes the size of the finger pad at

$$.250 * 2 + .125 + 2 * .030 \text{ (edge thickness)} = .685.$$

This also fixes the minimum spacing between adjacent pallets in the rack: they had to be far enough apart so that when the finger was at its worst case misalignment up or down, it would not contact the ear of the pallet above or below.

At first, four flat chamfers were put around the slot, which intersected in straight lines radiating out from the slot. Although the chamfer faces are all 45° slopes, the line of intersection of two 45° slopes is only sloped 35°. During testing, the 45° slopes were steep enough to pull the pallet into the slot, but if the pallet ear worked its way into the line of intersection of two slopes, which happened every time there was a misalignment in two axes, it would get hung up there.

To overcome this problem, the chamfer had to be curved around the slot. This was done by cutting it with the end of a 45° tip end mill. In this way, the slope of the chamfer is 45° at all points. The effect of this is to reduce the capture range from being a rectangle with .25" sides to being a circle of .25" diameter. Thus, rather than both axes being able to be off by .25", the root square sum of the errors could not exceed .25".

The Pallet / Furnace Interface

The furnace consists of a halogen bulb in an elliptical reflector. The radiation from the bulb is focused into an aperture in the bottom of the reflector. The sample pallets contain thin, flat films of various materials. These need to be accurately placed in the focus of the beam. The accuracy requirement was given as .020" in all three axes.

The bottom of the furnace was made flat, so the Z axis (up and down) positioning of the sample pallet is accomplished accurately by simply pressing the pallet flat against the bottom of the furnace. The rotational misalignments will be small, and the inherent compliance of the robot together with a positive pressure will ensure flush contact.

For the other two axes, the furnace has two .187" diameter pins which extend down on either side of the aperture. These engage two holes in the pallet, on either side of the sample (see figure 10). One of the holes is round, nominally .010" bigger than its pin. The other hole is a slot, with the short axis also .010" bigger than the pin. The long axis points toward the other hole and is .1" longer than the pin's diameter. This keeps the interface highly repeatable, and prevents it from being over constrained.

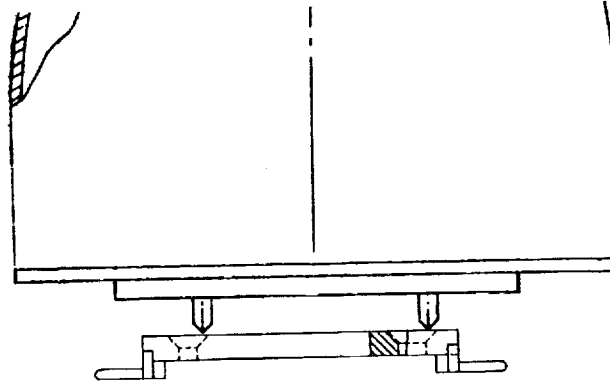


Figure 10): The pallet below the furnace, slightly misaligned in X.

To provide a capture range, the holes in the pallet have a 45° chamfer of .22", and the pins have rounded tips, with a radius of .090", for a total capture range of .31".

The Finger / Launch Lock Interface

Since the gripper is mounted to the rest of the robot via what is essentially a compliant spring, there is a concern that it might oscillate wildly during the high vibration environment of launch and landing, stressing the compliant device excessively. For that reason, the gripper will grab a launch lock fixture on the main Z-axis support post. This will relieve any loading from the compliant device during launch and landing. This interface had to be similar to the pallet / finger interface in that the launch lock needs to locate the finger precisely, to prevent rattling, yet large forces must not be able to pry the fingers out of the interface.

This interface was therefore designed in a similar way (see figure 11). The launch lock fixture is a block of metal with a slot cut into it, which the finger pad fits into. To lock the gripper down, the gripper inserts its fingers into the fixtures and closes them tight. Since the gripper drive train is a 1/4" diameter, 16 thread per inch acme screw, it is not backdriveable. The finger cannot be pried out of the fixture, but there is play, to ensure that the pads do not bind in the fixture on their way in or out. This play would allow the gripper to rattle during high vibrations, significantly increasing the contact stresses at the interface, the contact stresses at the finger linear bearings, and the bending stresses in the fingers.

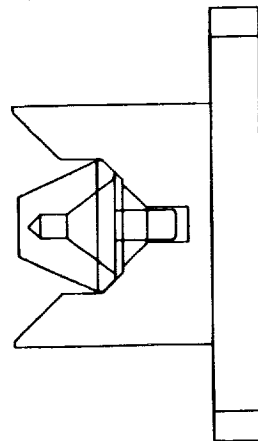


Figure 11): The gripper finger in the launch lock fixture.

To locate the fingers in the launch lock fixtures, the bottom of the slots in the fixtures have 45° slopes which snug up on matching 45° chamfers on the top and bottom edges of the finger pads as the fingers close all the way in the fixtures. This locates the fingers in the Z (up and down) direction. Because the grip force is in effect pressing a 45° wedge into a 45° slot, the normal force at that interface is quite high, and the friction force preventing radial motion of the finger pad in the fixture is large enough to prevent rattling in that direction. To prevent a large force from pulling the finger out of the fixture in the radial direction, the same pins in the finger pad that are used to depress the lock pins in the pallet storage racks fit into holes in the bottom of the launch lock fixture. These holes have chamfers to guide the pin in, in the radial direction. These holes are .030" oversized, to prevent binding.

Working Forces

The working force is the force that the robot is expected to actually use to do its work. It is the average maximum force the robot will need to apply, in a given axis, to perform the task at hand. The maximum force is the force which may be needed to overcome unexpectedly high friction, greater than average misalignment, or some slight binding. The robot's continuous force capacity is the force the robot can exert if the rated voltage is continuously applied to the joint motors, without overheating.

As an initial estimate, a working force level for the robot was set at five pounds in all three axes. Five pounds would be enough to actuate a mechanism or pull a pallet out against its detent springs, it was reasoned, and to provide a comfortably large pressure to ensure proper contact between two mating pieces. Yet five pounds was not such a large force that large motor currents would be needed, or that the motors and drive train would grow heavy and unwieldy. This is of particular concern in a serial-link robot in a gravity field, where the base joints must carry the outboard joint as well as provide a tip force.

As the design progressed, it became apparent that the azimuth joint was only needed to position the gripper, and not to apply any forces. Its maximum force requirement was therefore left as five pounds. The Z axis joint needed to apply a five pound load to press the pallet against the furnace, and the radial joint needed to apply five pounds to push and pull the pallets into and out of their storage racks against the detent springs. These axes' maximum force requirements were therefore multiplied by 5, to get 25 pounds, to ensure a positive torque margin. Additionally, the Z axis needs to lift the rest of the robot up during testing in a gravity field, so an additional 15 pounds was added to its maximum force requirement for a total of 40 pounds. The robot's joint motors were then selected to provide a continuous force capacity of at least three times the maximum force requirement.

The selection of the grip force was more complicated. The Z and radial axes had working forces of five pounds. This would be the force necessary to overcome an average misalignment. The average misalignment was assumed to be one half of the maximum misalignment. Assuming a linearly compliant spring, this set the force level necessary to deflect the spring by the maximum amount at ten pounds.

Therefore, the gripper fingers squeezing on the pallet ears at the gripper's maximum rated misalignment of .250" would have to build up to a ten pound restoring force if the gripper is to deflect the compliant device by .250". Figure 12 shows the free body diagram of the finger pads pressing on the pallet ear, providing the restoring force.

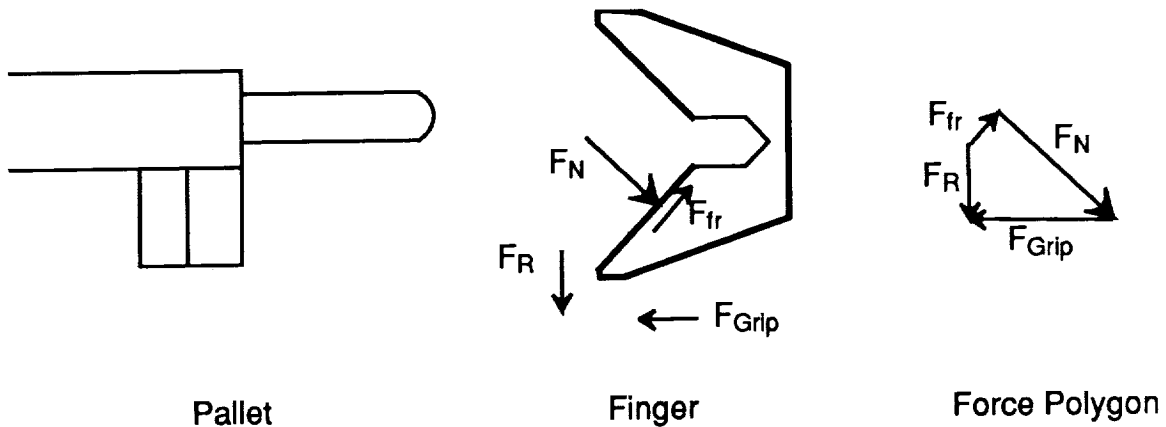


Figure 12): The free body Diagram of the finger pad. Forces shown for the case when the fingers are contacting the pallet ears, and the fingers are too high.

The restoring force is then given by

$$F_R = F_N \sin 45^\circ - F_{fr} \sin 45^\circ$$

$$F_R = (F_N - \mu F_N) \sin 45^\circ = (1 - \mu) F_N \sin 45^\circ$$

$$F_R = (1 - \mu) F_{Grip}$$

where

F_R = the restoring force

F_N = the normal force

F_{fr} = the friction force

F_{Grip} = the gripping force

μ = the coefficient of friction between the pallet ear and the finger

A conservative value for μ of .38 was used to yield a required maximum force of 16 pounds for the gripper. The gripper drive motor was selected for its inside diameter, to allow the acme screw to pass through the middle. Its continuous force capacity proved to be much higher than what was required.

Compliance

A summary of the compliance requirements is as follows:

For the Z axis: The compliance must handle up to .250" misalignment of the pallets entering the rack at 10 pounds of force. It must also press the pallets against the furnace with a positive force when the robot overtravels the oven's nominal position by .130" +/- .1".

For the radial axis: the compliance must also handle up to .250" misalignment at 10 pounds of force, when the pallet is pressed against the alignment pins in the furnace, and when the robot overtravels to ensure that the pallets enter the rack completely.

For the azimuth axis: the compliance must also handle up to .250" misalignment at 10 pounds of force, when the pallet is pressed against the alignment pins in the furnace, and when the robot stores the pallets in the rack.

For the gripper, the compliance must be able to handle an inaccuracy of the gripper fingers closure of up to .010", and still ensure a positive grip force. The compliance must not allow the grip to be opened enough to allow the pallet to be released.

To meet these requirements, two different compliant devices were used: one (figure 13) at the juncture between the radial axis and the gripper (the robot's "wrist"), and one in the fingers (see figure 3). The compliant device in the robot's wrist consists of two nested, double blade flexures, which allow .250" of travel in the Y (radial) and Z directions at a maximum force of 10 pounds. The double blade flexures were used because they each provide compliance in one axis only: they are very stiff in all five other axes. Nesting two of these together, rotated 90° with respect to each other, provides a plane of compliance. A spreadsheet program was used to size the blade width and thickness for a given length, spring constant, modulus, and stress level.

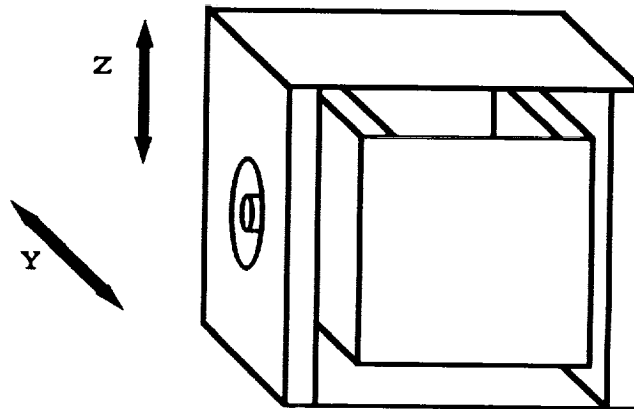


Figure 13): The wrist compliant device.

The compliant device for the grip and azimuth directions was simply a spring placed between the nut at the output of the finger drive train acme screw and the finger itself. This spring provides "give" when the gripper grasps a pallet. The accuracy of the gripper finger's positioning was estimated to be .020". Since no force control is being used, the only way a positive grip force could be assured without stalling the motor was to command the fingers to close past the point where the pallet would definitely be encountered, and to rely on the compliance to maintain a force close to that desired. The precise force level depends on the position accuracy.

A summary of the design values is given in figure 14.

Axis	Task	Working / Maximum force level	Repeat ability	Capture Range (min.)	Compliant device stiffness
Z	Press pallets against furnace, comply to rack, launch lock misalignment	5 lbs / 10 lbs	<.117 in.	.25 in. (finger/pallet)	40 lbs/in
Radial	Insert pallets into racks, comply to furnace, rack, launch lock misalignments	5 lbs / 10 lbs	<.117 in.	.25 in. (finger/pallet)	40 lbs/in
Azimuth	Free space moves, comply to furnace and rack misalignments	0 lbs / 10 lbs	<.117 in.	.31 in. (pallet/furnace)	40 lbs/in

Figure 14): A summary of the design parameters.

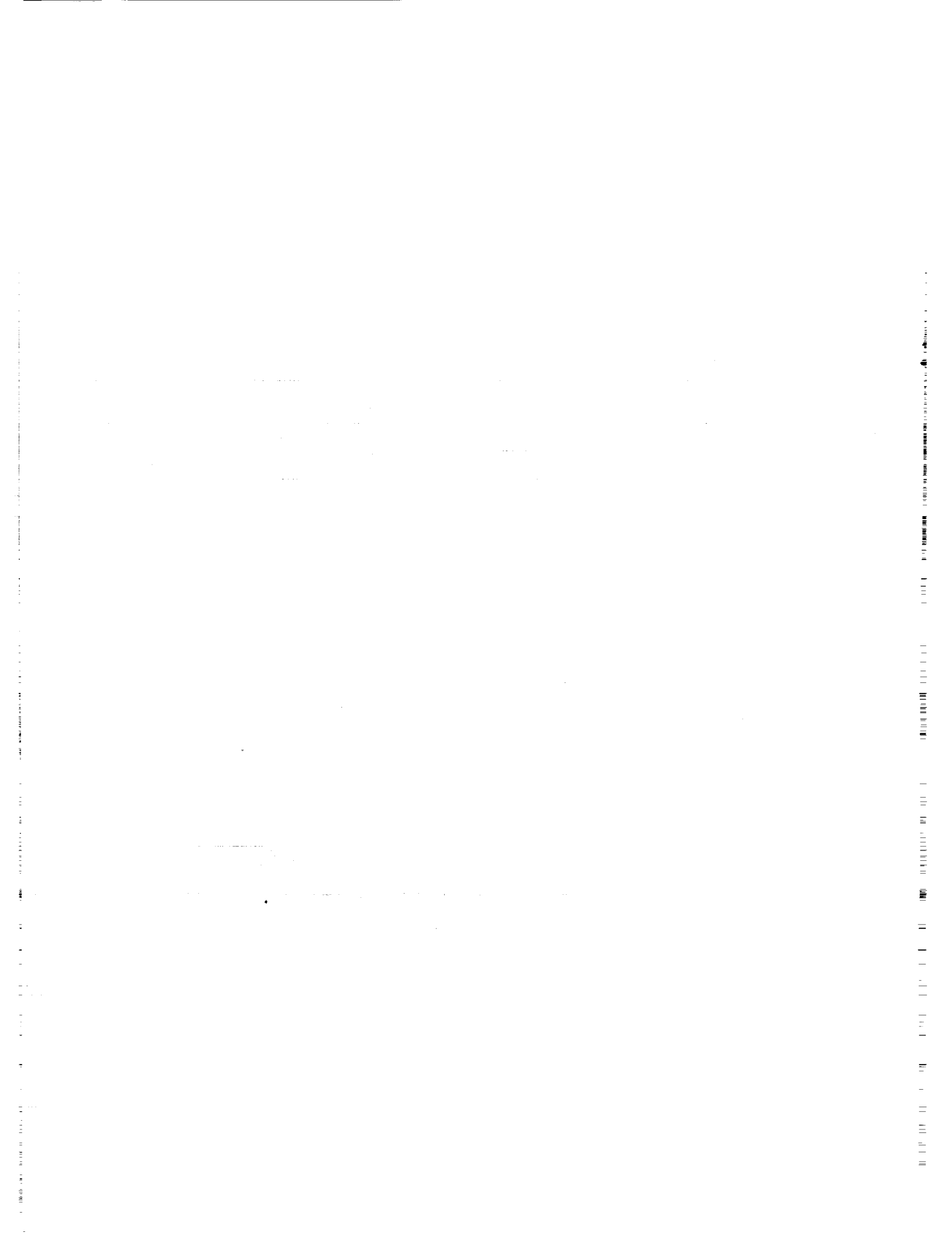
Extensions of This Technology

This type of logic is useful not only in designing traditional robotics mechanisms, but also when designing materials and object handling mechanisms. Although they may not "look" like robots, these mechanisms share attributes which make this design approach useful.

Another example would be docking and berthing mechanisms, wherein one mechanism aligns itself progressively to another mechanism, eventually locking down its position with a given accuracy.

Conclusion

Because of the interplay between capture range, compliance and applied force levels in a materials handling robot, a systematic, logical design process is required. The ground rules must be set: which variables should be accepted as fixed by the problem, and which dependent variables need to be calculated based on those. This is the starting point for all robotics and materials handling mechanism designs. In the ROMPS robot, targets for a) the capture range of the make/break interfaces and b) the joint torques were selected with the goal of minimizing the overall system cost. The required stiffness matrix was then calculated using these values. This stiffness matrix, taken together with other operational considerations, formed the basis for the design of the compliant elements in the robot.



THE DSI SMALL SATELLITE LAUNCHER

S. Nichols, D. Gibbons, J. Wise, D. Nguyen
DEFENSE SYSTEMS, INC.
McLean, VA 22102

ABSTRACT

A new launcher has been developed by DSI, that is compatible with the GAS canisters. It has the proven capability to deploy a satellite from an orbiting Shuttle that is 18 inches in diameter, 31 inches long, and weighing 190 pounds.

These DSI Launchers were used aboard the Discovery (STS-39) in May 1991 as part of the Infrared Background Signature Survey (IBSS) to deploy three small satellites known as Chemical Release Observation (CRO) satellites A, B, and C. Because the satellites contained hazardous liquids (MMH, UDMH, and MON-10) and were launched from GAS Cylinders without motorized doors, the launchers were required to pass NASA Shuttle Payload safety and verification requirements.

Some of the more interesting components of the design were the V-band retention and separation mechanism, the separation springs, and the launcher electronics which provided a properly inhibited release sequence operated through the Small Payload Accommodations Switch Panel (SPASP) on board the Orbiter.

The original plan for this launcher was to use a motorized door. The launcher electronics, therefore has the capability to be modified to accommodate the door, if desired.

INTRODUCTION

DSI developed the launchers because the presence of the hazardous payload required more safety inhibits than existing designs could provide. As the satellite design evolved, more volume and weight capability was needed. The new launcher has the electronics and spring drive outside the GAS canister envelope.

This paper will describe the design features, the qualification program that was performed that led to the approval to fly on the Shuttle, and the operational results.

The DSI launchers were used aboard the Shuttle, Discovery (STS-39) in May 1991 as part of the Infrared Background Signature Survey (IBSS). Fig. 1 shows the canisters and launchers mounted in the Shuttle payload bay. The SPASP was mounted on the aft flight deck, as seen in Fig. 2.

These launchers can be reused. Information is provided as to the processes required for reuse and possible modifications to adapt to other requirements.

DESIGN

Mechanical Details

The DSI launcher was designed to interface directly to the standard GAS canister cylinder. The launcher base plate interfaces to the cylinder via the standard attachment of 32 3/8" screws. The mounting to the Shuttle is a typical GAS canister technique, using 4 attach brackets and a shear pin.

The primary components of the launcher mechanism, as shown in Fig. 3A, are the pusher plate, v-band, mounting ring, separation springs (2), base plate, guide rod, retention springs, electronics/battery boxes, and the electronics enclosure. Most of the parts are made of aluminum. The springs are made of music wire; the guide rod is stainless steel; the bushings supporting the guide rod are bronze.

The launcher pusher plate sits inside the launcher mounting ring and mates with the inside edge of the satellite mounting ring. The segmented v-band, as shown in Fig. 3B, holds the rings together with approximately 3000 lbs tension. The springs were sized to provide a nominal separation velocity of 3.7 ft/sec for a 190 lb satellite. With these springs, the separation velocity will vary with the satellite weight. All components and hardware are mounted directly to the launcher base plate.

The launcher electronics system is contained in a single box as shown in Fig. 4. The batteries and electronics are mounted beneath the base plate in the payload bay, and protected by the electronics module cover plate, which provides an additional 8 inches of usable height inside the GAS can, while utilizing only 2 inches of height inside the canister for launcher volume.

The DSI launcher utilizes a 4-segment, aluminum v-band, using A-286 CRES links at two joints and separation pyrotechnics at the other two joints. The launcher mechanism is released by firing clamp separators, actuated by NASA Standard Initiators (NSI). Each half of the separated v-band is retained in the cylinder after deployment by retention springs. Damage to the GAS cylinder is prohibited by band stops, which retain the v-band and prevent flipping and resulting contact with the cylinder walls. As the v-band separates from the satellite and launcher mounting rings, the spring/pusher plate then pushes the satellite out of the cylinder. Fig. 5 is a photo of a launcher in flight configuration, after deployment.

Electrical Description

The launcher electronics system accommodates three launchers with control by the SPASP. As shown in Fig. 2, this panel has 6 switches and 6 indicators. Two of the switches were used for the launcher address code, three were used for the remaining three inhibits, and the final switch, "execute", was used to initiate the command selected by the other switches. The indicators were used to verify the commands.

The launcher electronics block diagram is shown in Fig. 6. Two 12-volt batteries provide power, each with six lead-acid cells with 4 amp-hour rating. Power converters include a 12V-28V unit for the indicators on the SPASP and a 12V-5V unit for the logic and relay drivers. The pyro circuit uses the 12 volts from the battery. Both batteries and both converters are protected by fuses.

The logic circuit is a set of static gates that convert switch actions into responses to satisfy operational and safety requirements. The circuit design does not allow the failure of a single device to cause an improper action, such as a premature or simultaneous release.

Toggling the execute switch turns the electronics on for 15 minutes. The logic circuit decodes the address switches and closes the select relay if the address is correct. The prearm switch closes the prearm relay which is on the return side of the pyro circuit, and a one minute inhibit timer is started. This timer prevents an premature release by inadvertently throwing the switches. The arm switch closes the arm relay. The deploy switch completes the pyro circuit and releases the satellite from the launcher.

Ground Support Equipment

Pallets were developed to support the CRO satellites and the DSI launchers. They were used during the fuel and oxidizer loading operations on CRO, for transport of the satellites, during the mating of the satellites to the launchers and the installation of the V-bands, and through final flight preparation until integration into the GAS cylinders.

The battery charger provided monitoring and charging of the batteries during testing, integration and prelaunch activities. Final battery charge is performed up to 2 months before launch.

The ordnance circuit monitor unit (OMU) is connected to the launcher in place of the Safe or Arm plug. This connection safes the ordnance by shorting the wires while monitoring the activity on the launcher ordnance circuit. When the fire voltage is applied, a light comes on in the OMU. This unit also verifies no operation during the environmental tests.

The function and power monitoring unit (FPMU) is used in conjunction with a SPASP to verify operation of the four inhibit relays and to monitor battery and converter voltages. Proper timer operation and addressing functions may also be verified using the FPMU.

An interface verification test (IVT) set was developed to verify the copper path of the interconnect wiring system from the SPASP to all three launchers. Each launcher has two connectors for system wiring which are wired together, with branch wiring to the launcher electronics. The first two launchers each have two cables connected, while the third launcher only has one cable connected.

By attaching the IVT set to the unused connector on the third launcher, all wiring could be verified in one test without disturbing flight connections. A test (GSE) SPASP was built to allow operational tests before integration with the Shuttle.

SHUTTLE QUALIFICATION PROGRAM

Design Verification Tests

These tests verified that the operations were in compliance with predicted and required performance characteristics. The GSE SPASP was used with two flight cables and one non-flight cable. All credible scenarios were verified.

A low voltage test was performed to verify the ability of the logic to perform as the supply voltage decayed. The test result showed that the relay drivers ceased operations at a higher voltage than the logic.

Environmental Tests

EMI and EMC testing was performed to verify the ability to operate in the Shuttle RF environment and that no inadvertent emissions from the launcher could effect the Shuttle.

The Thermal Cycling Test was performed to verify operation of the launchers over the temperature range of -30°C to +40°C. The Thermal Vacuum Test, performed at GSFC, was a 90 hour duration test with holds of up to 8 hours at both -20°C and +40°C, the low and high temperatures. The Vibration Test, was conducted with the launchers in the GAS cylinder with the CRO satellite attached in flight configuration. The vibration levels were 5.5 Grms, 7.7 Grms, 7.0 Grms in the X, Y, & Z axes respectively, as specified in the Orbiter Cargo Bay Random Vibration Payload Sidewall Adapters/Orbiter Interface Per ICD-A-17559. The Static Load Test, performed at GSFC, tested the launcher structure and separation mechanism, and showed minimum safety factors of 2.78 on yield and 3.34 on ultimate.

Operational Verification

As part of the design process, an extensive deployment velocity analysis was performed. The goal of the analysis was to provide a nominal separation velocity of 3.7 ft/sec for a 190 lb satellite. Deployment testing was performed to verify the analysis, and some surprising results were found. Deployment testing showed a separation velocity of approximately 60% the predicted value. The losses were discovered to be due to dynamic response of the spring mass system. All previous analysis considered only static properties. Design modifications were incorporated to achieve the required deployment velocity.

An analysis was required to ensure the launcher would not "jam", creating an unsecured, undeployed satellite situation. The inherent design prevents the launcher from jamming itself. Analysis also showed that all possible angles of incidence of the

satellites and the cylinder walls, given the coefficients of friction (minimized by placing delrin rails on the outer edges of the satellite) were too small to cause the satellites to jam within the cylinder after separation from the launcher. Flight experience shows that all three CRO satellites contacted the cylinder wall with no jamming.

Tipoff analysis was required to determine expected tumbling, interference, etc. The GAS cylinder walls limit tumbling due to tip-off, but is still possible, as post flight data indicates. Tip-off is a function of satellite mass properties, so a tip-off analysis must be performed for each mission. Post flight data does not correlate to previous analysis well, simply because tumbling was not of concern to the first mission.

V-band release testing was performed in numerous configurations to verify the structural design, the release capability, and the retention test. Ground tests verified that the v-band would release by firing only one of the two clamp separation bolts. Ground testing also verified the v-band attachment procedures as well as leading to the final v-band retention design, which was difficult to design based on analysis alone. The v-band was also test fired using bolts and a bolt cutter, instead of the recommended clamp separator. Tests proved the band released nominally in this configuration.

Flight Safety Qualification

The DSI launcher has passed extensive flight safety qualification and certification in accordance with NSTS 1700.7B, the STS Flight Safety Handbook. Extensive electrical, structural and kinematic analyses and tests were performed to certify that the launchers would pose no operational threat to the Orbiter. In addition, the launcher handling is controlled by a certified and approved Fracture Control Plan, generated in accordance with NHB 8070.1, the STS Fracture Control Requirements. In the event of a re-flight, the Fracture Control Plan is still applicable for all handling and screening of flight hardware.

OPERATIONAL RESULTS

On-Orbit results

CRO satellite C was successfully deployed with a confirmed ejection velocity of 4.0 ft/sec which was within 5% of the predicted release velocity of 3.9 ft/sec. No operational problems were encountered during the deployment sequence.

CRO satellite B was successfully deployed as shown in Fig. 7. The measured release of 3.7 ft./sec. was within 5% of the predicted release velocity of 3.6 ft/sec. Upon initial attempt to deploy B, the astronauts were unable to activate the launcher B electronics. After following the malfunction procedures, there was still no response from the launcher. Ground control commanded the crew to try launcher B again, before going to launcher/satellite AM (which was the planned contingent mode). Launcher B performed nominally

and satellite B was successfully deployed. This anomaly is discussed in the next section.

CRO satellite A was successfully deployed, with a measured velocity of 3.5 ft/sec, which is within 5% of the predicted release velocity of 3.4 ft/sec. Problems similar to those seen in the B deployment were observed here. Again, this anomaly is discussed in the next section.

Post Flight Activities

When the Shuttle returned to the Kennedy Space Center (KSC), a series of tests were performed during the deintegration as part of the anomaly resolution. In the Orbiter Processing Facility, operational and cable resistance tests were performed before any changes were made to the flight configuration. (Repeating the verification tests performed pre-flight.) Both tests were successful and showed no anomalies.

Stand-alone tests were performed by DSI both at KSC and in McLean, VA using the GSE. All tests were successful and no anomalies were found. The Shuttle payload bay operated at a cold temperature during the flight of STS-39. Therefore a cold temperature test was performed to simulate flight conditions. This test recreated the flight anomaly.

The flight anomaly was caused by the design of the electronic circuit. The execute switch is used for two functions: To turn on the electronics for 15 minutes; and to initiate switch selections. Due to a time delay caused by the toggling of a relay, the input voltage to the logic is applied before the logic is powered on. When the temperature is cold, this caused the logic to "lock-up" and not respond to further commands. Resetting the logic clears this condition and allows the logic to perform normally. The proper operation, in accordance with the electronics design, is to toggle the execute switch by itself to turn the launcher electronics on, and then to set the address switches and toggle the execute switch again.

Future Mission Capability

Refurbishment Requirements

Because the DSI launcher is flight proven, a minimal amount of refurbishment is required. In order for a payload to use the DSI launcher, there is a certain minimum hardware refurbishment and engineering support required.

Hardware Activities:

- Battery replacement.
- Mounting ring & v-band inspection and surface re-finish.
- Procurement of new clamp separators (although only 2 are required for flight, at least 20 must be procured due to STS ordnance qualification requirements).
- Standard testing (functional and temperature).
- Separation testing.

Analysis, Documentation, and Program Support:

- Separation analysis, which is spacecraft unique.
- Flight Safety Documentation. According to NSTS 1700.7B, must be re-certified for each flight. All analyses for flight 1 are in place, so it is a matter of verifying analyses are still adequate, re-submitting documentation as part of payload unique safety process.
- Support of system vibration testing and pyro shock testing (if customer required).
- Support Orbiter integration at KSC.
- Provide crew training (for SPASP operation).
- Support mission operations at JSC if required.

Baseline Capability

The baseline capability of the DSI launcher is a 3.7 ft/sec deployment velocity for a 190 lb payload. The separation velocity vs payload weight, using the standard separation springs, is shown in Figure 8. If the deployment velocity is too great, smaller, standard springs may be substituted for the existing ones. If additional deployment velocity is required, custom springs would have to be developed.

In addition to deployment velocity limitations, the launcher does have payload weight vs cg limitations, as shown in Figure 8. These are based more on Flight 1 qualification levels than structural capability. If payloads meet this requirement, then little or no additional structural analysis would be required. If the payload does not fit the weight/cg curve, additional analysis would be required.

Motorized Door Option

DSI originally planned to have the capability to operate the GAS fully deployable motorized door. For this reason, two sets of high energy batteries were installed and a switch function was intended to be used to control the door. The DSI launcher could be used with the door by modifying the electronics. The changes made would be to add a printed circuit card which would utilize the Pre-Arm switch as the motor control and the Pre-Arm indicator as the motor control indicator. The one minute timer would now be replaced by the time to operate the door.

Standard GAS Can Launcher

DSI originally intended to utilize the standard GAS Can launcher (known also as the TSI launcher) marman (V) band design. If a payload would like to be (or is) compatible with the TSI V-band, and is in the acceptable weight vs cg range, TSI compatible separation system could be incorporated at a minimal cost.

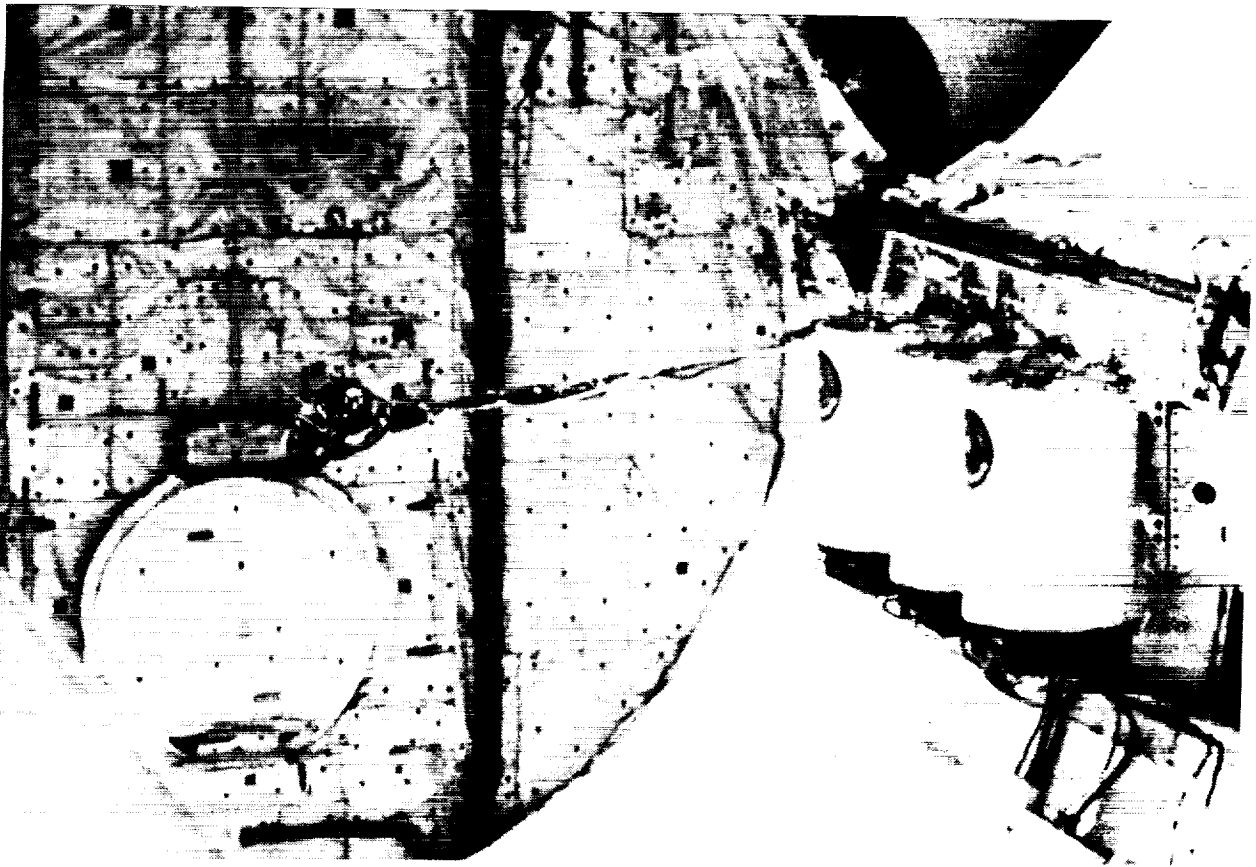


FIG 1. DSI Launchers Installed in Orbiter DISCOVERY

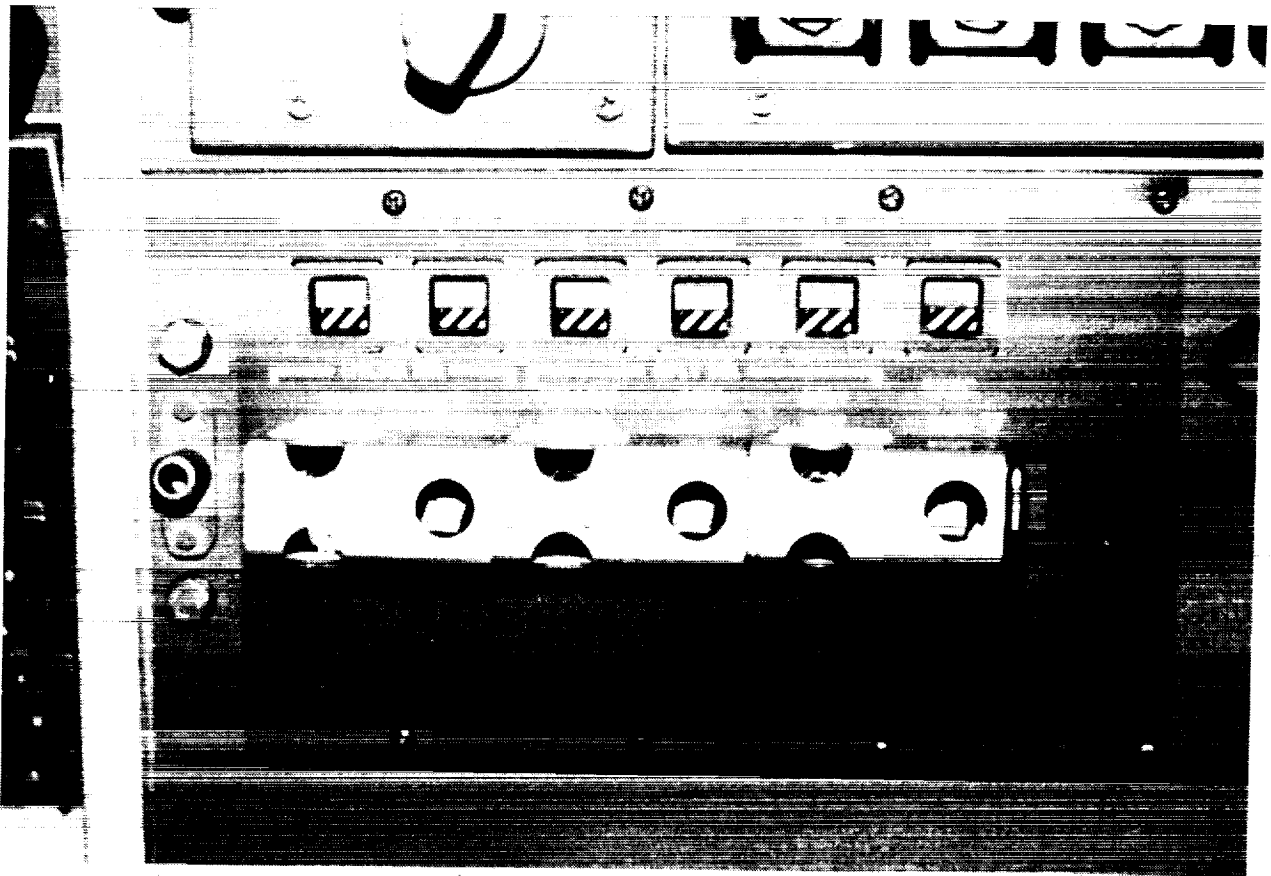


FIG 2. SPA Switch Panel in Aft Flight Deck of Orbiter

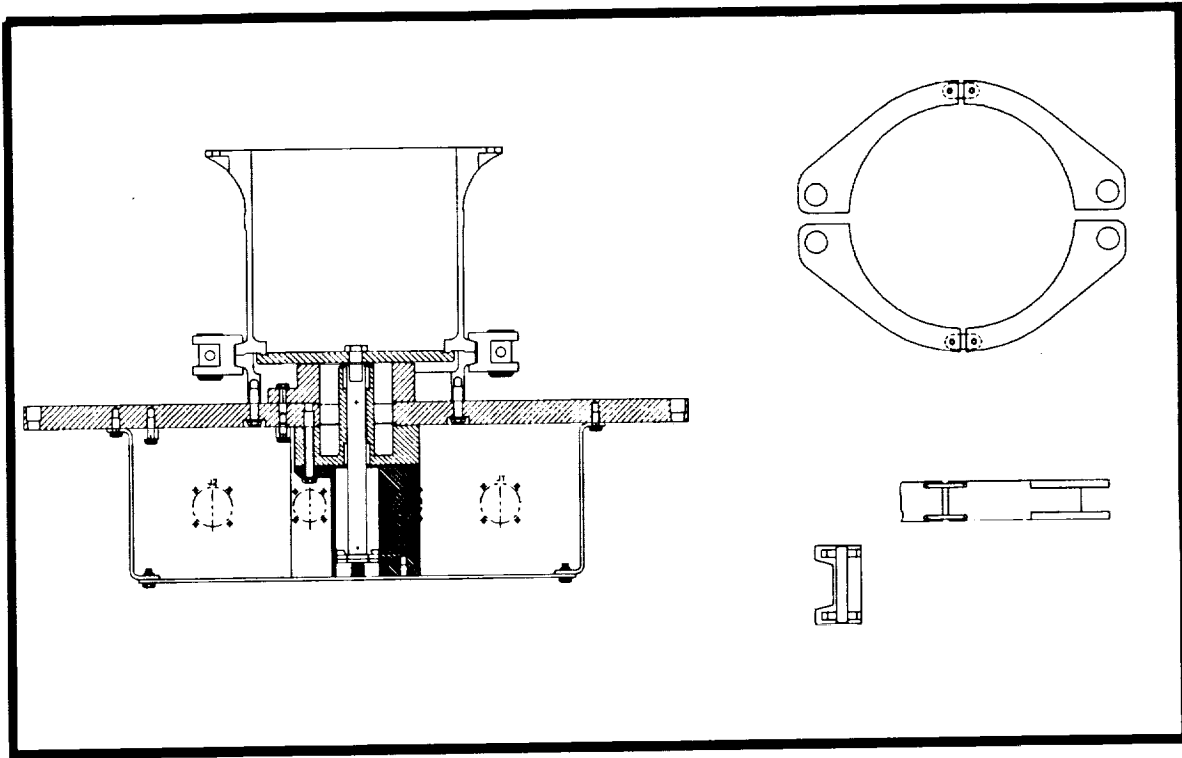


FIG 3. DSI Launcher Assembly With V Band
(A) Side View (B) V-Band

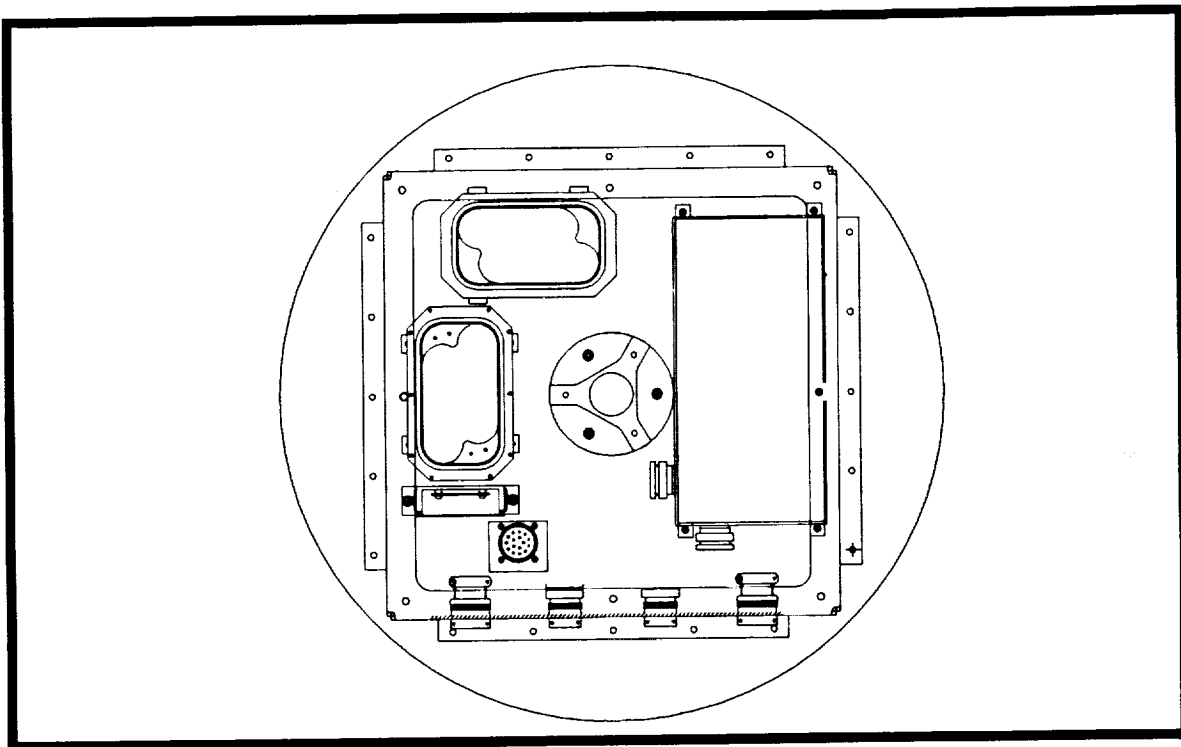


FIG 4. DSI Launcher Electronics Box



FIG 5. DSI Launcher in Flight Configuration

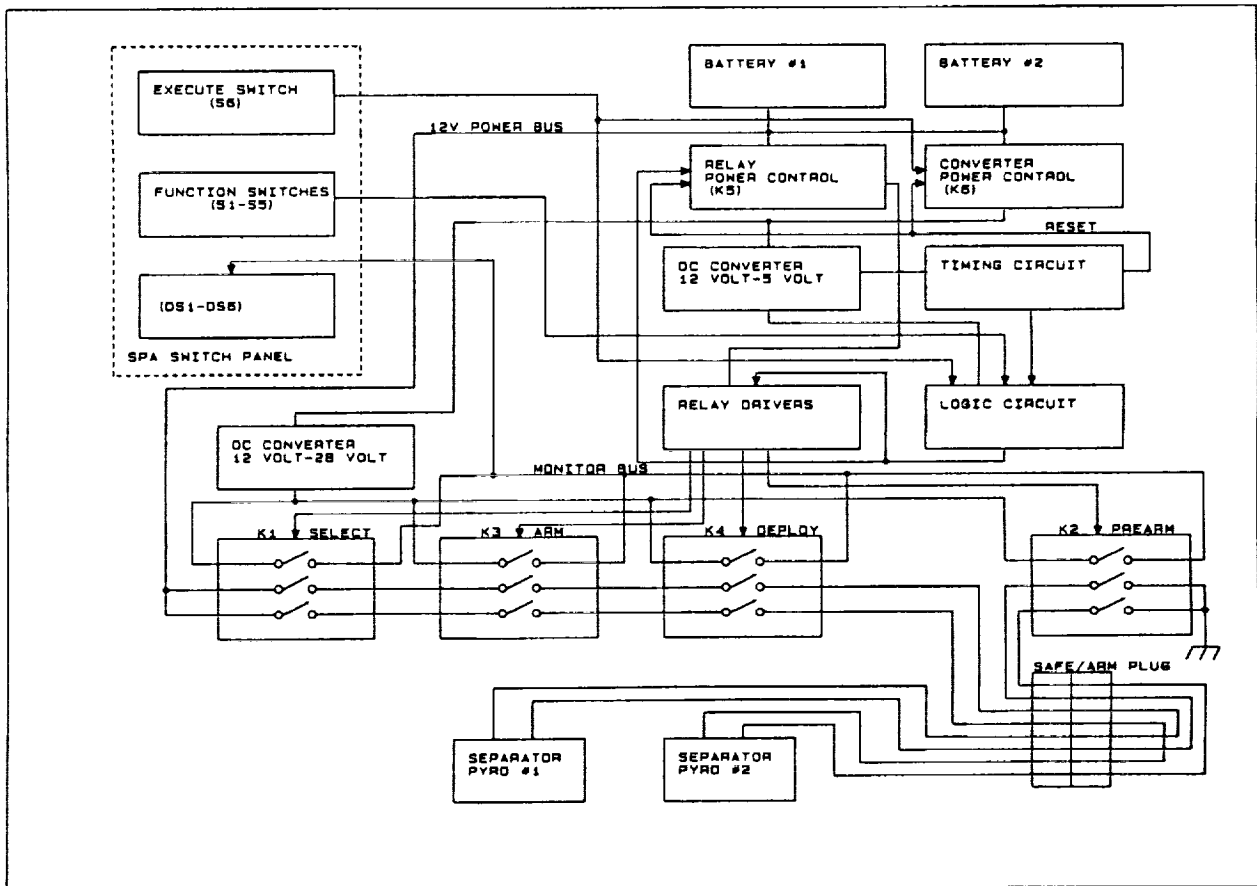


FIG 6. Electronics Block Diagram

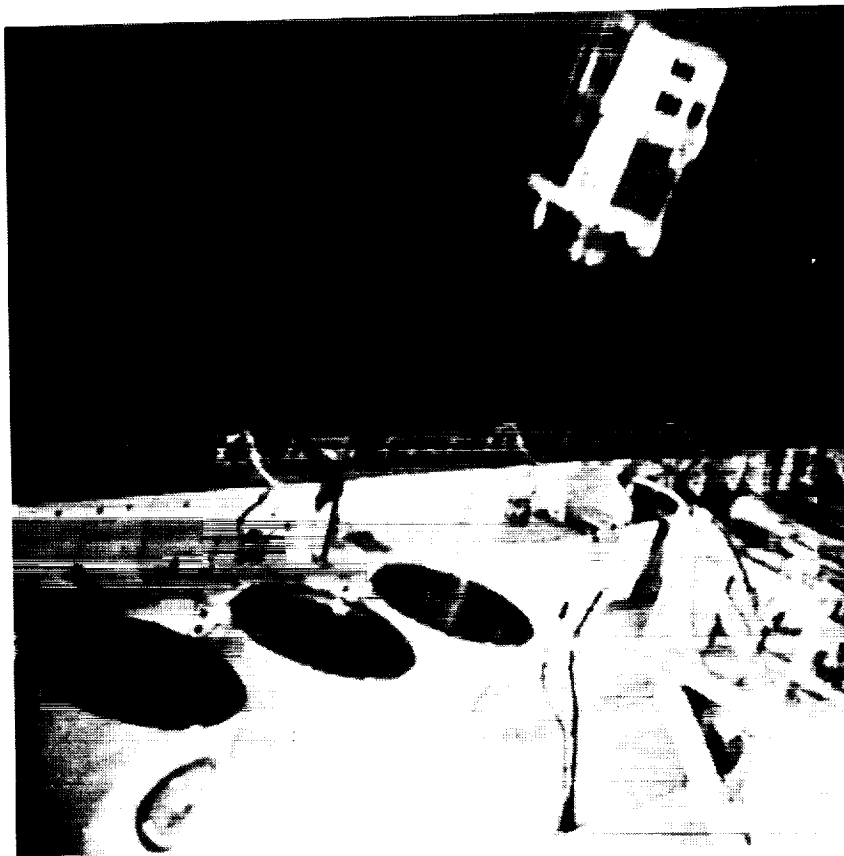


FIG 7. CRO Deployment from Shuttle

ORIGINAL PAGE
BLACK AND WHITE PHOTOGRAPH

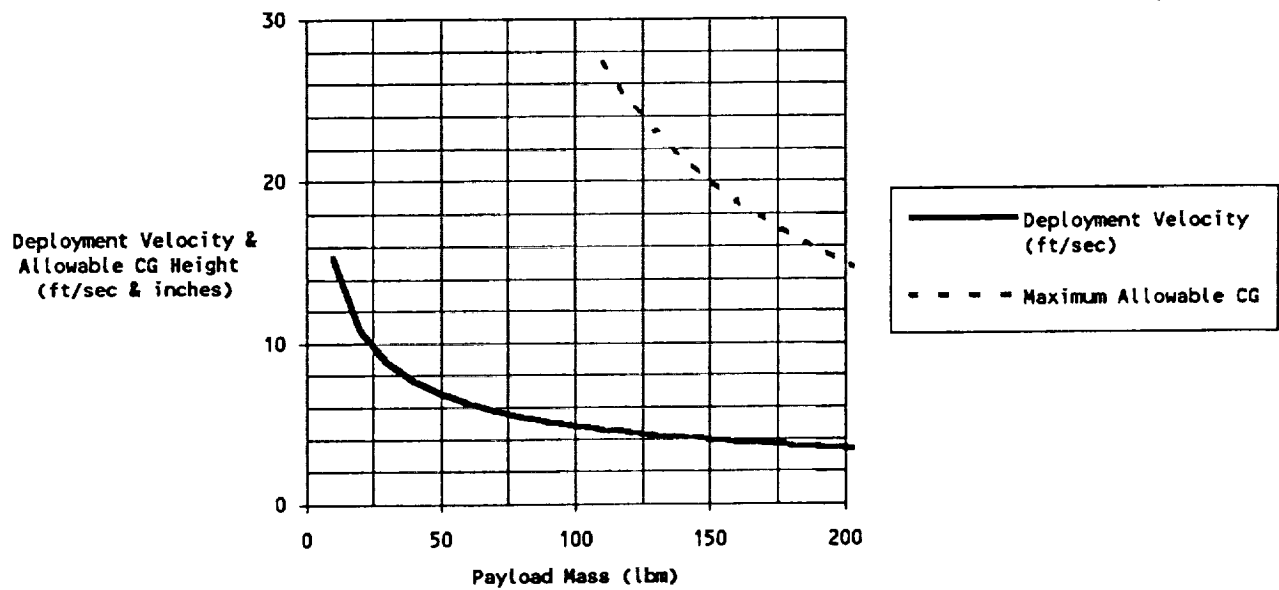


FIG 8. DSI Launcher Predicted Deployment Velocities and Allowable CG Heights as a Function of Payload Mass

**THE CAPILLARY PUMPED LOOP FLIGHT EXPERIMENT (CAPL)
A PATHFINDER FOR EOS**

D. Butler
NASA Goddard Space Flight Center
Greenbelt, MD
and
T. Hoang
NSI Technology Services Corp.
NASA Goddard Space Flight Center

ABSTRACT

The CAPL shuttle flight experiment will provide micro-gravity verification of the prototype capillary pumped loop (CPL) thermal control system for EOS. The design of the experiment is discussed with particular emphasis on the new technology areas in ammonia two-phase reservoir design and heat pipe heat exchanger development. The thermal and hydrodynamic analysis techniques and results are also presented, including pressure losses, fluid flow, and on-orbit heat rejection capability. CAPL experiment results will be presented after the flight, presently planned for 1993.

INTRODUCTION

The enhanced Capillary Pumped Loop Flight Experiment (CAPL) is a follow-on to the initial Capillary Pumped Loop flight experiments described in [1]. The CAPL is a much larger experiment and is designed as a prototype of the Earth Observing System (EOS) instrument thermal control system which is based on capillary pumped two-phase technology. The Capillary Pumped Loop (CPL) utilizes the latent heat of vaporization in a closed thermal control system to transfer large amounts of heat over long distances. Two-phase systems offer significant weight and power savings compared to single phase systems currently in use. The CPL is a completely passive loop in that it has no mechanical moving parts that can wear out or introduce unwanted vibrations to the platform. However, the CPL does have limited pumping capability of approximately $3,450 \text{ N/m}^2$ (0.5 psi), so the system components must be designed for low pressure losses.

Verification of the CPL technology in micro-gravity is required prior to its implementation on the EOS platform. Gravitational effects on pressure losses, heat transfer coefficients, and fluid management must be evaluated and tested. The initial CPL experiment proved that the CPL technology can work in micro-gravity. However, this experiment was only a small scale demonstration of CPL technology and did not address a number of system characteristics inherent with larger systems required for EOS. The CAPL is a full size prototype with features such as long liquid transport lines and heat pipe heat exchangers that were not tested in the first experiment. The CAPL

experiment is currently manifested for a shuttle flight in mid-1993. It is being developed by NASA Goddard Space Flight Center with NSI Technology Services Corporation as the prime contractor.

DESCRIPTION OF CAPL EXPERIMENT

A functional schematic for CAPL is illustrated in Figure 1. CAPL employs anhydrous ammonia as its working fluid. The main components of CAPL include two evaporator plates, a capillary starter pump, four heat pipe heat exchanger (HPHX) radiators, a subcooler, transport lines, and a two-phase reservoir. The CAPL components are packaged into the envelope shown in Figure 2. The experiment is mounted on top of a Get Away Special (GAS) bridge assembly through a Mission Peculiar Equipment (MPE) interface structure as depicted in Figure 3. The GAS bridge will be located near the rear bulkhead of the Space Shuttle.

Each of the two evaporator plates are made up by metallurgically bonding two capillary pumps to a rectangular aluminum block as shown in Figure 4. A capillary pump basically consists of an axially grooved aluminum extrusion and an annular porous wick insert [2]. In this controlled experiment, the heat source is simulated by heaters attached on the evaporator surface. Heat conducts into the capillary pumps where it vaporizes the liquid ammonia. The generated vapor travels along the vapor line to four heat exchangers where heat is removed to condense the vapor into saturated liquid. The removal of heat from each heat exchanger is carried out by radiating the heat to space via a heat pipe radiator as shown schematically in Figure 5. The saturated liquid ammonia must pass through a subcooler where heat is removed further to collapse any remaining vapor bubbles coming out of the heat exchangers in order to insure that no vapor could return to the capillary pumps to deprime (or dry out) the wicks inside them. The heat removal from the subcooler is provided by a radiator surface mounted to a portion of the liquid line. The 8 meter long vapor and liquid lines are intended to demonstrate the CPL pumping capability over long distances.

Another major component of CAPL is the two-phase reservoir. The reservoir serves as a storage for the liquid ammonia inside the loop. During the start-up process, heat is applied to the reservoir to vaporize a small amount of its liquid. The pressure building up inside the reservoir forces the remaining liquid out of the reservoir and into the loop. A porous wick structure is placed at the reservoir exit end to prevent vapor from coming out. Nevertheless the liquid coming out of the reservoir must pass through a subcooler, again to insure no vapor could reach the capillary pumps to deprime their wicks. The reservoir is also used to control the saturation temperature (set point) of the loop during operation by maintaining its temperature with heaters and a proportional power controller.

CAPL is currently designed to start-up with a fully flooded loop. That is, all components will be filled with liquid ammonia before the heaters on the evaporator plates can be turned on to commence the loop operation. This start-up method

guarantees that the capillary pump wicks will always be primed when heat is applied to the evaporator plates. However, there is a serious problem associated with the fully flooded start-up when the capillary pumps are used to clear the vapor line of liquid ammonia. During the initial boiling of the ammonia inside the capillary pumps, the backflow of superheated liquid from the vapor side to the liquid side of the pumps creates a vapor blockage in the pump liquid inlet which consequently cuts off the liquid supply to the pump wicks and causes them to deprime. To alleviate this problem, a capillary starter pump and vapor line heaters are incorporated in the CAPL design. The capillary starter pump or the vapor line heaters will be used to generate the initial vapor space in the vapor line during the start-up process. Also, a mechanical pump package was added to the CAPL experiment as a backup for start-up operations. It is a small positive displacement, magnetically driven gear pump that is plumbed in parallel along the liquid line (see Figure 6). It is used to force liquid into the capillary pumps to prime the wicks even though there may be vapor bubbles in the liquid inlet of the capillary pumps.

The CAPL experiment employs a variety of instrumentation to evaluate its performance. These include 180 thermistors distributed throughout the experiment, an absolute pressure transducer, and two differential pressure transducers. The absolute pressure transducer measures system pressure in the reservoir while the differential pressure transducers measure pressure losses across the evaporator plates and the vapor line. The experiment also has a thermal flow meter to determine the ammonia mass flow rate.

The CAPL experiment has been designed to emulate the EOS platform thermal control system. Table 1 presents a comparison of the major characteristics of both CAPL and EOS thermal loop, showing the close correlation between the two systems.

Table 1. CAPL vs. EOS Major Characteristics

<u>LATEST EOS</u>	<u>CAPL</u>
30 to 600 Watts	50 to 1,200 Watts
3 to 8 Meter Transport Lines	8 Meter Transport Lines
Fully Flooded	Fully Flooded
1/4" OD Vapor Line	1/2" OD Vapor Line
1/8" OD Liquid Line	1/4" OD Liquid Line
2 Pound Ammonia Charge	4 Pound Ammonia Charge
1/2" OD Capillary Pumps	1/2" OD Capillary Pumps
HPHX Radiator	HPHX Radiator

Design of Two-Phase Reservoir and Heat Pipe/Heat Exchanger Radiators

Three prototypes of different reservoir designs were built and performance tested in a ground based test loop, with one design selected for the CAPL flight unit. The performance requirements for the reservoir include: (i) elimination of vapor expulsion

under normal operations, (ii) minimization of exit port pressure drop, (iii) minimization of expulsion time, (iv) ability to control the CPL set point within $\pm 0.5^{\circ}\text{C}$, and (v) ability to expel 2,800 cc of liquid ammonia to the loop. Dynatherm Corporation was chosen to build the CAPL flight reservoir based on their prototype design. The flight reservoir consists of a stainless steel cylindrical shell (approximately 8.9 cm in diameter and 66 cm long) and six porous polyethylene tubes which are positioned circumferentially around the reservoir inner surface. These polyethylene tubes extend over the length of the reservoir and are held in place by several layers of wire meshes, which are in turn spot welded to the reservoir inner wall (see Figure 7). The primary function of the tubes is to deliver liquid ammonia from anywhere inside the reservoir to the exit and to the heater zone with minimal flow resistance. Heaters are attached to the outer wall of the reservoir in the heater zone at the opposite end of the exit. Test results have been encouraging with liquid ammonia being pumped out at high adverse tilts. Further information on this reservoir can be found in Reference 7.

The heat pipe/heat exchanger (HPHX) radiator is utilized for CAPL heat rejection instead of a more efficient direct condensation radiator (DCR) due to EOS requirements. Over the multi-year life span of EOS, the probability of a meteoroid hit on a radiator is substantial. A hit on a DCR could result in loss of the entire ammonia charge of the loop and, therefore, loss of the loop operation. With a HPHX radiator, only the affected segment of the radiator is lost, but not the entire loop. Two prototypes of the HPHX designs were built and performance tested in a ground based test loop. The requirements imposed on the HPHX design are: (i) heat exchanger must accept a maximum heat load of 350W with less than 5°C temperature differential between the CPL and the header heat pipe, (ii) header heat pipe must have a minimum heat transport of 430 Watt-meters at 35°C with 0.25cm adverse tilt, (iii) spreader heat pipe must have a minimum heat transport of 180 Watt-meters at 35°C with 0.25cm adverse tilt, (iv) flow regulation must be provided when multiple units are tested in parallel, and (v) must have provisions for non-condensable gas (NCG) collection. OAO Corporation was selected to build the flight HPHX units for the CAPL experiment based on their prototype design. The OAO HPHX employs helical fin heat exchangers [3], 2.86cm OD header heat pipes, and 1.91cm OD spreader heat pipes. The header heat pipes are rated at 711 Watt-meters at 35°C with 0.25cm adverse tilt. The spreader heat pipes are rated at 432 Watt-meters under the same conditions. Heavy walled extrusions were utilized in manufacturing the header heat pipes so that the helical grooves could be cut into the outer surface of the heat pipes to form fluid flow passages for the heat exchangers, i.e. each header heat pipe becomes an integral part of a heat exchanger (see Figure 8). The helical grooves promote annular flow, and consequently the heat transfer coefficient of the heat exchangers will improve in both 1-g and 0-g environments. However, this design does not provide flow regulation when two or more heat exchangers are tested in parallel. To remedy this problem, a stand-alone flow regulator is included in each HPHX unit. The flow regulator is plumbed downstream of a heat exchanger. It is simply a porous polyethylene wick barrier used to prevent vapor from blowing through. It is also designed to collect non-condensable gases which are detrimental to proper operation of the loop. Further information on the HPHX can be found in Reference 8.

System Pressure Drop Analysis

The pumping capability of the CAPL capillary pumps can only extend to the capillary limit of the pump wicks. The maximum capillary limit of a porous medium is proportional to the working fluid surface tension and inversely proportional to the wick pore size. If the system pressure drop exceeds this limit under any operating condition, the wick will not be able to prevent vapor from penetrating into the wick structure to dry it out. The system pressure drop of CAPL during normal steady state operation includes the fictional pressure losses due to (1) vapor flow in the vapor line, (2) two-phase flow in the heat exchangers, (3) liquid flow in the sub-cooler and liquid line, and (4) both liquid and vapor flows in the capillary pumps.

Single-phase and two-phase pressure drop correlations for annular flow were used to compute the pressure losses [4]. The component pressure drops for CAPL operating at maximum power of 1,200W are summarized in Table 2. For a CPL system, the total system pressure drop increases with the amount of heat applied to the evaporator plates. Therefore there is a limit to the maximum power that can be applied to the CAPL evaporator plates, above which the system pressure drop exceeds the capillary limit. Table 2 shows that there is a very large margin in the CAPL pumping capability and the high transport limit for CAPL operation may not be reached in the flight tests.

Table 2. CAPL Pressure Drops

CAPL Components	Pressure Drop (Pa)		
	@10°C	@25°C	@35°C
Vapor Line (1/2" OD)	668	417	312
Liquid Line (1/4" OD)	362	319	294
Cold Plates	87	69	60
Liquid Isolators	183	160	146
HPHX	700	700	700
Thermal Flowmeter	276	276	276
Solenoid Valve	276	276	276
Total Pressure Drop			
- Normal Operation	2,552	2,217	2,064
- One Pump Fails	2,822	2,446	2,270
Capillary Limit	4,723	4,003	3,523
Margin			
- Normal Operation	1.85	1.80	1.70
- One Pump Fails	1.67	1.63	1.55

Fluid Flow and Thermal Analyses for CAPL in Orbit

The two-phase fluid flow in CAPL is, by itself, a complicated hydrodynamic problem. When coupled with another complex thermal system of the Space Shuttle environment via the capillary pumps, HPHX radiators, reservoir, and subcooler, it is almost impossible to simulate the experiment transient behaviors in orbit efficiently with any available analytical tool. The transient of the CAPL fluid flow is caused by two main forcing functions: (i) variation in power profile to the evaporator plates, and (ii) variation in ambient conditions which change constantly with the Space Shuttle position in orbit. Simplifications must be made with regard to the analytical model of CAPL if there is any hope to simulate the CAPL behavior within a reasonable amount of computing time. The transient hydrodynamics of a CPL system is very explosive and very important to a CPL designer during the "clearing of liquid in vapor line" event of the start-up process [5]. This event lasts less than 5 minutes for CAPL. Therefore, the Space Shuttle thermal environment is assumed to remain unchanged during this period. On the other hand, once the system gets started the hydrodynamic event responds almost instantaneously with the forcing functions, i.e. the time constant for the hydrodynamic system is much smaller than that of the thermal environment. The fluid flow is assumed to reach a quasi-steady state from one computational time step to the next. The fluid flow and thermal analyses of CAPL are provided by two computer models - a transient model for the start-up process and a quasi-steady state model for on-orbit operation.

Transient Fluid Flow Model

As mentioned before, the CAPL experiment is designed to start up with a fully flooded system. The vapor line is initially filled with liquid ammonia. The capillary starter pump will be used to clear liquid in the vapor line and return it to the reservoir. As heat is applied to the starter pump, the pump body begins to heat up but nothing happens until its temperature exceeds the loop saturation temperature, at which time vapor starts to be generated. Due to the large amount of liquid in the vapor line, the pressure in the starter pump outlet must increase high enough to displace a large liquid flow rate to the reservoir. The liquid flow rate to the reservoir is equal to the rate at which vapor is generated in the starter pump times the liquid to vapor density ratio. Therefore there is a limit to how much heat can be applied to the starter pump so that the pressure rise in the pump will not deprime its wick. A SINDA85/FLUINT model was used to study the hydrodynamic transients of the CAPL start-up with the capillary starter pump. The results in Figure 9 show the maximum allowable power level of 250W for the starter pump during the start-up process.

Quasi-Steady Fluid Flow / Transient Thermal Model

When the capillary starter pump completes the liquid purge in the vapor line, heaters on the evaporator plates will be turned on to commence the CPL operation. The liquid-vapor interface of the loop is confined in the heat exchangers. A change in power input to the evaporator plates and/or a variation in ambient conditions will cause the liquid-vapor interface to move forward or backward inside the heat exchangers. Due to

large thermal masses of the evaporator plates and the HPHX radiators, sudden changes in power input or ambient condition will not cause an instantaneous increase or decrease in the mass flow rate in the loop. Hence the hydrodynamic transients become negligible in this case. Because the mass flow rate inside CAPL is very small and the rate of change of fluid mass flow rate is gradual, the fluid inertial effects were neglected. As a result, the fluid flow in the vapor phase can be assumed to be incompressible which leads to simplified energy and mass conservation equations.

A SINDA model was used to simulate the fluid flow in orbit. Correlations for two-phase flow pressure drop and heat transfer were utilized to determine the film coefficient between the fluid nodes and their thermal environment counterparts.

Heat Rejection Capability of CAPL Radiators / Radiator Model

There are wicks at both ends of the vapor line, capillary pump wicks at one end and flow regulator wicks at the other. Even though the high transport limit for CAPL may not be reached in flight tests at the maximum available power level, the capillary limit of the capillary pumps can still be exceeded if the heat exchangers cannot condense as much vapor as the pumps generate. The maximum heat rejection of the CAPL radiators depends on the Space Shuttle orientation, and the loop saturation temperature. The CAPL radiators consist of four 39cm x 254cm panels facing the same orientation in orbit. Each panel is used to remove heat from a heat exchanger.

A SINDA model was developed to study the performance of the CAPL radiator for different loop set points in various Shuttle orientations. The model was intended to determine the maximum power which CAPL can operate, either continuously or for some period of time in a particular orientation. The heat pipe conductances were provided by ground tests. The radiation couplings between the radiator panels and the environment nodes were computed by a TRASYS model [6]. Figure 10 shows the maximum heat rejection capability of the CAPL radiators when the experiment is in the bay-to-deep-space orientation.

CONCLUSION

Results have shown that CAPL can operate continuously at 1,200W in the bay-to-deep-space orientation and about 600W in the bay-to-earth orientation for at least 45 minutes. Sixteen 3 hour test cycles are requested for the CAPL flight experiment, four of which will be in the bay-to-deep-space orientation. Various power profiles and temperature set points will be tested. The CAPL experiment is currently manifested on STS-60 with a launch date of October 1993.

REFERENCES

1. Ku, J.; Kroliczek, E.; Butler, D.; McIntosh, R.; and Schweickart, R.: Capillary Pumped Loop GAS and Hitchhiker Flight Experiments. Paper No. 86-1248, AIAA/ASME 4th Thermophysics and Heat Transfer Conference, Boston, June 2-4, 1986.
2. Kroliczek, E.; Ku, J.; and Ollendorf, S.: Design, Development and Test of a Capillary Pumped Loop Heat Pipe. Paper No. 84-1720, AIAA 19th Thermophysics Conference, Snowmass, Colorado, June 25-28, 1984.
3. Fredley, J.E. and Braun, C.: A Low Pressure Drop Heat Exchanger with Integral Heat Pipe. Proceedings of the 1988 ASME National Heat Transfer Conference, Volume 1, pp 367-377.
4. Streeter, V.L.: Handbook of Fluid Dynamics. McGraw-Hill Book Company, Inc., 1961.
5. SINDA85/FLUINT User's Guide. JSC Contract NAS9-17448, Martin Marietta Corp., Sept. 1988.
6. Thermal Radiation Analyzer System (TRASYS) User Manual. JSC 22964, April 1988.
8. Ku, J.; Yun, S.; Kroliczek, E.: A Prototype Heat Pipe Heat Exchanger for the Capillary Pumped Loop Flight Experiment. Paper No. 92-2910, AIAA 27th Thermophysics Conference, Nashville, TN, July 6-8, 1992.

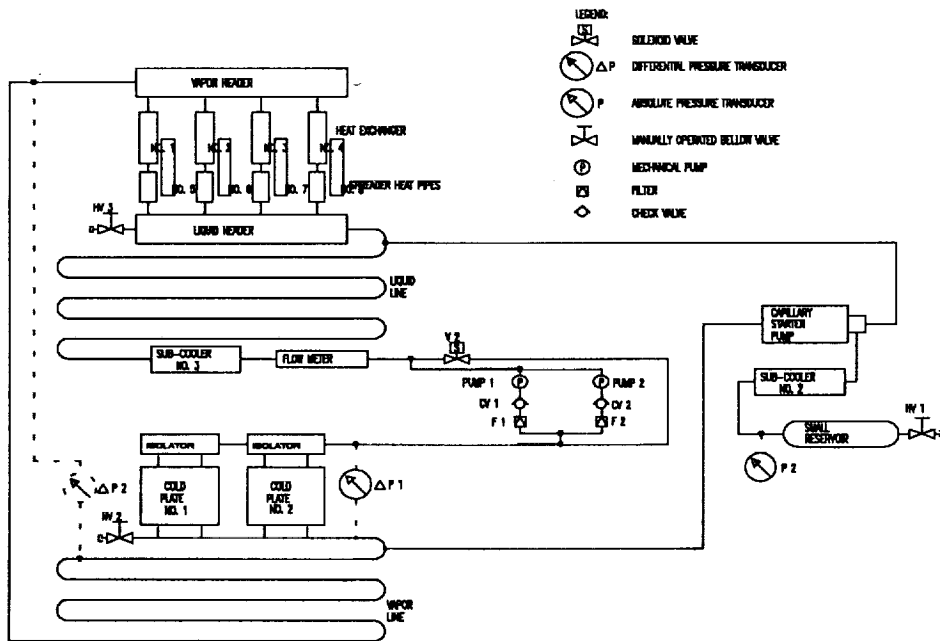


Figure 1. CAPL Functional Schematic

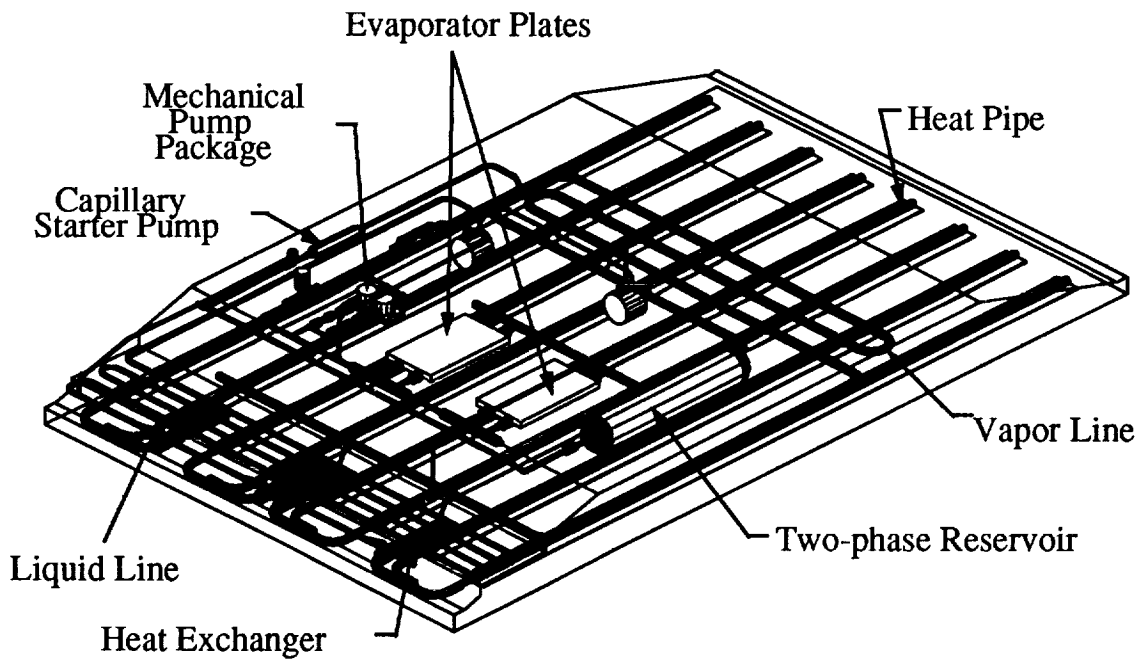


Figure 2. CAPL Flight Experiment

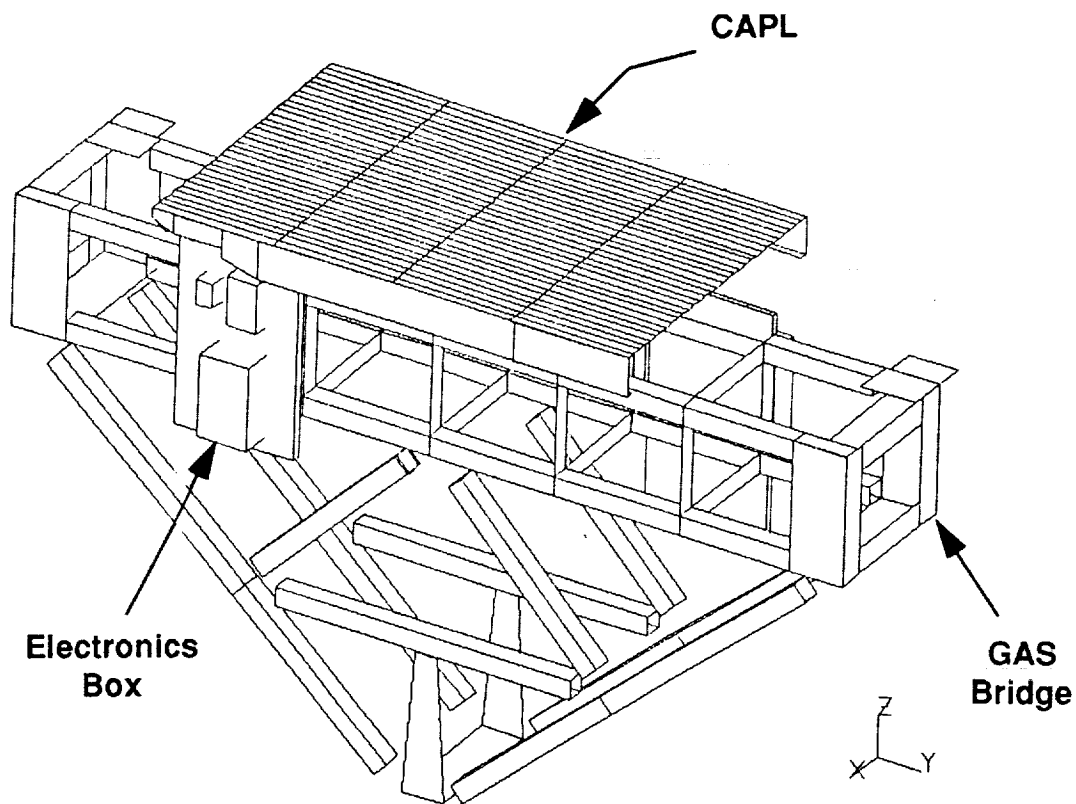


Figure 3

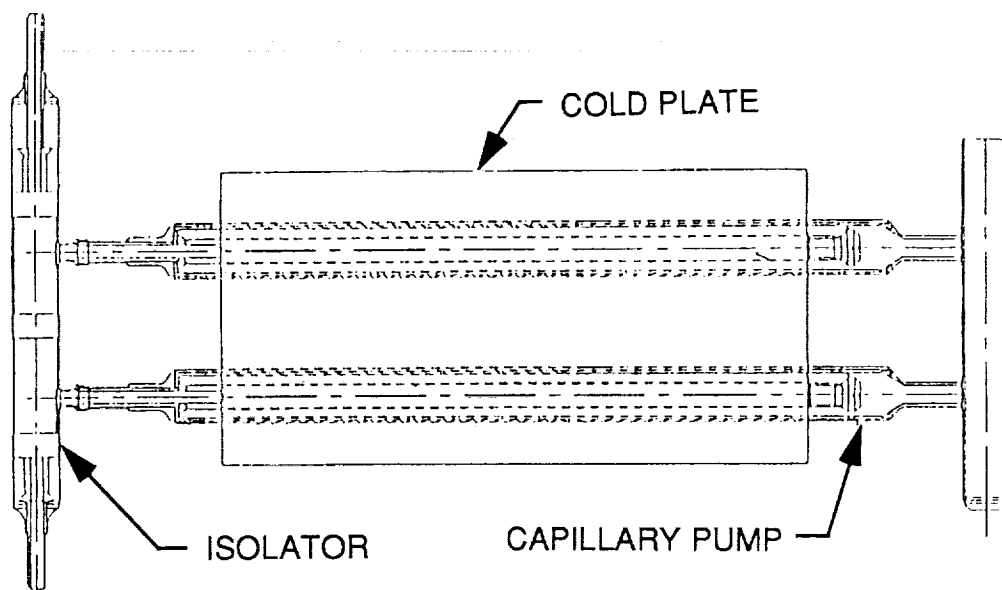
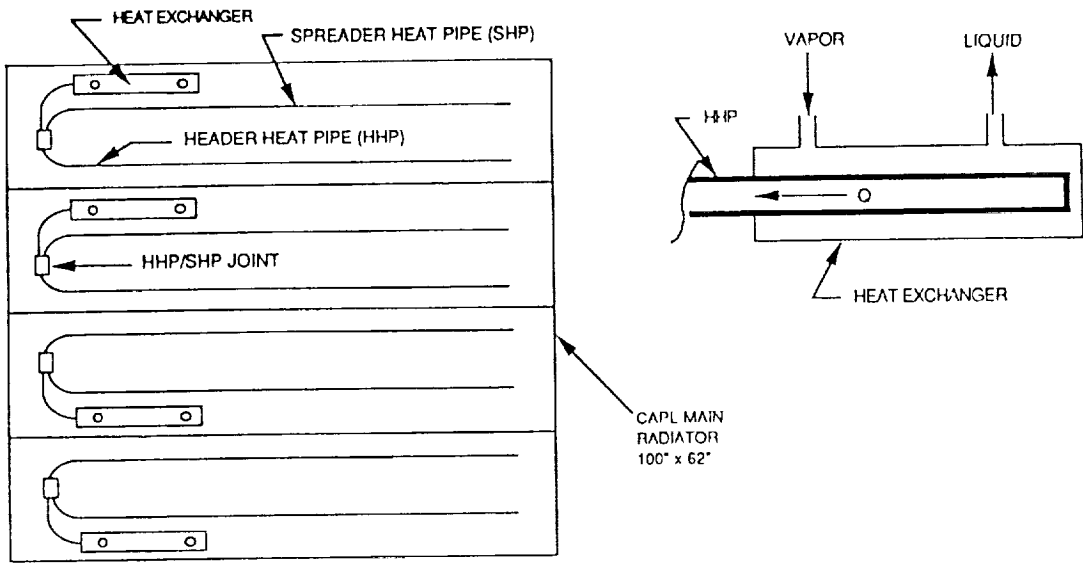


Figure 4



NOT DRAWN TO SCALE

Figure 5

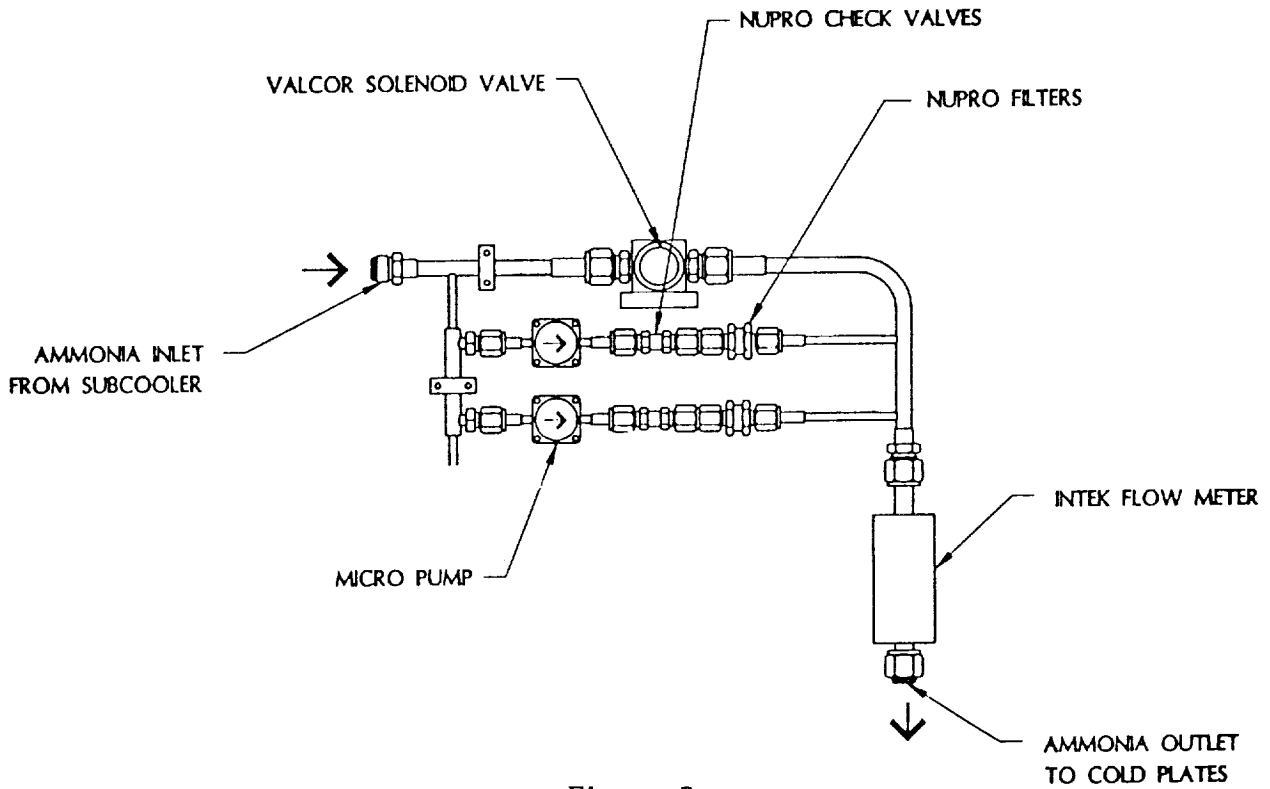


Figure 6

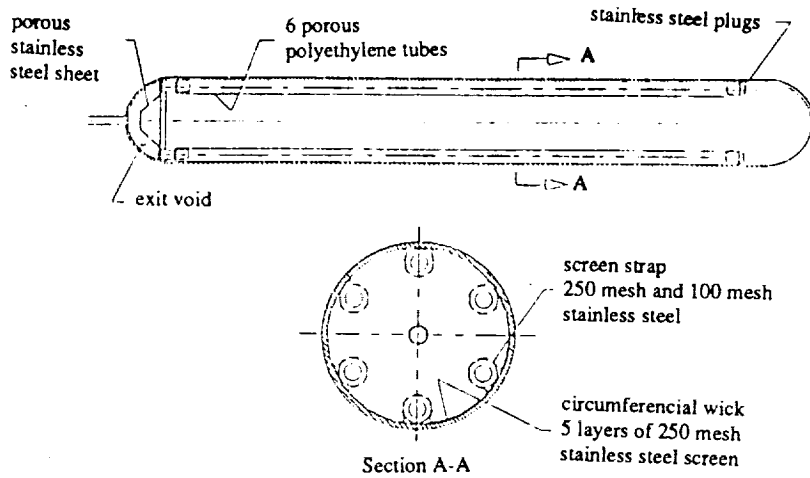
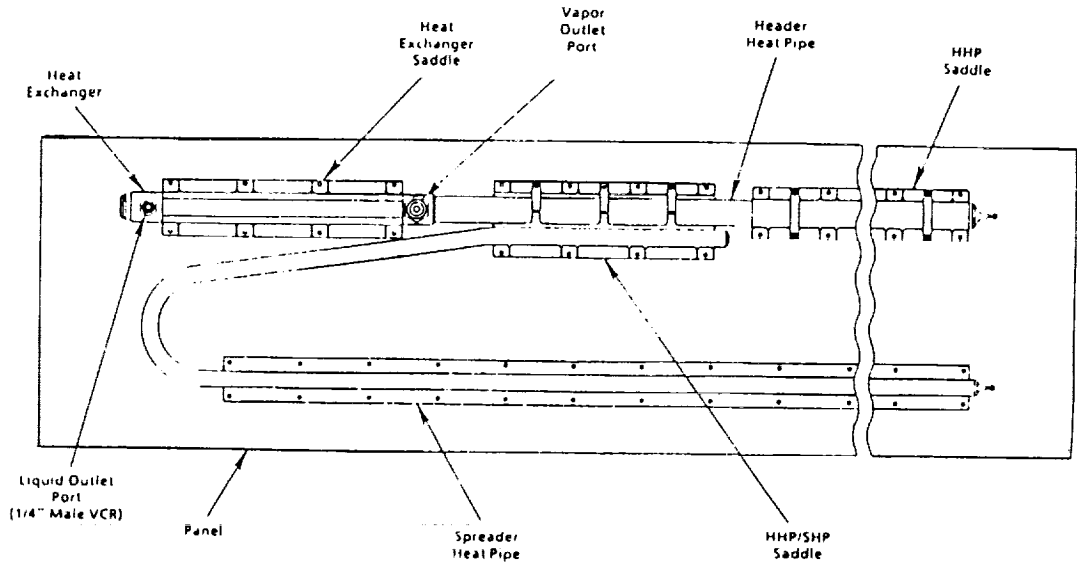
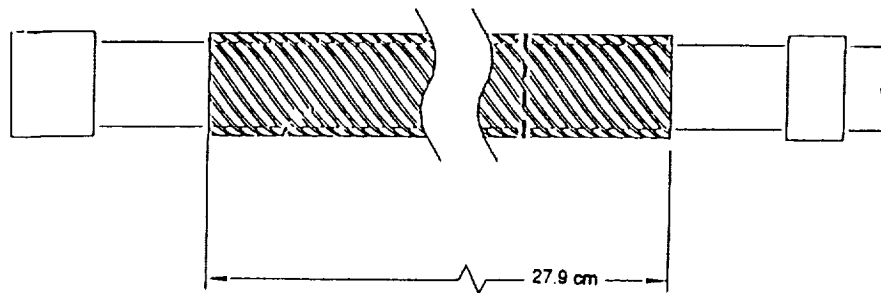


Figure 7



OAO HPHX Layout



OAO Heat Exchanger Design

Figure 8

Maximum System Pressure Drop During Start-up at 25C
 Capillary Pump Limit at 25C is 4,000 N/m²

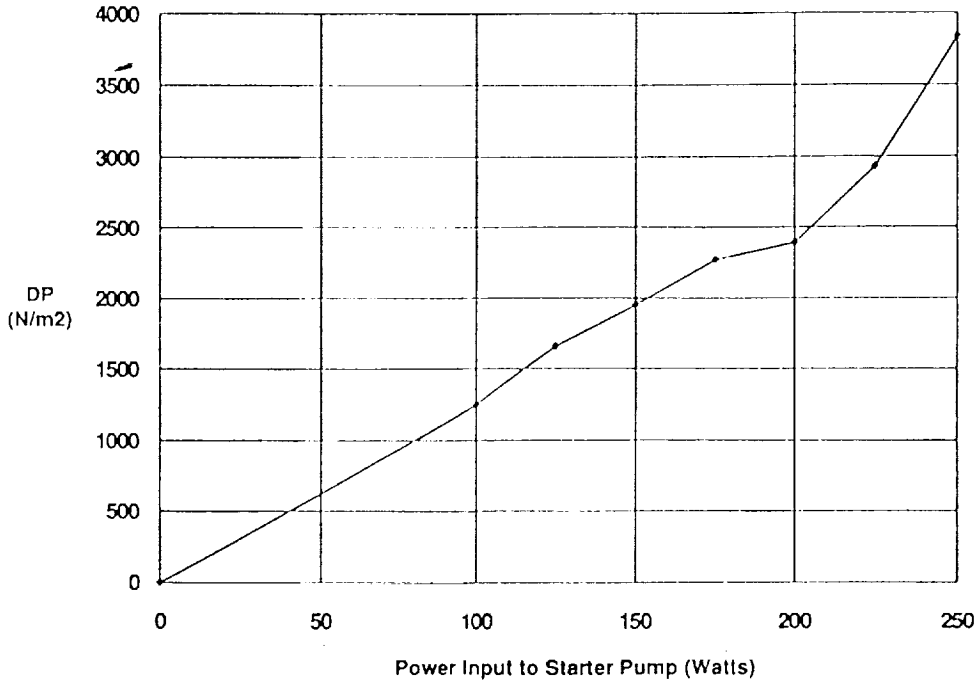


Figure 9

**BAY TO DEEP SPACE
 TOTAL HEAT REJECTED**

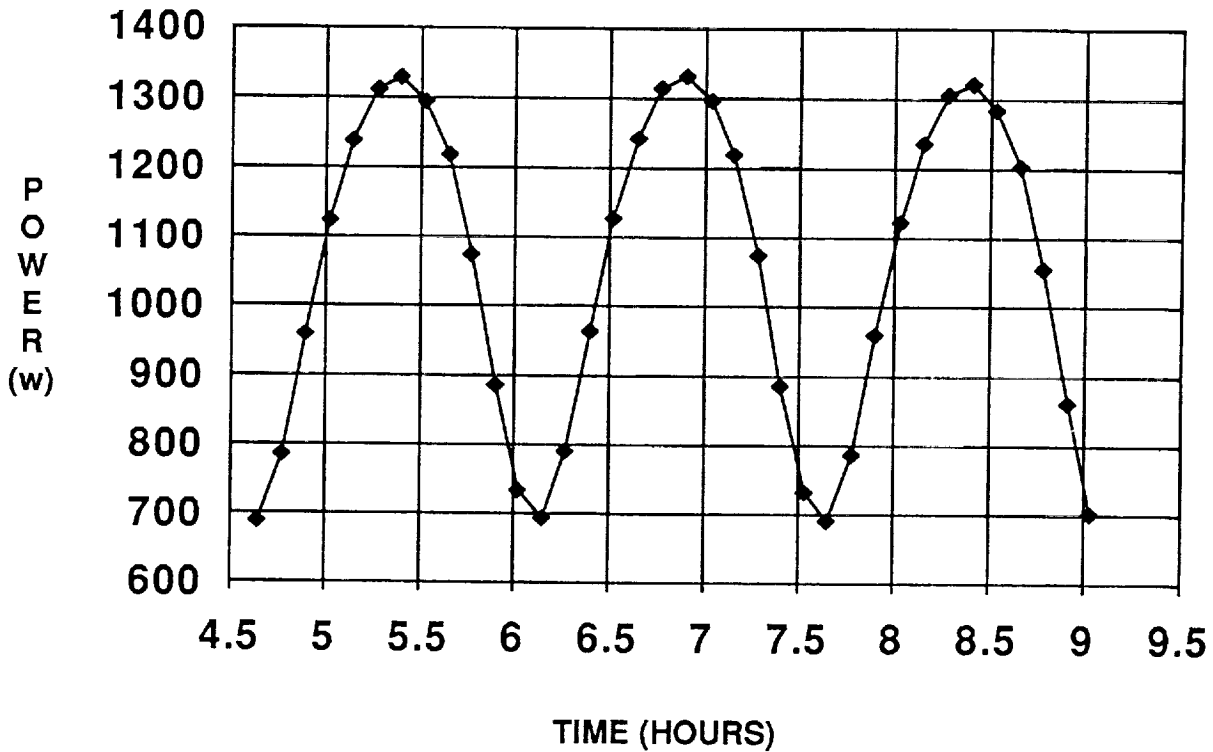
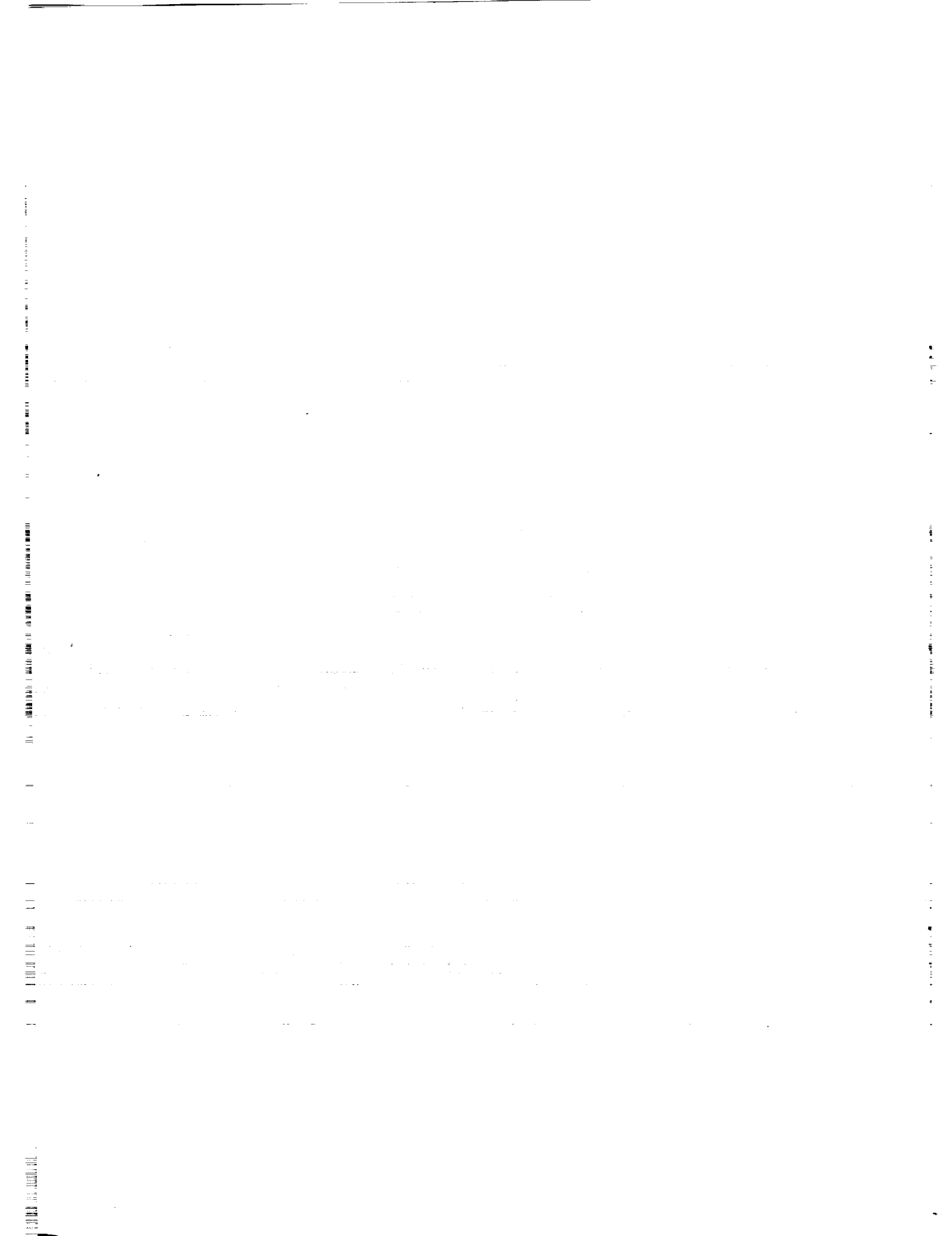


Figure 10



THE VTRE PROGRAM - AN OVERVIEW*

William J. Bailey and John P. Gille
Martin Marietta Corporation
Denver, Colorado

ABSTRACT

The Vented Tank Resupply Experiment (VTRE) Program is a NASA In-Space Technology Experiments Program (IN-STEP) that will develop and fly a small, low cost space experiment to investigate, develop, and acquire needed data to extend and advance the technology of capillary vane fluid management devices to applications requiring direct venting of gas from tanks in low-gravity. Gas venting may be required for control of pressure, or to allow low-g fill of a tank with liquid while holding a constant tank back pressure by gas venting. Future space applications requiring these fluid management capabilities include both cryogenic and Earth storable fluid systems. The experiment is planned as a Shuttle Hitchhiker payload, and will be developed around two transparent tanks equipped with capillary vane devices between which a test liquid can be transferred. Experiments will be conducted for vented transfer, direct venting, stability of liquid positioning to accelerations within and significantly above the design values, and fluid reorientation by capillary wicking of liquid into the vane device following intentional liquid upset.

INTRODUCTION

Strategies and hardware have been developed for space fluid management requirements for acquisition and delivery of liquid from part-filled tanks in the weightless, low-g space environment. Approaches used have included propulsive settling to establish a low-level artificial gravity; mechanical liquid-gas separation devices such as bladders, bellows and diaphragms; and "capillary" devices that exploit the small surface tension force of liquid-gas interfacial surfaces to collect liquid to a tank outlet port for delivery to using systems, such as propulsion and attitude control thrusters.

Capillary Fluid Management Techniques

Two types of capillary device are used. One relies on the characteristics of wetted fine-mesh woven screen, through which liquid flows in preference to gas. The screen devices are normally configured as a duct network (called channels or galleries) that connect various regions of the tank to the liquid outlet line. A part of the duct wall is made of very fine mesh screen. Gas entry into the duct is resisted by a significant "bubble pressure" required to force a bubble through the screen while liquid passes with little flow.

* The Phase B Conceptual Design Study for VTRE was performed for NASA Lewis Research Center under Contract NAS3-25977. Mr. Don Bresnahan & Mr. Al Seigneur were NASA Project Managers.

resistance. In this way, liquid is collected and gas is prevented from entering the duct. The second type of capillary device consists of a number of surfaces configured to draw liquid into regions between closely spaced vanes by capillary wicking action. Capillary vane devices can be configured to collect and transfer liquid to a tank outlet under very low-g conditions.

Both capillary devices depend on liquid wetting the materials of which the device is constructed, an inherent characteristic of all liquids of interest in contact with most materials of construction. For this reason, there is no analogy for collecting gas using similar devices to support tank venting. However, gas can be positioned by default if all liquid is collected to a defined location. Propulsive settling is one approach; the capillary vane concept, designed for total liquid wicking is another. Capillary screen devices do not position liquid and can not implement gas venting.

Direct tank venting has been required infrequently to date. The Centaur vehicle requires a programmed reduction of propellant tank pressure that is accomplished by directly venting gas after firing thrusters to settle liquid propellants away from the vent port. The Saturn launch vehicle had a similar requirement. The Viking Orbiter (VO-75) propellant tanks were provided a capability for direct venting of pressurant for emergency overpressure relief, using a capillary vane type liquid acquisition system, depicted in Figure 1. This system primarily provided for liquid delivery to the propulsion gas to the vent port in a very low g environment. However, venting was not attempted on either VO-75 mission.

Pressure reduction may result in formation of bubbles within the liquid bulk, by evolution of dissolved pressurant gas, as occurs when a carbonated beverage is opened, or when the boiling temperature is reached because of pressure reduction. To vent under these conditions, the vane device must be able to pump the bubbles toward the normal ullage region. This is accomplished by configuring the vanes so the size of a bubble that would not be constrained by the vanes increases toward the vent port. Bubbles of sufficient size to be squeezed by the vanes will be forced toward the more open region, and bubbles pushed together by this process will tend to coalesce into larger bubbles that will be further pumped toward the vent.

Many advanced missions will require space resupply of liquids, including Space Station Freedom, and the capability for resupply could be profitably used on current systems. An example is communications satellites whose life is normally limited by depletion of attitude control propellant, not by failure of the communications hardware. Only limited experience has been accumulated on liquid transfer in space, however. Soviet space programs have resupplied liquids using bellows type positive displacement tanks and NASA has demonstrated space servicing of a hydrazine tank equipped with a diaphragm type liquid management system (Orbital Resupply System - ORS). These capabilities are restricted to positive displacement fluid management

devices which are limited in their applicability to relatively small tank size and ambient temperature fluids.

The Vented Tank Resupply Experiment (VTRE) addresses capillary vane fluid management technology in space applications of direct gas venting and vented resupply of liquids of all types, including cryogenics & corrosive Earth storable oxidizers. The Viking Orbiter vane concept (Figure 1) represents a point of departure. This design was developed specifically for emergency vent of a relatively small tank in a very low drag environment with small and infrequent acceleration disturbances. Advanced systems must be designed for larger tanks, greater and more frequent disturbances (but still quite small), and venting to meet various mission needs. Vane systems must also be designed so capillary positioning strength exceeds the dynamic force of entering liquid during fill, positively controlling the liquid-gas orientation to assure only gas at the tank vent port. This capability will permit refill of tanks without loss of liquid with the approach normally used in the Earth environment, that is, maintain a constant receiver tank pressure by venting gas as required.

Background

There is significant research and development history relative to vent and resupply using capillary vane devices to support a flight investigation at this time. The most extensive effort was the development in the early '70s of the device for the VO-75 vehicles, which was provided by Martin Marietta Corp. Earlier (1969-72), NASA Lewis Research Center performed extensive drop tower testing of transfer of liquid into small cylindrical tanks free of internal hardware while venting, and established criteria for which stable fill could be achieved. Martin Marietta has continued low-g venting research (from 1976) under internal and contractual research and development programs. Venting and vented resupply tests have been conducted in KC-135 aircraft in spherical tanks of 10 and 32 cm (4 and 12.5 in.) diameter, and in 10 cm (4 in.) diameter spherical and cylindrical tanks in the Martin Marietta 2-second drop tower low-gravity facility, and vented fill tests are continuing at the present time under Independent Research & Development (IR&D) funding. Figure 2 illustrates the configuration of the current drop tower test articles including vane and tank inlet design. These tests have demonstrated the validity of the vane concept to control liquid location during fill, and dimensionless criteria for stable vs unstable fill have been bracketed.

VTRE Objectives

The mission of VTRE is to experimentally investigate capillary vane fluid management technology using the Shuttle Hitchhiker as the experiment carrier. VTRE experiments will specifically address direct tank venting and vented tank resupply. Secondary objectives are to determine positioning stability of the vane system under moderate acceleration disturbances, above the normal Shuttle background, and ability of the capillary vane system to reorient liquid following deliberate upset by adverse Shuttle thrusting. In addition, the VTRE transfer tests will inherently demonstrate the ability of the vane

devices to deliver all liquid to the tank outlets under a nominal Shuttle acceleration environment at significant transfer rates. These experiments will obtain data that will define critical design parameters, verify scaling relationships, and provide a database and design approach for design of advanced capillary vane fluid management systems.

EXPERIMENT DESCRIPTION

Experiments to be conducted as primary objectives of VTRE are vented transfer and direct tank vent tests. Secondary tests investigate the ability of the capillary vanes to maintain liquid position during low-level acceleration disturbances, and the ability of the device to relocate liquid after it has been upset by an adverse acceleration.

Experiments will be performed using two transparent test tanks that are viewed with video camera-recorders. Tank A is a cylindrical tank 31.75 cm inside diameter by 40.6 cm inside length (12.5 x 16 in.) with hemispherical domes. Tank B is spherical with 35.5 cm (14 in.) inside diameter. The two tanks are of equal net volume. They are connected for liquid transfer through a series of parallel and series valves configured to provide seven discrete transfer flow rates. Each can be connected to the pressurization subsystem, and each can be connected to the vent system that either maintains a fixed backpressure or provides any of seven discrete flow impedances to the overboard vent. The test liquid selected is Refrigerant 113, a non-flammable, non-toxic liquid with characteristics suitable for simulation of most liquids of interest. Nitrogen was selected as the pressurant.

Twelve vented transfer tests are planned. Test parameters include the direction of transfer, into tank A (cylindrical) or tank B (spherical), the transfer flow rate, and the target fill level in percent. The first eleven tests will be conducted while maintaining a constant backpressure of approximately 117 kPa (17 psia) on the receiving tank. The twelfth will start with the receiver tank pressure initially near the triple point pressure of the test liquid, and the pressure will be allowed to rise until it reaches the preset backpressure level, allowing observation of the effects of partial vaporization of the liquid as it enters the tank. Acceleration is a parameter, with most tests conducted with normal Shuttle background acceleration environment, and also the maximum drag acceleration of 2×10^{-6} g. Initial and target fill levels are also test parameters.

Fourteen vent tests have been defined. Test parameters include the tank being vented, the vent rate as established by choice of the vent impedance selection valves, initial and final pressure, and quantity of liquid at the start. Except for one, these tests are run at normal Shuttle background acceleration; the one will be conducted at the maximum drag condition imposing an approximate 2×10^{-6} g laterally.

Tests for determining the stability of the capillary vane device, response to imposed acceleration disturbances, and reorientation of liquid by capillary wicking action are conducted simultaneously for both tanks. Each test run is accomplished by establishing the

quantity of liquid required in each tank, actuating the lights and cameras, performing the Shuttle maneuver required to create the disturbance, and continuing the video record for sufficient time to permit the response to be completed. Test parameters are the accelerations imposed and the liquid fill level in each tank. For the stability tests, short accelerations on the order of 5×10^{-5} to 1×10^{-4} g are imposed. To assure large scale displacement of liquid from the vane device, an adverse (reverse relative to launch) acceleration of 4×10^{-4} or greater will be imposed for a period up to one minute depending on the Orbiter RCS firing configuration selected.

DESIGN

The VTRE system has been broken into various subsystems consisting of the following elements: Experiment Subsystem which is comprised of R-113 Test Tanks, GN₂ Pressurization, Fluid Distribution and Experiment sensor elements; and Support Subsystem Elements that are comprised of an Avionics Subsystem (which is further broken down into Electrical Power Subsystem, Command and Data Handling (C&DH) Subsystem, Video & Lighting Subsystem, and Experiment Electronics), Structural Subsystem, Cabling and Harness Subsystem and Thermal Subsystem. A flight Software element completes the system flight element definition. In addition there are two ground support elements: the Mechanical Ground Support Equipment (MGSE) and Electrical Ground Support Equipment (EGSE), that will be utilized to provide ground test support, ground servicing, handling support, and maintenance functions.

The experiment tanks, one cylindrical (A) and one spherical (B) are made of crosslinked acrylic with high craze resistance. The tanks will be assembled from blown or vacuum formed domes, machined flanges and a barrel section, and details are shown in Figures 3 and 4. The capillary vane configuration has been developed on the basis of drop tower test results, and includes 12 inner and 12 outer alternating radial vanes. The vane device as it appears for the spherical tank is depicted in Figure 5. The same design concept is followed for the cylindrical tank, but the vanes are shaped to conform to the tank cross section. The combined inner plus outer vane concept provides a capillary wick structure that will maintain liquid position against normal Shuttle accelerations, and the capillary pressure will be sufficient to arrest the momentum of the entering liquid at a typical velocity of 4-6 cm/s (0.13-0.2 ft/s), and to redistribute the flow into the vane system, keeping liquid out of the designated ullage region surrounding the vent port.

The experiment is depicted schematically in Figure 6. For transfer tests, a gaseous nitrogen pressurization system provides a blanket pressure of approximately 172 kPa (25 psia) in the supply tank, and a back pressure regulator maintains the receiver tank pressure at 117 kPa (17 psia), providing a differential of 55 kPa (8 psid) to drive the transfer. Three solenoid valves in the transfer line between tanks select any combination of three pre-adjusted flow regulating valves to provide seven flow rates. The initial test will be performed at a flow rate expected to be near the critical point above which liquid would break free of the vanes and be expelled in the

vent. A liquid-gas sensor will detect liquid in the vent, and if none is detected, a higher rate will be selected for the next test. If liquid is detected, experiment logic will select a lower rate instead, and subsequent tests will select from the seven available rates to bracket the critical flow below which the transfer will be successful. A Weber number relationship, a ratio of inertial flow forces to capillary restraining forces, is expected to characterize this stability criterion.

For venting tests, the pressurization system can be operated to establish an initial pressure in the tank, and the vent system will establish a vent flow to reduce the tank pressure. Three solenoid valves select three preadjusted control valves to select seven vent impedances, similar to the transfer flow selecting scheme. The liquid-gas sensor again provides the experiment software with information to determine whether the vent flow should be increased or decreased to bracket the critical vent flow.

FABRICATION AND TESTING

The VTRE has been classified as a Class D instrument payload, with relaxed reliability and product assurance requirements designed to permit development of low cost, single-flight, higher risk payloads, that must, however, meet all Shuttle safety requirements. VTRE is further classified as D-Modified, adding a rigorous test program to enhance confidence in the ability of the experiment to meet its performance objectives. To remain cost effective, the use of expensive flight qualified fluid mechanical and electrical/electronic/microprocessor hardware cannot be considered except on a selective component-by-component basis and only when other commercial off-the-shelf options pose unacceptable program risk. For the most part, commercially available hardware has been found that has an acceptable risk to justify using for flight.

An engineering model (EM) will be fabricated as a tool that will aid in developing confidence that a multitude of commercial off-the-shelf hardware, including the command and data handling (C&DH) system will perform in the Shuttle launch and space environments. The EM will be a high fidelity duplication of the envisioned VTRE flight design. It will aid in the implementation of the protoflight hardware approach required by the Class D payload. The EM will provide for in-line testing during fabrication and assembly, followed with both functional and qualification tests which will provide early verification of design. A prime function of the EM is to provide a test bed to resolve any remaining engineering issues that might impact the cost and schedule during build and verification of the flight hardware. Another is to permit development and verification of flight software while operating with actual hardware and performing ground test of all flight operations.

The VTRE flight system, and therefore the engineering model, will be designed with adequate margin that will in many cases reduce testing requirements. Verification of hardware for flight will generally be provided by system level testing of the integrated VTRE hardware and by previous demonstration of capability provided by EM testing.

INTEGRATION & FLIGHT OPERATIONS

The VTRE has been developed to the conceptual design level as a Shuttle Hitchhiker payload. The experiment has been packaged into three interconnected Hitchhiker sealed canisters, and can be manifested on either the Hitchhiker -M or -G carriers. The M carrier is a bridge structure to which companion payloads are integrated at NASA Goddard Space Flight Center (GSFC), and the bridge is integrated as a unit into the Orbiter. The G approach requires that each canister be separately mounted to the Orbiter sidewall adaptor beams, and that inter-canister piping and electrical cabling then be installed. Figure 7 shows the layout of VTRE subsystems in the three canisters. The M carrier approach has been selected as the preferred approach, and VTRE is being considered as an OAST-3 experiment to fly in the 1995-1996 time frame. An artist's concept of VTRE on the Hitchhiker M beam is shown in Figure 8.

As a HH-M payload, primary integration activities will occur at Goddard Space Flight Center. The VTRE will be thoroughly inspected, all systems will be functionally tested and leak checked, and the liquid and pressurant tanks will be serviced with fluids. The three canister assemblies, that are shipped assembled to modified HH cover plates, will be installed into canisters, and the canisters mounted to the HH-M beam and electrically connected to the HH avionics unit that provides electrical power and uplink command signals. The interconnecting piping is leak checked, the integrated system is electrically verified with the VTRE ground support equipment (GSE), and multilayer insulation is installed over the external piping. At Kennedy Space Center, the VTRE GSE will perform functional checkout, before the HH-M beam is integrated to the Orbiter as a single payload.

The VTRE operates autonomously, and no data is downlinked or displayed on Orbiter systems. Experiments are, however, divided into seven groupings that will normally be run in sequence. In order to coordinate the experiments with Shuttle operations, and to work around unplanned changes in the Shuttle schedule, these sequences can be selected and initiated from the Payload Operations Center at GSFC. This capability, using the HH Bi-level uplink lines permits coordination of the stability and repositioning experiments with Shuttle maneuvers & thruster firings.

Postflight operations will include offloading data that is stored in computer memory and in 8 mm video cassettes, deservicing fluids, removing interconnecting piping and cabling, and removing the canisters from the beam and the experiment elements from the canisters. Inspection of the hardware will determine if any anomalies developed, and viability of the experiment for reflight. Analysis of the flight data will reconstruct all experiments and reduce all numeric and video data. Critical parameters that must be met to achieve successful venting and transfer will be determined. Test results will be compared with pre-flight analyses and modeling, and these analytical tools will be updated. Results will be extrapolated to full size systems of interest, and a final report, as well as a summary video presentation, will be prepared.

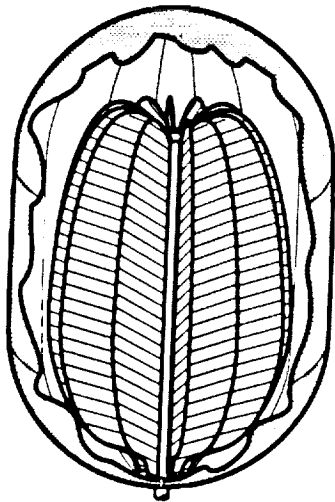


Figure 1 Capillary Fluid Management Concept Used In Viking Orbiter

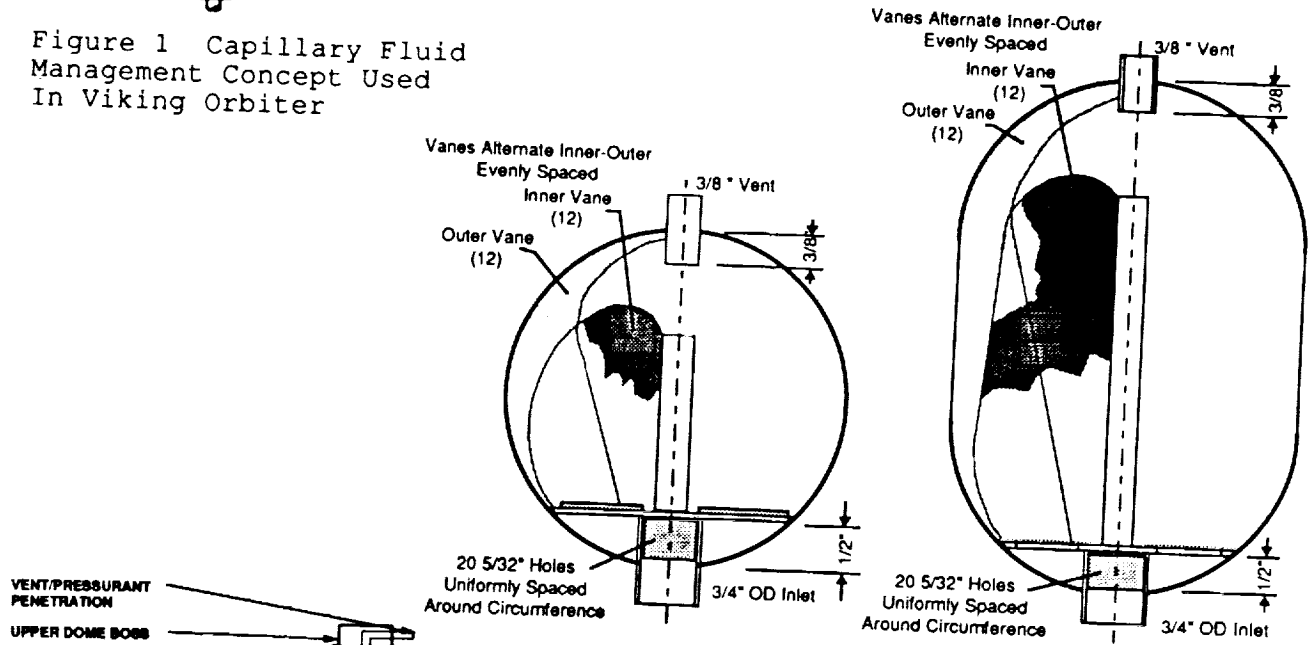


Figure 2 Capillary Vane Test Articles for Recent Vented Fill Drop Tower Test Program

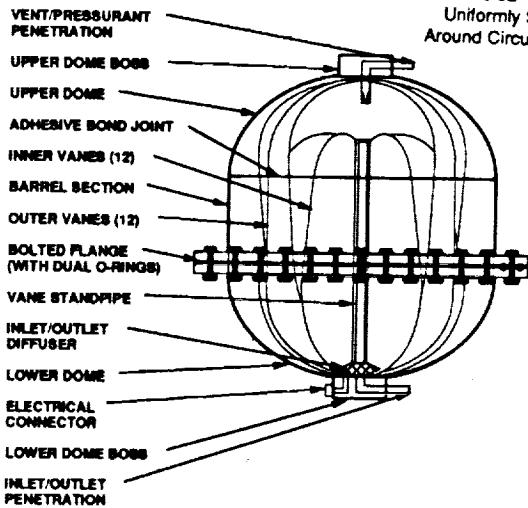


Figure 3 VTRE Cylindrical Tank

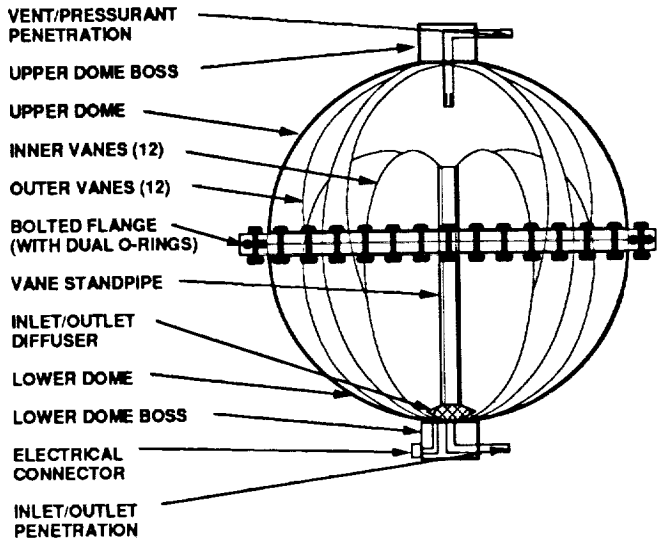


Figure 4 VTRE Spherical Tank

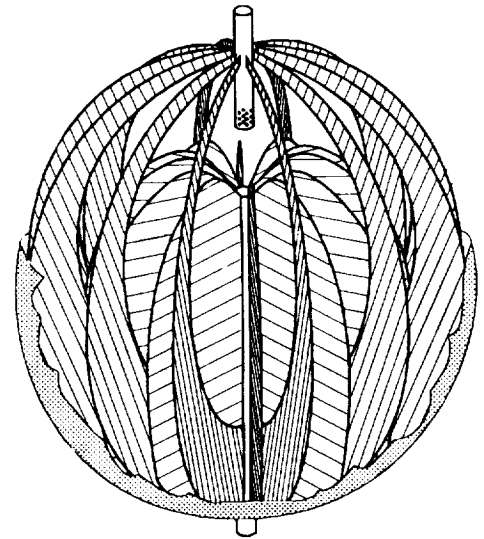


Figure 5 Capillary Vane Concept - Spherical Tank

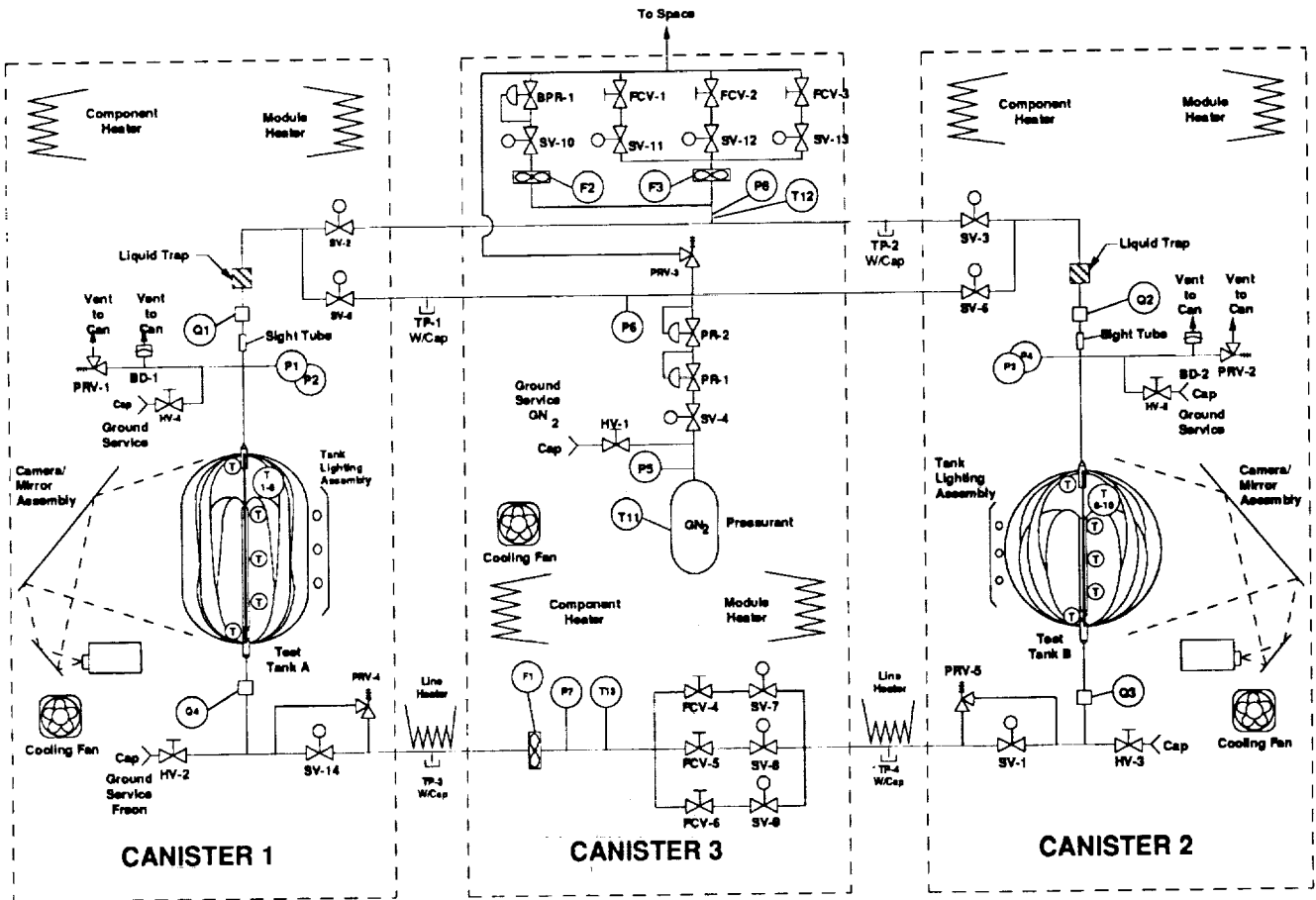


Figure 6 VTRE Schematic

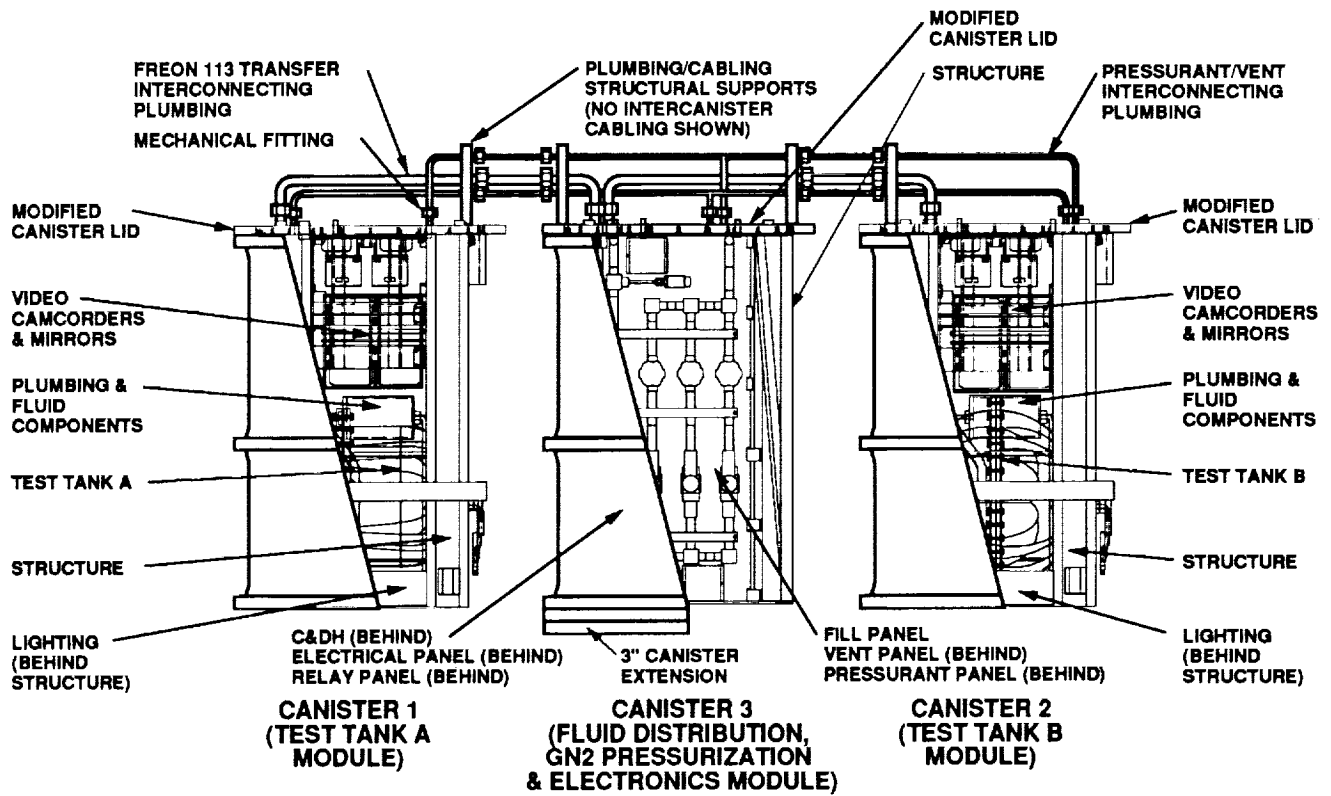


Figure 7 VTRE Flight System Elements Mounted Into Hitchhiker Canisters

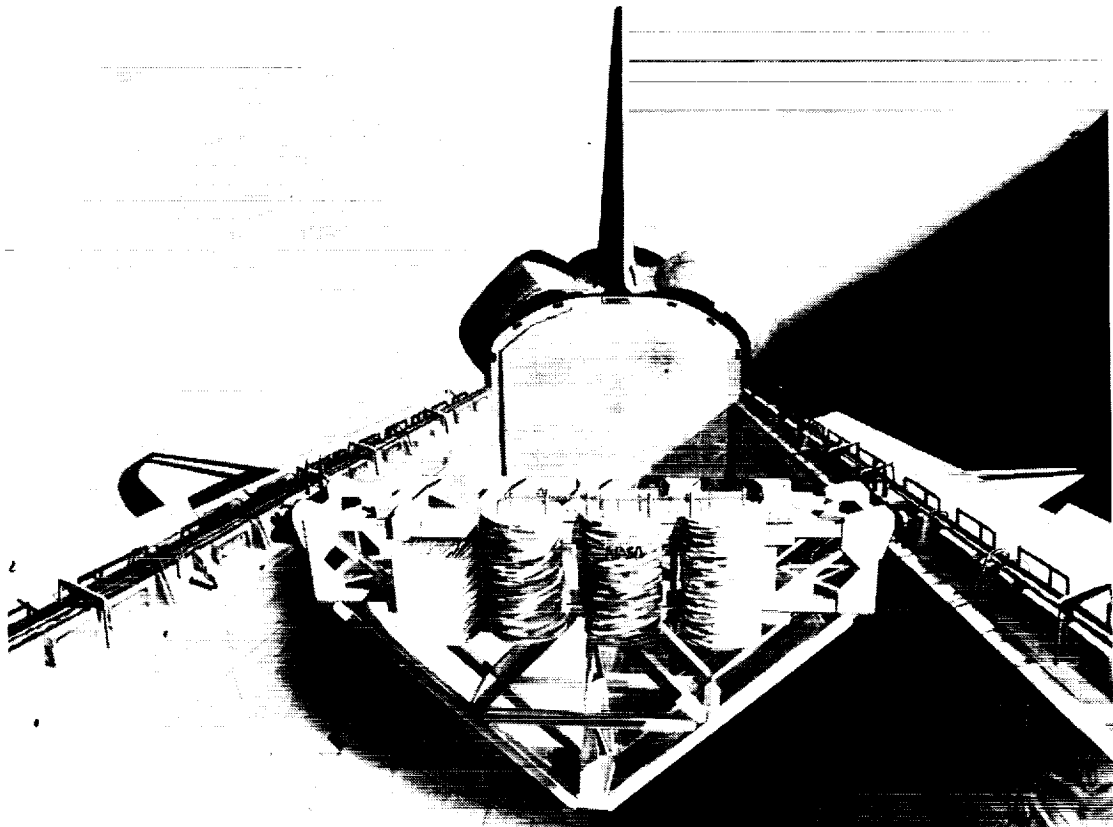


Figure 8 VTRE Flight Installation on Hitchhiker M Carrier

The LDCE Particle Impact Experiment as flown on STS-46

Carl R. Maag*, William G. Tanner**, Janet Borg+, Jean-Pierre Bibring+,
W. Merle Alexander** and Andrew J. Maag++

*Science Applications International Corporation; Glendora, CA 91740 USA

**Baylor University; Department of Physics; Waco, TX 76798 USA

+Institut d'Astrophysique Spatiale; 91405 Orsay Cedex, France

++Stanford University, Palo Alto, CA 94305 USA

ABSTRACT

Many materials and techniques have been developed by the authors to sample the flux of particles in Low Earth Orbit (LEO). Through regular *in-situ* sampling of the flux in LEO the materials and techniques have produced data which compliment the data now being amassed by the Long Duration Exposure Facility (LDEF) research activities. Orbital debris models have not been able to describe the flux of particles with $d_p \leq 0.05$ cm, because of the lack of data. Even though LDEF will provide a much needed baseline flux measurement, the continuous monitoring of micron and sub-micron size particles must be carried out.

A flight experiment was conducted on the Space Shuttle as part of the LDCE payload to develop an understanding of the Spatial Density (concentration) as a function of size (mass) for particle sizes 1×10^{-6} cm and larger. In addition to the enumeration of particle impacts, it is the intent of the experiment that hypervelocity particles be captured and returned intact. Measurements will be performed post flight to determine the flux density, diameters, and subsequent effects on various optical, thermal control and structural materials.

In addition to these principal measurements, the Particle Impact Experiment (PIE) also provides a structure and sample holders for the exposure of passive material samples to the space environment, e.g., thermal cycling, and atomic oxygen, etc. The experiment will measure the optical property changes of mirrors and will provide the fluence of the ambient atomic oxygen environment to other payload experimenters.

In order to augment the amount of material returned in a form which can be analyzed, the survivability of the experiment as well as the captured particles will be assessed. Using Sandia National Laboratory's hydrodynamic computer code CTH, hypervelocity impacts on the materials which comprise the experiments have been investigated and the progress of these studies are reported.

INTRODUCTION

Orbital debris is becoming a major concern for many of the space systems presently considered. This concern is due to a combination of fundamental issues. The debris environment is a dynamic process in which fragmentation due to collisions create

additional objects of different sizes. Collision models combine the effect of pieces reentering the atmosphere and fragmentation due to collisions. Some of the small particles are washed out by solar pressure and some of the larger particles deorbit due to aerodynamic drag, if they are in a low orbit. The size distribution as a function of altitude, of the total effect, is yet unknown but it has been estimated that a uniform increase of 6% over the entire size range envelopes all uncertainties. Immediate detection of meteoroids, orbital debris, and other space debris is extremely important for successful space missions, particularly those of long duration. Impacts may cause damage to manned habitable modules, sensors, reflective or refractive optics, etc. It has been observed that a major source of very small particles come from solid rocket motors (SRM's) fired in space. A single motor, when fired, can emit 10^{20} particles, ranging in size from 1×10^{-4} to 1×10^{-2} cm. Most of these particles, which are aluminum oxide spheres, reenter quickly. However, the small fraction that remain in orbit (~5%/motor/year) produce a flux which exceeds the meteoroid flux, i.e., for a similar size.

Space-based systems exposed to the extreme environment of Low-Earth Orbit (LEO) will avoid catastrophic failures only if the materials which compose them can provide a "shield" against the effects of continuous hypervelocity impacts. Extensive research has been conducted to characterize the effects on materials subjected to hypervelocity impacts by large masses. Even though the large mass impactors carry the highest probability of precipitating a catastrophic event, the number of large mass objects which might be encountered by an exposed surface in LEO is believed to be quite small. However, the size distribution of objects a surface will encounter in LEO has not been adequately characterized; especially for that portion of the distribution which contains the largest number of objects, i.e., the smallest. In order to provide *in-situ* data depicting the size distribution of the most numerous objects in LEO, an experiment has been designed and flown aboard the STS-46 mission.

EXPERIMENTAL DESIGN

Characterization of the orbital debris and micrometeoroid complex which any surface will encounter in LEO implies an implementation of several concurrent processes. Foremost, there should be a means to sample *in-situ* the flux with a frequency which can establish good statistics for multiple samples. There also should be access to that environment for an extended period, e.g., Solar Max, LDEF, so that the existence of any temporal fluctuations in that flux can be identified. The experiments flown can be passive sensors if the materials can be easily returned to Earth. In fact, the complete analysis of the LEO environment cannot be adequately conducted without repeated examinations of materials which have been exposed to the extremes of space. Hence the experimental design which can provide a much needed investigation of small grains, $D_p \leq 10$ cm, would be a passive sensor which could both detect and capture constituents of the orbital debris and micrometeoroid complex.

Passive Sensor Development

In an effort to develop such a system of sensors, the authors have designed and tested several prototypes on many STS missions. The primary means to test these devices has been on the Interim Operational Contamination Monitor (IOCM) developed under the auspices of the United States Air Force/Space and Missile Systems Center. The IOCM contains an array of passive and active sensors which continuously sample three

orthogonal directions in the STS cargo bay. The IOCM has successfully flown on four (4) shuttle missions, the two (2) most recent being STS-32 and STS-44.

Although the primary objective of the STS-32 and STS-44 passive sensor experiments was to sample the LEO orbital debris and micrometeoroid complex, an additional design goal for these experiments was to test the survivability of thin films with a thickness of less than 750 Å and which possessed a density of less than 3.0 gm/cm³. When the ratio of the particle diameter, d_p , to the film thickness, T_f , viz., D_p/T_f , is large and the density of the material composing the film is comparable to the impacting grain ($r_p = r_f$), one can reduce the degree to which the penetrating particle would fragment and thus large fragments or complete grains will impact the plate or capture material below.

STS-46 Experiment

The Center for the Commercial Development of Space: Materials for Space Structures (CCDS) is located at Case Western Reserve University (CWRU), Cleveland, Ohio. CWRU is currently involved in several spaceflight programs to expose materials to the space environment. The Limited Duration Space Environment Candidate Materials Exposure (LDCE) experiment will be launched for CWRU on STS-46. LDCE-1 and -2 are mounted in GAS canisters with door assemblies. LDCE-3 is mounted on the top of the Space Complex Autonomous Payload (CONCAP). Figures 1, 2, and 3 depict the layout of the LDCE-1, -2, and -3 exposure plates prior to integration into the GAS canisters. The PIE sensors are protected by a hard cover (to be removed before flight) and are not visible in the figures. The GAS canisters are located in Bay 13 of OV-104. Figure 4 shows the location of the GAS canisters relative to the other payloads. The samples mounted on LDCE-3 will be exposed for the entire duration of the mission. After the door assemblies of GAS canisters open, the samples mounted in the LDCE-1 and -2 will be exposed for a period of forty (40) hours. The exposure will occur towards the end of the mission, near 130 nm, with a continuous payload bay attitude into the velocity vector.

The LDCE will expose numerous samples to the environment. As can be seen in Figure 5, the PIE samples are primarily discs, nominally one (1) inch diameter (4.1 cm² exposed area). The discs are held in place, by compression, between highly baked out Nylon washers. Two (2) non-standard size samples were also accommodated.

The LDCE-1 and -3 PIE primarily house sensors for the detection of hypervelocity impacts. The LDCE-1 and -3 PIE sample strips are exact duplicates except for a polished graphite specimen onto which a Niobium grid was deposited. This sample will be used to deduce the LDCE-3 mission atomic oxygen fluence. The LDCE-1 PIE contains a gold foil (nominal $T_f \sim 4.0 \mu\text{m}$) that covers a low density micropore foam. The foam has been used on past missions to collect hypervelocity particles, intact. A similar piece of gold foil covers a highly polished aluminum strip coated with vacuum deposited gold. This will aid in the understanding of the distribution of ejecta material. Also included is a thin aluminum film (nominal $T_f < 500 \text{ \AA}$) stacked above a coated substrate. An estimate of the trajectory of grains within the experiment can be derived from analysis of penetrations made in the thin film and impact sights. The last group of passive sensors are high purity metallic surfaces used for the collection of all grains down to sub-micron size. During any impact, a characteristic crater is formed, with rounded habits and a depth to diameter ratio characteristic of the encountered metal. During impact, the particle is destroyed and

the remnants are mixed with the target material, concentrating in the bottom of the crater or on the surrounding rims. Its chemical and isotopical properties can be identified by analyzing the rim material.

LDCE-2 contain materials and sensors useful in understanding the effects of both atomic oxygen and hypervelocity impacts on the optical properties of engineering materials. Two (2) low scatter mirror specimens, a Kapton material sample and an aluminum film (nominal $t_f < 500 \text{ \AA}$) are used. The LDCE-1 and -2 aluminum films, with a total surface area of $3.24 \times 10^{-4} \text{ cm}^2$, should see 5.2 particles in ten days while in LEO. This estimate was based on Pegasus data published in 1970. Using a foil thickness of $7.24 \times 10^{-5} \text{ cm}$, a density of 2.8 g/cm^3 , and a velocity of 7 km/s , the minimum mass which could penetrate the thin film was calculated. The thin films could be penetrated by a grain which possesses a mass greater than a picogram.

OTHER DEBRIS EXPERIMENTS

Few laboratory hypervelocity impact experiments have investigated the mechanisms of ejecta creation. Consequently, a significant uncertainty accompanies predictions of the effects high-speed ejecta can have on surfaces lying near the site of a hypervelocity impact. For this reason, the effect on materials which will be incorporated into the design of future Earth-orbiting vehicles needs to be investigated by exposure to long-duration space flight conditions. This experiment has been devised to afford opportunities to assess a wide range of the dynamics of ejecta created by hypervelocity impacts on various substrates. Experimental data suggest that an oblique angle hypervelocity impact can create much more ejecta particles than normal incidence impacts, and that the velocity distribution of these ejecta particles will be skewed toward higher values. Therefore, ejecta created in oblique impacts will transfer a significant portion of the impactor's kinetic energy to the surrounding structures. The effects of this energy transfer can be examined through a characterization of the morphological properties of impact craters on witness plates using a Scanning Electron Microscope (SEM), and a digital image processing system. In order to examine this phenomenon further, there is a need for an experiment which can capture hypervelocity ejecta so that an ejecta size and velocity distribution may be derived from a non-destructive study. The effects which a variation in the density of the substrate might have on ejecta production must also be investigated. Hydrodynamic and molecular dynamics computer programs will assist in theoretical establishment of relevant hypervelocity impact parameters for the full regime of impact events from ultra thin film penetrations to semi-infinite targets composed of mixed material systems, viz., metallic surface evaporated onto a substrate.

As a consequence of the experimental data developed during earlier STS missions and the data expected from this mission, the authors have produced and delivered an experiment for the European Space Agency's European Retrievable Carrier (EuReCa 1) which will provide a nine-month exposure at 500 km for similar thin film experiments. EuReCa 1 is also manifested on STS-46. The data to be returned by the EuReCa 1 experiment will be produced through an examination of the morphology of primary and secondary hypervelocity impact craters. Primary attention will be paid to craters caused by ejecta produced during hypervelocity impacts on different substrates, e.g., gold, aluminum, palladium, and at different angles of incidence, viz., 45° , 35° , 25° , 0° . From these data one will be able to determine the size distribution of ejecta by means of witness plates and collect fragments of ejecta from craters by means of momentum

sensitive micropore foam. With an established ejecta size distribution via witness plates and with the determination of total momenta of each ejected particle, a velocity distribution by angle will be derived, [given that the ejecta number density is a strong function of the angle taken with respect to the surface normal of the impact target].

COMPUTER SIMULATIONS OF THIN FILM PENETRATION

During the decades ahead, a significant amount of material which has been exposed to the LEO environment will be returned for analysis. Interpretation of the evidence presented by these materials will require extensive knowledge concerning the failure modes of similar materials subjected to hypervelocity impacts. An accurate assessment of the properties of objects which might have created the features evident on the returned materials will insure that an exact "picture" of the orbital debris and micrometeoroid population can be developed. To this end, extensive experimental investigations have measured the penetration parameters of several types of metallic substances in the velocity and size regimes commensurate with that of Interplanetary Dust Particles (IDP's) and orbital debris. Through numerous hypervelocity impact investigations, Baylor University Space Science Laboratory (BUSSL) researchers have accumulated experience which has been applied to hydrodynamic computer program development and the utilization the multi-dimensional hydrodynamics code CTH (McGlaun, S.L. Thompson, and M.G. Elrick, 1990; Thompson and Lauson, 1984) produced by Sandia National Laboratory. Primarily, CTH will be used to investigate the relationship between the particle diameter, d_p , and the diameter, d_h , of the hole created in an aluminum thin film [500 Å thick (T_f)] for relevant particle sizes, densities and velocities. The results of these CTH runs will be employed to analyze the penetration parameters of the thin films flown on STS-46 and EuReCa 1.

EMPIRICAL ESTIMATIONS OF PENETRATION PARAMETERS

Extensive experimental work has established several empirical relationships (McDonnell, Carey, and Dixon, 1984; Carey, McDonnell, and Dixon, 1985) which describe the hypervelocity impact event of thin film penetration. Interpretations of the solutions derived by use of CTH must be substantiated by a clear connection with parameters derived by experiment. Though by no means an exhaustive list of penetration equations, the four listed below are representative equations of the empirically derived penetration limits for thin films. One important aspect about these equations to notice is the apparent continuity between early work dating back to 1965 and even the most recent empirical equations.

Thin Film Penetration Equations:

$$\frac{T_f}{D_p} = 0.055 D_p^{0.056} \left(\frac{\rho_p}{\rho_T} \right)^{0.476} \left(\frac{\sigma_{Al}}{\sigma_T} \right)^{0.134} V_p^{0.739}; \quad \text{McDonnell \& Sullivan (1991)}$$

$$\frac{T_f}{D_p} = 0.772 D_p^{0.2} \epsilon^{-0.06} \rho_p^{0.73} \rho_T^{-0.5} (V_p \cos \alpha)^{0.88} \quad \text{Pailer \& Grün (1980)}$$

$$\frac{T_f}{D_p} = 0.57 D_p^{0.056} \epsilon^{-0.056} \left(\frac{\rho_p}{\rho_T} \right)^{0.5} V_p^{0.875}$$

Fish & Summers (1965)

Although not presented here, the above equations have been plotted versus velocity as well as versus particle diameter. In order to analyze by empirical means the penetration parameters of thin films like those flown on STS-46 and EuReCa 1, one may utilize the Fish-Summers (Fish, and Summers, 1965) penetration formula. Given that the thickness of the metallic foil is 5.00×10^{-6} cm, density of 2.7 g/cm^3 , and velocity of 7 km/s , then the minimum mass which could penetrate the thin film would be:

$$T_f = K r_p^{0.148} M_p^{0.352} V_p^{0.667} \quad \text{or} \quad M_p = \left[\frac{T_f}{K r_p^{0.148} v_p^{0.667}} \right]^{2.84} = 2.2 \times 10^{-15} \text{ g},$$

where $K = 3.56 \times 10^{-4}$ for aluminum. A recent empirical equation reported by McDonnell (McDonnell et al, 1990) which gives a measure of the penetration limits for metallic films exposed to the LEO orbital debris and micrometeoroid complex can be used to derive the following penetration mass limit:

$$M_p = K'' T_f^3 \left[\frac{\rho_p}{\rho_t} \right]^{-0.78} \left[\frac{\sigma_t}{\sigma_0} \right]^{0.24} v_p^{-3\beta} = 1.00 \times 10^{-15} \text{ g}; \quad \text{with } \beta = 0.69 \left[\frac{\rho_p}{\rho_t} \right]^{0.09}$$

where $K'' = 2.42 \times 10^{-18}$ is an empirically derived constant. These mass calculations suggest that the thin films can be penetrated by a grain which possesses a mass greater than a picogram. Using a more recent equation (McDonnell and Sullivan, 1991) one finds that :

$$D_p = \frac{T_f}{0.055} \left[\frac{\rho_T}{\rho_P} \right]^{0.476} \left[\frac{\sigma_t}{\sigma_0} \right]^{0.134} v_p^{-0.739} = 3.82 \times 10^{-7} \text{ m}; \quad M_p = 7.91 \times 10^{-14} \text{ g}.$$

Of particular interest to these investigations is a specific empirical form which relates penetration hole size with the diameter of the penetration hole. This experimentally derived equation for the description of the penetration relationship for iron projectiles impacting aluminum films of various thicknesses was developed by Carey, McDonnell, and Dixon (CMD) (Carey, McDonnell, and Dixon, 1985). The Carey, McDonnell & Dixon (CMD) empirical equation has been compared with the results of computer simulation of hypervelocity impacts, and has been plotted for various velocities of interest for surfaces flown in LEO. The CMD equation is shown as:

$$\frac{D_h}{D_p} = 1 + 1.5 \left(\frac{T_f}{D_p} \right) v_p^{0.3} \left(\frac{1}{1 + \left(\frac{T_f}{D_p} \right)^2 v_p^{-n}} \right); \quad \text{Where } n = 1.02 - 4 \exp(-0.9 v_p^{0.9}) - 0.003 (20 - v_p)$$

The most general form of the CMD equation utilizes the ratio of the target density to the particle density raised to the 0.6.

$$\frac{D_h}{D_p} = 1 + 2.9 \left(\frac{\rho_f}{\rho_p} \right)^{0.6} \left(\frac{T_f}{D_p} \right) v_p^{0.3} \left(\frac{1}{1 + 2.9 \left(\frac{\rho_f}{\rho_p} \right)^{0.6} \left(\frac{T_f}{D_p} \right)^2 v_p^{-n}} \right);$$

where n is unchanged.

SUMMARY

Data from two-dimensional (2D) computer simulations of the hypervelocity impact events which will most probably penetrate the STS-46 and the EuReCa 1 thin films conform to a high degree with the CMD equation, for all densities tested. The CMD relationship between the particle diameter, D_p , and the diameter, D_h , of the hole created in a 500 Å aluminum thin film (T_f) for relevant particle and film parameters when compared with other thin film penetration data, is found to agree. The CMD relationship will be compared with experimentally derived penetration data to be collected this year as well as with further CTH computer simulations at higher velocities, i.e., 9, 11, and 15 km/s. These extended computer simulations suggest that the CMD relationship may be used to analyze *in-situ* data of the thin film experiments flown on LDCE, and to determine the size distribution of particles which penetrate the thin films.

REFERENCES

1. Carey, W. C., J.A.M. McDonnell, and D.G. Dixon (1985). An empirical penetration equation for thin metallic films used in capture cell techniques. *Properties and Interactions of Interplanetary Dust*, 85th Proceedings of IAU.
2. Cour-Palais, B. G. (1979). Space vehicle meteoroid shielding design. *The Comet Halley Micrometeoroid Hazard*, ESA S-153.
3. Fish, R.H., and J.L. Summers (1965). The effect of material properties on threshold perforation. *Proc. Seventh Hypervelocity Impact Symposium*, Vol. 6.
4. McDonnell, J.A.M., W. C. Carey, and D.G. Dixon (1984). Cosmic dust collection by the capture cell technique on the Shuttle Pathfinder mission, *Nature* 309.
5. McDonnell, J.A.M., S.P. Deshpande, S.F.Green, P.J. Newman, M.T. Paley, T.J. Stevenson, and K. Sullivan (1990), First results of particulate impacts and foil perforations of LDEF, In *Proceedings of the XXI Lunar and Planetary Science Conference*.
6. McDonnell, J.A.M., and K. Sullivan (1991), Hypervelocity impacts on space detectors: decoding the projectile parameters, In *Proceedings of the Hypervelocity Impacts in Space Symposium*.
7. McGlaun, J. M., S.L. Thompson, M.G. Elrick (1990), CTH: A Three-Dimensional Shock Wave Physics Code, *Int. J. of Impact Engng*, Vol. 10.
8. Pailer, N., and E. Grün (1980). The penetration limit of thin films, *Planetary Space Science*, Volume 28.
9. Thompson, S. L., H.S. Lauson (1984). Improvements in the Chart D radiation-hydrodynamic CODE V: 1972/1973 modifications, *Sandia National Laboratory Report*, SC-RR-71 0714.

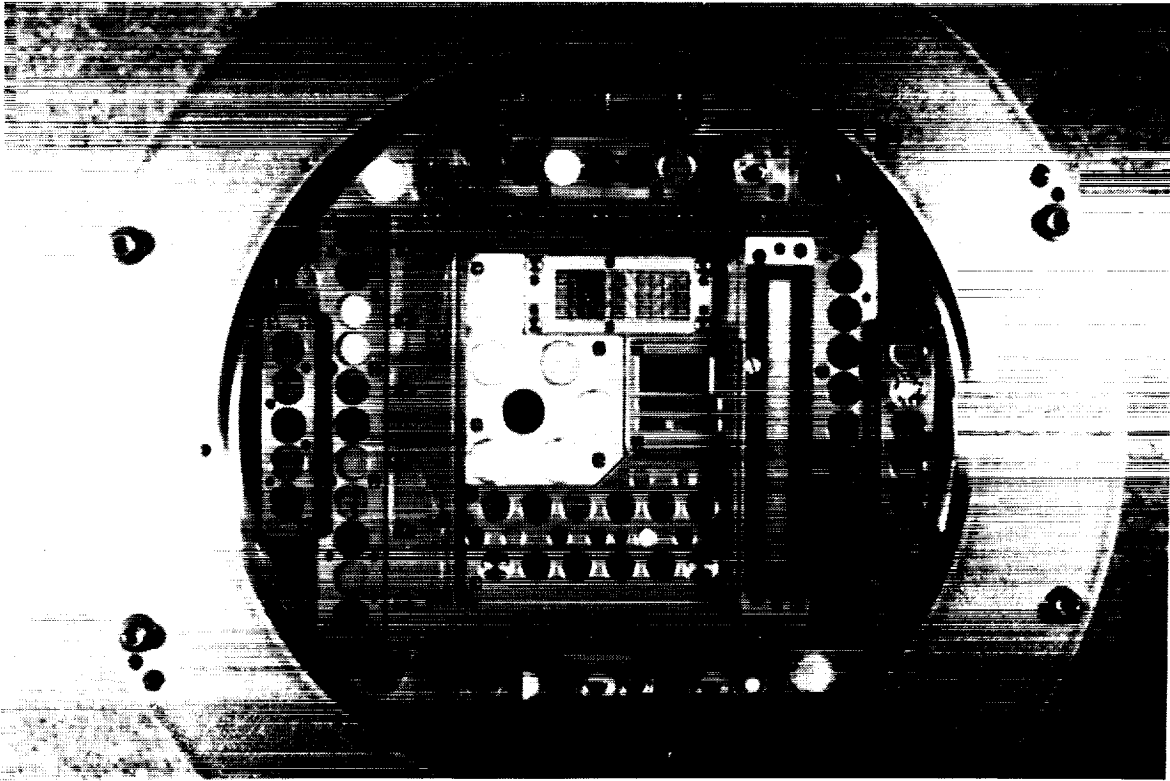


Figure 1. LDCE-1 Exposure Plate Prior to Integration

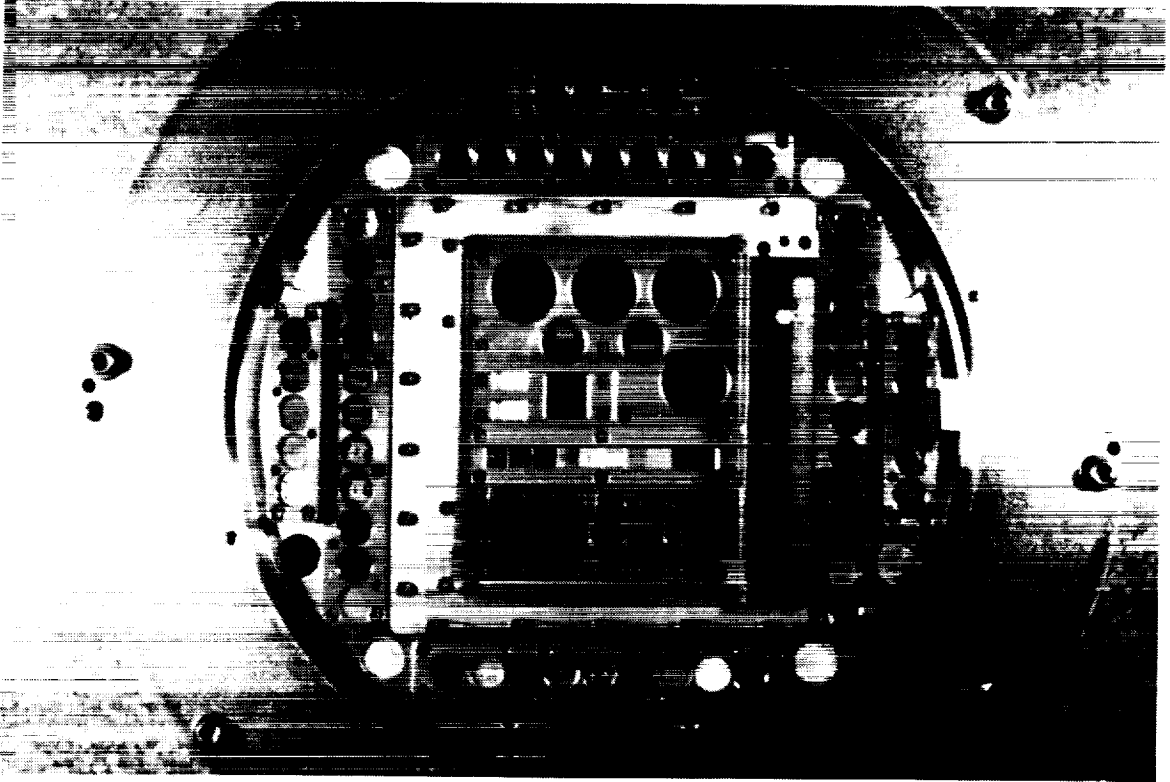


Figure 2. LDCE-2 Exposure Plate Prior to Integration

ORIGINAL PAGE
BLACK AND WHITE PHOTOGRAPH

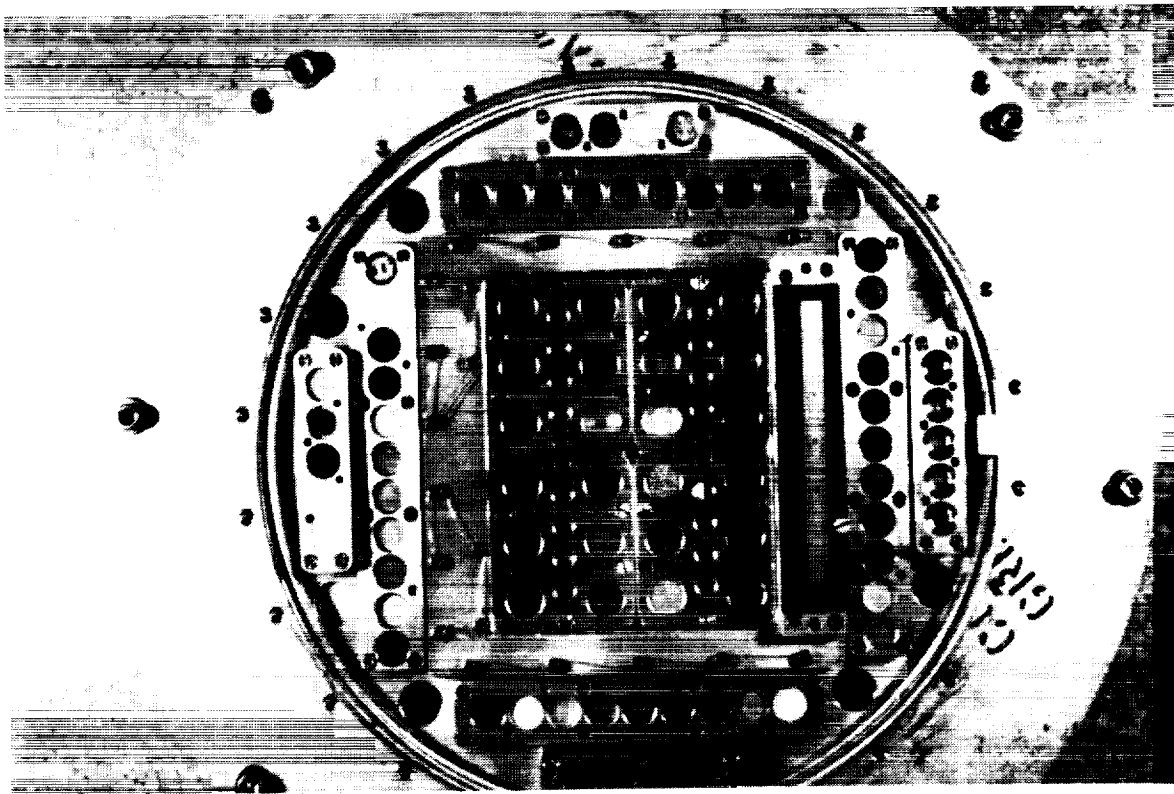


Figure 3. LDCE-3 Exposure Plate Prior to Integration

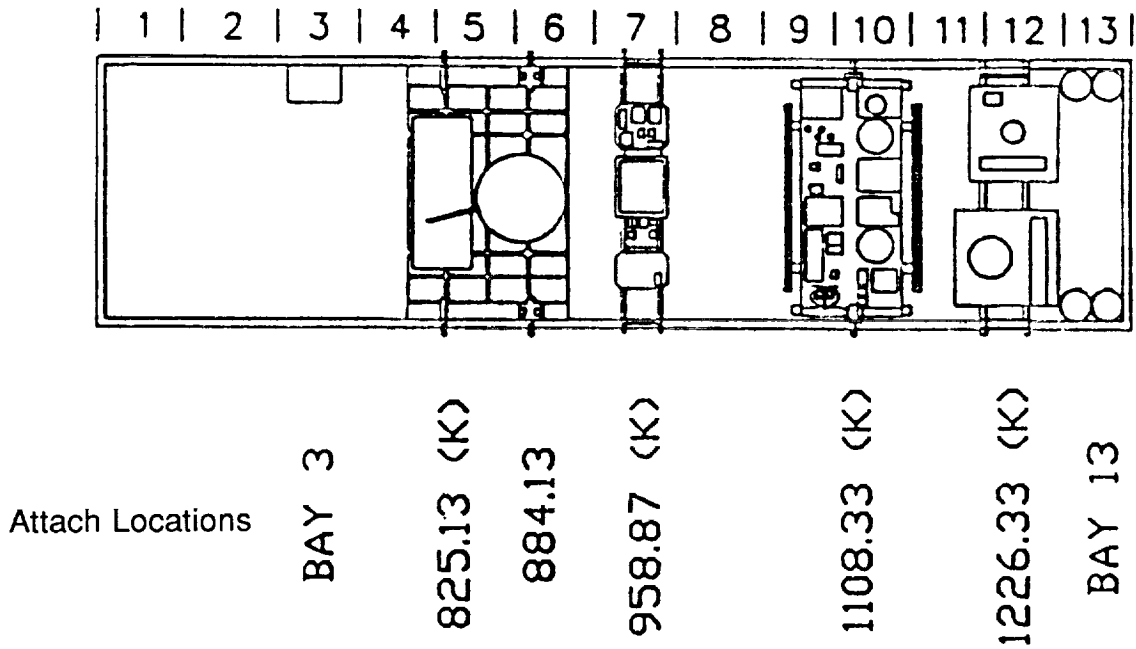


Figure 4. GAS Canister Locations: OV-104, Bay 13.

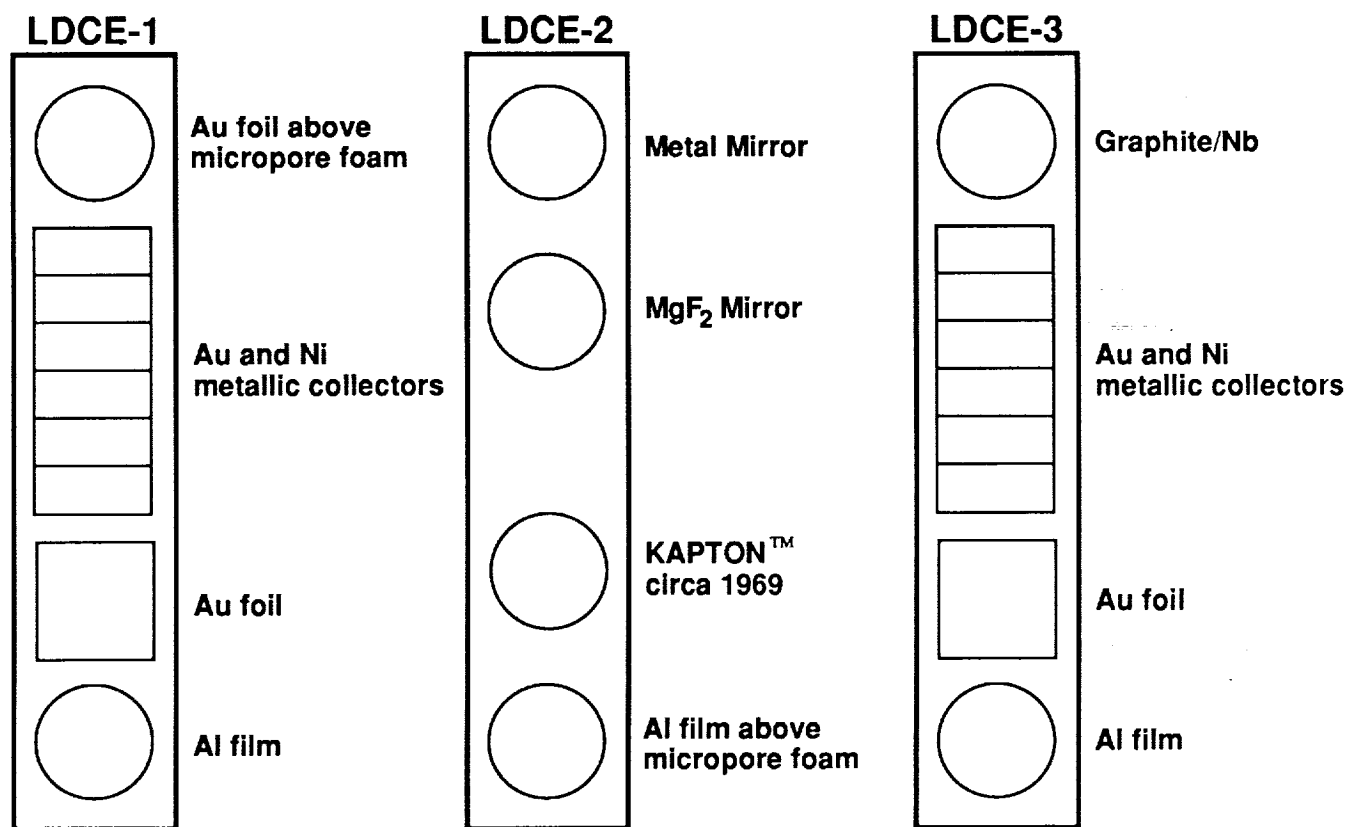


Figure 5. PIE Sample Mounting for LDCE-1, -2, and -3.

Battery Selection for Space Experiments

David R. Francisco
NASA-Lewis Research Center

Abstract

This paper will delineate the criteria required for the selection of batteries as a power source for space experiments. Four basic types of batteries will be explored, lead acid, silver zinc, alkaline manganese and nickel cadmium. A detailed description of the lead acid and silver zinc cells while a brief exploration of the alkaline manganese and nickel cadmium will be given. The factors involved in battery selection such as packaging, energy density, discharge voltage regulation, and cost will be thoroughly examined. The pros and cons of each battery type will be explored. Actual laboratory test data acquired for the lead acid and silver zinc cell will be discussed. This data will include discharging under various temperature conditions, after three months of storage and with different types of loads. A description of the required maintenance for each type of battery will be investigated. The lifetime and number of charge/discharge cycles will be discussed.

Space Experiment Battery Selection Overview

When designing a space experiment (for the purpose of this paper a space experiment is defined as hardware that is flown on the shuttle or any other vehicle that provides a platform for microgravity research) one of the primary concerns is the power source for the experiment. If a battery is selected, many factors contribute to this selection. Complete load characteristics, power requirements, energy requirements, and storage period must be considered in order to choose the correct battery. The available weight, volume restrictions and the environment in which the experiment will be operated is also critical in determining the correct battery for a space experiment.

Other factors that contribute to the selection of a battery is the location in which the experiment will operate. If the experiment will operate in an inhabited environment, then additional precautions must be taken. The cost of the battery and the maintenance required also plays a major role in selection of a battery. In this paper all of these factors will be considered in the description of each battery type.

Battery Terminology

Before a detailed description of each battery type can be started, a understanding of battery terminology is necessary. The following sections explain the relevant terms needed in understanding the application of batteries.

Capacity

The capacity (C) of a battery is usually defined as the number of amp-hours that a fully charged cell can supply. The capacity is affected by the rate at which the battery will be discharged, the temperature of the battery when discharging, and the state of charge. The capacity listed on a battery is valid only when the battery is discharged at 1/10 (C/10) of the listed amp-hours (i.e. a 15 amp-hour battery discharged at 1.5 amps for 10 hours). If the battery is discharged at a faster rate, the capacity will significantly decrease. Different types of batteries perform better at higher discharge rates than others, this will be discussed in each of the battery type descriptions.

Cycle

A cycle on a battery is one sequence of charging and discharging. Only secondary batteries have cycles.

Charging

The process of returning electrical energy to a battery. Secondary cells require charging.

Discharge Voltage Regulation

Discharge voltage regulation is defined as the stability of the batteries voltage during discharge. Some batteries, such as lead acid cells, will slowly decrease in voltage as they are discharged until the voltage drops quickly at the end of capacity. Other cells such as silver zinc cells will remain at one voltage level for a majority of the discharge cycle, then it will drop dramatically.

Depth of Discharge (DOD)

This is the percent of the capacity discharged in relation to rated capacity from a battery.

Electrolyte

Electrolyte is the medium used to transport ions within the battery.

Energy

Energy is the total amount of power delivered by the battery over time. This is calculated by taking the capacity (amp hours) times the average discharge voltage (= watt-hours).

Open Circuit Voltage (OCV)

The OCV of a battery is voltage measured when no load is applied to the battery. Measurement of the OCV is an indicator of the state of charge for many types of batteries.

Power

Power is defined as the number of watts discharged from a battery at a specific instance in time (such as the peak power was 150 watts).

Primary Battery

A primary battery can not be charged and is only used once.

Sealed Cells

Sealed cells do not require maintenance and are usually equipped with a high pressure vent. Most of these types of cells contain the minimal amount of electrolyte (see the section on Lead Acid Cells).

Secondary Battery

A secondary battery is one that can be recharged to the original full capacity. This type of battery is rated for the maximum number of charge/discharge cycles.

Self-Discharge Rate

Self-discharge rate is the rate at which a battery (or cell) loses capacity while standing idle (in storage). This rate is affected by the temperature at which the battery is stored. This parameter is critical when selecting a type of battery for a space experiment.

This concludes the discussion of battery terminology. The following sections will discuss the use of lead acid, silver zinc, alkaline manganese and nickel cadmium cells with respect to space experiments.

Sealed Lead Acid (SLA) Cells

Description

Lead acid cells are secondary cells that are commonly used in the automotive industry. The cells used in autos have a liquid electrolyte (H_2SO_4 - sulfuric acid), where as the cells considered for space

experiments are sealed lead acid cells (SLA). The SLA cells have a minimum amount of electrolyte and are maintenance free because they operate on a gas recombination principle (the oxygen and most of the hydrogen generated within the cell are recombined, therefore no additional water is needed). The anode is made of lead and the cathode consist of lead dioxide (PbO_2). The cases are made of metal (isolated) and are sealed with a resealable pressure valve.

Capacity

Lead acid cells have a low internal resistance (on the order of 5 m Ω) which allows the cells to source high current. A 12.5 amp-hour cell (rating at C/10 discharge rate) is rated at 9.0 Amp-hours when discharged at 12.5 Amp/hour rate (1C). In comparison to most other batteries SLA cells are much heavier for the same capacity.

Cycles

The number of cycles that can be obtained from a lead acid cell can vary between 200 to 2,000 depending on the use of the cell. The two factors that affect the life are the depth of discharge and the charging method. If the cells are discharged 100% during each cycle and charged without a current limit, then the life will end at about 200 cycles. If the cell is only discharged 25% and charged with a current limit of 2 Amps the life will be closer to 2,000 cycles.

Storage

Stored SLA cells should be trickle charged with a voltage approximately 2.25V to 2.30 V per cell. If the cells are not trickle charged, then they will loose a noticeable amount of capacity during storage. At room temperature the specifications indicate that these cells will loose 20% of their capacity after 6 months. Test data reveals that SLA cells stored at room temperature decreased in capacity by 35% after 5 1/2 months. At lower temperatures the cells will retain more capacity.

Temperature Performance

Lead acid cells perform better than other types of cells at lower temperatures. As per the specifications of sealed lead acid cells, a 15% reduction in energy is seen at a temperature of 0 C for a discharge rate of C/10. If the cells are discharged at a rate of 1.2C the reduction energy is approximately 35 %. A battery made of 16 cells with a capacity of 12.5 Amp hours was discharged at 32 F. These cells were discharged at a C/6 rate. Approximately a 8 % reduction of energy from a room temperature discharge was documented during this test.

Voltage Characteristics

The discharge voltage of lead acid cells varies from approximately 2.15 volts when fully charged to 1.6 volts when completely discharged. The temperature at which the discharge occurs will affect the discharge voltage. At 0 C the discharge voltage will be slightly (0.05 volts) lower.

Maintenance

These cells required very little maintenance. No additional electrolyte has to be added during the life of the cells. Charging of the cells requires a constant voltage between 2.4-2.6 volts per cell. Standard battery chargers may be readily purchased. Determining the state of charge of SLA cells is easily achieved by taking the open circuit voltage (OCV) and substituting this voltage in the following equation: % charge = $(OCV - 1.98V) / 0.05$. The only characteristics of the cells that may require additional maintenance is that these cells may need to be cycled (discharged deeply -90% of rated capacity) after an extended storage in order to achieve full capacity.

SLA Conclusion

SLA cells are very inexpensive, require very little maintenance and can withstand many cycles. The voltage regulation and the storage charge capacity retention is average. The major disadvantage to these cells is the weight and volume required to obtain the desired energy. Relative to other battery types, these cells require the most weight and volume to achieve the same capacity. Therefore if minimal energy (< 300 watt hours) is required and considerable weight and volume is available (30Kg and .36 m²) then SLA cells should be considered.

Silver Zinc

Description

Silver zinc cells are secondary cells that are usually used in military and aerospace applications. Silver zinc cells have a liquid electrolyte of potassium hydroxide (KOH) with the negative electrode of zinc and the positive electrode as silver. For space experiment applications the cell has a resealable vent valve. The case is made of a styrene plastic that is very durable.

These cells are purchased "dry, uncharged" or "dry, charged." Either type requires filling the cells with electrolyte. The dry uncharged cells require a formation process (see the maintenance section) and the dry charged cells may be used immediately after the filling of electrolyte. Both types of cells have the same characteristics, which are described in the following sections.

Capacity

Silver zinc cells have a low internal resistance (on the order of 3.5 mΩ) which allows the cells to source high current. A 15 Amp-hour cell is rated at 20 Amp-hours when discharged at C/10 at the beginning of life. The capacity at C/3 rate was tested at the beginning of life (initial cycle), a 15 amp hour cell supplied approximately 20 amp hours. Subsequent cycles showed a slight decrease (10%) in capacity. In comparison to most other batteries silver zinc cells are much lighter and much more energy dense (5 times greater than SLA cells).

Cycles

The number of cycles that can be obtained from a silver zinc cell can vary between 100 to 200 depending on the use of the cell. The major factors that affect the life are the depth of discharge, maintenance and storage conditions.

Storage

Silver zinc cells may be stored in the dry state (no electrolyte) for at least five years in a dry environment. Once the cells are wetted (filled with electrolyte), the active life is usually 1 to 2 years depending on the number of cycles.

Once the cells are wetted and charged, they are specified to retain 85% of their capacity when stored at room temperature for 3 months. Testing has verified this specification.

Temperature Performance

Silver zinc cells do not perform as well as lead acid cells at lower temperatures. As per the specifications of silver zinc cells, a 22% reduction in energy is seen at a temperature of 0 C for a discharge rate of C/10. Testing of a 19 cell 15 amp-hour battery at 0 C indicated a 18% reduction in capacity.

Voltage Characteristics

The discharge voltage characteristic of silver zinc cells is a dual plateau (two separate and distinct voltage levels during discharge). The first plateau is 1.75 volts/cell for approximately 20% to 30% of capacity and for the remainder of the capacity the voltage is at 1.5 volts/cell. Once the second plateau is reached the voltage is very stable for silver zinc cells.

Maintenance

These cells required a considerable amount of maintenance. Initially the cells must be filled with

electrolyte which requires safety precautions (KOH is a caustic) and is time consuming. If the uncharged cells are used, then a formation process is required. This process requires the cells to be charged initially and then discharged at a C/3 rate. If the rated capacity is not achieved then the cycle must be repeated. These cells have a resealable vent valve and they do vent during their lifetime. This requires the box that encloses the cells (and any components in contact with the cells such as an electrical connector) to be impervious to KOH. In most cases an epoxy is used to pot the cells with a opening for the vent valve. Charging of the cells requires a constant current with a shutoff of approximately 2 volts per cell. Usually a custom battery charger is required. Some manufacturers produce battery chargers that may be readily used. Determining the state of charge of silver zinc cells from their open circuit voltage (OCV) may be done. The OCV will tell if the cells are greater than 70% capacity (cell voltage approximately 1.85 V) or less than 70% (cell voltage approximately 1.6 volts).

Silver Zinc Conclusion

Silver zinc cells are very expensive, require considerable maintenance, and can withstand a limited number of cycles. Packaging also requires additional provisions. The voltage regulation and the storage charge capacity retention is excellent. The major disadvantages to these cells is the maintenance required and the cost. Relative to other battery types, these cells require the least weight and volume to achieve the same capacity. Therefore if weight and volume is a concern and considerable energy is required, silver zinc cells should be considered.

Alkaline Manganese Dioxide

Description

Alkaline cells are primary cells that are used for most household electronic appliances. The type of alkaline most widely used is alkaline manganese dioxide ($Zn-MnO_2$). These cells utilize zinc as the anode and manganese dioxide as the cathode and potassium hydroxide as the electrolyte. These cells are cylindrical and the case is usually made of steel.

Electrical Characteristics

Alkaline cells have an internal resistance of less than 1 Ω and are suited for low current draw over a long period of time. A nominal D-cell will deliver 0.8 amps for 15 hours. The starting voltage will be 1.5 volts/cell and its end of life will be at approximately 1.0 volts/cell. The charge retention after storage for alkalines is excellent and is not a concern when used for space experiments. These cells are specified to retain less than 75% of their capacity at 0 C. The overall cost is low and the maintenance required is minimal.

Alkaline Cell Conclusion

Alkalines offer excellent storage capabilities and are very inexpensive. One disadvantage is that if substantial amounts of current (> 1.0 Amps) is required, parallel batteries are needed which adds weight, volume and complexity to the fusing and wiring of the batteries. The voltage regulation during discharge varies significantly and the loads must be able to accommodate this variation. The operation of these cells at lower temperatures is a concern and should be thoroughly tested.

Nickel Cadmium

Nickel cadmium cells are secondary cells that use KOH as the electrolyte, cadmium as the anode and nickel (NiOOH) as the cathode. These cells are commonly used for household electrical appliances that are rechargeable. The case is made of nickel plated steel and is very rugged.

Electrical Characteristics

The internal resistance of nickel cadmium cells is on the order of $15 \text{ m}\Omega$. These cells are suited for moderate rates of discharge. Most cells have a capacity (C) in the range of 1 to 3 amp hours. The discharge voltage ranges from 1.35 volts/cell at full capacity to 1.05 volts/cell at the end of capacity. Nickel cadmium cells lose approximately 1% of capacity per day. The capacity retention due to storage is not suitable for space experiments.

Nickel Cadmium Conclusion

Even though new higher capacity nickel cadmium cells have been developed, the limiting factor with nickel cadmium for space experiment applications is their storage retention. Since most space experiments are stored for 3 months before flight with no access, nickel cadmium cells would not have sufficient capacity to operate an experiment. Nickel cadmium cells should not be considered for space experiments with an extended storage period.

Conclusion

Table I summarizes the characteristics of each type of battery discussed. The most important consideration when choosing a battery type for a space experiment application is the conditions in which the battery will operate. Details of the loads (power profile) of the experiment, the environment (temperature) of operation, and the available weight, volume and funds available are required to accurately choose the correct battery. Detailed testing under the worst case conditions that the space experiment will experience should also be conducted before choosing a specific battery type. It is also worth noting that there are many other types of batteries that may be used for space experiments.

BATTERY COMPARISON				
	LEAD ACID	SILVER ZINC	ALKALINES	NICKEL CADMIUM
TYPE	SECONDARY	SECONDARY	PRIMARY	SECONDARY
CAPACITY	2 TO 25 A-HRS	1 TO 600 A-HRS	< 20 A-HRS	< 8 A-HRS
CYCLES	200 TO 2000	100 TO 200	1	500
VOLTAGE REG /CELL	2.15 - 1.6V	1.7 - 1.5V	1.5 - 1.0V	1.3 - 1.1V
STORAGE CAP RETENTION	3 MON./65%+	3 MON./85%	3 MON./95%+	3 MON./0%
TEMPERATURE CAP AT 0 C	85%	68%	<75%	90%
MAINTENANCE	MEDIUM	HIGH	LOW	MEDIUM
CONCERNS	WEIGHT	MAINTEN./COST	CURRENT CAP.	STORAGE

TABLE I

REFERENCES

1. Battery Energy Data Manual, Whittaker-Yardney Power Systems.
2. Duracell Battery Data Guide For Designers, Duracell U.S.A., Tarrytown, New York, 1981.
3. Duracell Technical Bulletin, Alkaline, Duracell Inc. Bethel, CT, October 1991.
4. Gates Energy Standard Cyclon Battery Catalog, Gates Energy Products, Denver, Colorado, January 1986.
5. Gates Sealed Nickel Cadmium Rechargeable Cells, Gates Energy Products, Gainesville, Florida, October 1987.

THE UNIQUE CHALLENGE OF MANAGING AN
UNDERGRADUATE GET-AWAY-SPECIAL EXPERIMENT

Peter W. A. Roming, Mark K. Spute, Memorie K. Williams,
Branton J. Campbell, and J. Ward Moody^a
Department of Physics and Astronomy
Brigham Young University, Provo, UT 84602
Phone #: (801) 378-4361, Fax #: (801) 378-2265

ABSTRACT

A group of Brigham Young University (BYU) undergraduate students has undertaken an experiment to design and build a normal incidence soft x-ray robotics telescope for solar observations. The design phase of this, GOLDHELOX project, has now been completed and final construction and modifications are in progress.

The GOLDHELOX project was conceived by a group of undergraduate students in 1988. It has proceeded since then with only a minimal input from faculty and graduate students.

The project is under the direction of a four part administration consisting of a faculty advisor, cabinet, administrative assistants, and team leaders. The faculty advisor is the principle investigator and is ultimately responsible for grant money and setting and maintaining a schedule. The de facto program management is the responsibility of the cabinet and administrative assistants. The design and manufacture of the payload is under the direction of the team leaders and a system's integrator.

A goal of this project is educating and furnishing experiences in space engineering and physics for undergraduate students. Well over a dozen former project members have gone on to graduate school in engineering or physics.

Our main source of funding is NASA and the BYU Colleges of Physical and Mathematical Sciences and Engineering and Technology. Other sources of funding have come through advertising and voluntary professional services.

This project is possible because of the NASA Get-Away Special (GAS) program. The only feasible alternative is using an expensive sounding rocket. We estimate the sun tracking and guidance package alone would cost upwards of a million dollars -- at least ten times our entire budget. Because of the GAS program, we simplified the construction, operation, and programming of the instruments with resulting savings in weight, cost, and time spent.

^aAuthor to whom correspondence should be addressed.

INTRODUCTION

A group of Brigham Young University (BYU) undergraduate students has undertaken an experiment, The GOLDHELOX^b Project, to design and build a normal incidence soft x-ray robotically controlled telescope for solar observations. GOLDHELOX, identified by NASA as space shuttle payload number G-133, will fly above the earth's atmosphere to make unobstructed observations of the sun in the 171-181 Å wavelength region. The telescope will make these observations by utilizing the Get-Away Special (GAS) can with a Motorized Door Assembly (MDA).

The design phase of the GOLDHELOX project has now been completed. Final modifications and construction are in progress (a more detailed discussion of this project is found in another paper in this publication¹). Under the supervision of Dr. J. Ward Moody the project is operated and administered by undergraduate students.

Undergraduate students are a resource in research which is both under-utilized and underestimated, primarily because of the many difficulties associated with operating a large undergraduate student project. High student turnover creates a continually evolving leadership void. Limited student knowledge and experience make progress on a complicated experiment slow and difficult. Also, a volunteer research project such as ours competes with the already limited time available to undergraduate students.

In this paper we discuss our approach to overcoming each of these problems while emphasizing areas in which we have been particularly successful. We highlight how to motivate students to get involved in undergraduate research for reasons other than the need for a part time job, and how appropriate incentives can make participation a beneficial endeavor for students.

We also discuss project administration, funding, and the organization of our project into various interactive teams and sub-teams. Finally, we discuss our interaction with the NASA GAS program, the ways in which the GAS program has been most helpful to our project, and how collaboration with other groups doing similar research has helped our undergraduate team overcome difficult problems.

PROJECT ADMINISTRATION AND ORGANIZATION

As in all organized projects, we required a strong administration to oversee the design and construction of the payload. Our administration is divided into four main groups: the principle investigator, cabinet, administrative assistants, and team leaders (see figure 1).

Dr. J. Ward Moody, of the physics and astronomy department, is the project's Principle Investigator (PI) and faculty advisor. Under his supervision the project is operated and administered by undergraduate students. His role is to monitor progress and expenditures, and see that deadlines are made and kept.

The Cabinet coordinates the operation of the project and is ultimately responsible in practical terms for its success. The Cabinet consists of a Project Coordinator (PC), Assistant Project Coordinator

^bGOLD for the color of the sun and HELOX for HELiocentric Observations in X-rays.

(APC), Systems Integrator (SI), and Payload Manager (PM).

The main responsibility of the PC and the APC is to oversee the project and its administration. Some of their duties include organizing and conducting project meetings to coordinate the efforts of the different teams, obtaining weekly status reports, helping team leaders establish goals and deadlines, and recruiting and integrating new members.

One of the difficulties encountered by our project is a continually evolving leadership void created by a high student turnover. Most of the undergraduates participating in our project are upperclassmen. They usually enter the project sometime in their junior year, spending a year on the project as a team member, and then functioning for another year in some leadership position. Since leaders only act in their capacity on the average of a year, keeping an experienced administration is difficult.

Our solution to this problem is to keep the administration aware of future leadership vacancies. The PC and APC are responsible for finding replacements three to six months before someone leaves the project, so that a new leader can be trained properly and completely by the retiring leader.

The SI is responsible for the preparation of the requirements^c and specifications^d documents. The SI's duties include approving any specification changes, preparing a project schedule, and overseeing the construction and assembly of the instrument.

The PM acts as sole interface between the GOLDHELOX team and NASA. The PM is also responsible for preparing all documentation required by NASA, informing each team of the safety concerns which relate to them, and helping each team prepare the safety reports required by NASA.

The administrative assistants consist of a Librarian, an Accountant, and a Quartermaster. The Librarian's responsibilities are obtaining and cataloguing materials and documentation to be used as reference material. The Accountant monitors the project budget and informs the Cabinet of monthly expenditures. The Quartermaster acts as an assistant to the SI and organizes, maintains, and issues all project equipment.

The payload design and construction are handled by four independent teams: the Electrical, Mechanical, Optical, and Science teams. Each team has a Team Leader (TL) whose responsibilities include coordinating their team members efforts by holding regular meetings and reporting weekly to the PC. All teams also have a faculty advisor who works closely with the TL and provides assistance for the students on the team.^e

The Electrical Team, mainly consisting of electrical engineers, is responsible for specifying, designing, and assembling the electrical components. This includes all the motors, heaters, power supply, computer circuitry, programming, etc.

The Mechanical Team, primarily comprised of mechanical engineers, is responsible for specifying, designing, and building the physical and

^cThe requirements document consists of NASA requirements, spacial limitations, functional and power requirements, mission parameters, etc.

^dThe specifications document includes the specifications of every mechanical and electrical component, and every other device that will be a part of the instrument.

^eGOLDHELOX Project Charter, January 1992.

structural components of the payload.

The Optical Team, composed mostly of physicists, is responsible for designing and aligning the mirror, filters, and other optical elements.

The Science Team is responsible for establishing the mission parameters and procedures. They are responsible for defining the scientific purposes of the mission and for making certain that the ultimate design and construction can meet these purposes.

The overall organization is essentially a pyramidal structure comprising no more than four levels from the team member to the PC. Because each team consists of one or more sub-teams containing three to five members, and there are four different teams; there is room for a lot of student involvement without becoming top-heavy with management. The result is a lean structure that is flexible enough to adjust to changing requirements quickly and yet remain in control of the project. It allows, and requires, that each student have ample decision making opportunities to incorporate their ideas into the final design. We value the unique abilities and experiences that each student brings into the project and endeavor to ensure that no suggestion that a student makes is treated lightly.

MOTIVATING STUDENTS

Essentially one hundred percent of the work on the GOLDHELOX project, in the last four years, has been initiated or completed by over a hundred undergraduate students. Nearly all of this work has been on a volunteer basis. However, we have learned that before students will volunteer, they must be interested in the nature of the project itself. Of course no one will volunteer unless they know the project exists and that participation is welcome. Large displays in the lobbies of the physical science, engineering, and technologies buildings advertise the existence of this project to a large number of students. These advertisements detail the project's progress and invite students of all majors and in all class levels to participate. Occasional articles in the student newspaper² and flyers posted around campus also serve to recruit interested students.

Even though students may be interested, they still need to devote the majority of their waking hours to their course work. As a result, progress was slow and painful in the early stages of the project. Although the students involved were interested in the project's success, their priorities rightfully rested on their homework and classes. As a result, the project was frequently neglected. It was only after we organized a research class in which progress was demanded and grades were given that the project really started to advance.

Since the project personnel are mainly physics, electrical engineering, and mechanical engineering students, the research class was set up by using a course option already available in each of these majors, whereby students would ordinarily help professors with their individual research in exchange for credit.

A large work force is recruited each year. Each recruit is evaluated and given assignment that are matched to the capability, experience, and the number of research credit hours for which that student has registered. In lieu of class attendance, all project members meet weekly with their team leader who is familiar with the students' assignment as well as the project's construction. Weekly and semester progress reports are required from the students and graded by professors in their individual

departments. The advice of the professors is critical to the success of the project, but the students must first formulate their own solutions to problems. After doing this, they may then seek counsel on the feasibility of their solution. This approach encourages the students to exercise their own creativity.

The research course is a catalyst that encourages participating students to work longer and become more experienced and useful with time. In the beginning stages of the project monetary incentives were generally used to obtain results. With the research class, the grade is sufficient motivation for most students.

Another point of this project that makes it attractive to student volunteers is that it is entirely student run and administered. There is a lot of pride in this. The students feel that they are working for themselves, have a say in the progress and performance of the project, and are an integral part of the project administration. Because they have assumed responsibility for the project, it has become in a very real way "their project" and it will rise or fall based on their efforts alone. The faculty does not manage or administer the day to day aspects of the project.

Most of the students involved in GOLDHELOX are interested in space and space exploration and have used it to gain actual hands on experience with practical problems in space exploration. Several students have been invited to present papers about the project to various professional groups. Well over a dozen former GOLDHELOX project members have gone on to graduate schools such as Arizona, Cal Tech, Colorado, Illinois, and BYU.

OBTAINING FUNDING

Most of our funding was obtained as a result of writing three proposals: one to the BYU College of Physics and Mathematical Sciences, one to the BYU College of Engineering, and one to NASA.

Our project received some publicity when a local magazine³ and newspaper⁴ published our efforts. National recognition came when news of our project was picked up by the Associated Press⁵ and published throughout the country. As a result of this publicity, we received several small contributions.

We have also received several significant voluntary professional services from different companies and individuals that would have otherwise cost us thousands of dollars. These voluntary private contributions have helped keep us under our budget of approximately \$100,000.

THE NASA GAS PROGRAM

This project is possible only through the NASA GAS program. The only feasible alternative to using a GAS can is a sounding rocket. Using a sounding rocket would have required the telescope to have a sophisticated tracking, guidance, control, and recovery or telemetry system. If telemetry was used, arrangements would have to be made for ground based tracking of the payload. If recovery was selected, a tracking and recovery crew would be necessary, and the use of a testing area would have to be arranged so that the descending package would not endanger human

life or property. The cost of all of this would be enormous. We estimate that the sun tracking and guidance package alone would cost upwards of a million dollars -- at least ten times as much as our entire budget.

Using a GAS can in the Space Shuttle allows us to worry only about the control of our package. NASA provides the launch vehicle, a stable tracking platform, recovery services, and six astronaut "operations" which we have used to control the warm-up, activation, and deactivation of our instrument. NASA has verbally stated at least twenty minutes of solar facing time, with the solar disk within thirty degrees of the instruments zenith. Because of the six astronaut operations, we simplified the construction, operation, and programming of the instrument considerably with resulting savings in weight, cost, and time spent in development, programming, and testing.

NASA has also been helpful with suggestions, advice, and financing. They have provided us with specifications for various materials and tests, working drawings of the MDA to ensure our camera can "see" adequately and to localize blind spots. NASA seems to be doing all it can to ensure the success of this experiment. We are grateful to them for the timely assistance they have given us.

COLLABORATION

Collaborating with other research groups, who have worked on similar projects, is beneficial. Many of the groups we work with, including those participating in the NASA GAS program, have already solved many of the problems we are encountering.

The Utah State University GAS group has utilized several NASA GAS cans and has been invaluable in helping prepare our project for launch. Stanford University, who conducted an experiment similar to ours⁶, and Lockheed have offered indispensable technical advice. Without the cooperation of these groups we would have spent much more time and money on problem solving.

SUMMARY

We have undertaken a complex project using undergraduate students as the primary engineers and technicians. We have found that undergraduate students are useful in research but must be administered properly. Working on GOLDHELOX is worthwhile to the students in terms of educational experiences and to the University in terms of finances. Although using undergraduates requires more time and patience, it prepares them better for careers in space exploration and science.

This research is supported by grant NAGW-2612 from the NASA Education Division and Space Physics Division and by funding from the BYU Colleges of Physical and Mathematical Sciences and Engineering and Technology.

^f. An "operation" is defined as an astronaut throwing a switch from off to on, or from on to off. We need one operation each to warm up the instrument, open the MDA, turn on the camera, turn off the camera, close the MDA, and shut down the instrument. Hence six operations.

REFERENCES

1. Williams, M. K.; Campbell, B. J.; Roming, P. W. A.; Spute, M. K.; and Moody, J. W.: G-133: A Soft X-Ray Solar Telescope. 1992 Combined GAS/Hitchhiker Shuttle Small Payload Symposium. NASA CP-_____, 19___. (Paper _____ of this compilation.)
2. Kim, A. Y.: BYU Student Project to 'Blast Off' with NASA. The Daily Universe, Provo, UT, vol. 42, no. 59, Thursday, Nov. 17, 1988, p. 1.
3. Walker, J. H.: NASA Provides Funding for Student Space Research Project. BYU Today, vol. 45, no. 5, Sept. 1991, pp. 14-16.
4. Adams, B.: BYU's Telescope Could Shed Light on Sun's X-Rays. The Deseret News, Salt Lake City, UT, Utah County Edition, Thursday, August 2, 1990, pp. B4.
5. BYU's 'GOLDHELOX' is Spacebound. The Herald, Provo, UT, Friday, August 3, 1990, p. B2.
6. Walker, A. B. C.; Barbee, T. W., Jr.; Hoover, R. B.; and Lindblom, J. F.: Soft X-Ray Images of the Solar Corona with a Normal-Incidence Cassegrain Multilayer Telescope. Science, vol. 241, Sept. 30, 1988, pp. 1781-1787.

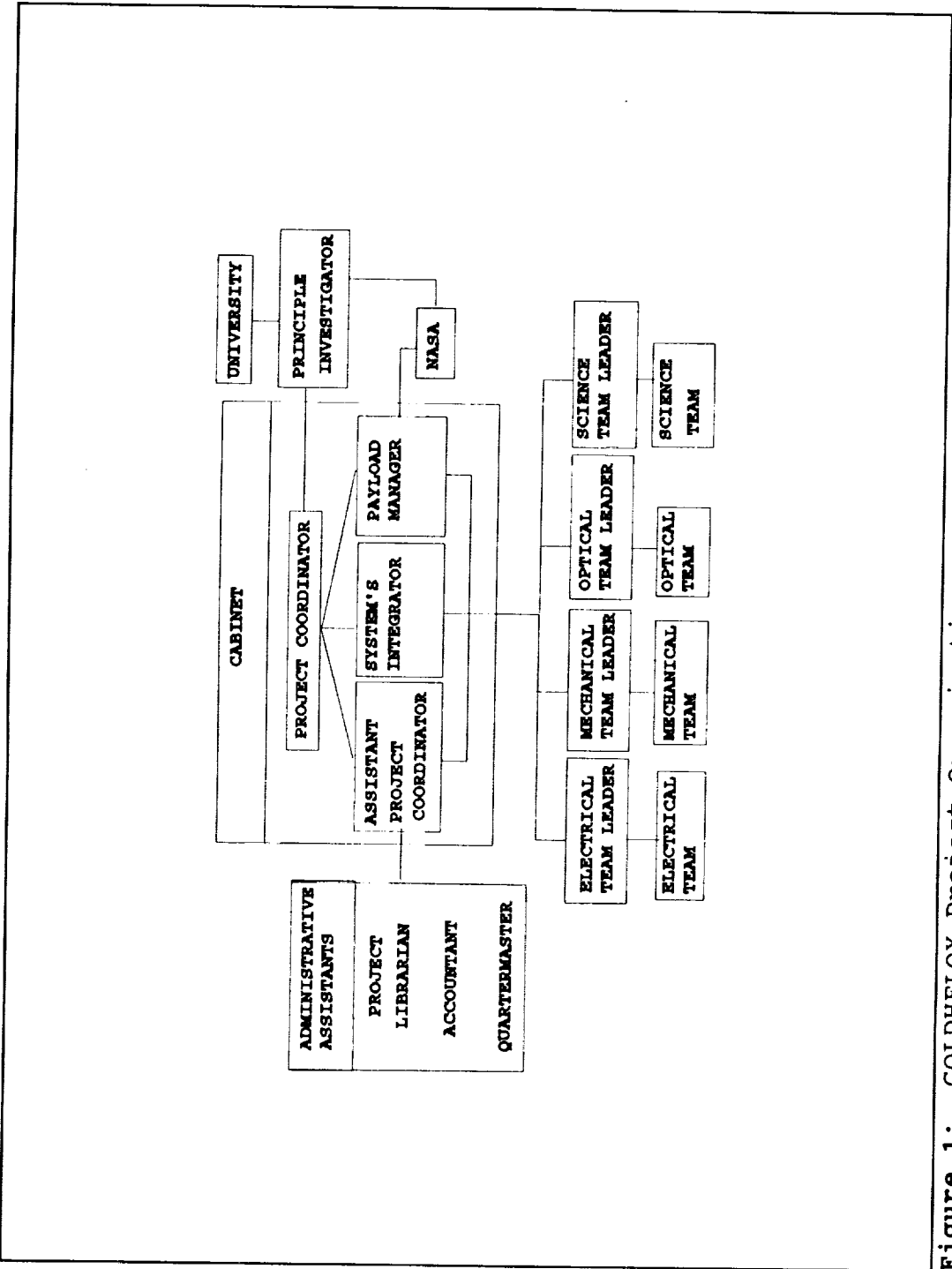


Figure 1: GOLDHELOX Project Organization.

Preparing Safety Data Packages for Experimenters Using the Get Away
Special (GAS) Carrier System

by

Jerome Kosko
GAS Project Safety Manager
Goddard Space Flight Center
Greenbelt, Maryland 20771

ABSTRACT: The implementation of NSTS 1700.7B and more forceful scrutiny of data packages by the Johnson Space Flight Center (JSC) lead to the development of a classification policy for GAS/CAP payloads. The purpose of this policy is to classify experiments using the carrier system so that they receive an appropriate level of JSC review (i.e. one or multi-phase reviews). This policy is based on energy containment to show inherent payload safety. It impacts the approach to performing hazard analyses and the nature of the data package. This paper endeavors to explain the impact of this policy as well as the impact of recent JSC as well as Kennedy Space Flight Center (KSC) "interpretations" of existing requirements.

The GAS canister does adequately contain most experiments when flown in the sealed configuration (however this must be shown, not merely stated). This paper also includes data package preparation guidelines for those experiments that require an opening door which often present unique safety issues.

INTRODUCTION

The GAS carrier system was originally intended to fly inherently safe experiments in a sealed canister that provided an adequate level of containment. As additional carrier system features were acquired (e.g. opening doors and ejection systems) and more dangerous experiments were accepted in the program the assumption of inherent safety became questionable. Moreover a new program, CAP (Complex Autonomous Payloads), was recently introduced. CAP payloads also use the GAS carrier system but are manifested as secondary Space Transportation System (STS) payloads whereas GAS payloads are tertiary payloads of flight opportunity. Although programmatically distinct the carrier system hardware is identical. The implementation of the CAP program, the acquisition of additional carrier system capabilities, and the visibility of increasingly dangerous experiments lead to a reassessment of the manner in which Safety Data Packages (SDPs) are processed at the Goddard Space Flight Center (GSFC) and JSC. The implementation of a new policy classifies payloads for inherent danger and directly relates to the logic of hazard analyses and the manner in which SDPs are prepared.

BACKGROUND

GSFC had routinely processed GAS payloads in accordance with mutual agreements among the centers that were forged years ago at the inception of the GAS program. The purpose of these agreements or understandings was to simplify the processing of payloads and the development of all documentation related to flight approval. The nature of these agreements considered the inherent danger of the user's hardware/operations within the context of the standard carrier system which provides containment by the canister as a fundamental and incontrovertible hazard control. Unfortunately, these agreements were never formally documented and over the years as the experiments became more complex and the carrier system acquired additional features, the "ground rules" became more and more subject to interpretation. In the recent past these interpretations have differed significantly and the distinction between design "guidelines" versus design requirements has become muddled even though the original GAS concept (i.e. inherent safety by containment) remains consistent for a majority of the payloads flown.

The purpose of the classification scheme for payloads utilizing the GAS carrier system is to determine the appropriate level of JSC scrutiny in the phased safety review process based only upon the inherent danger posed to the Orbiter or its crew by the payload regardless of programmatic considerations. An overview of the carrier system, the initial safety review process, and the approach for classifying and reviewing GAS/CAP payloads is presented below.

CARRIER SYSTEM OVERVIEW

The basic GAS carrier system is comprised of either a 5 or 2.5 cu ft. canister that is mounted to either an adapter beam in the cargo bay or to the GAS bridge structure which straddles the cargo bay. Each beam can accommodate 2 canisters whereas the bridge can carry up to 12 GAS canisters. Additionally, each canister configuration can vary depending upon the needs of the experiment that is contained in the canister. However, the majority of GAS/CAP payloads utilize the most basic configuration which is the sealed canister with no intentional venting and an inerted (i.e. no oxidizers present) internal atmosphere at 1 atm. The bridge, adapter beams, associated mounting hardware, as well as the canisters and the canister components are reflow hardware that is systematically tracked and refurbished or replaced in accordance with procedures approved by JSC.

The canister itself is made of two 0.625 in. thick aluminium end plates mounted to opposing ends of a 0.125 in. thick aluminium cylinder. The canister design has been verified by proof pressure testing to 115 psig. The basic canister configuration includes two pressure relief valves in the bottom endplate set at 30 and 45 psid. After the experiment is integrated into the canister and the endplates are mounted, the canister is leak checked and later backfilled with dry nitrogen prior to launch.

The fundamental premise of the basic carrier system configuration is the control of hazards via containment. In the case of solids (e.g. failed structure) it has been shown by analysis that the canister will contain

any failed structure up to 200 lbs. (which is the weight constraint for GAS/CAP payloads) under all possible STS loading conditions. This analysis has been reviewed and approved by JSC. There are only 2 constraints for payloads related to structures: the Center of Gravity (CG) envelope which is virtually impossible to violate, and the requirement that the payload's fundamental frequency be greater than 35 Hz. These requirements relate to the attachment points of the can to either a beam or the bridge and not directly to the hardware sealed inside the canister.

The fact that the canister has been shown to contain failed experiment support structure does not obviate the need for a structural analysis of the experiment as such an incident would damage the GAS avionics and associated equipment. Furthermore, the analysis pertains only to unaccelerated debris and does not envelope dynamic situations (e.g. exploding pressure systems).

As mentioned above the canister is leak tested, post-payload integration and prior to launch which, in GSFC's view, confirms the asserted control of primary containment for fluids as long as the fluid is compatible with the canister and does not degrade the endplate or relief valve seals. Material usage in the canister is reviewed and approved by the GSFC Material Branch for the purpose of compatibility with the particular application.

The GAS carrier system may also be configured to vent through the endplate on ascent via a filtered port or through a check valve (in the former the canister repressurizes upon reentry while in the latter it lands at vacuum). Any portion of the canister or any sealed container within the canister may be vented to space through one of the purge ports. The canister may be equipped with a Standard Door Assembly (SDA) which can be opened on - orbit exposing the experiment to space. Additionally, an ejection system to launch small satellites has been developed and been approved by JSC as have the SDA.

There are two other hardware options available to the GAS carrier user. Each canister may be equipped with a redundant battery vent system that is used to vent a sealed battery box outside of the canister through filtered pressure relief valves set at 15 psid. This option is highly recommended and frequently used as a control for the potential of accumulating gases from discharging batteries inside the canister. The other option is a baroswitch which can be used to turn the payload on/off at a predetermined altitude during ascent/descent. Ordinarily the payload is turned on/off by the crew via the APC (Autonomous Payload Controller) in the cabin.

INITIAL GAS/CAP SAFETY REVIEW PROCESS

By mutual agreement GSFC conducts what is analogous to the Phase 0, I, and II Safety Reviews. This process is often multi-iterative involving the user and GSFC personnel from the Special Payloads Division (code 740) and the System Safety Branch (code 302). When necessary specialized experts are available and consulted for specific issues (e.g. electrical, thermal, mechanical). Each Payload Organization (PO) is

required to submit a materials list which is reviewed by the GSFC Materials Branch (Code 313) and a structural analysis which is reviewed by a Code 740 contractor. The PO is also required to submit a Preliminary, a Final, and a Phase III Safety Data Package in accordance with certain milestones in the payload processing timeline. GSFC acts essentially as a surrogate safety review panel for all but the ultimate Phase III SDP which is submitted to JSC (1).

The review critique by GSFC considers the configuration of the carrier system as well as that of the contained hardware. The original concept of GAS was safety via containment as described above in the overview. The majority of GAS payloads are in the truly sealed configuration; they do not vent and they do not have SDAs. This concept of containment seems to have been lost in recent times at both GSFC and JSC. The logic of requiring a fuse on two seriesed "AA" alkaline battery cells inside a sealed canister made of 0.125" thick aluminum with 0.625" endplates that has been proof tested to 115 psig is not apparent.

There are some GAS payloads for which the containment argument is not true and the review logic is accordingly adjusted. For example, in a vented or MDA canister two "AA" cells could represent a viable ignition source which would need some kind of circuit protection or environmental isolation. The absence of the containment control gives rise to more potential hazards in terms of possibilities and magnitude.

Until the classification scheme was adopted there was no systematic approach to evaluate the inherent risk that the payload poses within the context of the carrier system in its various configurations.

CLASSIFICATION OF PAYLOADS USING THE GAS CARRIER SYSTEM

The classification strategy is based upon the degree of containment offered by the carrier system which depends upon the characteristics of the user's payload as well as the configuration of the carrier system.

Structures/Fluid Containment Properties

A properly assembled GAS canister has been shown by analysis to be capable of containing fractured structure weighing up to 200 lbs. which is the maximum mass allowed by GSFC. The proper assembly of the canister at the launch site is assured by following standard assembly procedures performed by GSFC field operations personnel.

Beyond the containment control for failed structure the structural integrity of the user's hardware is designed and verified to margins of safety in excess of those required for STS payloads. This is imposed by GSFC for although failed structure inside the canister would not pose a threat to the Orbiter it most likely would damage the carrier system hardware.

In a truly sealed GAS canister primary fluid containment is also verified in the field by a leak test of the canister in accordance with the standard assembly procedures.

Energy Containment Properties

The sealed GAS canister is capable of fully containing a limited amount of energy that may be released by the enclosed system. Additionally, it is also capable of releasing energy to the ambient environment in a controlled fashion via the pressure relief valves and by the passive thermal control system. The amount of stored energy used to operate the payload inside the canister is known and limited. For the most part, energy is in the form of potential energy that is chemically stored in the battery pack, however other devices such as pressure vessels are also to be considered in the analysis.

The rate at which the contained payload can release this energy depends upon the characteristics of the possible processes that can transform the stored energy of the payload into other dissipative forms of energy (heat, kinetic, and rf energy).

For example, all of the energy in the battery could be dissipated over a short period of time as heat via a dead short across its terminals resulting in a temperature rise of the battery. There is also the potential outgassing of combustibles from the battery. Some of the generated heat would cause an increase in the temperature and pressure in the canister but, this value can be calculated and compared to the canister pressure containment tolerance.

In the above example a dead short of a battery was assumed for the purpose of illustrating the concept. Batteries are particularly important devices as they provide all of the power to run the payload. It is not the intent of this approach to compromise prudent battery design features such as fusing the primary battery pack to prevent dead shorts. However, the need for fusing very low energy batteries in innocuous applications (e.g. flash bulbs, clocks, and memory backup) in sealed and inerted canisters is questionable and is evaluated in the context of energy containment.

Alternatively, the payload may contain a sealed fluid system or pressure vessel. If all of the battery energy is consumed by heating the fluid which overpressurizes the system then the energy may be released instantaneously depending upon the fracture mechanics of the fluid system. However, the amount of energy that can be released is known and limited. Again, if it can be shown that the instantaneous release of energy is the worst possible case and that the canister contains it or dissipates it in a controlled manner, we see no hazard to the Orbiter.

The canister is equipped with one filtered relief valve set at 30 psi and an unfiltered relief valve set at 45 psi (the canister has been proof tested to 115 psi) that provide accelerated pressure relief. As long as it can be shown that the rate of the pressure increase is less than the venting capacity of the pressure relief system and that the vented fluid is not intrinsically hazardous or incompatible with the Orbiter bay environment in any phase of the mission, we see no hazard to the Orbiter.

With respect to RF energy release the truly sealed canister has been shown to exhibit 70 db attenuation. Nevertheless all payloads that have significant EMI sources are required to show compliance with the STS ICD.

GSFC proposed that truly sealed GAS canisters in the most basic standard configuration as described above, and whose energy containment capabilities and materials compatibility are satisfactorily demonstrated be classified as class "B" (for benign) GAS/CAP payloads. The analysis of energy containment will be included in the SDP and will demonstrate containment in the worst case energy dissipation scenario possible and will evaluate the margin of the analysis.

GSFC also proposed that SDA payloads with no batteries (essentially exposure experiments) be included in the class B category. The structures hazard report will include fracture control requirements compliance.

GAS/CAP payloads that do not meet the criteria described above will be classified as "C" (for controlled) GAS/CAP payloads. These payloads will include ejectables and most of the other SDA canisters as well as some canisters that are not truly sealed (i.e. vent in part or in whole on ascent).

It must be recognized that the energy containment analysis is not a trivial exercise. It will involve an analysis of all energy storing devices (i.e. batteries, pressure vessels, chemical reactions, springs, flywheels, etc.) and the possible ways in which that energy can be transformed, possibly accumulated, and released. The intent of the modeling effort used to evaluate energy containment will initially be simplistic but may have to be refined to more accurately reflect the system if necessary. For example, assuming that all of the stored energy is consumed in an adiabatic process which raises the temperature (and pressure) of the nitrogen is a theoretical upper bound but in most instances it does not represent a process that is physically possible. However, if such a calculation confirms containment then there is no need for a more sophisticated model, otherwise the model will be refined.

This may sometimes involve complex thermodynamic analyses including transient multi-media heat transfer problems as well as other processes that are characteristic of the system and its environment.

SAFETY REVIEW PROCESSING

GSFC and JSC have determined that class B payloads be processed in much the same manner as most GAS/CAP payloads were initially processed. The only submittal to JSC will be the Phase III data package which can be processed "off line" without the need for a formal "face-to-face" review with the panel, however GSFC will support a formal review if deemed necessary by JSC. In short, return to the original concept of GAS payloads being considered as benign ballast.

When containment, as defined above, cannot be shown analytically (Class C) or when the margin of safety is questionable GSFC will issue a Phase 0/I SDP submittal with an option for a formal "face-to face" review. The second and third submittals will be the Phase II and III SDPs (or a combined Phase 2/3 if mutually agreed to) for which there will be a standard STS safety review.

THE SAFETY DATA PACKAGE

Much of this paper has been dedicated to defining the JSC/GSFC policy on safety reviews while foregoing any discussion as to its impact on the data package itself. Simply, the new policy is significant, yet minimal. All data packages should contain the information in a format as adeptly described by Gum. Compliance with JSC 13830B and NSTS 1700.7B must be shown. The minimal impact is the required inclusion of the containment analysis, particularly energy containment, in the safety assessment section of the document.

This analysis must show whether or not the payload is Class "B" for benign or "C" for controlled. In the former case it is acceptable to include information regarding system controls that limit certain experimental parameters (e.g. thermostats on heaters) within the descriptive narrative of the experiment. However, it should be emphasized throughout the document and especially in the safety assessment that such devices relate only to mission success and are not hazard controls. The class "B" payload, by definition, assumes total loss of all controls with no safety consequences. This must be shown not just merely asserted. It is anticipated that such payloads will have a minimum of 2 hazard reports: one for structural failure and one for asserting energy containment as described above. In some cases it may be necessary to include others (e.g. secondary fluid containment or batteries).

The SDP for the class "C" payload must show that hazard controls are either single or dual fault tolerant as appropriate pursuant to the criteria in NSTS 1700.7B. The proper approach in preparing a SDP is to perform a hazard analysis to determine if there are any hazards. If found, the level of control is defined by assessing the potential magnitude (i.e. Catastrophic or Critical) of the hazard. It is inappropriate and unacceptable to forgo the hazard analysis and arbitrarily include hazard controls in experimental designs. This applies to all "B" and "C" class payloads.

Beyond the technical requirements and results of analyses/tests the SDP must be clear and concise. It must be appreciated that the JSC review is usually conducted off-line so that there is no real time dialogue among GSFC and JSC during the evaluation of the SDP. The SDP must accurately and unambiguously describe the experiment, how it works, what the hazards (if any) are and how they are controlled.

References

- 1) Gum, M. "STS Safety Approval Process for Small Self Contained Payloads", GAS Experimenter's Symposium (Proceedings) 1988
- 2) JSC 13830B "Implementation Procedure for STS Payloads System Safety Requirements"
- 3) NSTS 1700.7B "Safety Policy and Requirements for Payloads Using the Space Transportation System"
- 4) KHB 1700.7 "STS Payload Ground Safety Handbook"



REPORT DOCUMENTATION PAGE			Form Approved OMB No. 0704-0188	
Public reporting burden for this collection of information is estimated to average 1 hour per response, including the time for reviewing instructions, searching existing data sources, gathering and maintaining the data needed, and completing and reviewing the collection of information. Send comments regarding this burden estimate or any other aspect of this collection of information, including suggestions for reducing this burden, to Washington Headquarters Services, Directorate for Information Operations and Reports, 1215 Jefferson Davis Highway, Suite 1204, Arlington, VA 22202-4302, and to the Office of Management and Budget, Paperwork Reduction Project (0704-0188), Washington, DC 20503.				
1. AGENCY USE ONLY (Leave blank)	2. REPORT DATE October 1992	3. REPORT TYPE AND DATES COVERED Conference Publication		
4. TITLE AND SUBTITLE 1992 Shuttle Small Payloads Symposium			5. FUNDING NUMBERS Code 740	
6. AUTHOR(S) Lawrence R. Thomas and Frances L. Mosier, Editors				
7. PERFORMING ORGANIZATION NAME(S) AND ADDRESS(ES) NASA Goddard Space Flight Center Greenbelt, Maryland 20771			8. PERFORMING ORGANIZATION REPORT NUMBER 92B00110	
9. SPONSORING/MONITORING AGENCY NAME(S) AND ADDRESS(ES) National Aeronautics and Space Administration Washington, D.C. 20546-0001			10. SPONSORING/MONITORING AGENCY REPORT NUMBER NASA CP-3171	
11. SUPPLEMENTARY NOTES Lawrence R. Thomas: NASA Goddard Space Flight Center, Greenbelt, Maryland, 20771. Frances L. Mosier: Interstel, Inc., Beltsville, Maryland, 20705.				
12a. DISTRIBUTION/AVAILABILITY STATEMENT Unclassified - Unlimited Subject Category 12			12b. DISTRIBUTION CODE	
13. ABSTRACT (Maximum 200 words) The 1992 Shuttle Small Payloads Symposium is a continuation of the Get Away Special Symposia convened from 1984 through 1988, and is proposed to continue as an annual conference. The focus of this conference is to educate potential Space Shuttle Payload Bay users as to the types of carrier systems provided and for current users to share experiment concepts.				
14. SUBJECT TERMS Space Shuttle Small Payloads, Carrier Systems and Experiments--Past, Present and Future			15. NUMBER OF PAGES 296	
			16. PRICE CODE A13	
17. SECURITY CLASSIFICATION OF REPORT Unclassified	18. SECURITY CLASSIFICATION OF THIS PAGE Unclassified	19. SECURITY CLASSIFICATION OF ABSTRACT Unclassified	20. LIMITATION OF ABSTRACT Unlimited	